Tomas Bata University in Zlín

Doctoral Thesis

Drug Self-Delivery Systems for Enhanced Targeted Cancer Therapy

Systémy dávkování léčiv pro léčbu rakoviny

Author:	**M.S. Haijun XIAO**
Degree programme:	Material Science and Engineering
Degree course:	Biomaterials and Biocomposites
Supervisor:	Prof. Ing. Vladimír Sedlařík, Ph.D.

Zlin, August 2020

Key words: *irinotecan, curcumin, surfactant, nanoparticle, drug delivery systems*

Klíčová slova: *irinotecan, kurkumin, surfaktant, nanočástice, systémy pro dávkování léčiv*

Acknowledgments

First and foremost, I express my Deepest Gratitude to my supervisor Prof. Vladimír Sedlařík for providing this excellent scientific platform and granting me the maximum freedom in the field of scientific researches. His integrity, sagacity and tolerance impress me greatly. His clear guidance will illuminate my way and help me Soar in my life.

A special gratitude goes to all the technicians at Polymer Centre for their kind support for my research.

Last but by no means least, I am grateful to my grandma, my parents and my siblings, who have provided me through moral and emotional support in my life. I am also grateful to my other family members and friends who have supported me along the way.

Thanks for all your encouragement.

CONTENTS

ABSTRACT

This research work is focused on development and characterization of the easily manufacturing nanostructured systems for enhanced delivery of cytostatic agents based on irinotecan and curcumin. Developed nano-systems only consist of active therapeutic substances and possess good physiochemical stability and redispersibility of its lyophilisates. Both *in vitro* and *in vivo* tests showed improved effectivity of the prepared nanoformulations in comparison with pure cytostatic analogues with simultaneous significant suppressing of the side effects that is promising for further clinical trials.

ABSTRAKT

Tato výzkumná práce je zaměřena na vývoj a charakterizaci snadno připravitelného nanostrukturovaného systému pro zlepšené dodávání cytostatik na bázi irinotekanu a kurkuminu. Vyvinuté nanosystémy se sestávají pouze z aktivních chemoterapeutických látek a vykazují velmi dobrou fyzikálně chemickou stabilitu a redispergovatelnost jejich lyofilizátu. Testování in vitro a in vivo prokázaly zvýšenou účinnost připravených nanoformulací oproti čistým analogickým cytostatikům při významném potlačení negativních vedlejších účinků, což přináší dobré předpoklady pro následná klinická testování.

1. INTRODUCTION

Cancer becomes the second leading cause of death globally. Chemotherapy based on small molecules remains one of the most effective ways to fight against various cancers *via* utilising chemical substances to stop cancer growth either by directly killing the cells or preventing these cells from division. Nevertheless, more than 80% of drug candidates and 40% of marketed drugs show very poor water solubility and limited bioavailability[1, 2], severely hindering their clinical formulation and translation. Free drugs, when administered into bloodstream, are subjected to various metabolic processes, primarily renal clearance and distribution in non-target tissues. These processes not only reduce the drug concentration at the target sites but also increase the likelihood of unwanted side effects.

In order to overcome the intrinsic shortages of these useful small molecules, a dramatically large amount of materials have been developed and optimised as carriers for the delivery of these molecule, including those directly obtained from natural resources, such as various kinds of natural polysaccharides, and those synthesised by human beings, such as the synthetic polymers. The materials are usually covalently conjugated with the free molecules to alter the chemical structures and chemophysical properties of the small molecules[3, 4] or utilised as carriers *via* forming different nanoparticular systems with various nanostructures to transport these small molecules[5], such as nanoparticles, dendrimers, micelles, polymersomes and so on.

The specific nanostructures of these unique carrier forms provide the small molecules many different features compared to those traditional formulations. For instance, the tumour-specific deposition feature, also known as the enhanced permeability and retention effect, occurs when the nanoscale particles extravasate out from the tumour vasculature, causing the particular accumulation of drug molecules in the solid tumour interstitia[6]. These materials used as carriers in the drug formulations may not only change the apparent behaviour of drug molecules inside the body but also provide them with more functional possibilities.

However, the utilisation of these materials in drug formulations also brings more uncertainty at the same time because of the compatibility and safety problems. Considering these, until now only very few polymers have passed the clinical screening and been approved by the U.S. Food and Drug Administration (FDA) to be used inside human bodies. Another obstacle which heavily limits the clinical translation of the carrier-based drug formulations is the uniformity of these nanoparticles during preparation and the physiochemical stability after lyophilisation.

In this research, we aim to develop an easy-manufacturing drug self-delivery system based on drug molecules themselves without the extensive use of carrier materials in the nano formulations, which can be used to enhance the anti-cancer efficacy of the chemotherapeutic agents as well as to ameliorate their side effects caused to the bodies.

In the theoretical part, a review of cancer treatment methods based on the modern therapeutic technologies is reported, including the strategies used for the treatment of different cancers, the chemophysical properties of materials used for the delivery of a diversity of chemotherapeutic agents, the drug delivery systems with various nanostructures suitable for delivery of different drug molecules, and the problems faced during the construction of these drug delivery systems.

In the experimental part, a drug self-delivery system based on the anticancer agents has been constructed. Their physiochemical properties are explored and their enhanced therapeutic efficacy and ameliorated side effects are verified on both *in vitro* and *in vivo* models.

2. CANCER TREATMENT

2.1 Global Cancer Burden

Cancer is a group of diseases associating with the uncontrollable growth of cells which may further invade other parts of the body. According to the statistical data from world health organisation (WHO)[7], cancer becomes the second largest cause of death globally and is responsible for a nearly 10 million deaths in 2018, which means 1 in 6 deaths is caused by cancer. The most common confirmed cancer types include lung cancer[8], breast cancer[9], colorectal cancer[10], stomach cancer[11] and skin cancer, and more than 1 million cases are confirmed in each cancer type in 2018. While the most common causes of cancer deaths involve lung cancer, colorectal cancer, stomach cancer, liver cancer and breast cancer.

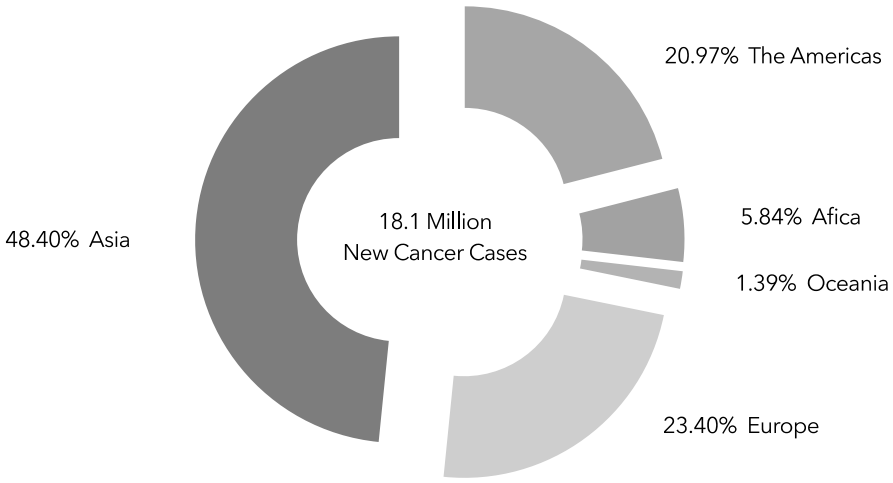

Figure 2.1-1 Global cancer incidence in 2018

These high incident cancers show very close relationships with genetic factors of people and their personal characteristics and habits, such as the ages which dramatically increase the cancer incident rates as getting older[12, 13], the physical inactivity[14] which is connected to the personal immunity, exposure to strong ultraviolet and ionising radiation interrupting the normal cell activities[15], the abuse of tobacco and alcohol[16], the possible microbial infections[17] and so on.

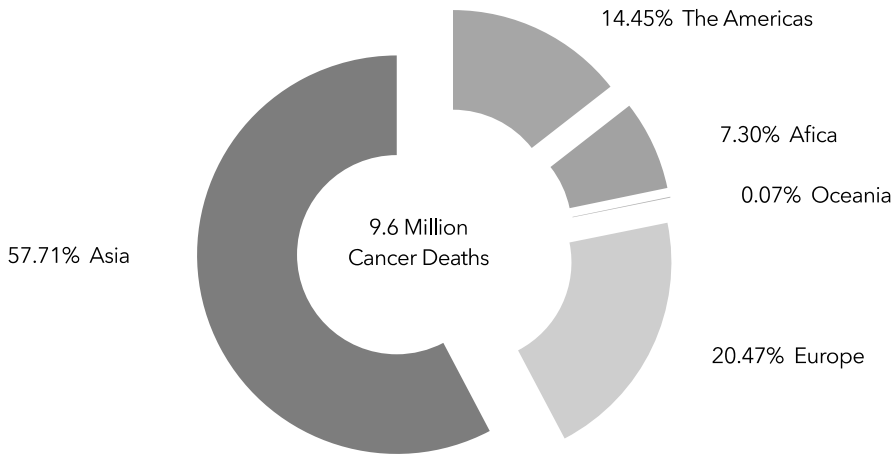

Figure 2.1-2 Global cancer mortality in 2018

Generally, to reduce the cancer burden is to avoid the related key risk factors, which could significantly reduce the incidence of most cancers. For instance, the use of tobacco is one of the most important high risk factors, which causes around 1 in 5 cancer-related deaths globally in 2016[18]. Besides, early detection such as early diagnosis and screening is another effective way to dramatically reduce the incidence of cancer mortality because cancer is more likely to be controlled when identified and treated early. Usually, significantly positive results can be expected in the lives of cancer patients by early detection and avoidance of delay in palliative care.

2.2 Methods for Cancer Treatment

The primary goal for cancer treatment is simply to cure cancer or significantly prolong the lifetime of cancer patients. Another aspect of cancer treatment is to improve the life quality of patients, which also plays a pivotal role for cancer patients.

While the correct cancer diagnosis is usually the very important first step for the later cancer treatment as individual patients may require a specific therapeutic regimen according to the different cancer types and the various physical conditions of patients. Besides, for a specific cancer case at different stages, more than one treatment modalities are usually combinatorially used in order to maximally control the development of caners, such as radiation therapy in combination with chemotherapy. During the decades researches on the treatment of cancers, many therapeutic methods have been developed and used in clinical to help prolong the lifetime of cancer patients, such as surgery[19], radiation therapy[20], chemotherapy[21], immunotherapy[22], stem cell therapy[23] and hormone therapy[24].

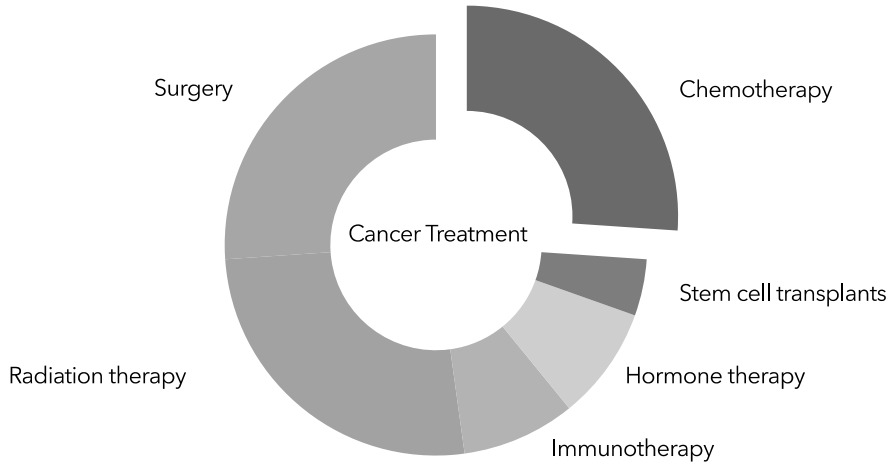

Figure 2.2-1 General cancer treatment methods

2.2.1 Surgery

Surgery, when used for the treatment of certain types of solid cancers, is a procedure in which the surgeons directly remove cancer tumours from the body. Depending on the physical conditions of the patients, the part of body that requires surgery and the amount of tumour tissues that need to be removed, the processes of surgeries may be open or minimally invasive, which essentially cause different degrees of trauma to patients and take varying time to be recovered from surgeries.

Surgery is especially suitable for the treatment of solid tumours at very early stages, which generally indicates that the tumour tissues are still contained in one local area without spreading to other parts of the body. According to the actual situation, surgery can be used to remove the entire tumour or just parts of the tumour tissues if the entire removing would cause the dysfunction or damage of some other organs[25]. Sometimes surgery is also utilised to just ease the pressure to a particular organ caused by tumour tissues inside the body.

However, surgery may also cause some symptoms. Many people may suffer from the pain after surgery for a long time, which totally depends on the extent of surgery, the part of the body where surgery is operated on and the sensitivity of patients to pain. In some cases, pain control is necessary for some patients[26]. Another common risk for surgery treatment is the infection occurs at the wound sites after surgery, which may need to be treated with some antibiotics for a certain range of time[27]. Some other related problems of surgery include bleeding, damage to the nearby organs and so on. Therefore, the possible palliative care and other supports should be provided for the patients to ease their suffering after surgery, which would help people live more comfortably.

There are also some limits of surgeries to be used for the treatment of cancers. For instance, surgery cannot be used for leukaemia which is a type of blood cancer. In some other cases, because of the weak physical conditions of patients or the late stages of cancers which means the cancers have already spread to other parts of the body, surgery can only provide very limited help. Therefore, in addition to surgery, some other methods are also used to treat cancers.

2.2.2 Radiation therapy

Radiation therapy[20] (also called radiotherapy) is another common treatment method which has been widely used in clinical to treat various cancers as well as to ease the caner symptoms. Radiation therapy uses high doses of radiation to kill cancer cells and shrink the tumour seizes. At high doses, the radiation would permanently damage the DNA of cancer cells whose proliferation therefore are prevented. Finally, these damaged cancer cells would die and be removed by the body. Usually, this process would last for several weeks or months to keep the cancer cells dying after radiation therapy ends because the radiation would not kill the cancer cells right away.

According to the sources of the radiation, radiation therapy can be classified into two main classes, namely external beam radiation therapy[28] and internal radiation therapy[29]. External beam radiation therapy is based on a large machine which aims its radiation at the local cancer sites. For instance, patients with lung cancers might only be exposed to radiation at the chest instead of the whole body. Internal radiation therapy is a treatment method whose radiation source is inside the body. Internal radiation therapy with solid radiation sources (also called brachytherapy[30]) coming from seeds, ribbons or capsules which are placed near the tumours inside the body would only produce local anti-cancer effects as well. While internal radiation therapy with liquid radiation sources would take a systemic therapeutic effect as the treatment agents would travel in the blood to the whole body before being eliminated from the body[31].

Many factors would affect the practical applications of this method for cancer treatment, such as the cancer types, the tumour sizes, the location of tumours, the physical conditions and ages of patients and so on. External beam radiation therapy can be used for the treatment of various cancers because of its machine-based local therapeutic effects. Brachytherapy is usually utilised to treat eye[32], head[33], neck[34], breast[35] and prostate[36]. While the systemic therapeutic radiation therapy is often used for thyroid cancer[37] and advanced prostate cancer[38].

Usually, radiation therapy would be used in combination with other cancer treatment methods to achieve a better therapeutic effects. For instance, radiation therapy might be given before, during or after other cancer treatments. Radiation therapy might be given before surgeries to significantly shrink the cancers which hold large sizes. Radiation given during surgeries would directly go to the cancer tissues without interrupting any normal tissues. The duration of radiation therapy would depend on the cancer types and primary goal of this treatment, namely treating the cancer or easing the symptoms.

The limits and drawbacks of radiation therapy are also obvious. For instance, over the course of lifetime, an area of body can only safely receive limited amount of radiation. Besides, radiation therapy would cause damage to the nearby healthy cells during treatment, which would further produce some other side effects, such as fatigue, hair loss, skin changes, test changes and so on[39].

2.2.3 Immunotherapy

Immunotherapy is another cancer treatment method which helps the own immune system of the body to fight against cancers. Generally, the body immune system, which consists of a complex network of cells and proteins, could detect and try to destroy the abnormal tumour cells to prevent the growth of cancers. However, these cunning cancer cells have their own ways to avoid being eliminated by the immune system by changing their genes or directly turning off the immune cells through expressing some specific proteins on their surfaces, which is why immunotherapy is needed for the body immune system to better fight against cancers.

According to the different action mechanisms, several types of immunotherapy have been used to treat cancers, including immune checkpoint inhibitors[40], T-cell transfer therapy[41], monoclonal antibodies[42], treatment vaccines[43] and immune system modulators[44].

Immune checkpoints are a part of the body immune system, which basically helps to reduce the sensitivity of an immune response to normal cells and avoid killing these healthy cells in the body. The proteins on the immune cells are called immune checkpoint proteins. When the proteins on the tumour surface bind to the immune checkpoint proteins, an "off" signal would be sent to the immune cell, which stops the immune system from killing the cancer cells.

Immune checkpoint inhibitors (also called immunotherapy drugs) would prevent the immune checkpoint proteins from binding to their partner proteins on the tumour

surface and inhibit the "off" signal which silences the immune cells, subsequently allowing the immune system to kill cancer cells. Drugs which work as immune checkpoint inhibitors include CTLA-4 and PD-1. Immune checkpoint inhibitors have been approved to be treat various cancers, such as breast cancer, colon cancer, liver cancer, lung cancer and so on. This cancer treatment would also cause some adverse effects, including rash, diarrhoea, fatigue and widespread inflammation.

T-cell infusion is another type of immunotherapy, which works by boosting the natural ability of T cells in the body to fight against cancers. There are two main types of T-cell transfer therapy, namely tumour-infiltrating lymphocytes therapy[45] and CAR T-cell therapy[46]. With this treatment method, T cells would be collected from the patients and then infused back into the patients after massive cultivation in the laboratory. Two CAR T-cell therapies, namely tisagenlecleucel[47] and axicabtagene ciloleucel[48], have been approved by the Food and Drug Administration for blood cancers.

T-cell infusion has also been studied to treat solid cancers, such as breast cancer and brain cancer. However, one known serious side effect caused by CAR T-cell therapy is the cytokine release syndrome. Cytokines are immune substances which would be largely released when the immune cells respond to the new T cells. A sudden increase of cytokine levels in the blood would cause unexpected adverse effects, such as fever, headache, rash, nausea, rapid heartbeat and so on. Besides, although the CAR T cells are specifically designed to bind to the tumour cells, sometimes they might be also recognised by normal cells causing organ damages.

Monoclonal antibodies are also called therapeutic antibodies, which are immune system proteins specifically designed and synthesised in the laboratory to interact with the targeted cancer cells[49]. They may be used to mark the cancer cells for being better recognised by the immune system or to directly help bring the immune cells close to cancer cells and kill cancer cells[50]. Many monoclonal antibodies have been developed to treat a large variety of cancers. Like other immunotherapies, monoclonal antibodies would also cause unexpected problems, such as skin reactions, flu-like symptoms, serious infections and capillary leak syndrome.

Cancer treatment vaccines[51] are another type of substances which work by strengthening the response of immune systems to cancer cells. These vaccines are designed to work against cancers instead of preventing the factors those cause cancers because cancer cells would usually express some tumour-specific antigens which are

not identified on normal cells. The treatment vaccines can help the immune system to better recognise the cancer cells.

According to the different sources, the cancer treatment vaccines can be made from the tumour cells or dendritic cells of a specific cancer patient[52] or tumour-specific antigens that are isolated from cancer cells of many people with one same type of cancer[53]. Another type of cancer treatment vaccine is the oncolytic virus[54], which could infect and destroy cancer cells without harming the healthy cells. Cancer treatment vaccines have been used to treat spread prostate cancer[55] and melanoma that returns after surgery[56]. Cancer treatment vaccines would produce some side effects, such as allergic reaction, stroke, flu-like symptoms.

One more type of immunotherapy is called the immune system modulator[57] which is used to enhance the response of the body immune system to cancer cells. Some modulator substances can work locally on some specific parts of the immune system while some others may affect the whole immune system in a more general way.

Several immune system modulators have been developed and utilised to work against cancers in different ways. For instance, interferons could enhance the body immune response to cancers by activating certain white blood cells, such as the natural killer cells and dendritic cells. Interleukins can boost the number of some kind of white blood cells in the body, including killer T cells and natural killer cells, to strength the immune response[58]. They can also help B cells to produce some substances which can target cancer cells. Some other immune modulators (Hematopoietic growth factors) are used to reduce the side effects caused by cancer treatment. A variety of blood cells may be also damaged during cancer treatment while the immune modulator substances could promote the growth of these blood cells. For instance, Erythropoietin has been used to promote the production of red blood cells[59] and interleukins -11 can increase the platelets in the blood[60]. Immune modulators can cause some flu-like side effects, such as fever, chills, weakness, dizziness, headache and fatigue[61]. Sometimes cytokines may produce many serious unexpected adverse effects, including trouble breathing, abnormal blood pressure, severe allergic reactions, skin reactions or even organ damage.

Immunotherapy has been developed to act against many types of cancers. However, until now they are not yet widely used as surgery and radiation therapy. Besides, immunotherapy can also cause many side effects.

2.2.4 Hormone therapy

Hormone therapy is a cancer treatment method which works by adjusting the hormone levels in blood to slow or stop the growth of cancer cells. Hormones are secreted from some endocrine glands, such as thyroid, pancreas and ovaries, which can further act on the targeted cells throughout the body via blood circulation to bring out particular changes of cells. By communicating with the specific cells, some hormones may promote the growth of cancers[62] while some may prevent their growth[63]. Based on these action characteristics, hormone therapy has been carried out to treat cancers by adjusting the hormone levels which cancer cells rely on or ease the symptoms caused by cancer via interfering with the behaviour of hormones in the body. For instance, hormone therapy has been used for the treatment of prostate and breast cancers whose growth depends on the consumption of certain hormones.

Hormone therapy can also introduce some unwanted side effects because of the changes of hormone levels in blood, such as fatigue, hot flashes and so on. Usually, hormone therapy is used with other cancer treatment methods together.

2.2.5 Stem cell transplants in cancer treatment

Stem cells exist throughout the body in adults to provide a way to reaerate and repair the most tissues in the body via replication and differentiation[64]. Stem cells play an important role in the body and they can grow into different types of blood cells, such as white blood cells, red blood cells and platelets, which work together to remain the body to be healthy.

Stem cell transplant is a procedure which restores the blood-forming stem cells in patients. Once inside the blood circulation, they would travel to the bone marrow to replace the destroyed cells. Usually, stem cell transplants do not act on the cancer cells directly. Instead, they provide a way to restore the stem cells the body needed and help the patients to recover the ability to produce stem cells. These stem cells sued for transplants can be collected from the bone marrow, bloodstream, or umbilical cord of the patient himself (autologous transplant)[65], or another person (allogeneic[66] or syngeneic transplant[67]). Stem cell transplants are usually used for patients with leukaemia[68], lymphoma[69] or myeloma[70]. Stem cell transplants can also cause some problems if the stem cells transplanted do not match the patients well. For instance, the called graft-versus-host reactions engages when the cells from the donor recognise the blood cells in the patients as foreign and begin to attack them.

2.3 Chemotherapy

Chemotherapy is a drug treatment that uses powerful chemical molecules to stop the growth of cancers by directly killing cancer cells or preventing them from proliferation. These chemical drug molecules are designed to interrupt the physiological functions of cancer cells. The use of chemical molecules to treat cancer can be traced back to the beginning of the 20th century[71]. Until now, many chemical small molecules have been verified to be strongly effective in controlling the abnormal activates of cancer cells.

Once inside the cancer cells, these drug agents are able to interact with other molecules in cancer cells to stop the cell growth. During the whole life cycle of cancer cells, every phase of the cell cycle could be the possible action target for these small therapeutic molecules. For instance, the vinca alkaloids would prevent the microtubule from assembly in the mitotic phase to stop the cell division process[72] while the taxanes, such as docetaxel and paclitaxel, would inhibit the cell division *via* blocking the disassembly of microtubules during cell proliferation[73].

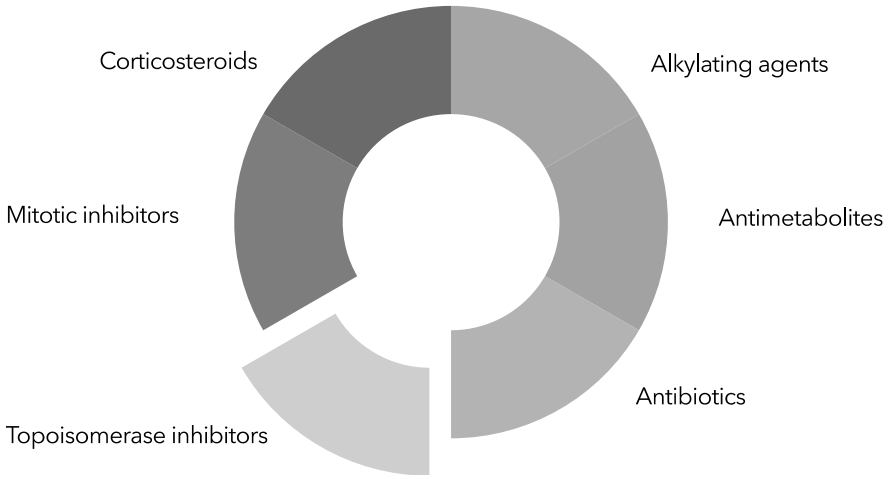

Figure 2.3-1 Types of chemotherapeutic agents

2.3.1 Types of chemotherapeutic agents

Based on the factors such as molecular mechanisms of action, chemical structures, sources and so on, the small anti-cancer agents can be classified into several classes[74], including alkylating agents which directly damage DNA, anti-metabolites that take place of the building components of genetic materials, antibiotics interfering with the enzymes involved in the replication of DNA, topoisomerase inhibitors, mitotic inhibitors that block the cell division and corticosteroids which are used to ease the

unwanted adverse effects of other drugs. Some drug molecules may be categorised into different classes as they may satisfy different criteria.

Alkylating agents

Alkylating agents are compounds that work by altering the structures and functions of DNA through crosslinking and/or fragmenting the genetic materials[75], which are one of the first classes of drugs used for cancer treatment.

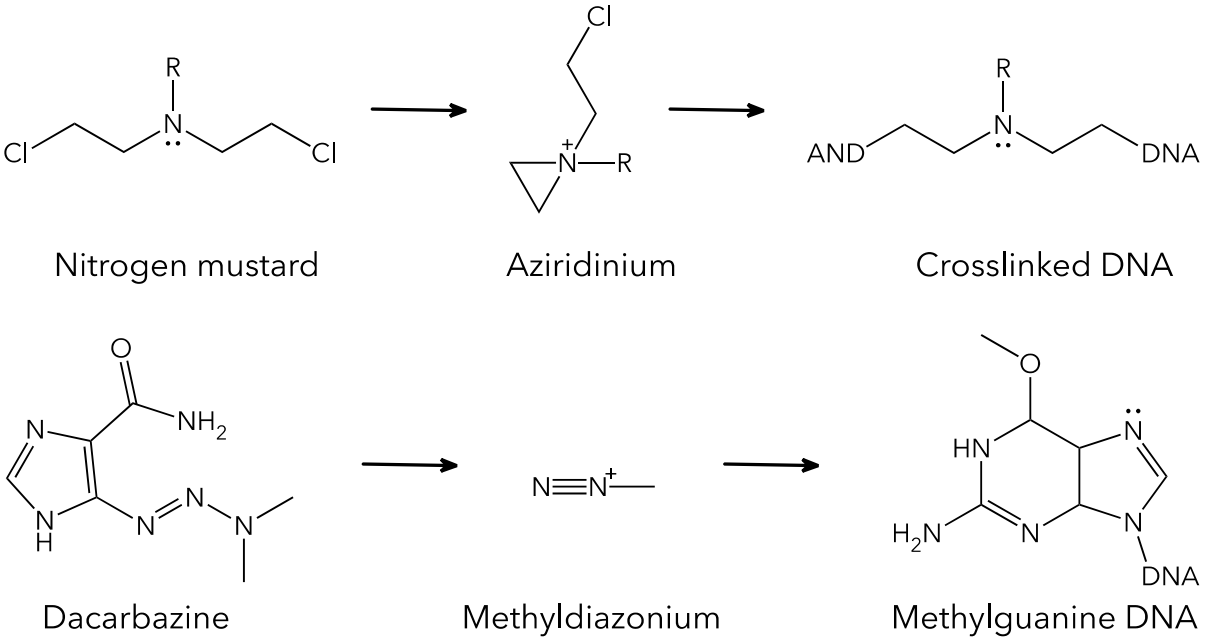

Figure 2.3-2 General action mechanisms of alkylating anticancer agents

Because of their effectiveness of action during every phase of the life cycle of cancer cells, alkylating agents can be used to effectively treat a wide variety of cancers, such as leukaemia, lymphoma, multiple myeloma, retinoblastoma, brain cancers, breast cancers, lung cancers, ovarian cancers, prostate cancers and so on[76, 77]. There are four traditional categories of alkylating agents, namely nitrogen mustards, nitrosoureas, alkyl sulfonates and ethylenimines and three non-classical categories of alkylating drugs including hydrazine, triazines and altretamines[78].

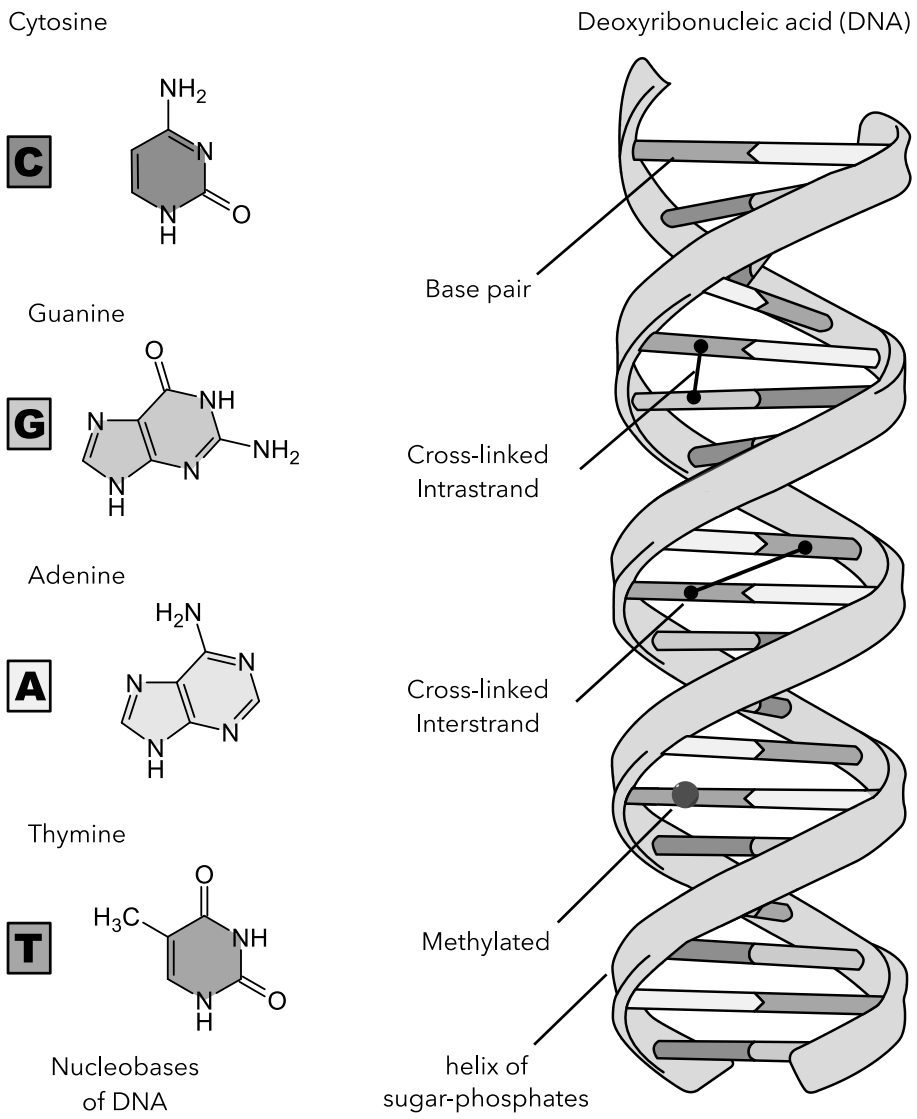

Figure 2.3-3 Alkylating agents caused errors during base pairing in DNA

Nitrogen mustards are a class of nonspecific DNA alkylating agents containing the functional chloroethylamine group, which were also the first approved agents for the treatment of various cancers. After being absorbed into the body, nitrogen mustards are hydrated and transformed to aziridinium ions or carbonium ions, which can be further cross-linked to the bases of DNA, interrupting the separation during DNA replication and damaging the normal functionalities of genetic materials through inhibiting their mitosis.

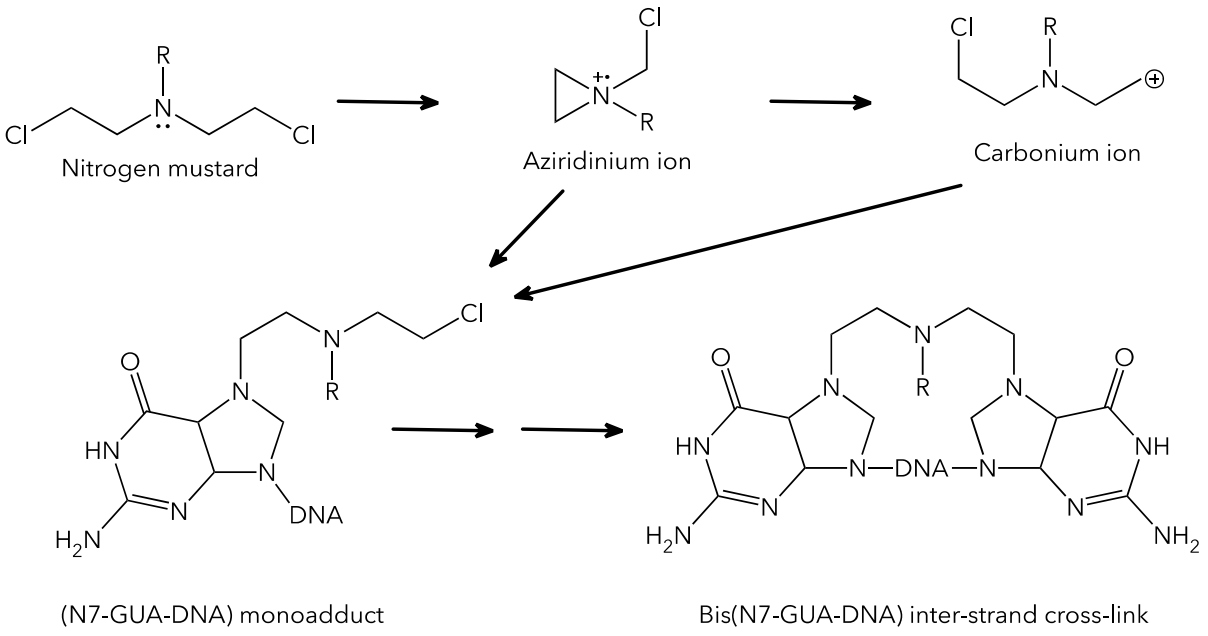

Figure 2.3-4 Nitrogen mustard mechanism of action

In 1929, Berenblum at the University of Leeds in England firstly applied sulphur mustard gas to mouse ears along with tar and discovered the inhibition effect of sulphur mustard gas on skin cancers[79]. The therapeutic effects of nitrogen mustards on various cancers were then experimented and investigated by different researchers all around the world. Many different nitrogen mustard drugs have been discovered. For instance, chlorambucil, which showed milder toxicities, was discovered and developed by W.C.J. Ross *et al.* in 1953 and approved by the FDA in 1957 as the first aromatic nitrogen mustard drug for the treatment of various cancers[78]. However, nitrogen mustards also cause many side effects, such as low blood counts, infection, bleeding, vomiting, hair loss, mouth sores, fever, diarrhoea and so on. The representative agents of nitrogen mustards include mechlorethamine, cyclophosphamide, ifosfamide, chlorambucil, melphalan and so on.

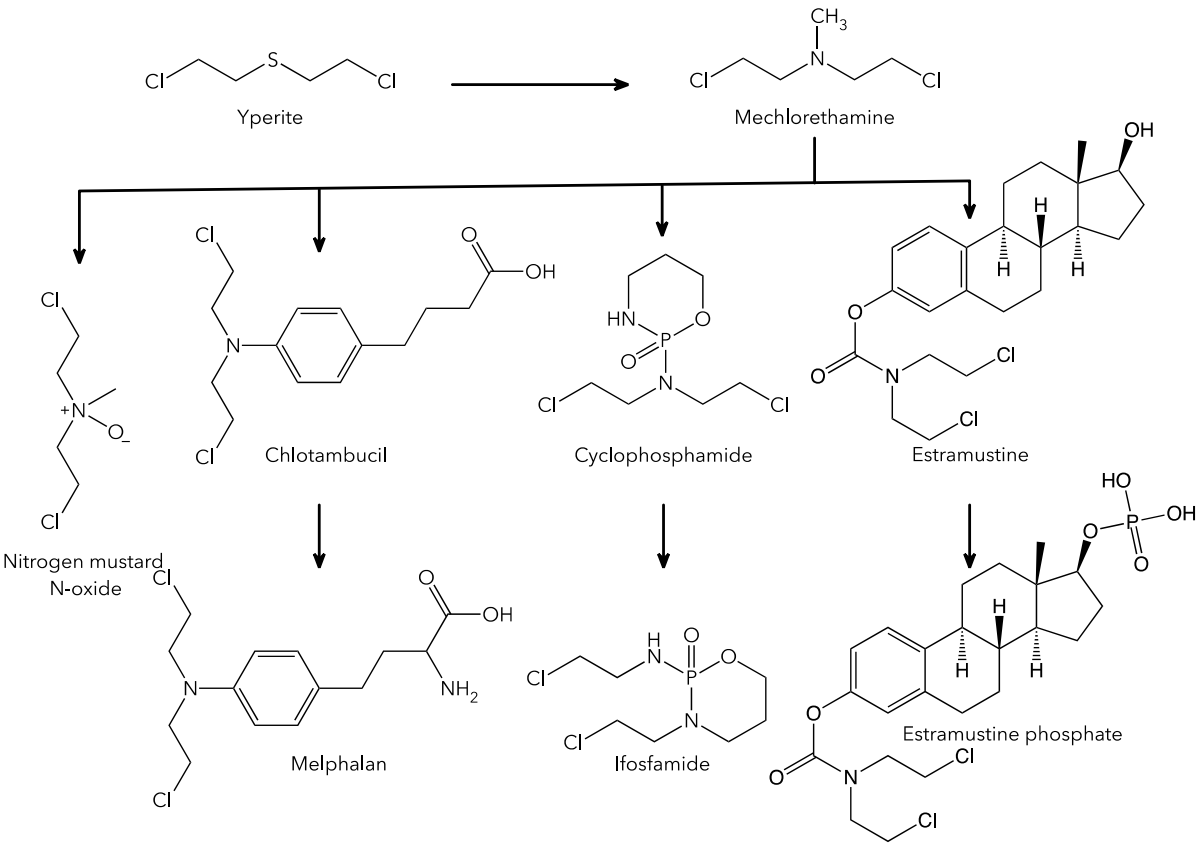

Figure 2.3-5 The structure of nitrogen mustard drugs

Alkyl sulfonates, such as Busulfan, are esters of alkane sulfonic acids which are another type of alkylating agents showing anti-cancer effects. Busulfan was first identified by A. Haddow and G.M. Timmis at the Chester Beatty Research Institute in 1951[80]. It contains two methanesulfonic acid at both ends of the buthane chain and can effectively interact with DNA stands to interrupt their replication. Busulfan was found to have excellent therapeutic efficacy and reduced bone marrow suspension compared to nitrogen mustard, which was approved by FDA as a chemotherapeutic agent for the treatment of chronic myeloid leukaemia in 1954.

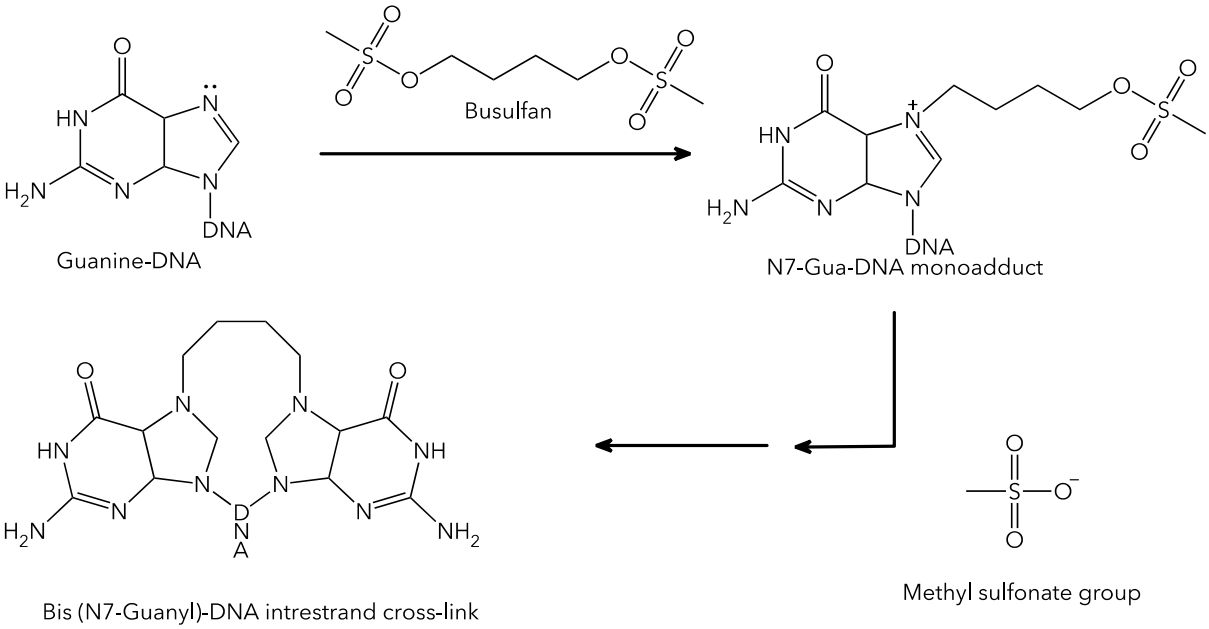

Figure 2.3-6 Mechanism of action of Busulfan

Ethylenimines are another class of alkylating agents which show similar therapeutic effects as nitrogen mustards but they are not electronically charged in their structures. They can trigger the DNA inter-strand cross-linking reactions and interrupt the DNA replication. Two main drugs in this class are thiotepa and mitomycin C.

The anticancer effect of thiotepa was first reported by A.L. Walpole's research group at the Imperial Chemical Industries Inc. in England and J.H. Burchenal's group at the Sloan-Kettering Cancer Centre in 1950, respectively. In 1959, thiotepa was approved by FDA as a chemotherapeutic drug. Now thiotepa has been used for several solid cancers, such as Hodgkin's disease, leukaemia, thyroid cancer, bladder cancer and so on, either alone or in combination with other therapeutic drugs. The main side effects of this drug used for cancer treatment is that it causes the bone marrow suppression which further leads to leukopenia, thrombocytopenia or anaemia in patients[81].

Mitomycin C is a kind of mitomycins which are a class of natural compounds containing the aziridine group. Mitomycins are isolated from *Streptomyces caespitosus* or *Streptomyces lavendulae*, including mitomycin A, mitomycin B, and mitomycin C. Mitomycin C has been used to treat different cancers, such as oesophageal carcinoma, anal cancers, lung cancers, breast cancers, pancreatic cancers, bladder tumours and so on. In 2020, the mitomycin gel was approved by FDA to treat low-grade upper tract urothelial cancer in the United States. However, this drug molecule would also lead to many side effects, such as haemolysis, ureteric obstruction, flank pain, urinary tract infection, renal dysfunction, fatigue, nausea, abdominal pain and so on.

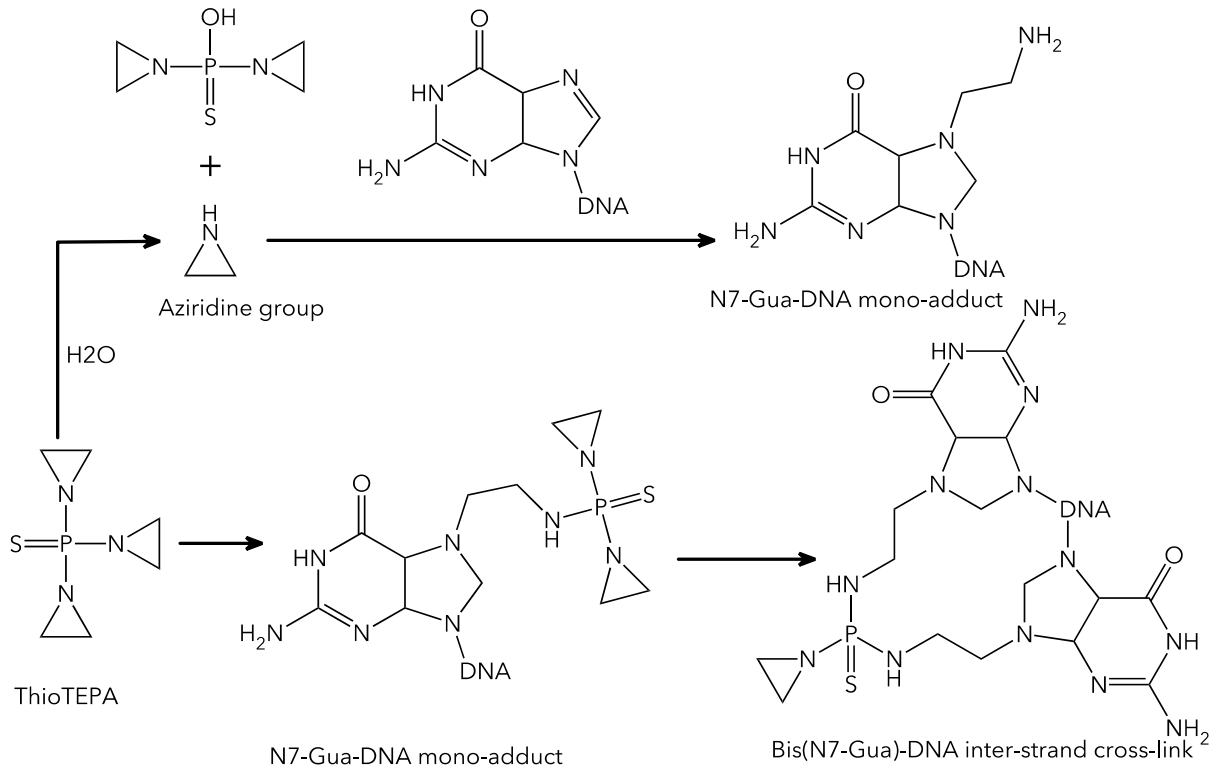

Figure 2.3-7 Mechanism of action of Thiotepa

Nitrosoureas are a class of alkylating anti-cancer agents which have a nitroso group and urea bound in their structures. They will hydrolyse into substances which show alkylating and carbamoylating activities in the body. These hydrolysed substances would induce the alkylation of DNA and transformation of proteins, subsequently preventing the replication and transcription of DNA. The representative drugs in this class include carmustine, lomustine and streptozocin. Carmustine and lomustine have been found to be easily come across the blood-brain barrier due to their suitable molecular sizes and their strong lipophilicity. Lomustine was first approved by FDA to treat brain tumours in 1976 and carmustine was first approved as a therapeutic drug by FDA in 1977. Now these two drugs are still using in clinical to treat several types of brain cancers, such as glioma, glioblastoma multiform, multiple myeloma, lymphoma and so on. Streptozocin is approved by FDA for treating metastatic cancers of the pancreatic islet cells since streptozocin can effectively shrink the tumour sizes and dramatically reduce the symptoms of disease. Streptozocin has also been used in scientific studies to model the Alzheimer's disease[82] and induce insulitis and diabetes[83] on some experimental animals because of its high toxicity to beta cells.

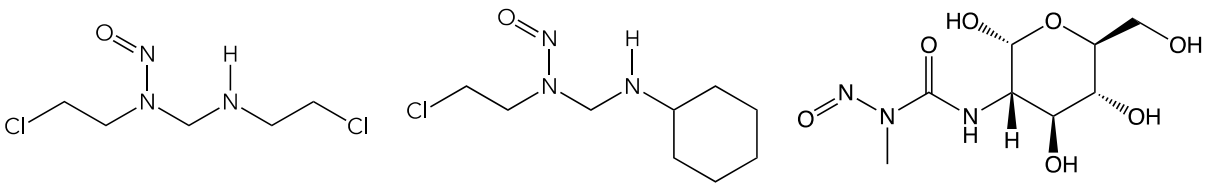

Figure 2.3-8 The structure of nitrosourea drugs

There are some other synthetic inorganic compounds which have been used as non-classical alkylating anti-cancer agents because most of them only induce the methylation of guanine bases instead of causing the DNA crosslinking activities exhibited in classical alkylating drugs. The representative non-classical alkylating drugs include hydrazines, triazenes, and altretamines.

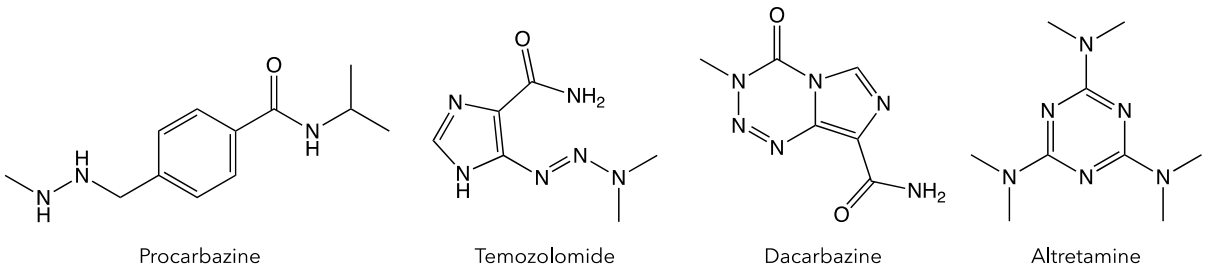

Figure 2.3-9 The structure of non-classical alkylating drugs

Hydrazines (R_2N-NR_2) are a class of chemicals which have two nitrogen atoms linked together through a covalent bond and one to four alkyl or aryl substituents[84]. Procarbazine, which was developed by Hoffmann-La Roche in 1950s, was the first approved anti-cancer agent among this class. Procarbazine has been used to treat brain cancers and Hodgkin's lymphoma alone or in combination with some other therapeutic agents. The common side effects caused by procarbazine include low blood cell counts, tiredness, vomiting, depression and so on.

Triazines are another family of non-classical alkylating agents containing the functional group –N(R)–N=N–, where R represents H, alkyl or aryl[85]. The representative anti-cancer drugs in this class include dacarbazine and temozolomide. Dacarbazine and temozolomide act as prodrugs which would be activated by cytochrome P450 inside the body and converted into monomethyl compounds. The monomethyl chemical would be hydrolysed into a diazomethane which further forms a methyl diazonium ion and methylates guanine in DNA.

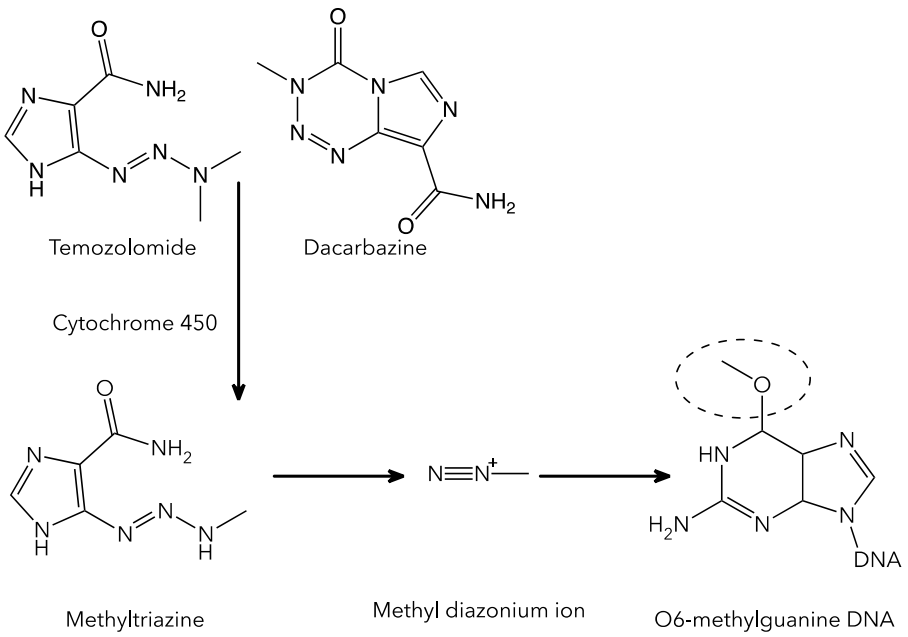

Figure 2.3-10 Mechanism of action of dacarbazine and temozolomide

Dacarbazine has been utilised to treat different cancers, including melanoma and Hodgkin's lymphoma, soft tissue sarcomas, neuroblastoma, rhabdomyosarcoma, islet cell carcinoma and medullary carcinoma of the thyroid and temozolomide are used for the treatment of anaplastic astrocytoma and glioblastoma multiforme. The therapeutic efficacy of these drugs would rely on the levels of DNA methylation in tumour tissues and epigenetic silencing of MGMT gene in brain tumour cells has been considered to be a predictive factor for response to temozolomide treatment. Therefore, patients with high expression levels of MGMT gene are selected for the related researches of temozolomide[86].

Altretamine is also an anti-cancer agent which was first approved by the U.S. FDA in 1990 for the treatment of ovarian cancers because of its superior therapeutic efficacy[87]. The precise mechanism of action of altretamine acting as an anti-cancer agent remains unknown, but it is clarified by Me-SH as a non-classical alkylating agent[88]. The unique chemical and molecular structure of altretamine has been considered as the key factor for its anti-cancer efficacy[89]. Altretamine will be metabolised into the formaldehyde with weak methylation activities, which will further interact with DNA to damage the tumour cells. Altretamine also cause some side effects, such as nausea, vomiting, anaemia and peripheral sensory neuropathy[90].

Antimetabolites

Anti-metabolites are another type of anti-cancer agents which work by inhibiting the use of a metabolite in normal metabolisms and interrupting the regular activities of cells[91]. These drug molecules are usually the analogues with similar chemical or molecular structures of gene units. They would masquerade as gene units and prevent them from being incorporated into DNA. Hence, the presence of anti-metabolites would particularly interfere with the actives of cells during synthesis phase (S phase), stopping the normal development and division processes of cells. As tumour cells usually have more rapid division rates than other cells, the incorporation of antimetabolites shows a stronger inhibition effect on cancer cells. The antimetabolites have been used for the treatment of various cancers, such as leukaemia, ovarian cancer, breast cancer, intestinal cancer and so on.

The antimetabolite drugs can be mainly classified into four classes. The first category is base analogues (also called nucleobases), which can be substituted as normal nucleobases in nuclear acids to prevent the proliferation of cells. This type of antimetabolites includes purine analogues and pyrimidine analogues, which mimic the structures of metabolic purines and pyrimidines, respectively. The representative examples of antimetabolites used for cancer treatment in this class include thiopurines, fludarabine, 5-Fluorouracil (5-FU), 6-Mercaptopurine (6-MP), gemcitabine (Gemzar®) capecitabine (Xeloda®), cladribine, clofarabine, cytarabine (Ara-C®), floxuridine, pentostatin and so on.

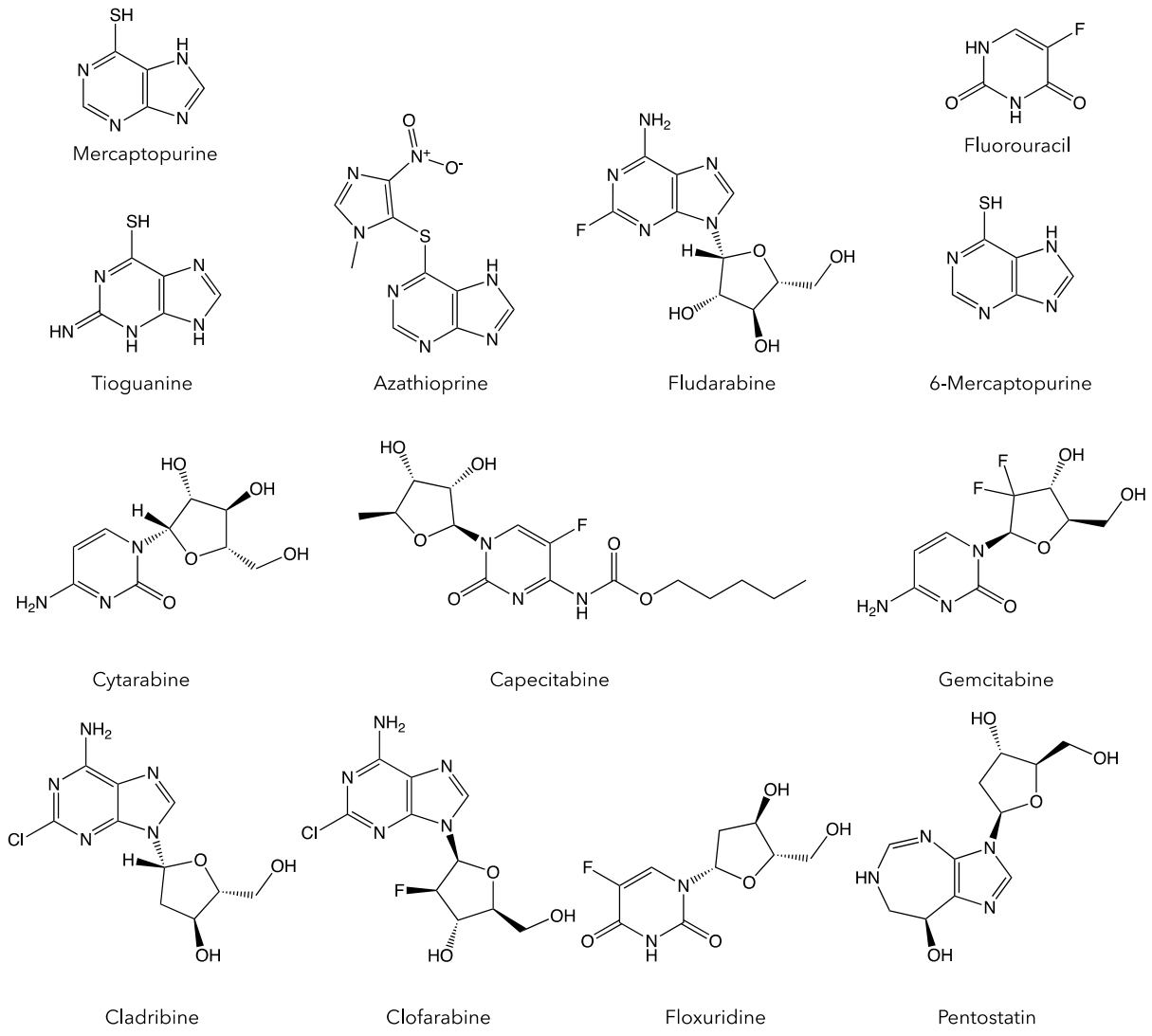

Figure 2.3-11 Chemical structures of base analogues and nucleoside analogues

Nucleoside analogues are another class of antimetabolites consisting of a nucleic acid, a sugar molecule and/or one to three phosphonates. They are similar to the components used to build cellular DNA but different enough that the cell proliferation will be inhibited after being added into the DNA structures. Anti-folates are also used as anticancer agents because they can block the actions of folic acid which is needed during cell division. Examples of anti-folates include dihydrofolate reductase inhibitors (such as aminopterin, methotrexate, pemetrexed and pralatrexate) and thymidylate synthase inhibitors (such as pemetrexed and raltitrexed).

Antibiotics

Some natural antibiotics targeting the enzyme which are incorporated into DNA replication are also widely used for the treatment of various cancers. These anti-cancer

antibiotics are cell-cycle nonspecific which means they can affect all phases of the cell cycle. They work by interfering with DNA and RNA in cancer cells and preventing the synthesis of certain proteins needed for cancer cells.

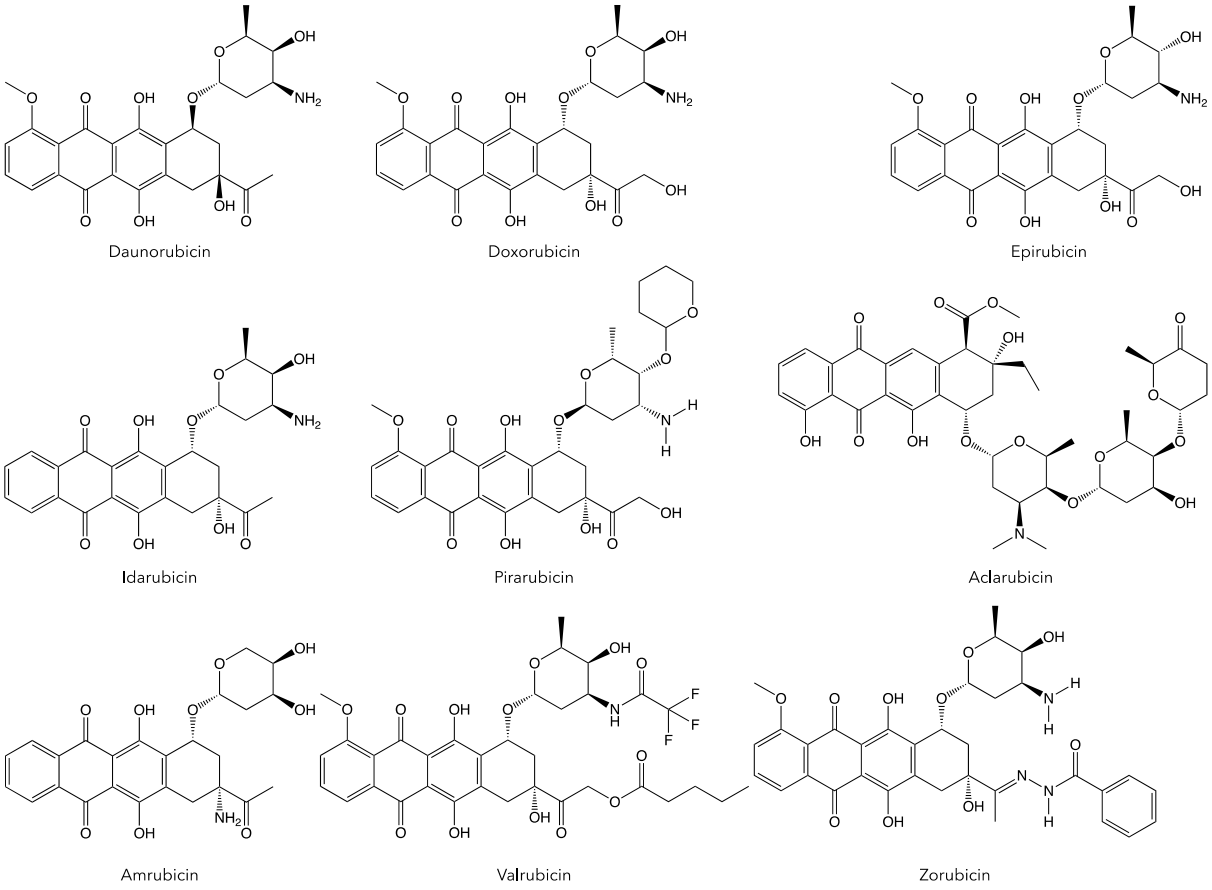

Figure 2.3-12 The chemical structures of antibiotics used to treat cancer

Anthracyclines are a large family of antibiotics used for cancer treatments, including aclarubicin, amrubicin, daunorubicin, doxorubicin, epirubicin, idarubicin, pirarubicin, valrubicin, zorubicin and so on. Some other antibiotics that do not belong to the anthracycline include mitoxantrone, bleomycin and other antibiotics. However, the damaging effects of these drugs heavily hint at their clinical usage in cancer treatment. Additionally, dose limits for a lifetime are determined for these molecules because exceeding a critical limit can permanently damage the heart, which is a major cause of heart disease.

Topoisomerase inhibitors

Topoisomerases are enzymes which participate in the alteration of the supercoiled structure of a DNA molecule by catalysing the breaking and re-joining of the phosphodiester backbone of DNA strands. During the replication and transcription

processes, DNA molecules become overwound ahead of the replication fork. Topoisomerases can bind to the DNA molecules to cut the phosphate backbones of DNA strands and temporally unwinds the DNA molecules. At the end of the processes, the DNA molecules will be resealed again. Since the overall chemical composition and connectivity of the DNA molecules keep the same while the substrates and product of DNA molecules are chemical isomers with different topologies, these isomerase enzymes are named topoisomerases which act on the topology of DNA molecules[92].

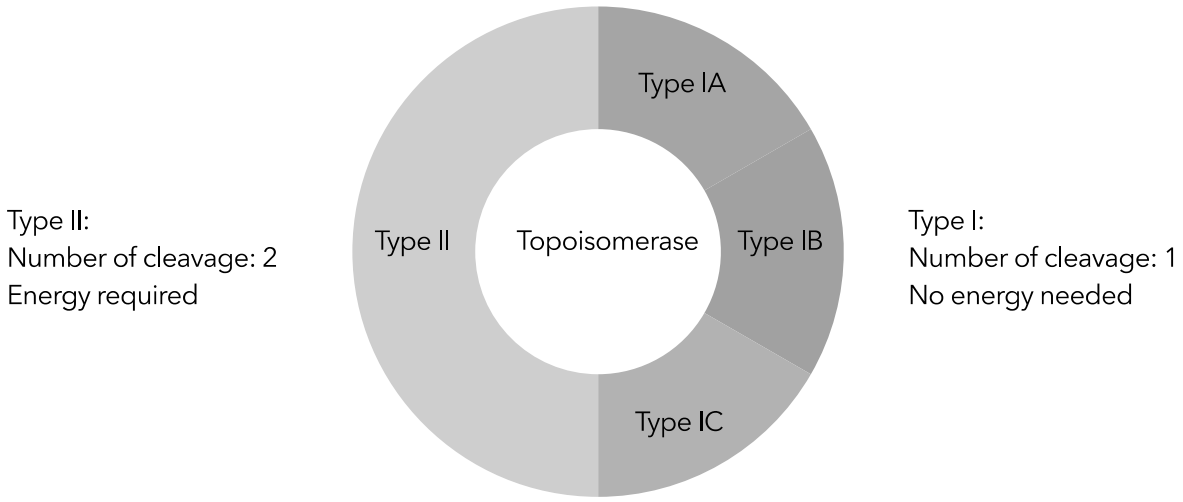

Figure 2.3-13 The types of topoisomerases

Topoisomerases are used to solve the topological problems during DNA replication and transcription. Depending on the number of DNA strands they cut in one round of action, topoisomerases can be classified into two different types with different structures and action mechanisms. Type I topoisomerases only cut one strand of a DNA molecule. After the release of the stress in the double-helix structures, the cut strand will be re-ligated again by the enzymes. Type I topoisomerases can be further subdivided into three subclasses with different structural and mechanistic features, namely IA, IB and IC subfamilies. Additionally, no ATP is required during the action process of type I topoisomerase. Type II topoisomerases cut both strands of a DNA molecule and pass another unbroken DNA helix to through it to reduce the degrees of DNA twist. The cut double strands would be re-ligated again by the enzymes. During the action process, ATP is required. Type II topoisomerases are subdivided into two subclasses with similar structure and mechanisms.

Topoisomerase inhibitors are chemicals that inhibit the actions of topoisomerases. Topoisomerase inhibitors can prevent the re-ligation process, which produces the

breaks of single or double strands of DNA. The breaks of DNA strands would initiate the apoptosis of cells and lead to cell death[93]. According to the types of the topoisomerases they act on, the topoisomerase inhibitors are simply divided into topoisomerase I inhibitors and topoisomerase II inhibitors.

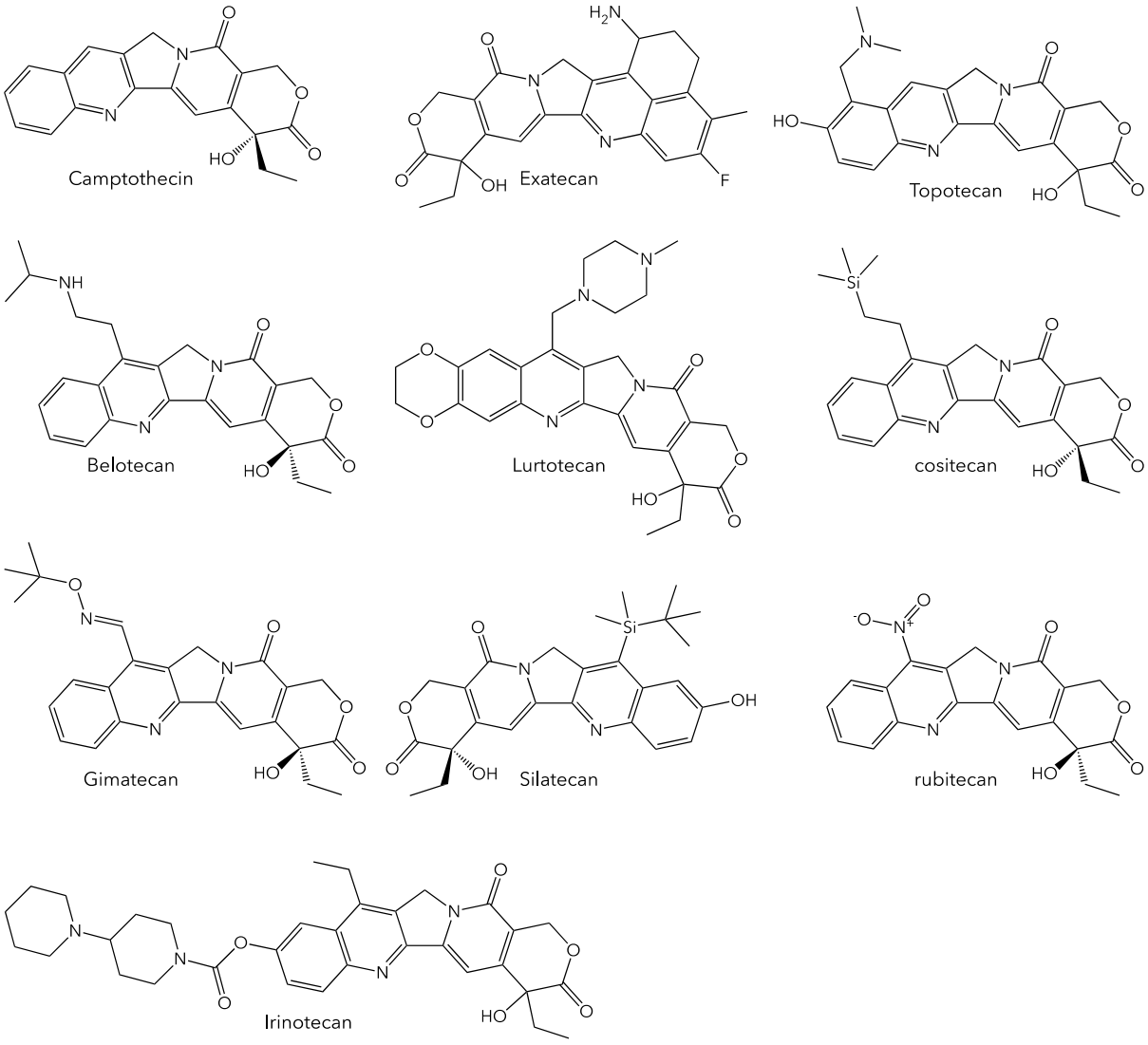

Figure 2.3-14 The chemical structures of representative topoisomerase I inhibitors

Type I topoisomerase inhibitors would stabilise the cleavable complexes of DNA and topoisomerases[94] and produce the breaks of DNA strands, which further induce cell death. The representative examples of type I topoisomerase inhibitors include camptothecin and its derivatives, such as irinotecan, topotecan and belotecan. Some of these small molecules have been approved by FDA to be used for the treatment of various cancers while others are under investigation. For instance, irinotecan hydrochloride has been approved to treat colorectal cancer and pancreatic caners either alone or in combination with other cancers. Topotecan hydrochloride

was approved to treat ovarian cancer, cervical cancer and small cell lung carcinoma in 1996, 2006 and 2007, respectively. However, these camptothecin derivatives used for cancer treatment also exhibit certain clinical problems, such as the dose-limiting side effects of server delayed diarrhoea, the inactivation to a lactone form in blood stream.

Type II topoisomerase inhibitors can be classified into two main categories. One is called the topoisomerase II poisons which act on the complexes of DNA and topoisomerases and the other category is the topoisomerase II inhibitors which interfere with the catalytic turnover. The representative examples of type II topoisomerase inhibitors for eukaryotes include anthracyclines such as doxorubicin, daunorubicin and amrubicin, anthracenediones such as mitoxantrone and pixantrone, and podophylum such as etoposide and teniposide. Some of the topoisomerase poisons would improve the cleavage reactions during DNA replication and transcription while others may block the re-ligation of DNA, disrupting the normal activities of DNA during cell life cycles. The topoisomerase II inhibitors which act on the N-terminal ATPase domain of type II topoisomerases to prevent the enzymes from tinging over include genistein which is an isoflavone[95] and ICRF-193 which locks down the dimerization of the ATPase domain[96].

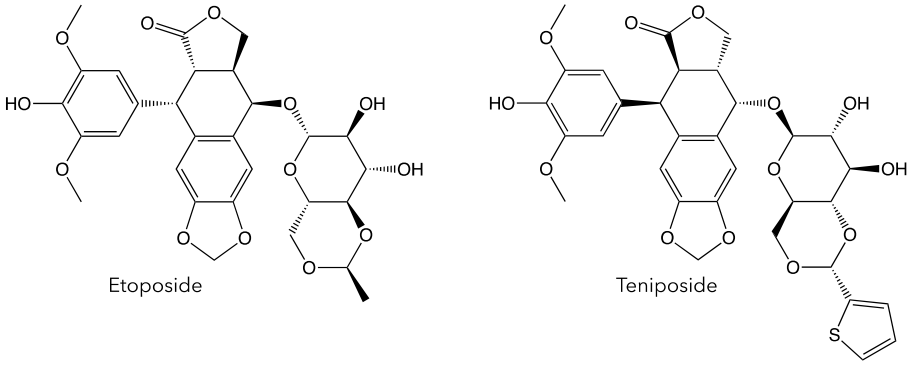

Figure 2.3-15 The chemical structures of representative topoisomerase II inhibitors

Mitotic inhibitors

Mitotic inhibitors are chemical compounds inhibiting the mitosis of cells. These drug molecules interfere with the microtubules which pull the chromosomes apart during cell division. Microtubules are long rope-like proteins made up of tubulin. These proteins are polymerised to separate chromosomes and other components during cell division. The treatment of mitotic inhibitors can prevent cancer cells from continuous mitotic division.

Some of the them work by preventing the microtubules from assembly. The representative example includes griseofulvin[97], colchicine[98] and vinca

alkaloids[99], such as vinblastine used for leukaemia, Hodgkin's lymphoma, non-small cell lung cancer, breast cancer and testicular cancer, vincristine for lymphoma, breast cancer, lung cancer, and acute lymphoblastic leukaemia, vindesine used to treat leukaemia, lymphoma, melanoma, breast cancer and lung cancer, and vinorelbine for the treatment of breast cancer and non-small-cell lung cancer[100-106].

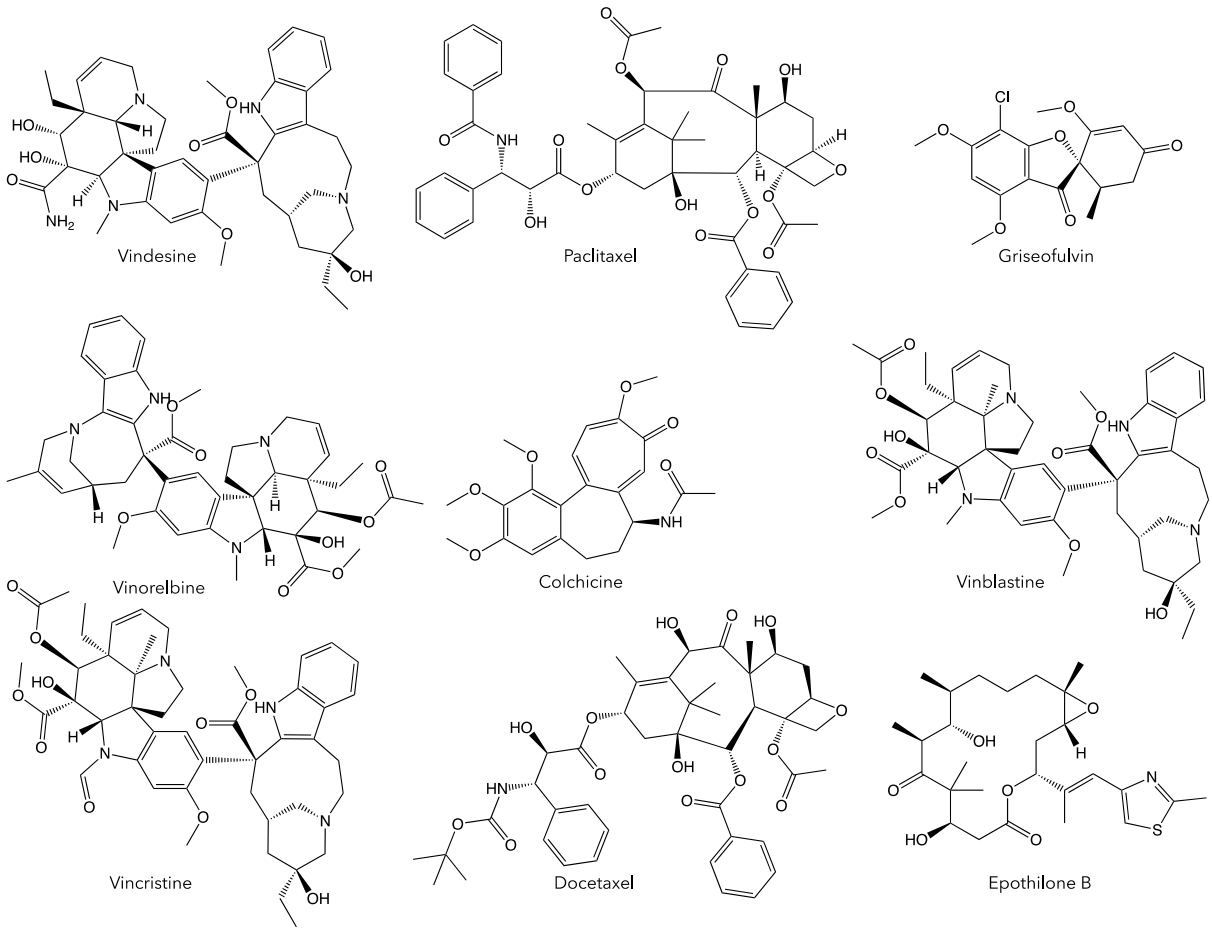

Figure 2.3-16 The chemical structures of representative mitotic inhibitors

Some other mitotic molecules can block the disassembly of microtubules to interrupt the normal cell activities, such as taxanes and epothilones. Taxanes are complex terpenes originally isolated from Pacific yew tree and now are artificially synthesised. The representative examples include docetaxel and paclitaxel, which are used to treat lung cancer, ovarian cancer, breast cancer and other cancers[107].

Corticosteroids

Corticosteroids are a class of hormones used to relieve the adverse effects caused by other therapeutic agents, such as inflammation, swelling, itching, redness and allergic reactions[108]. Corticosteroids resemble the cortisol and show similar biological functions as cortisol which is naturally produced by adrenal glands and takes part in a

wide range of processes happened in the body, such as the metabolism and immune response.

Based on the chemical structures, corticosteroids can be generally divided into four main groups, namely the acetonide type steroids, the hydrocortisone type steroids, Betamethasone type steroids and the ester type steroids. There are more than ten steroids in each group. The chemical structures of common corticosteroids are shown below.

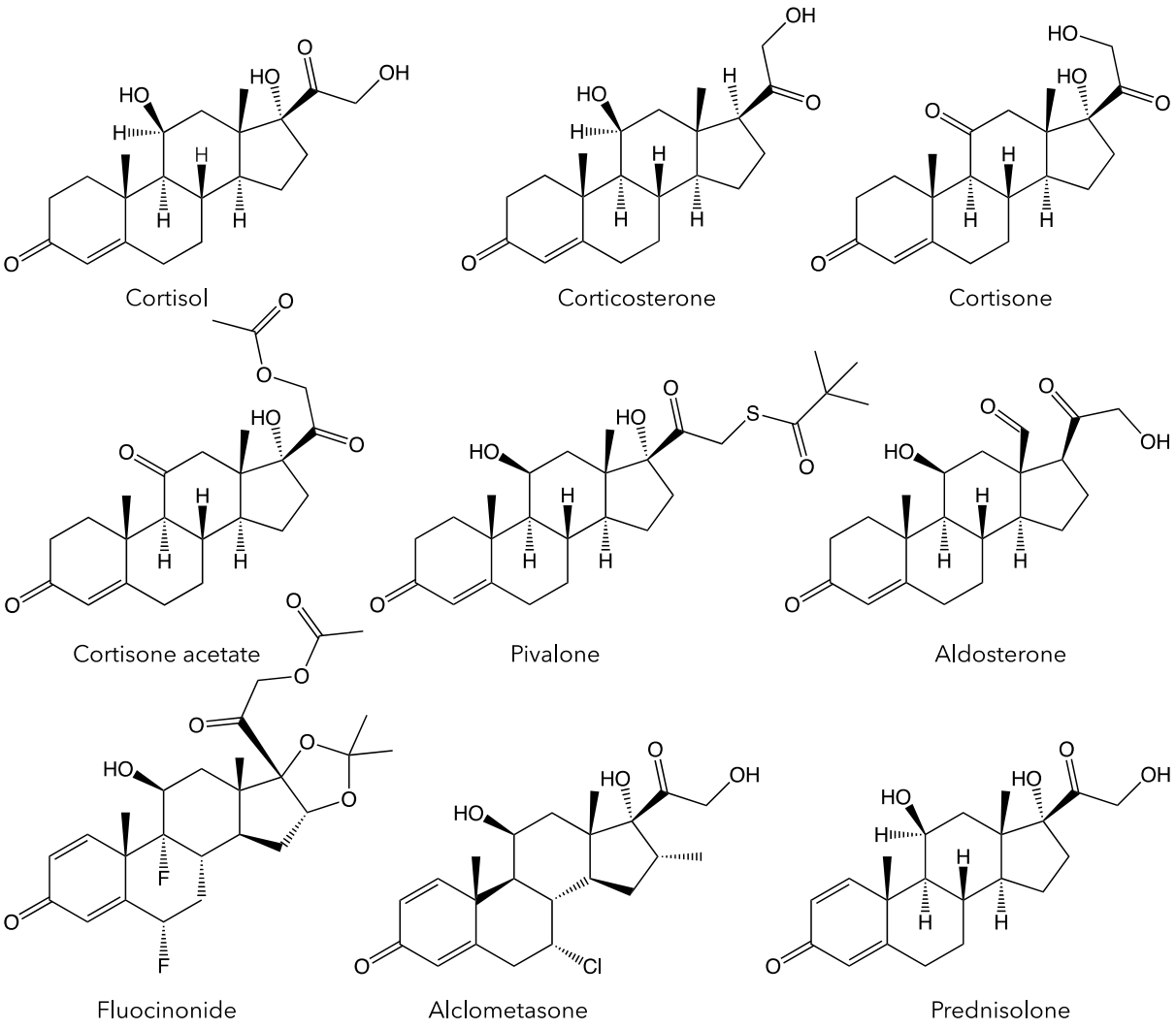

Figure 2.3-17 The chemical structures of common corticosteroids

The synthesised pharmaceutical agents with corticosteroid-like activities are used in lots of conditions. They can be used systemically or locally. Localised corticosteroids aim at a specific part of the body, such as eyes, ears and skin for the treatment of asthma

and hives. While they can be also delivered systemically through the blood circulation to treat conditions like lupus and multiple sclerosis.

However, the use of corticosteroids may cause numerous unwanted side effects, such as severe amoebic colitis[109], steroid psychosis[110], anxiety[111], depression[112], cardiovascular diseases[113], corticosteroid-induced lipodystrophy or "moon face"[114], hyperglycaemia[115], insulin resistance[116], diabetes mellitus[117], steroid-induced osteoporosis[118] and so on. Additionally, according to the "Coopman classification", if someone is allergic to one steroid in a group, typically he/she would be intolerance to all the steroids in this group[119].

2.3.2 Challenges of chemotherapy

Chemotherapy based on small molecular agents has been widely used in clinical for the treatment of various cancers and it is one of the most effective ways to fight against cancers. However, there are also potential risks and challenges associated with this therapeutic strategy. For instance, the intrinsic properties of many anti-cancer small molecules, such as poor water solubility, limited bioavailability and severe adverse effects, significantly hinder their therapeutic efficacy for cancer treatment and limit their clinical usage.

Poor water solubility

Poor water solubility of many drugs remains one of the major obstacles impeding the development of highly potent pharmaceutics and clinical applications because the absorption and bioavailability of these drug molecules would be significantly limited due to the low water solubility[120].

Biopharmaceutics Classification System (BCS) is a classification criterion used to differentiate the drug molecules based on their water solubility and permeability. According to the BCS classification criterion, drug molecules can be divided into four categories with varying degrees of water solubility and permeability.

It has been reported that more than 80% of drug candidates and around 40% of marketed drugs show poor water solubility[1, 2], severely impeding their clinical formulation and translation. For instance, the bioavailability of molecules in class II with high permeability and low water solubility would be heavily limited by their solvation rate while compounds in class IV with both poor solubility and poor permeability possess a poor bioavailability because of their poor absorbability over the intestinal mucosa, such as curcumin[121].

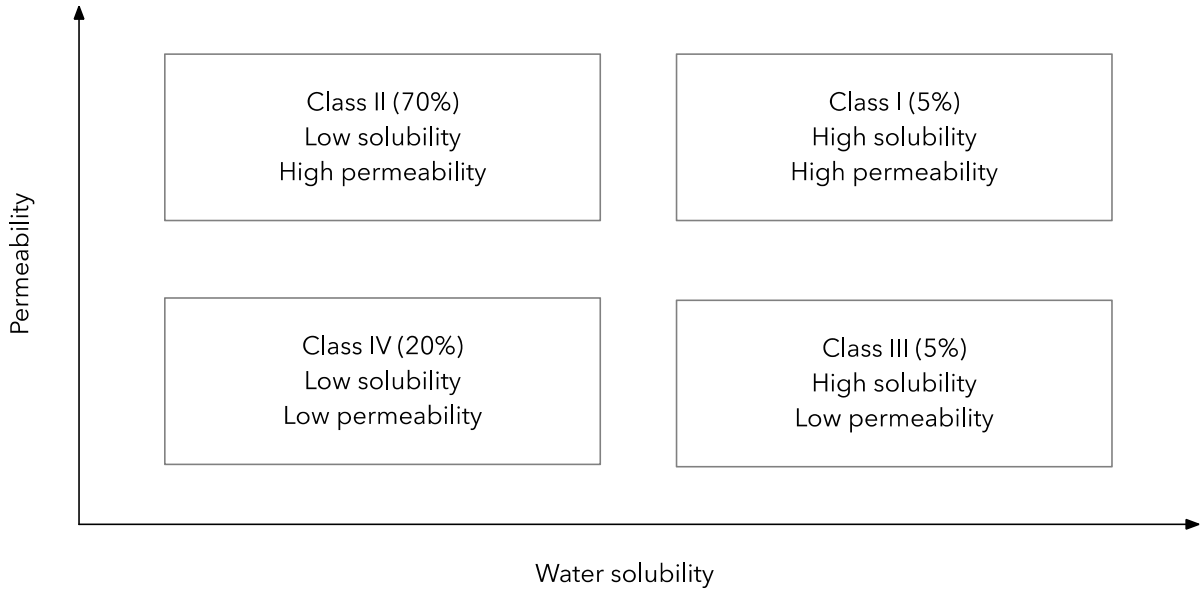

Figure 2.3-18 The biopharmaceutics classification system

Curcumin is a tautomeric molecule existing in both di-keto and keto-enol forms. The conformational equilibrium of curcumin shifts to the enol form, which remains its planar structure[122], in its favourable solvents respect to the solubility[123, 124]. Curcumin is also a weak Bronsted acid and has three pKa values (around 7.8, 8.5 and 9.0) for the dissociation of three acidic protons (*Figure 2.3-19*), namely one active methylene hydrogen of β-diketones and two other phenolic hydrogens[125-127]. In an acidic environment, curcumin mainly exists in the neutral form and exhibits better stability[128]. With the increase of pH, curcumin dissociates to anionic forms, whose stability decrease as well[129].

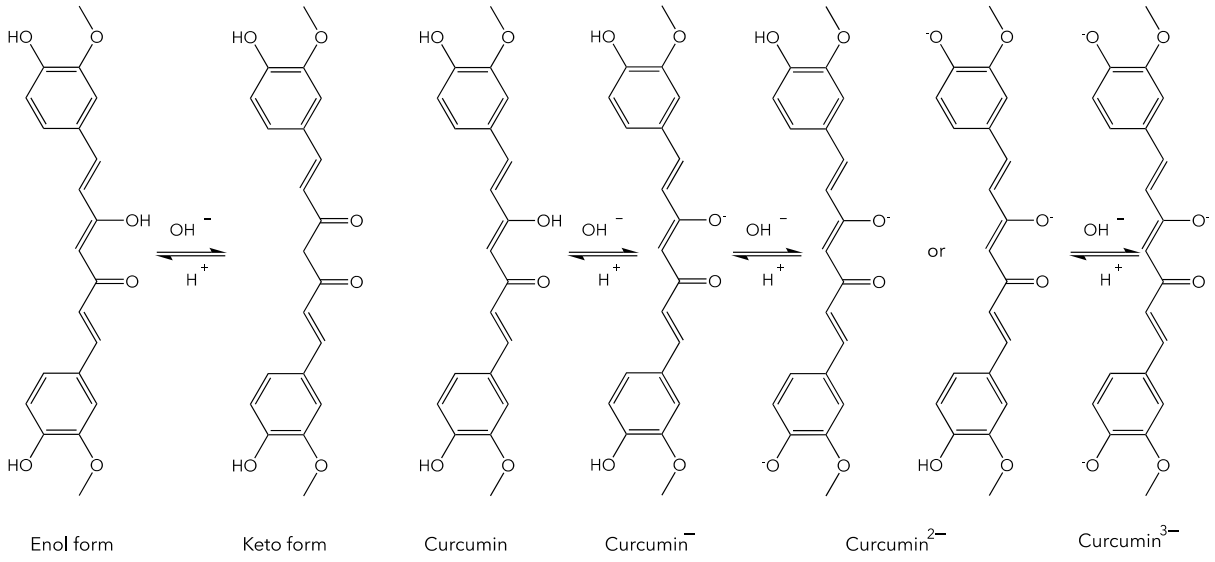

Figure 2.3-19 Keto-enol tautomeric equilibrium and dissociation equilibrium of curcumin

In order to enhance the water solubility of these drug molecules, improve their bioavailability and eventually augment their therapeutic efficacy, several strategies have been employed in the pharmaceutical formulations, such as covalently conjugating with hydrophilic moieties to form prodrugs[130], changing the salt formation of ionisable drug molecules[131] and the utilisation of co-solvents[132]. These strategies have been shown to successfully improve the solubility of drugs. Other nanotechnology-based strategies, such as increasing the ratios of surface area to volume of drug powders, changing the crystalline forms and designing novel materials with various nanostructure which can be used as carriers, have also provided the key driving force for the development of novel pharmaceutics[120].

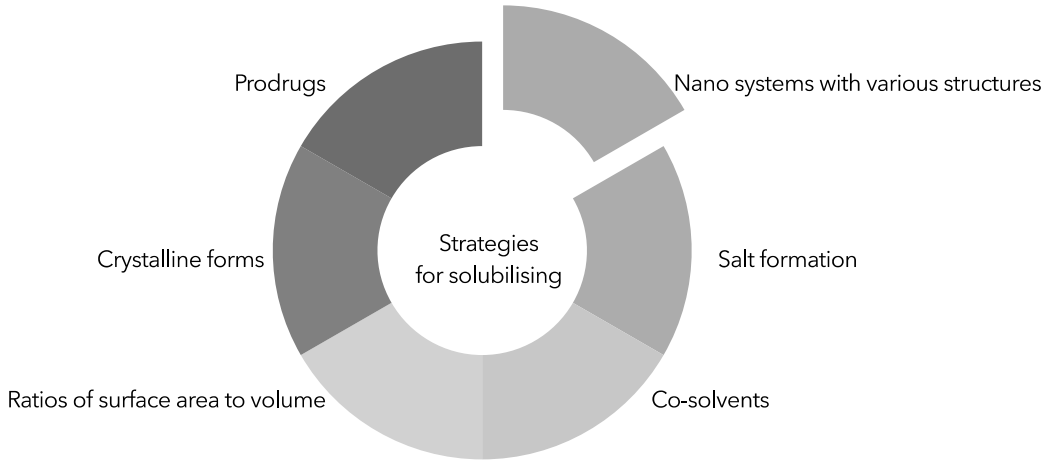

Figure 2.3-20 Strategies to increase drug solubility and bioavailability.

Non-specificity

Another challenge of chemotherapy is the non-specificity (lack of targeting ability) of drug molecules used for cancer treatment. Drug targeting is defined as the ability of drug molecules to selectively accumulate in certain targeted organs or tissues so that the concentration of the drug molecules at the preferred disease sites would be significantly higher than that in non-targeted organs[133], which can dramatically increase the therapeutic efficacy of the drugs. However, most drug molecules used for cancer treatment exhibit no targeting ability and these agents showing multiple targets of action in the body would usually be systemically delivered to the whole body through the blood circulation system, resulting in the decreased therapeutic efficacy at the disease sites as well as the unwanted toxicities to normal tissues[134].

In order to endow these drug molecules with the targeting abilities, various pharmaceutical strategies have been explored. They can be mainly divided into two

categories, namely the active targeting formulations with the utilisation of specific targeting moieties[135] and the passive targeting systems which are based on the physiological features of the body[136] and the modern nanotechnologies[137]. Taking advantages of the physiological properties of tumour tissues, such as the pH values[138], temperatures[139], redox potential[140] and other feathers, the drug molecules can be passively delivered and take effect on the cancer tissues. Moreover, the enhanced permeability and retention (EPR) effect based on modern nanotechnologies also play a pivotal role in the passive targeting delivery systems[141].

Active targeting strategy based on the site-specific ligands has been utilised to selectively deliver the drug molecules to the targeted tissues. The drug formulations decorated with specific ligands would lead to their targeting to selected cells and take effect on the desired sites. The targeting ligands can be broadly divided into several categories, including proteins (antibodies[142] and transferrin[143]), peptides[144], aptamers (nuclear acids[145]), polysaccharides[146] and other small molecules[147] (such as folate[148], phenylboronic acid[149]).

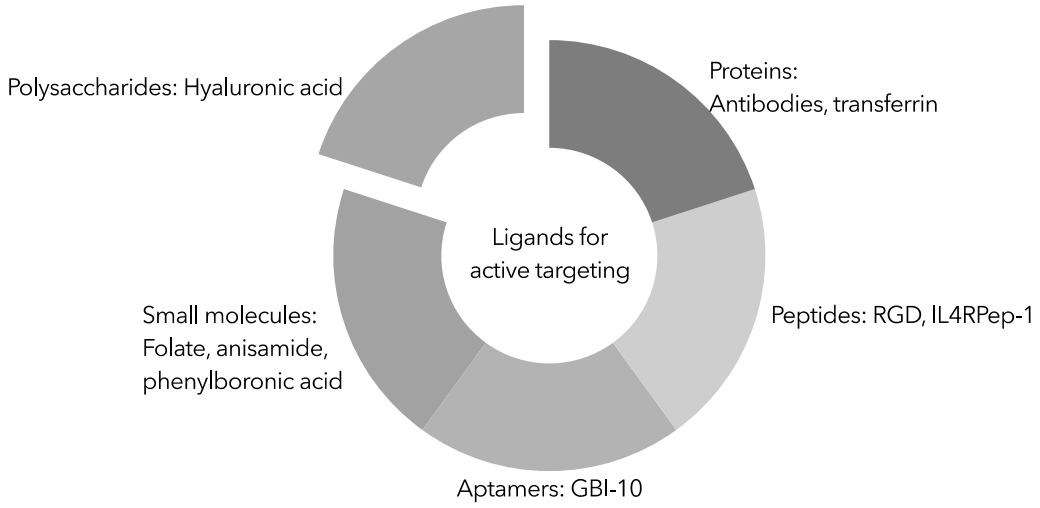

Figure 2.3-21 Typical types of ligands used for active targeting

However, although these strategies have been proposed to improve the specificity of the drug molecules for cancer treatment, there are many challenges in developing these targeted delivery systems. The first one is the uniqueness of each delivery system, which means they must be evaluated separately as new formulations before being considered for clinical applications. Major developmental concerns, such as the physiological stability of these formulations, the large scale manufacturing of sterile preparations and so on, need to be resolved[133].

Side effects

Just like other cancer treatment methods, chemotherapy based on small anti-cancer drug molecules would also cause many unwanted side effects during or after cancer therapy. Due to the non-specificity, the drug molecules travelling throughout the body in the blood stream would also affect the normal activities of healthy cells, such as the hair follicles, blood-forming cells in the bone marrow and so on, which would most likely be damaged to cause some common side effects to the body. Some therapeutic drug molecules may damage the cells in some organs, such as the heart, kidneys, bladder, lungs and nervous system, which would cause the dysfunction of related organs.

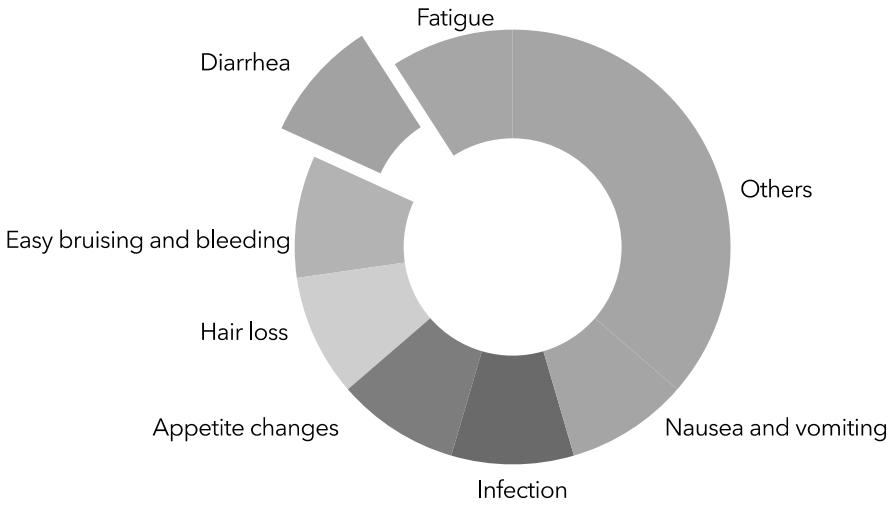

Figure 2.3-22 Common side effects of chemotherapy

For example, irinotecan, which is a derivative of anti-cancer molecule camptothecin, has been used as the first line treatment method for colorectal cancer which is the third most commonly diagnosed malignancy (1.8 million new confirmed cases in 2018) causing the second largest number of cancer –related mortality (0.86 million deaths in 2018). However, this small molecule can cause some common side effects, such as nausea, vomiting, weakness, low blood cell count, infection, loss of hair, poor appetite, fever, chills, loss of weight, diarrhoea and so on[150]. Except for these common side effects, there are also some less common side effects including cough, headache, shortness of breath, skin rash, dehydration, sores of mouth and swelling. Some of the side effects can cause discomfort but are not fatal while some may cause severe problem, such as the life-threatening diarrhoea[151].

Usually these side effects exhibit individual differentiation. The severity and duration of certain side effects on patients vary greatly from person to person. For

instance, some side effects would disappear fairly quickly on some patients while may last for months or even years on some other patients. Therefore, some other drugs may be utilised together with the chemotherapeutic agents to reduce the severity of some side effects and to improve the life quality of cancer patients. Besides, based on these realities, precision medication or personalised therapy has been proposed as a better strategy for the treatment of diseases[152].

Drug resistance

Another huge challenge for cancer treatment by using chemotherapeutic agents is the drug resistance. Drug resistance can be defined as the decrease in the efficacy and potency of a drug to produce therapeutic merits[153], which is one of the major impediments to the survival of patients with advanced stage cancers[154]. Of particular note, the tumour tissues in some cancer types, such as renal cancer, carcinoma cancer and malignant melanoma, intrinsically show resistance to chemotherapeutic agents without prior exposure to anti-cancer drugs, leading to a naturally poor chemotherapeutic response[155]. The intrinsic drug resistance can also be attributed to multiple factors which alter the interaction between the drug molecules and their targets on tumour cells. These factors include the breakdown of drugs, the decreased expression of drug targets, the altered drug transport across the cell membrane and the decreased interaction efficiency between the chemotherapeutic agents and their molecular targets[156].

The intrinsic drug resistance of cancer cells is largely relied on the activities of various membrane proteins which either directly pump out the drug molecules to reduce the accumulation of drug molecules in cells or adjusting the net accumulation of drugs via some physiological processes[157]. Two major classes of protein families associated with drug resistance have been identified. First is the ATP-binding cassette (ABC) transporter superfamily which directly pumps out the hydrophobic chemotherapeutic agents from cancer cells, subsequently decreasing the net accumulation of drug molecules and reducing their therapeutic efficacy. Another big class of membrane proteins involved in the drug resistance is the solute carrier transporters which would enhance the drug resistance by interrupting the uptake of hydrophilic drug molecules by cancer cells[157].

Until now, about 50 kinds of ABC transporters have been identified in human genome which can actively transport various chemical compounds out of cancer cells. These ABC transporters can be classified into seven families according to the classification by the Human Genome Organisation[158] and exhibit different functions in the body. In the ABC superfamily, some transporters have been widely

studied, such as the well-known ATP-dependent efflux pump P-glycoprotein (Pgp or ABCB1) whose overexpression would result in the multiple drug resistance in several kinds of cancers[159]. ABCG2 is another member of the ABC superfamily, which is responsible for transporting the lipids, drug substrates, bile, steroids and so on. This protein is also referred to as the breast cancer resistant protein (BCRP) which is overexpressed in human-derived breast cancer cells and may play a role in multiple drug resistance to chemotherapeutic agents including mitoxantrone and the derivatives of camptothecin.

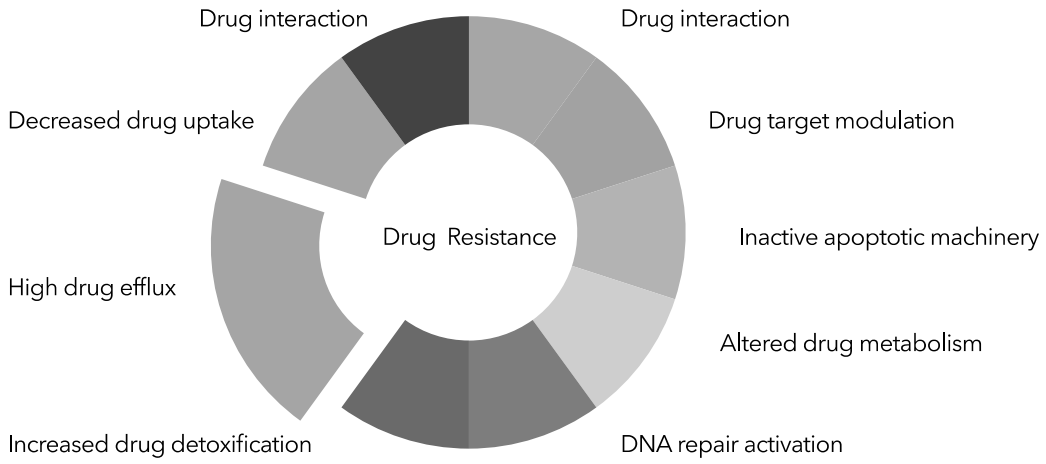

Figure 2.3-23 Mechanisms of multiple drug resistance

While in some other cases, poor therapeutic response would usually be expected after the initially positive cancer treatments because of the development of acquired drug resistance to a certain class of chemotherapeutic agents[153]. The acquired drug resistance can be resulted from the genetic or environmental factors which facilitate the proliferation of drug-resistant cancer cells and the mutation of certain enzymes associated with relevant metabolic pathways[156]. The relatively poor stability of gene materials, such as the aneuploidy, deletions, point mutations and gene amplifications, results in the intra-tumour heterogeneity, the distant metastatic lesions, caner relapse after treatment failure[160].

3. MATERIALS FOR DRUG DELIVERY

Drug carriers refer to any substances used to ameliorate the delivery and the effectiveness of drugs[161]. Materials can be mainly clarified as natural and synthetics. Many different materials have been utilised in various drug delivery systems to modify various physiochemical properties of therapeutic agents.

3.1 Natural Materials

Natural materials are those directly obtained from natural resources. Discovery of suitable materials for drug delivery from the nature has generated a great deal of interest because of the large abundance of natural resources. Natural polymers, inorganic materials and other materials based on cells, bacteria and viruses have been widely studied.

3.1.1 Natural polysaccharides

Polysaccharides are one type of natural polymers consisting of monosaccharide units which are linked together through glycosidic bonds[162]. Because of the relatively good bio-safety of natural polysaccharides, various natural polysaccharides have been employed to produce nanoparticles with different architectures to explore their use in drug delivery as well as to investigate more pharmaceutical applications.

Polysaccharides are those containing more than ten monosaccharide units while oligosaccharides contain three to ten monosaccharide units. Polysaccharides can be hydrolysed (reacted with water) by using amylase enzymes as catalysts to produce monosaccharides and/or oligosaccharides. Depending on the number and types of repeating units, polysaccharides usually show a big difference in molecular weights and range in structure from linear to highly branched. They also exhibit different bio-functionalities, such as structure construction, energy storage in living systems, and so on. Starch and glycogen are two kinds of storage polysaccharides used in plants and animals, respectively. While cellulose and chitin are used for the construction of biological structures.

Natural polysaccharides are usually composed of simple carbohydrates, which generally math the formula of $C_x(H_2O)_y$. They can be obtained from various natural resources, such as plants, algae, bacteria, animals, and so on. They are usually heterogeneous because of the slight difference of the repeated units. Polysaccharides usually have distinct physiochemical properties compared to their building monosaccharide blocks, such as the phase states. Polysaccharides may be in an amorphous state and show extremely limited solubility in water[163]. Based on the

structures of the constructing monosaccharides in a polysaccharide are the same or not, polysaccharides can be classified into homoglycans or heteroglycans, respectively[164].

Polysaccharides possess many unique physiochemical properties according to their composition and architecture, such as low osmotic effect, good water solubility and gelation[165]. Because of the various derivable groups on molecular chains, polysaccharides can be easily modified via chemical and biochemical reactions, leading to many kinds of polysaccharide derivatives[166]. As a structurally diverse class of macromolecules, polysaccharides play diverse and pivotal roles in many biological processes, such as energy storage, signal recognition, cell communication, fertilization, pathogenesis prevention, blood clotting and system development, thus showing good biocompatibility and biodegradability[162]. Many polysaccharides themselves are also bioactive, showing many therapeutic efficacy, such as anti-cancer activities and antibacterial effects [162]. Besides, they have also been applied as carriers to delivery various therapeutic agents.

Starch

Starch is a glucose polymer, inside which the glucose units are linked together by alpha-linkages. Starch is a mixture of amylose and amylopectin (*Figure 3.1-1*). Generally, amylose is a linear polymer consisting of several hundred glucose units and amylopectin is a branched polymer with thousands of glucose units. Both constituents can be digested *via* breaking the alpha-linkages by humans and some animals. Starch molecules remain semi-crystalline state in plants and the sizes of starch granules vary largely from different plant species.

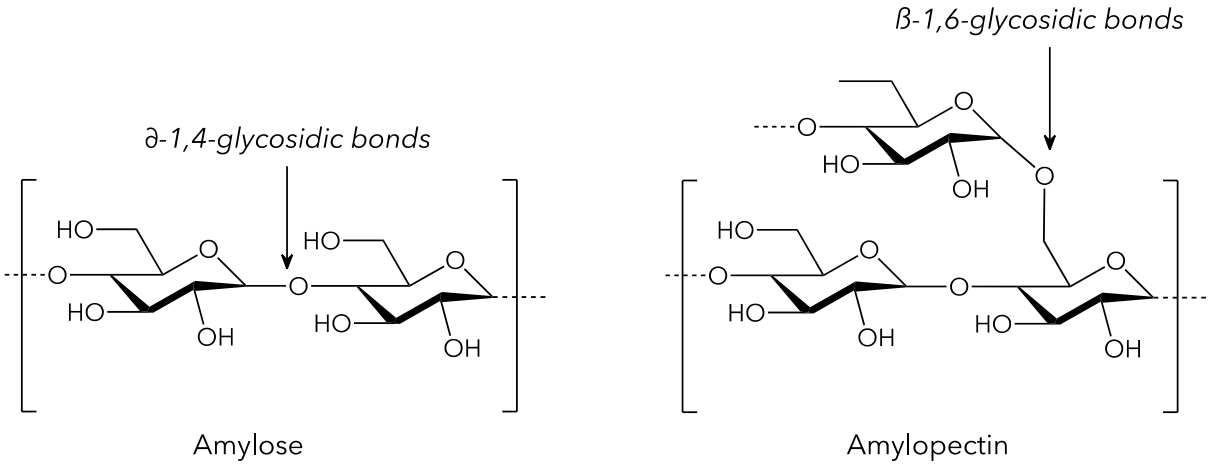

Figure 3.1-1 Chemical structures of two constituents of starch.

Generally, starch is insoluble in water. The starch-based materials are specially tailored for the targeted delivery and controlled release of various anticancer drugs. Starch was covalently modified with biotin or glycyrrhetinic acid by forming eaters between molecules, which was then self-assembled into nanoparticles for the delivery of doxorubicin[167]. The obtained drug-loaded nanoparticles showed a controlled release profile according to the environmental acidity. Starch was also coupled with doxorubicin *via* carboxymethyl groups to modify the intrinsic properties of drug molecules, which was then coated on superparamagnetic iron oxide nanoparticles as potential antitumor cargo[168]. Starch was also used to improve the solubility and stability of curcumin in water by forming nano micelles, which exhibited stronger antioxidant and anticancer activity than the free drug[169].

Glycogen

Glycogen is another structurally similar glucose polymer with denser branches. It is analogous to starch and stored in liver and muscles. Only the glycogen stored in liver can be used by other organs. Glycogen can be quickly metabolised to meet the sudden need for glucose by animals[170].

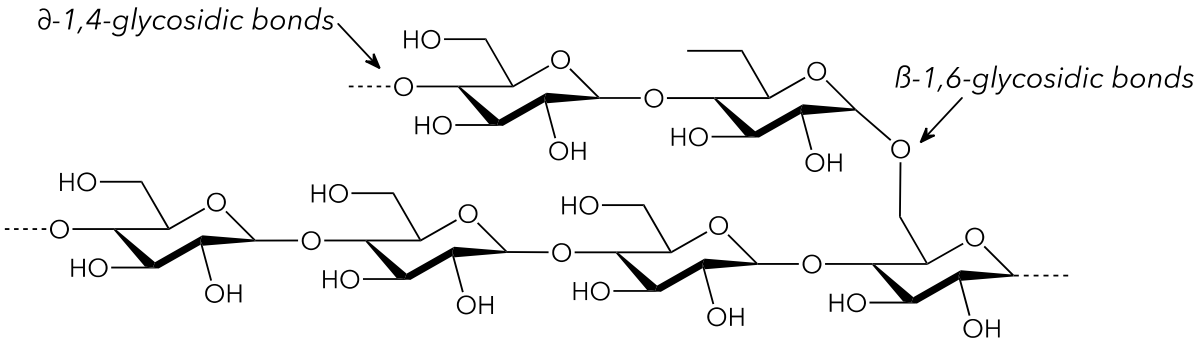

Figure 3.1-2 Chemical structure of glycogen

Glycogen is insoluble in water and has been utilised as carriers to deliver various drugs. Glycogen was covalently linked to anti-cancer drug doxorubicin *via* schiff-base and decorated with the beta-galactose for the liver cancer cell targeting. The obtained nano-system exhibited a pH-dependent drug release and enhanced drug accumulation at tumour sites[171]. Glycogen was also used as cores of nanoparticles to deliver doxorubicin after being decorated with other functional groups, such as the targeting RGD peptides[172]. The prepared nanoparticles exhibited augmented chemophotothermal therapeutic effects and reduced systemic toxicity, which significantly inhibited the tumour growth.

Cellulose

Cellulose is a natural polysaccharide consisting of a linear chain of hundreds to thousands linked D-glucose. Cellulose is used as the primary structural component of cell walls of green plants, algae, and some oomycetes. Therefore, cellulose is one of the most abundant organic polymers on earth.

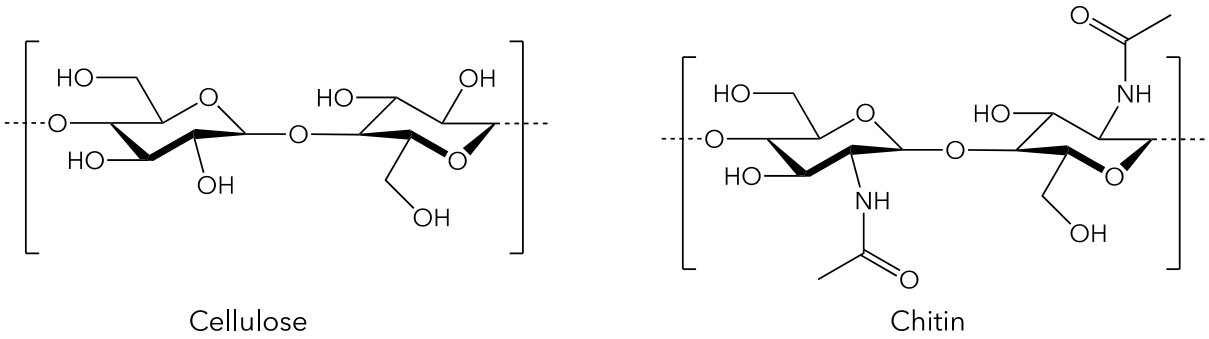

Figure 3.1-3 Chemical structures of cellulose and chitin

Cellulose is odourless, tasteless, water soluble, and non-digestible, which has been used as the component of hydrophilic bulking agents. Compared to starch, cellulose behaves more crystalline, which needs a temperature of 320°C and 25 MPa to become amorphous in water[173]. Depending on the chain length, the properties of cellulose vary largely. For instance, cellodextrins with very small chain length, which are broken down from cellulose, exhibit excellent solubility in water and organic solvent.

Cellulose has widely used in our daily life duo to its ideal physiochemical properties. Cellulose is the major constituent of paper products, textiles, pharmaceutics, and many other products. Mirocrystalline celluloses (E460i) and powdered cellulose (E460ii) has been utilised as the inactive fillers in drug tablets. While many other cellulose derivatives, such as E numbers from E461 to E469, are used as emulsifiers, thickeners, and stabilisers. Cellulose has also been used to construct different carriers for drug delivery. A novel pH-sensitive hydrogel based on cellulose, graphene and chitosan was constructed *via* a cross-linking process, which was used for the co-delivery of doxorubicin and curcumin to improve their water solubility and the drug stability under physiological conditions[174]. Another hydrogel based on cellulose and polyvinyl alcohol was synthesised, which was used to deliver curcumin for accelerating the full-thickness skin wound healing.

Chitin

Chitin is a natural polymer existing as a structural component in many animals to support structure and provide strength. Chemically, the structure of chitin is close to

cellulose with a long linear chain of glucose derivatives containing nitrogen (*Figure 3.1-3*). The introduction of acetyl amine provides the chitin-polymers increased strength compared those based on cellulose.

Chitin has been widely used in different fields, such as agriculture, industry, and so on. Chitin has been used to induce the defence mechanisms of plants to control the plant diseases[175]. It also shows great potential for use as a soil conditioner to enhance the soil fertility and plant resilience[176]. In industry, the chemically modified chitin has been used in food processing as additive to improve the stability of food emulsion[177]. Chitin is also used in pharmaceutics. Researchers designed a pH/ROS sensitive nanoparticle system by using hollow mesoporous silica as cores and carboxymethyl chitin as gates for the targeted co-delivery of doxorubicin and α-tocopherol succinate for cancer therapy[178]. The drug loading capacities of doxorubicin and α-tocopherol succinate were 4.06% and 7.64%, respectively. The fabricated drug-loading nanoparticles had an average at about 260 nm and showed good biocompatibility. The enhanced anti-cancer efficacy of this nanoparticle system was approved by both *in vitro* and *in vivo* studies.

Pectins

Pectins are a class of complex polysaccharides containing 1,4-linked α-D-galactosyl uronic acid residues. Fruits, such as apples, pears, guavas, quince, plums, gooseberries and oranges, are rich in pectin[179]. The main raw materials for the production of pectin are dried citrus peels[180] and apple pomace[181]. Pectin is usually extracted by adding hot dilute acid (pH 1.5-3.5) into the raw materials. The extract is then filtered and concentrated in a vacuum before being precipitated by ethanol.

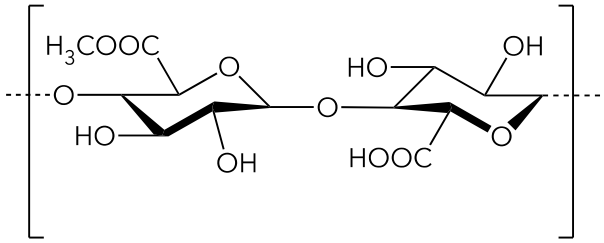

Figure 3.1-4 Chemical structure of pectin

Generally, pectin and its monovalent salts are soluble in pure water, and the dry pectin powders trend to hydrate rapidly in water[182]. Pectin is mainly used in food as a gelling agent. Adding pectin into jellies would result in a good gel structure. In medical, pectin can increase the viscosity of stool so that it is used to prevent diarrhoea. It is also used as a demulcent in throat lozenges[179]. In pharmaceutics, pectin was used to prepare a doxorubicin loaded nanoparticle encapsulated with a liposome-like

membrane. This nano systems exhibited enhanced cellular uptake, augmented anti-cancer efficacy, and significantly reduced systemic toxicity on tumour-bearing mice. In another research, the water soluble pectin was covalently connected to the hydrophobic doxorubicin molecules *via* disulphide bonds to form an amphiphilic prodrug, which could further self-assemble into nano-scale particles. These prodrugs exhibited anti-cancer efficacy on mouse colon cancer cells, which might be suitable for building platforms for colorectal cancer[183].

Many polysaccharides have been employed to construct nanostructures as carriers for the delivery of various drugs. Drug molecules may also be covalently cross-linked with the large amounts of hydroxide groups on polysaccharides *via* some cleavable space linkers, such as glutaraldehyde, to form some polymer conjugates. Unfortunately, the toxicity of glutaraldehyde on cell viability limits its utility in the field of drug delivery. Some other cross-linkers are developed to ameliorate the biocompatibility, such as the water-soluble condensative carbodiimide. The condensation reaction was performed between the carboxylic groups of natural acids and the pendant amino groups of chitosan, through which biodegradable chitosan nanoparticles were obtained. This method allows the formation of polycations, polyanions, and polyampholyte nanoparticles[166].

3.1.2 Natural inorganic materials

Many natural inorganic materials are also studied by researchers to explore their potential applications in pharmaceutics. Inorganic materials, such as gold, iron oxide and silica, have been utilised for the construction of different functional nanoparticles.

Gold nanoparticles

Gold nanoparticles have a broad spectrum of application fields, such as medicine, food industry, water purification and so on[184]. In pharmaceutics, they are applied to drug delivery, bio-imaging and antimicrobials. They are considered as biocompatible materials except that the conventional reduction methods could leave some toxic chemicals on their surface, which to some extent compromise their usages[185]. Gold nanoparticles intrinsically exhibit dramatically antibacterial effects on some pathogens[186, 187]. Gold nanoparticles are used for diagnostic imaging based on their unique plasmonic and magnetic properties, which produce imaging contrast by computed tomography (CT), magnetic resonance (MR) or positron emission tomography (PET)[188].

Gold nanoparticles are also utilised as carriers for drug delivery in pharmaceutics. Gold nanoparticles were coated with hyaluronic acid for the treatment of

neovascularization processes in the eye[189]. In this system, the surface functionalisation significantly enhances the particle stability, the abilities of nanoparticles to cross the eye barriers and their biodistribution in retina. These functionalised nanoparticles dramatically inhibited the advanced glycated end products and neovascularization. Gold nanoparticles were also used for gene delivery due to their cationic surface charges which can be electrostatically connected with negatively charged nucleic acids [190]. Other functionalisation methods, such as PEGylation[191] and peptide coating[192], are also used to modify gold nanoparticles for specific purposes.

Silver nanoparticles

Silver nanoparticles are one of the most commercialised particle products, which shows excellent physiochemical properties, such as the good antibacterial effect and limited toxicity to human cells[193, 194]. They are widely used in many fields, such as textiles, cosmetics and water purification systems. In addition to the effects on microbial, silver nanoparticles also possess many other activities, such as antioxidant, antiviral and anticancer properties. Compared to vitamin C, silver nanoparticles exhibited greater antioxidant effect[193]. Silver nanoparticles are also used as an antiviral agent to treat African swine fever virus. In this study, the microbial contamination in the pig house was dramatically reduced after spraying the silver nanoparticle solution, which can be used to prevent the transmission of the African swine fever virus.

Silver nanoparticles were also functionalised as drug carriers for various applications. Silver nanoparticles, for instance, were coated with poly-dopamine for the effective treatment of acute myeloid leukaemia, which exhibited similar *in vitro* toxicity of doxorubicin against Murine C1498 cells[195]. Silver nanoparticles were also used to delivery drug molecules *via* coating chitosan as a reducing and stabilizing agent. The formed spherical nanoparticles were encapsulated with doxorubicin and was used for the effective treatment of human breast cancer[196].

Despite of such advantages, the successfully use of inorganic nanoparticles in clinical is limited because of their undesirable toxicity limitation[197]. Besides, their positively charged surfaces may bind to negatively charged proteins to form aggregates after injection. Even though PEGylation prevent them from forming aggregates, low excretion of gold nanoparticles is observed[198], which still hinders their clinical applications. In addition, inorganic nanoparticles usually show limited drug loading capacities[199].

3.2 Synthetic Materials

Synthetic polymers are made by human beings. To fulfil the various requirements of pharmaceutical researches and applications, lots of polymers with different properties have been synthesised and investigated. Some polymers are still under early research stages and some have been approved by the Food and Drug Administration (FDA) in United States for clinical use.

3.2.1 Synthetic polyethers

Polyether generally refers to polymers that contain the ether group in their backbone. Several polyethers have been approved by the FDA for clinical uses, such as the polyethylene glycol (PEG), polypropylene glycol (PPG) and polyglycerol (PG).

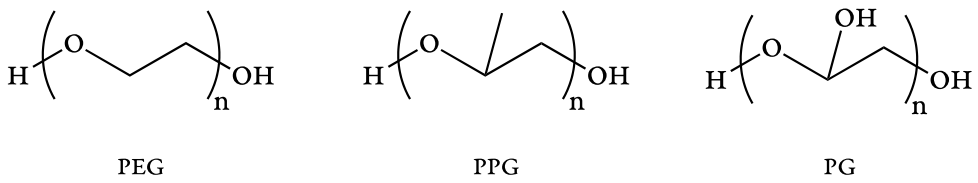

Figure 3.2-1 Chemical structures of several polyethers

Polyethylene glycol (PEG)

Polyethylene glycol (PEG) is a synthetic polymer which was first isolated by A. V. Lourenço and Charles Adolphe Wurtz separately in 1859[200]. Generally, PEG can be synthesised by the interaction of ethylene oxide with water, ethylene glycol, or ethylene glycol oligomers with the help of various catalysts, such as cationic or anionic catalysts. Ethylene glycol and its oligomers are usually preferable because they allow the creation of polymers with narrow distribution of molecular weights. Besides, it is easy to control the length of PEG chains by simply adjusting the ratios of the reactants.

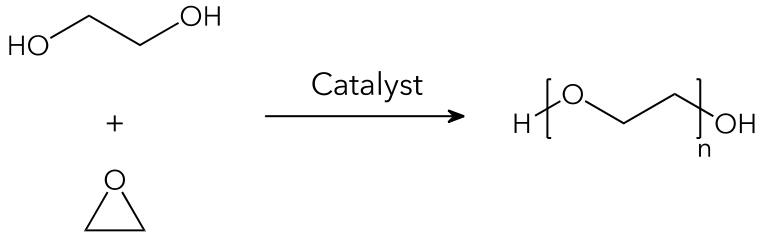

Figure 3.2-2 Synthesis of PEG

Depending on the types of catalysts used for initiating the polymerisation, the mechanism can be cationic or anionic. The preferable polymerisation is anionic which can be used to synthesise PEG with a low polydispersity. Besides, the polymerisation of ethylene oxide is an exothermic process, which would runaway the reaction if the reactants are overheated or contaminated. The PEG with high molecular weights (also known as polyethylene oxide, PEO) is usually synthesised by a suspension polymerisation method, which is a radical polymerisation procedure. During this process, the monomer or mixture of monomers are mixed mechanically in a liquid phase to form polymer spheres in solution. Catalysts like magnesium-, aluminium-, or calcium-organoelement compounds are used to initiate the polymerisation process. While the chelating additives, such as dimethylglyoxime, are used to prevent the coagulation of polymer chains from solution.

PEG has been widely used in various pharmaceutical researches and applications for their excellent water solubility, lack of ions, non-toxicity and good biocompatibility. It has been approved by the FDA for different applications in foods, cosmetics and pharmaceuticals[201]. In the medical field, for instance, PEG has been utilised as the matrix of several laxatives, which can be further used to irrigate the whole bowl before surgery or colonoscopy. One significant modified property of polymers decorated with PEG (PEGylation) is their improved water solubility. PEG is used as the hydrophilic block of amphiphilic block copolymers to deliver many hydrophobic drug molecules for the therapeutic effects, which would dramatically improve their bio-availability. Another advantage of PEG is their stealth-effect[202, 203], which protect themselves from being rapidly cleared in the body, leading to an enhanced *in vivo* stability and significantly elongated blood circulation times[203].

However, the accumulate of PEG within certain organs increases with the increase of their molar mass[204], causing *in vivo* toxicity. Another problem of PEG is that it may activate the compliment C and provoke the immune system, leading to the hypersensitive reactions and, consequently, to an anaphylactic shock[205].

Polypropylene glycol (PPG)

Polypropylene glycol (PPG) or polypropylene oxide is the polymer synthesised from propylene glycol. Polypropylene glycol is usually mentioned for polymers with low to medium molar mass and their ending groups (hydroxyl groups) still play a functional role, which would affect their properties. While polypropylene oxide is usually for polymers with high molar mass whose end-groups no longer affect the properties of these polymers.

PPG is usually synthesised by a ring-opening polymerisation of propylene oxide. The polymerisation process is usually initiated by a base catalyst from an alcohol. When ethylene glycol, or water is used as the initiator of the polymerisation, a linear polymer is usually obtained. Polymers with multiple branches can also be synthesised by using initiators like glycerine, sorbitol, or pentaerythritol.

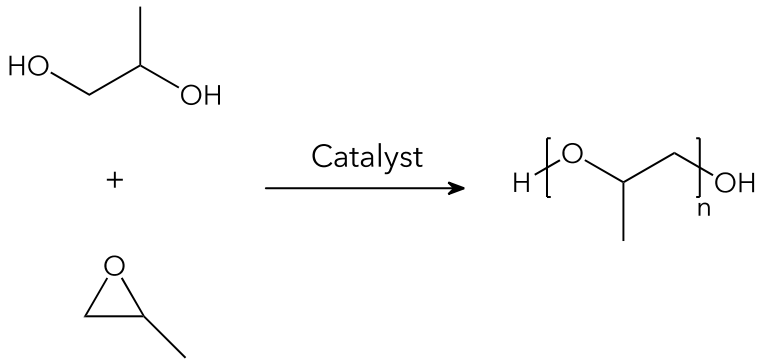

Figure 3.2-3 Synthesis of polypropylene glycol

PPG also possesses good biocompatibility whereas its water solubility decreases considerably compared to PEG. At room temperature, polypropylene is a liquid and its solubility in water decreases rapidly as its molar mass increases. However, the toxicity of polypropylene is less than PEG, which are used in many biotechnological productions. PPG, for instance, is used as a rheology modifier in many formulations for polyurethanes. PPG is also employed as a surfactant, wetting agent, or dispersant in leather finishing. The triblock copolymers PEG-b-PPG-b-PEG with various molecular weights (named poloxamers) are proved by the FDA for pharmaceutical applications and known by their trade names Pluronic®. Because of their amphiphilic property, poloxamers can self-assembly into polymeric micelles in aqueous solution and encapsulate various poor water-soluble drug molecules inside their hydrophobic cores, attracting considerable interests from pharmaceutical researchers.

Polyglycerol (PG)

Polyglycerol is a polyol formed by dehydration between the hydroxyl groups of glycerol molecules. There are three hydroxyl groups in glycerol molecules and all the hydroxyl groups are reactive. Depending on the reactive sites and the different numbers took part in the reaction, polyglycerol can be linear, cyclic, or branched.

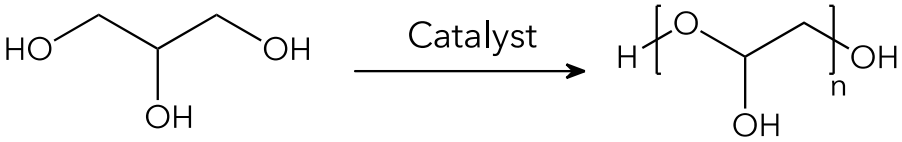

Figure 3.2-4 Synthesis of polyglycerol

PG is usually used as an alternative of PEG. Compared to PEG, the difference of PG is the presence of hydroxyl groups at their backbone, which can be used to covalently introduce other moieties and offer more functionalities[206]. Besides, polymers connected with PG also leads to an elongated circulation time.

3.2.2 Synthetic polyesters

Polyester is a class of polymers made of monomers which are bonded together by ester bonds[207]. Ester bonds (-COO-) are a kind of covalent bonds formed between a carboxylic group (-COOH) and an alcohol group (-OH).

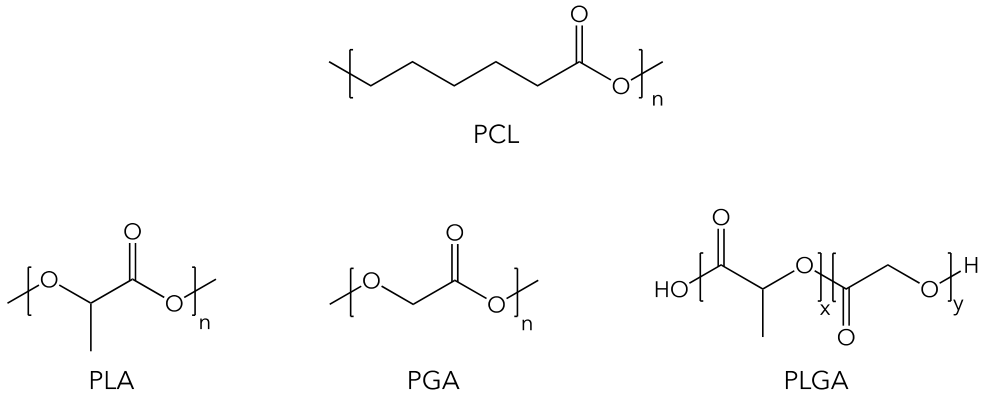

Figure 3.2-5 Chemical structures of PCL, PLA, PGA and PLGA.

These polymers are mostly hydrophobic. Some of the synthetic polyesters show good biodegradability, which have been approved to be safely used in the human body by the FDA. For instance, polylactic acid (PLA), poly glycolic acid (PGA) and the copolymer polylactic-co-glycolic acid (PLGA) are hydrophobic aliphatic polyesters which have been approved by the FDA for various applications, such as drug carriers in in pharmaceutical industry. Their excellent biocompatibility, biodegradability and mechanical strength make them powerful tools for *in vivo* applications. They are usually covalently connected with hydrophilic moieties to form amphiphilic polymers which are then utilised to deliver various pool water-soluble drug molecules by forming micelles.

Polycaprolactone (PCL)

PCL is one of the earliest synthesised polyesters. It is a nontoxic polymer exhibiting good biodegradability. PCL is synthesised by ring-opening polymerization of ε-caprolactone with the help of a catalyst such as stannous octanoate. This polymer has a relatively low melting point at around 60°C and its glass transition point stays at about -60°C[208]. PCL is often used as an additive for resins to modify the processing characters and also mixed with other polymers, such as starch, to improve the biodegradability.

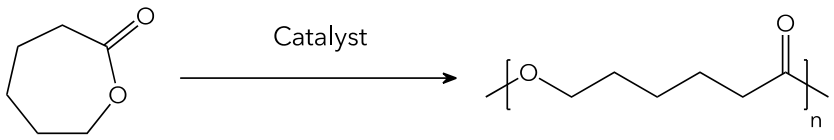

Figure 3.2-6 Synthesis of PCL

Because of the good biocompatibility, PCL has been approved by the FDA to be sagely used in drug delivery systems, sutures, long-term implants and adhesion barriers[209]. The degradation of PCL under physiological conditions is very slow due to the lack of suitable enzymes to hydrolyse the ester, which is why PCL is expected to prolong the circulation time under physiological conditions and applied for controlled drug release in many drug delivery systems. PCL is water insoluble and shows a high permeability for many therapeutic drugs, which has been used as the hydrophobic part of amphiphilic synthetic block copolymers to form various vehicles with different nano structures, such as polymersomes and micelles, in aqueous phase. These vehicles can be further used as carriers for drug delivery. A lot of drugs have been encapsulated inside PCL beads to control the drug release profiles under physiological conditions.

Polylactic acid (PLA)

Another class of synthetic polyesters is polylactic acid (PLA) which is a highly versatile polymer showing good biodegradability. PLA can be produced from 100% renewable sources, such as corn, wheat, rice, and sugar beets. This polymer can be synthesised by both the ring-opening polymerisation of the cyclic lactide dimer and the direct condensation of lactic acid[210]. Most work has been focused on the ring-opening polymerisation process because the direct condensation route for the synthesis of PLA is an equilibrium reaction, which generally limits the molecular weight of the ultimate polymer due to the difficulties of removing the trace water produced in the late stage of the reaction.

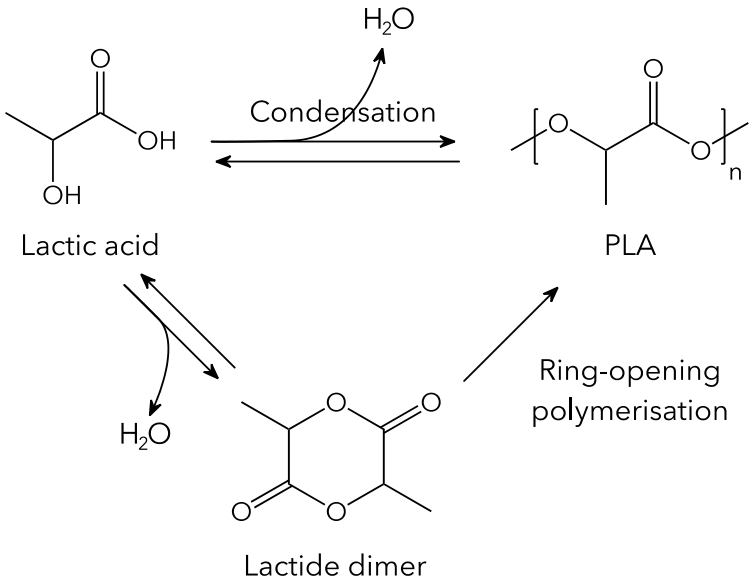

Figure 3.2-7 Synthesis of PLA

The first commercially viable biodegradable polymer made from renewable resources was achieved by the Cargill Dow LLC which patented a low-cost continuous process for the synthesis of PLA. This process synthesises both lactide and PLA in the melt instead of in solution. The process starts with a continuous condensation reaction to produce PLA pre-polymer with low molecular weight from the aqueous lactic acid. The pre-polymer is converted into a mixture of lactic stereo-isomers in the presence of the catalyst tin which enhances the selectivity of the intramolecular cyclisation reaction. The molten mixture of lactide dimer is then catalysed into high-molecular PLA polymers though a ring-opening lactide polymerisation process, which completely eliminates the use of costly and environmentally unfriendly solvents.

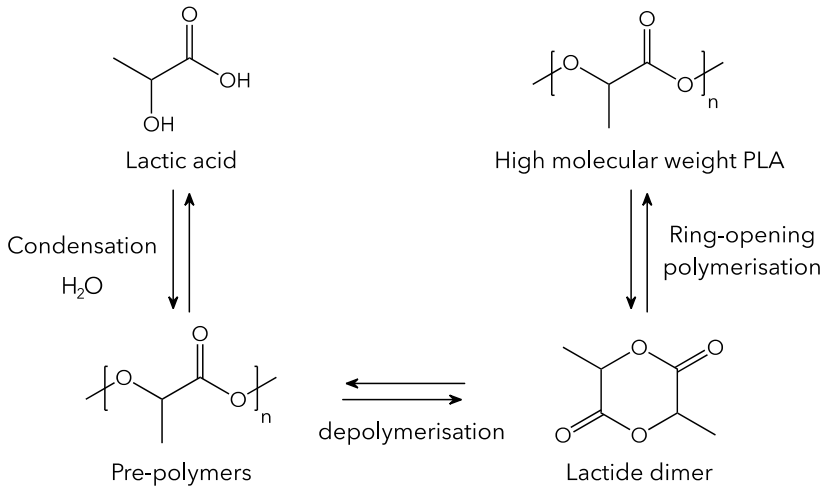

Figure 3.2-8 Synthesis of PLA through the pre-polymer and lactide dimer

PLA shows many advantages compared to other synthetic polymers. The lifetime of PLA is Eco-friendly. The raw materials of this polymer are 100% from renewable resources, such as corn, wheat, and rice. It is biodegradable, recyclable and compostable. And the production of PLA also consumes carbon dioxide, making PLA an attractive synthetic polymer. Another advantage of PLA is the good biocompatibility. PLA would hydrolyse into alpha hydroxyl acid in the human body, which will be excreted though the tricarboxylic acid cycle. PLA also show good processibility due to its better thermal characteristic. It can be processed by injection moulding, film extrusion, blow moulding, and so on. Lastly, during production of PLA, less energy is required, which also makes the PLA production potentially advantageous[211].

However, there are also some limitations of this polymer, such as the poor toughness, the slow degradation rates, hydrophobicity, and the lack of reactive side chains, which to some extent limit its applications. But the hydrophobicity and relatively low degradation rates of PLA are used to control the drug release profile in many drug delivery systems.

Polyglycolic acid (PGA)

PGA or polyglycolide is also a biodegradable polymer, which has been known since 1954 as a tough fibre-forming polymer. It's the simplest aliphatic polyester. PGA has a glass transition temperature between 35 and 40°C. The melting point of PGA stays at around 228°C. This polymer also shows an elevated degree of crystallinity (about 45-55%), which leads to the low water solubility in aqueous phase.

PGA can be synthesised through several different routes starting with different materials, including the polycondensation of glycolic acid, ring-opening polymerisation of glycolide, and solid-state polycondensation of halogenoacetates.

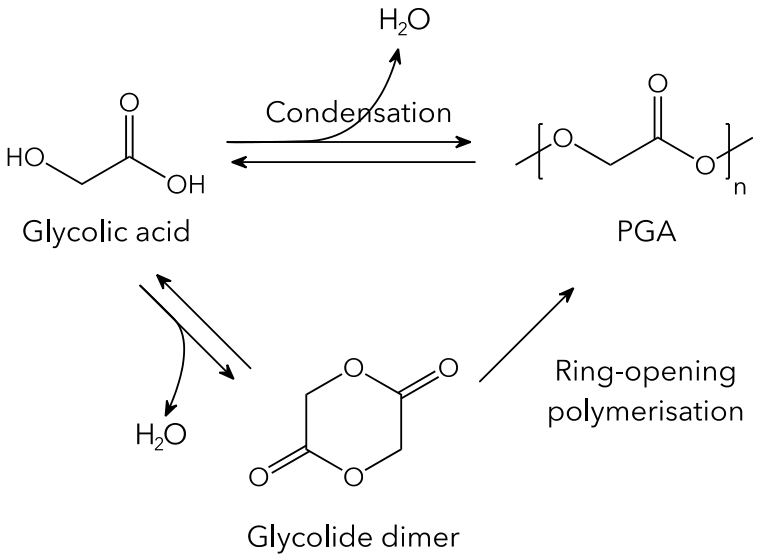

Figure 3.2-9 Synthesis of PGA

The simplest way to prepare PGA is the polycondensation process starting with glycolic acid. However, the simplest way is usually not the most desirable process because it only obtains low molecular PGA polymers. Briefly, to produce PGA with this method, glycolic acid is heated (around 180°C) at atmospheric pressure and the temperature is maintained until the water ceases to distil. Then the pressure is reduced to 150 mm Hg while the temperature keeps the same for another 2 hours to get the low molecular weight polyglycolide[212].

To produce PGA polymers with high molecular weights, the ring-opening polymerisation of glycolide is a more common way. Firstly, glycolide can be collected by distillation after heating the low molecular PGA polymers under reduced pressure. Then a catalytic amount of catalysts is added into glycolide to imitate the reaction under a nitrogen atmosphere. The reaction temperature is kept at 195°C for about 2 hours before being raised to 230°C to solidify the polymers. Then the PGA polymers with high molecular weights are obtained[212] .

Another procedure to synthesis PGA consists in the thermally induced solid-state polycondensation of halogenoacetates, which results in the production of polyglycolide with small crystal forms. Briefly, this polycondensation process is initiated by heating an halogenoacetate at around 170°C under nitrogen atmosphere. During this process, the PGA polymer is formed with chloride salts which can be removed by washing with water. Recently, researchers find a more direct way to synthesis relatively high molecular weight PGA polymers[213]. With this method, high molecular weight PGA polymers can be directly synthesised from melting

polycondensation of glycolic acid by using zinc acetate as the catalyst. It is also found that the high vacuum contributes much to the molecular weight of the final polymers.

PGA has been traditionally modified with some amino acids, like L-lysine, to prepare the PGA suture, which also leads to its application in other biomedical fields, such as the implantable medical devices and tissue engineering scaffolds. Because of the good biocompatibility of PGA, this polymer has been modified with some hydrophilic moieties to alter their water solubility so that they can be used as drug carriers in human body[214].

Poly lactic-co-glycolic acid (PLGA)

Another biodegradable polymer which has drawn considerable attention is poly lactic-co-glycolic acid (PLGA). Due to the long clinical experience, the unique degradation properties, and the good biocompatibility, PLGA has shown immense potential in the biomedical fields, such as being used as drug delivery carrier and as scaffolds for tissue engineering. Much literature has been focused on the controlled release of drugs at the desirable sites in the human body because of the favourable degradation of PLGA. The physical properties of PLGA can be tuned via easily changing some parameters, such as the molecular weights of polymers and the ratios of lactide to glycolide in the polymers, which can be further used to control the behaviours of various drug molecules in the body.

Basically, PLGA is a copolymer of poly lactic acid (PLA) and poly glycolic acid (PGA). PLGA polymers are usually synthesised via a ring-opening copolymerisation of two different monomers, namely the cyclic dimers of glycolic acid and lactic acid. During this procedure, common catalysts, such as tin(II) 2-ethylhexanoate, tin(II) alkoxides, and aluminium isopropoxide, are usually used to initiate the reactions. The successive monomeric units are linked together by ester linkages in PLGA, which leads to the linear, aliphatic polyester as the final product. Copolymerising PLA with crystalline PGA would reduce the degree of crystallinity of PLGA, which increases the rate of hydration and hydrolysis. Generally, PLGA with higher content of PGA would result in quicker degradation rates.

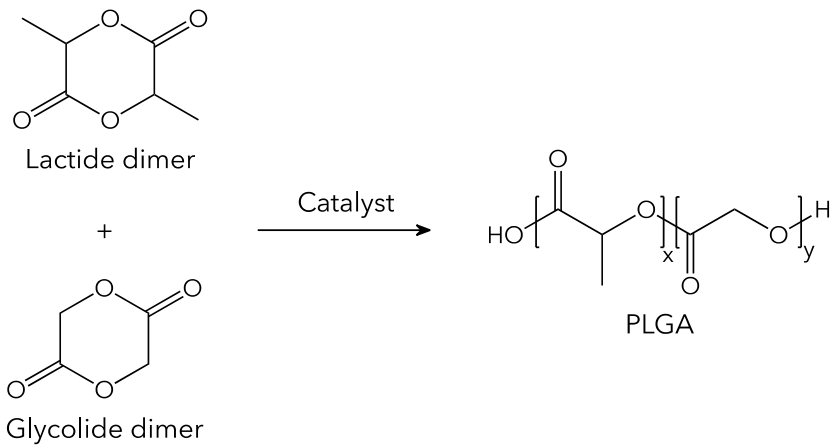

Figure 3.2-10 Synthesis of PLGA

PLGA can be processed into various shapes and sizes which are capable of encapsulating molecules with different sizes. It can be dissolved into a large wide of common organic solvents, such as chlorinated solvents, tetrahydrofuran, acetone, ethyl acetate, and so on. PLGA is not soluble in water but it can undergo hydrolysis of its ester linkages. The physiochemical properties of PLGA have shown a close relationship with the initial molecular weight, the ratio of lactide to glycolide in polymer, the sizes of the devices, exposure to water, storage temperature, and so on. Due to the hydrolysis of PLGA, many parameters of this polymer can change with time, such as the glass translation temperature (*Tg*), moisture content and molecular weight. And thesis physiochemical properties would affect the abilities of polymers to be formulated into drug delivery devices and control the behaviours of drug molecules. Researches have shown that the degree of crystallinity of the PLGA would affect the mechanical strength, swelling behaviours, and degradation rates.

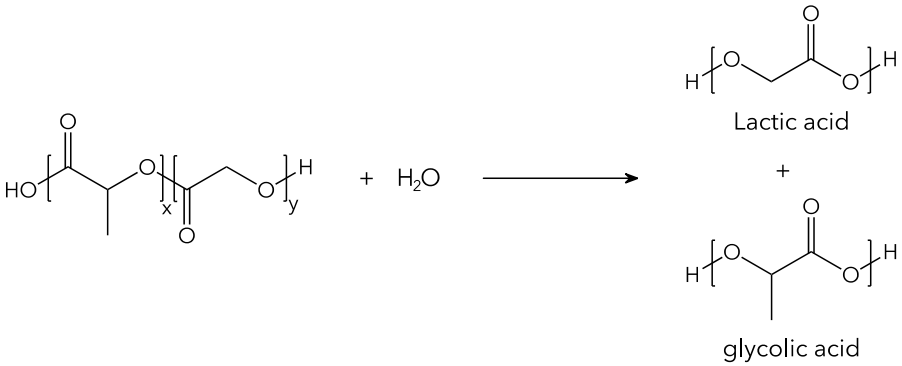

Figure 3.2-11 hydrolysis of PLGA

These biodegradable polymers have been used as carriers to deliver its payloads to the targeted sites for the intended therapeutic effect. Researchers have found that the biodistribution and pharmacokinetics of PLGA follows a non-linear and dose-

dependent profile in the body[215]. Besides, the dose and composition of PLGA carriers may also affect its blood clearance and uptake by the mononuclear phagocyte system (MPS)[216]. For instance, some formulations of PLGA with nano-structures, such as nanoparticles, would rapidly accumulated into liver, bone marrow, lymph nodes, spleen and peritoneal macrophages. Besides, PLGA shows a quick degradation phase in the early stage and is eventually cleared by the respiration in the lung[217].

Many new polymers with various properties have also been synthesised and investigated as carriers for the delivery of many drug molecules. However, only a few types have been approved by the FDA to be used in medicinal applications because of the biocompatibility and biodegradability problems. Besides, polymers with suitable physiochemical properties for drug delivery also need vigorous trials before clinical use and carrier-based nanomedicine display a more complicated path through the clinic.

4. DRUG DELIVERY SYSTEMS

Drug delivery systems (DDS) refer to approaches for transporting active pharmaceutical ingredients (APIs) to the target sites of pharmacological actions in the body. The technologies employed mainly involve those concerning pharmaceutical preparation, administration, site targeting, distribution, metabolism and biocompatibility. Thus, drug delivery focuses on the development of technologies to deliver APIs to the desired sites so as to maximize their therapeutic efficacy, minimize their side effects and ameliorate the compliance of patients.

4.1 Carrier-based Drug Delivery Systems

During the last decades, many DDS with various composition and carrier architectures have been developed and investigated, including liposomes, polymersomes, polymeric micelles, virusomes, inorganic nanoparticles and cell-based delivery systems.

4.1.1 Polymer-drug conjugates

In polymer-drug conjugates (*Figure 4.1-1*), drug candidates are covalently bonded to polymers via cleavable space linkers to form prodrugs, which are typically designed to reduce the systemic toxicities of their parent compounds and ameliorate the therapeutic effects[218]. The polymers used in polymer-drug conjugates are specially synthesised to be sensitive to specific environments, such as the acidic tumour micro-environment, so as to alter their *in vivo* behaviour because the drug molecules remain attached to the polymers and are not activated until they are navigated to the targeted sites[219]. Compared to their parent drugs, these specially designed polymer-drug conjugates usually exhibit improved circulation time, ameliorated bio-distribution and reduced systemic toxicities[218]. An example that uses polymer-drug conjugates for cancer treatment is the [N-(2-hydroxypropyl)meth acrylamide] (HPMA) copolymer-doxorubicin conjugates, which has completed the Phase II study and revealed that polymer-bound therapeutics can have modified and enhanced anticancer activities[220]. Another polymer-drug conjugate that has entered phase III trials is the Poly-L-Glutamic acid-Paclitaxel Conjugate (PG-TXL), which exhibits significantly enhanced standard of living for patients who undergo paclitaxel therapy for non-small cell lung cancer[221, 222].

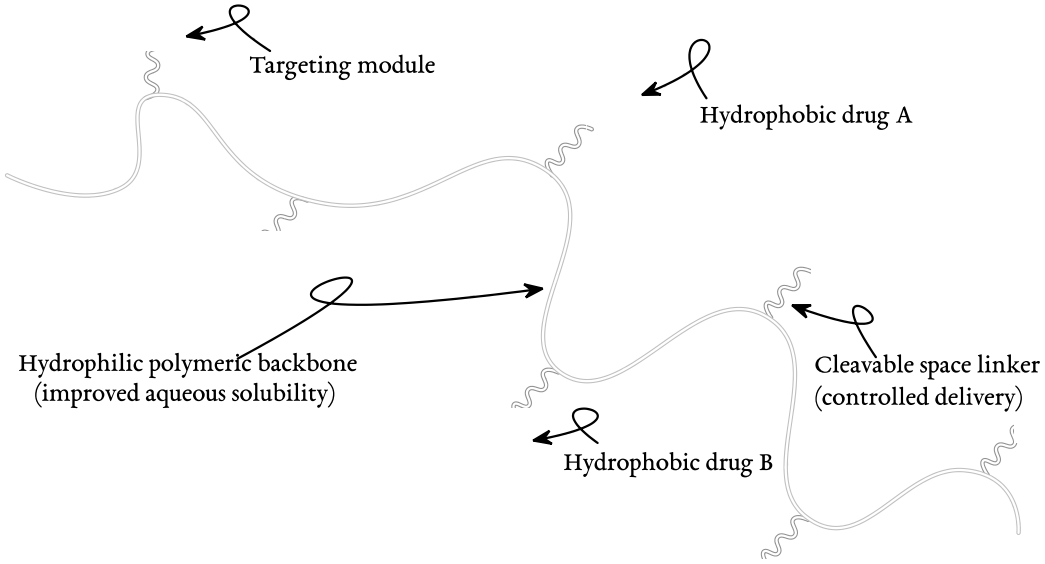

Figure 4.1-1 Illustration of polymer-drug conjugate systems

4.1.2 Liposomes

Liposomes (*Figure 4.1-2*) are spherical structures in which an aqueous volume is entirely enclosed by a membrane consisting of one or more lipid bilayer[223]. Their sizes vary from around 10 nm to several micrometres. Two major structural components of liposomes are phospholipids and cholesterol. Phospholipids are the main ingredient used for construction of the liposome membrane while the introduction of cholesterol molecules can ameliorate the separation between choline head groups, leading to reduced hydrogen bonding and electrostatic interactions. The formation of liposomal structures of lipid bilayer reduces the unfavourable hydrophobic and hydrophilic phase interactions and decreases the large free energy difference existing between the hydrophilic and hydrophobic environment because spherical structures possess minimum surface tension[224]. Liposomes are used as vehicles for accommodation of drugs with varying hydrophilicity because of the hydrophobic lipid bilayers and the inner aqueous cores[223].

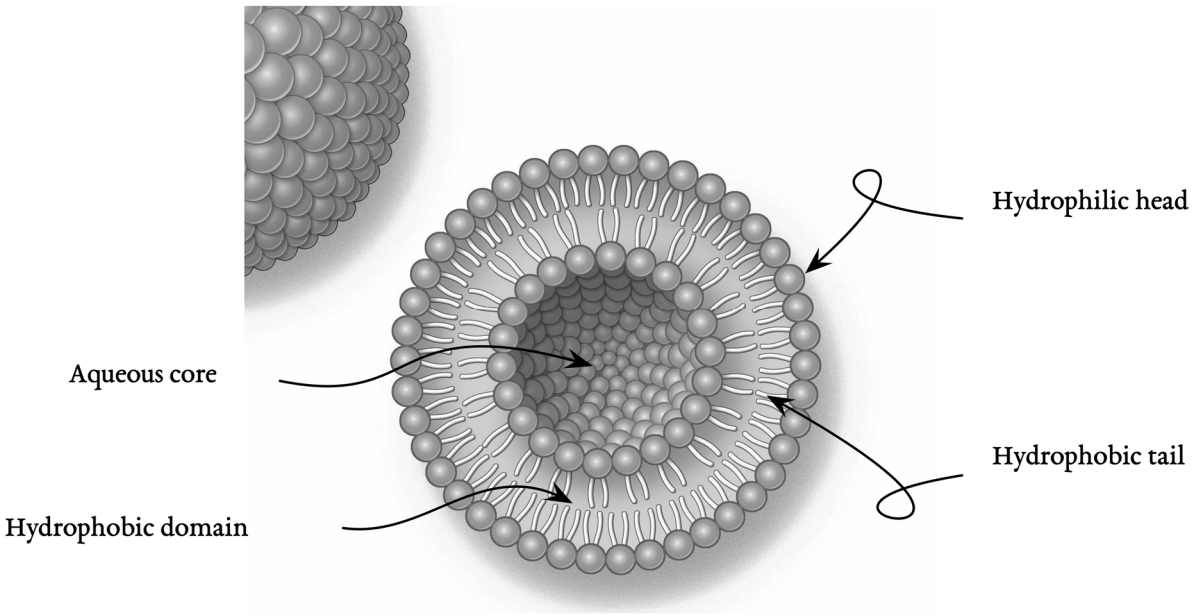

Figure 4.1-2 Illustration of Liposomes. [225]

They are also used to study the membrane mechanics in a cell during exocytosis due to their similar composition and structure[223]. The major obstacles associated with liposome drug delivery systems mainly include low encapsulation efficiency, fast burst release of drugs, short shelf life, relatively weak stability, rapid removal from circulation by the reticuloendothelial system (RES) and poor modular chemical functionality[224, 226].

4.1.3 Polymersomes

Polymersomes (*Figure 4.1-3*) are a class of artificial vesicles having similar bilayer structure to liposomes. They are hollow spheres containing an aqueous core surrounded by a bilayer membrane[227]. The big structural difference for polymersomes is that their membranes are composed of various polymeric amphiphiles, such as amphiphilic polypeptides[228], which have thicker membranes, thus possessing high membrane stability, low membrane permeability and prolonged circulation time in blood[229]. For liposomes, their typical membrane thickness is within 5 nm while the hydrophobic membrane thickness of polymersomes can easily exceed 5 nm via simply increasing the molecular weight of hydrophobic blocks[230].

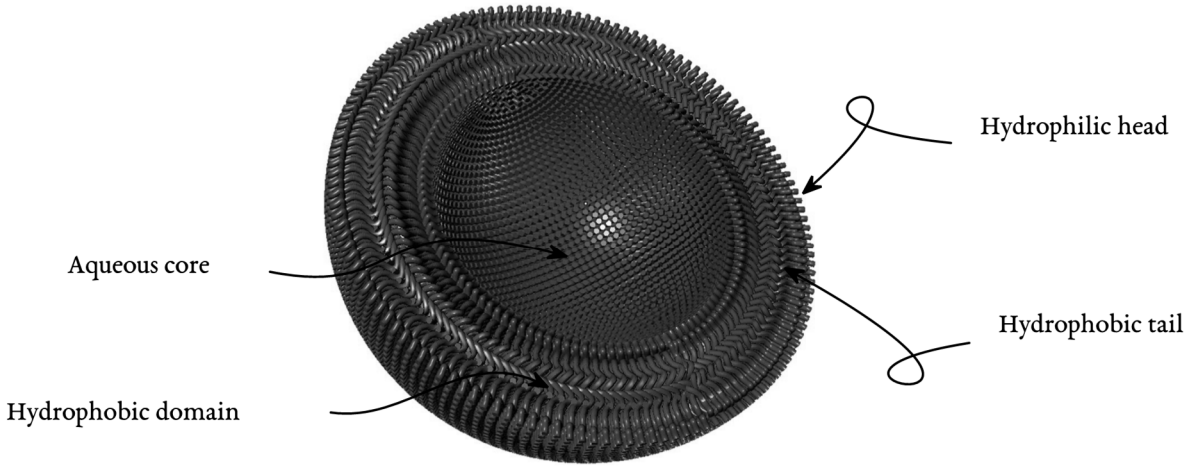

Figure 4.1-3 Illustration of polymersomes[227].

Similar to liposomes, the aqueous domain of polymersomes can accommodate hydrophilic cargo while the bilayer membrane integrates hydrophobic drugs into its hydrophobic domain through hydrophobic interactions, showing an improved drug encapsulation capacity because of the stronger abilities caused by polymers. Besides, the incorporation of ligands with various properties can easily provide polymersomes more functionality and make them become versatile drug delivery systems[229], such as pH-responsive polymersomes[231, 232], temperature-responsive polymersomes[233], magnetic field-sensitive polymersomes[234, 235] and double-responsive polypeptide-based polymersomes [236].

4.1.4 Polymeric micelles

Polymeric micelles (*Figure 4.1-4*) are also drug carriers composed of amphiphilic polymers. Their hydrophobic blocks spontaneously aggregate to form inner hydrophobic cores to reduce the surface tension in aqueous medium, while the hydrophilic parts of polymers interact with water molecules to form a hydrated corona to support the cores, consequently leading to the formation of good spherical micelles. It is important to differentiate polymeric micelles from polymersomes even though both of these macromolecular complexes are spherical and consist of amphiphilic polymers.

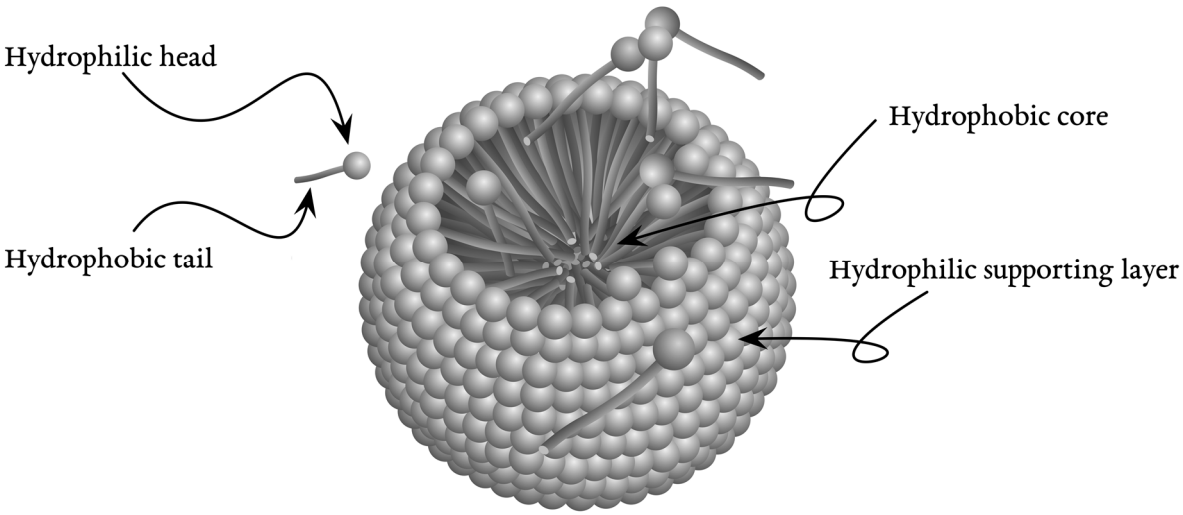

Figure 4.1-4 Illustration of micelles[237].

Micelles are composed of only a single layer of polymers and the non-polar blocks are clustered together in the centre to form hydrophobic cores. The lack of aqueous cores makes them less accommodating to a variety of hydrophilic drugs on the interior, whereas spherical polymersomes with aqueous cores are constructed from a bilayer that allows hydrophilic molecules on the inside. Disadvantages associated with micelles mainly include poor drug-loading efficiency, poor physical stability *in vivo* and insufficient cellular interaction of neutral micelles with malignant cells for uptake[238].

4.1.5 Dendrimers

Dendrimers (*Figure 4.1-5*) are nano-sized, radially symmetric polymer matrix with well-defined, homogeneous, and monodisperse structures[239]. These polymeric complex are initiated through a core molecule and branched via highly controllable polymerisation reactions. The regulated synthesis for dendrimer construction enables excellent control over their shapes and sizes which are important parameters for medical applications[240].

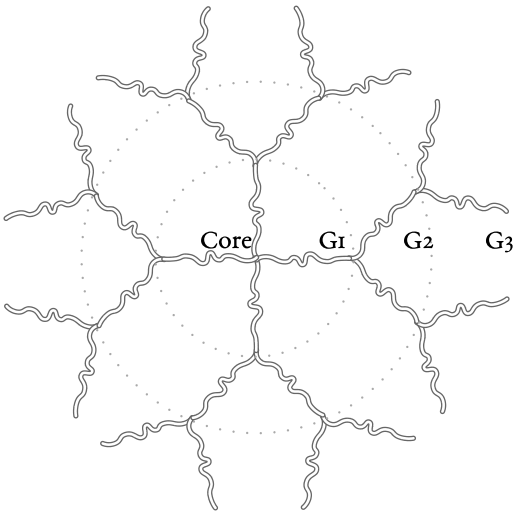

Figure 4.1-5 Typical structure of dendrimers with 3 generations.

According to the number of repeated branching cycles performed during synthetic construction, dendrimers can be classified by generations. The molecular weight of each new generation is roughly doubled compared to the previous one. Dendrimers with higher generations also expose more functional groups, leading to a more customizable surface of the dendrimers for different applications. Dendrimers also exhibit good water solubility and non-immunogenic[241]. Although dendrimers show several advantages, the researches regarding to their biocompatibility and toxicity are still ongoing[240].

4.1.6 Virosomes

Virosomes (*Figure 4.1-6*) are viral envelopes which are reconstructed to serve as vehicles for the cellular delivery of various preventive and/or therapeutic molecules, such as antigen, drug molecules and genes[242, 243]. They are regenerated empty virus envelopes without replicability, showing no toxicity and auto-immunogenity. They usually have a typical diameter around 100 nm. Compared other drug delivery systems, virosomes exhibit many advantages.

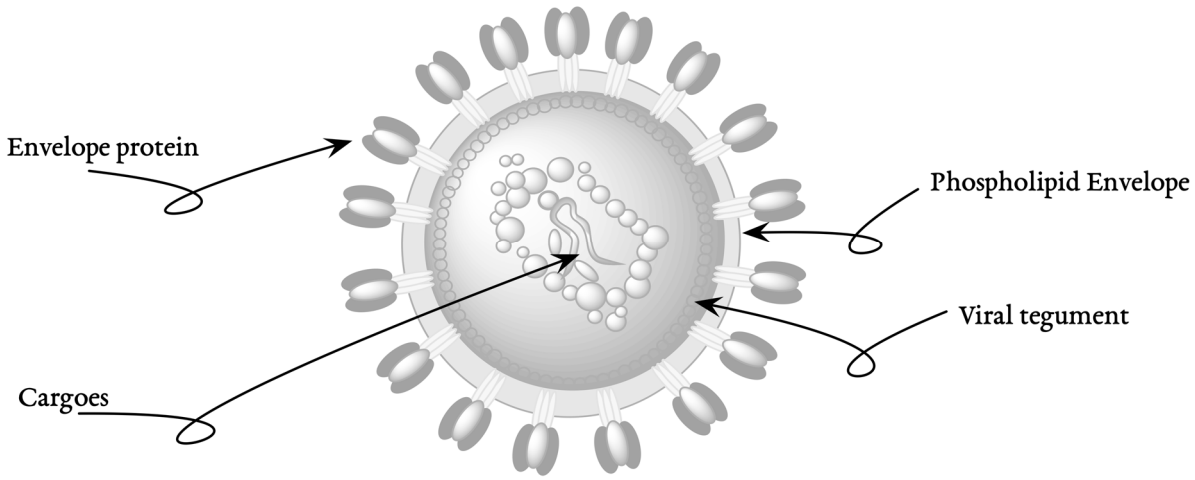

Figure 4.1-6 Typical structure of virusomes.

They possess good biocompatibility and biodegradability because of Their phospholipid membrane and the incorporated virus derived proteins naturally allows them to fuse with target cells and delivery the cargo molecules into the cytoplasm of target cells[243]. They can also promote combination movement in the endolysosomal pathway. Viruses used for virosomes include influenza virus, sendai virus, epstein-burr virus and herpes simplex virus. The achievement of intracellular delivery of cargoes also extensively relies on modern nanotechnology to prepare the bio-active materials and to incorporate them into the virosomes.

4.1.7 Inorganic nanoparticles

Various inorganic nanoparticles, such as gold nanoparticles[244, 245], quantum dots (QDs)[246] and iron oxide nanoparticles[247, 248] have been extensively developed and investigated for the biomedical applications.

Inorganic materials provide these nanoparticles more possibilities by incorporating multifunctional moieties. For instance, gold nanoparticles with controllable sizes and shapes have been decorated with antibodies to achieve both selective imaging and photo-thermal therapy by using light with longer wavelengths for tissue penetration[249]. These inorganic nanoparticles can also conjugate with fluorophores, tumour-targeting ligands, anticancer drug molecules and/or genes to simultaneously achieve fluorescence-based real-time self-imaging tracking, active targeting property and synergistic therapeutic efficacy[250].

QDs are tiny colloidal semiconductor nanocrystals and have specific optical and electronic properties. When excited by light with certain energies, they can emit light at frequencies which can be easily tuned by modifying the sizes and shapes of quantum

dots[251, 252], thus QDs are good candidates as theranostic platforms. For instance, CdTe@CdS@ZnS QDs were loaded with paclitaxel in nano-structured lipid carriers to achieve a theranostical effect[253]. Compared to organic fluorophores, QDs usually exhibit high fluorescence emission intensities, high photo-stability, narrow emission spectra and broad excitation spectra[254].

However, inorganic particles with sizes smaller than a few nanometres may also induce cytotoxicity while their cellular uptake efficiency decreases dramatically as particles sizes increase[255].

4.1.8 Cell-based delivery systems

Erythrocytes (red blood cells, RBCs, *Figure 4.1-7*) have been investigated as drug carriers for a long time[256, 257]. They are one common type of blood cells with typically biconcave disc shapes, which is a principal means of transporting oxygen to the body tissues via blood flow. RBCs usually have microscale diameter and for mature RBCs, the absence of nuclei and organelles allows them to contain more hemoglobin and, thus, carry more oxygen[258].

Their availability, large inner cavities, long half-life in the circulation (close to 120 days for human), high biocompatibility and natural mechanisms for safe elimination make them the ideal carriers for drug delivery[259]. Various therapeutic enzymes encapsulated in carrier RBCs are studies under different stages, including galactosidase[256], glucocerebrosidase[257, 260], thymidine phosphorylase[261], adenosine deaminase[262], thiosulfate-cyanide sulfurtransferase[263], phosphothioesterase[264] and alcohol oxidase[265].

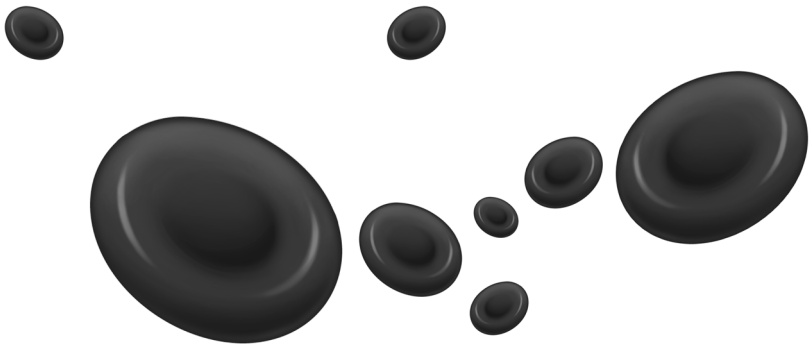

Figure 4.1-7 Erythrocytes with biconcave disc shapes.

Mononuclear phagocytes are widely distributed, biosynthetically active cells[266], which have also been studies as drug carriers for their penetration of blood brain barrier and delivery of therapeutic agents into the brain[267, 268]. Besides, other types of cells

like bacterial membranes[269] and cancer cell membranes[270, 271] have also attracted large interest duo to their unique feathers.

4.2 Drug Self-Delivery Systems

Drug Self-Delivery Systems (DSDS) are formed through self-assembly of therapeutic molecules without the addition of any carriers. Compared to conventional carrier-based drug delivery systems, the novel excellent paradigm could not only significantly improve drug-loading capacity (even up to 100% for pure drug nanocrystals) but also allay concerns about the biosafety of those materials used as drug carrier[272]. Besides, DSDS can protect the drugs from rapid blood/renal clearance by altering their aggregation state. They can also facilitate drug accumulation at tumour tissues through the enhanced permeability and retention (EPR) effect due to their nanoscale features[273]. The combinational delivery of multiple drugs can also promote the DSDS to overcome multidrug resistance (MDR). In addition, the fabrication process is easy to achieved because of their relatively simple structures and composition, suitable for large-scale practical industrial manufacture[274].

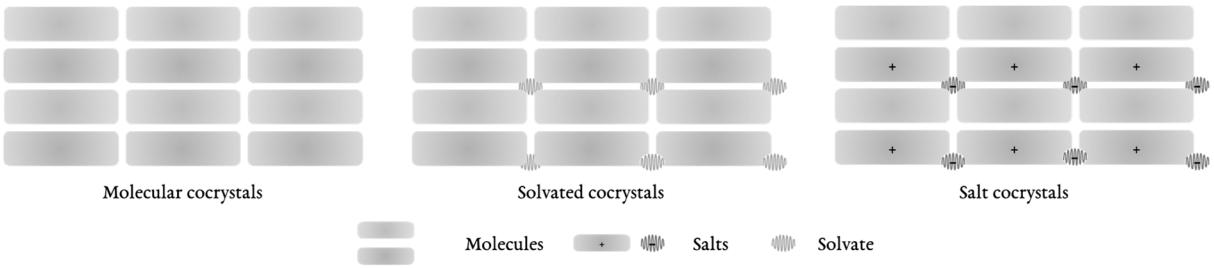

Figure 4.2-1 Illustration of pharmaceutical cocrystals.

According to the composition and the aggregation mechanism, DSDS can be classified into amphiphilic drug self-assembled nanoparticles and pharmaceutical cocrystals. Because of the hydrophilicity of most anticancer drugs, they are usually covalently connected with some small hydrophilic moieties, such as water-soluble drugs, via some susceptible linkers to achieve an amphiphilic structure which can self-assemble into nanoparticles. The self-assembled nanoparticles are usually in amorphous states.

Pharmaceutical cocrystals are another class of DSDS. Cocrystals are crystalline materials composed of two or more molecules in the same crystal lattice, which are considered the same as polymorphs or salts of Active Pharmaceutical Ingredients (APIs) in the latest version of FDA (2018) Guidance for Industry[275]. Depending on the compositions and the interactions between components, cocrystals can be further

classed into molecular forms and salt (charge assisted) forms[276-278]. Cocrystals enable an expedient way to modify the physicochemical properties of APIs by simply altering the solid-state arrangement of each component through intermolecular non-covalent interactions without utilising any carriers or changing their chemical structures, hence, minimising the alteration of their pharmacological properties. Besides, cocrystals can not only improve the water solubility[279-281] and permeability[282] of APIs, but also provide many other features, such as decreased hygroscopicity[283-285] and better stability[286, 287].

All the drug delivery systems prepared with different nanotechnologies have been utilised to modify the physiochemical properties of various active pharmaceutical agents to improve their druggability and help to transport them into the targeted sites in the body to maximise their therapeutic efficacies as well as to reduce their systematic toxicity.

5. Aims of the Study

On the basis of literature review, it is evident that the clinical research of curcumin is hampered due to its poor water solubility, fabricated formulation composition and complicated manufacturing processes, in spite of the fact that curcumin has been formulated into various kinds of micro-particles (MP) to improve its water solubility. In addition, although irinotecan hydrochloride has been used as the first line treatment of colorectal cancer, its life-threatening side effects, such as delayed diarrhoea, heavily limit its practical convenience and applications.

In this study, we aim to develop an easily manufactured self-delivered platform suitable for the combinational delivery of irinotecan hydrochloride and curcumin without utilising any carriers. Meanwhile, the water solubility of curcumin can be improved by formulating with irinotecan and the side effects caused by irinotecan can be reduced by involving curcumin. Furthermore, the possible mechanisms of evaluated side effects would also be explored.

The particular aims of the dissertation are summarised in the following major points:

- Development of a drug self-delivery nano-formulation for the combinational delivery of irinotecan and curcumin;
- Exploration of the suitable conditions for preparing the drug self-delivery system and optimisation of its formulation;
- Preparation and characterisation of the developed nano-formulation;
- Development and validation of an analysis method based on HPLC for simultaneous determination of irinotecan and curcumin in the developed nano-formulation;
- *In vitro* evaluation of the cytotoxicity, uptake efficiency and internalisation pathways on cells;
- *In vivo* evaluation of safety and therapeutic effects on nude mice, including the anticancer effects and the reduced side effects of the nano-formulation.

6. MATERIALS AND METHODS

6.1 Materials

Curcumin (≥ 80%, powder), irinotecan hydrochloride (≥ 98% HPLC, powder), poloxamer 105, mannitol, glucose, paraformaldehyde, acetonitrile (ACN, HPLC grade), methanol (MeOH, HPLC grade), dimethyl sulfoxide (DMSO, HPLC grade), acetic acid (HPLC grade), hydrochloride and sodium dodecyl sulfate (SDS, ≥ 98% GC, powder) were purchased from Sigma-Aldrich (Czech Republic) and utilized as received. Wortmannin, cytochalasin D, genistein and methyl-β-cyclodextrin were purchased from Meilun Biotechnology Co. Ltd (Dalian, China). Chlorpromazine was obtained from Selleck Chemicals (China). Disodium phosphate (DSP, Na_2HPO_4) was provided by PENTA s.r.o. (Czech Republic). Phosphate buffered saline (PBS, pH=7.4) was prepared in laboratory and ultrapure water was prepared in laboratory using a Milli-Q integral water purification system.

6.2 Nanoparticle Optimisation and Characterisation

6.2.1 Preparation and optimisation of the nanoparticles

Surfactant stabilised irinotecan hydrochloride and curcumin nanoparticles (SICN) was prepared based on a simple precipitation method. Briefly, irinotecan hydrochloride and curcumin were dissolved in dimethyl sulfoxide (DMSO), inside which the injectable non-ionic surfactant poloxamer 105 was added. The obtained organic solution was added into ultrapure water with magnetic stirring to get a suspension which was then dialyzed to remove the organic solvent. Nanoparticle powder was obtained after lyophilisation with mannitol, which was then dispersed into ultrapure water containing glucose to get an injectable nanoparticle suspension. Irinotecan hydrochloride curcumin nanoparticles without surfactants (ICN) was also prepared using the same procedures without adding surfactants.

The nanoparticle formulation was optimised through simple parameter exploration, which was operated by simply changing the composition of the formulation. The particle sizes, surface charges and their polydispersity index (PDI) in suspension were took as the evaluation parameters.

6.2.2 Physiochemical property characterisation

The particle sizes, surface charges and the polydispersity of the of nanoparticles in different conditions were characterised by dynamic light scattering (DLS). To investigate the morphologies of nanoparticles, a drop of nanoparticle water suspension was evaporated on an aluminium foil. All nanoparticles were coated with a thin layer

of gold (conductive coating) before investigation under a scanning electron microscope (SEM). The diffraction and thermal behaviour was characterized by powder x-ray diffraction (PXRD) and differential scanning calorimetry (DSC), respectively.

6.3 Analytical Method based on HPLC

6.3.1 Development of HPLC analytical method

Preparation of stock solution

Curcumin stock solution (1.05 mg/mL) was prepared by accurately weighing 10.5 mg of curcumin and dissolving it into 10 mL of ACN. Irinotecan hydrochloride stock solution (1.05 mg/mL) was prepared by weighing 10.5 mg of irinotecan hydrochloride and dissolving it into 10 mL of ACN. Additionally, to prepare a combined stock solution containing both curcumin and irinotecan hydrochloride, 10.5 mg of curcumin and 10.5 mg of irinotecan hydrochloride were accurately weighed and dissolved into 10 mL of ACN. All the prepared stock solutions were stored at 4°C in darkness for further use.

Development of Analytical Method

Chromatographic separation was carried out on a C_{18} column (Kinetex 2.6μ C_{18} 100A, 150 mm x 4.6 mm) fitted with a pre-column (WATREX 50 mm x 4 mm, ReproSil 100 C18, 5 μm). ACN and ultrapure water containing DSP (0.002 mol/L), SDS (0.08 mol/L) or acetic acid (4%, v/v) were used as the mobile phase. The flow rate was set to 1.0 mL/min., and the temperature in the column oven was maintained at 40°C. The volume injected for all injections equalled 0.5 μL. The UV-Vis absorption of curcumin or irinotecan hydrochloride was determined by HPLC, on the aforementioned system equipped with a DAD detector.

6.3.2 Validation of HPLC Analytical Method

Validation of the method was carried out according to current guidelines issued by the International Conference on Harmonization (ICH), ref. Q2 (R1) (ICH, 2017) [288].

Specificity

Blank ACN, standard curcumin solution, standard irinotecan hydrochloride solution, mixed irinotecan hydrochloride curcumin solution and ICN nanoparticles diluted with ACN were injected into HPLC so as to determine the specificity of the analytical method.

Linearity and Range

Serial dilutions were prepared of a mixture of curcumin and irinotecan hydrochloride in ACN at concentrations ranging from 2.05 μg/mL to 1.05 mg/mL. The calibration curve was plotted in triplicate, displaying peak area versus concentration. Analysis of least square regression was conducted on the data obtained and ANOVA test ($\alpha = 0.05$) was used to assess the regression significance.

Sensitivity

The sensitivity of the analysis method was observed with respect to the limit of detection (LOD) and limit of quantitation (LOQ). The LOQ was determined as the first concentration of calibration curves. The LOD was estimated based on the standard deviation (σ) of y-intercepts and the slopes (s) of the regression lines. The equations are represented below:

$$LOD = 3.3\ \sigma / s$$

Accuracy

To evaluate the accuracy of the method, a recovery experiment was performed. Three different levels (30 μg/mL, 200 μg/mL, and 500 μg/mL) of curcumin and irinotecan hydrochloride were added to the matrix samples: ACN and nanoparticle ACN solution. Their responses were estimated from the relevant calibration curve. Accuracy was determined by recovery with a relative error based upon actual and estimated concentrations.

Precision

Repeatability was analysed by injecting three different levels (30 μg/mL, 200 μg/mL, and 500 μg/mL) of curcumin and irinotecan hydrochloride solution into the HPLC system in three replicates within a single day. Intermediate precision was also determined by analysing the same three concentrations of curcumin and irinotecan hydrochloride solutions on two days in five replicates. Relative standard deviation (RSD, %) with a confidence interval pertaining to the estimated concentrations was calculated for each set of data according to the calibration curve.

Robustness

The robustness of the proposed method was determined by changing a chromatographic condition, such as the mobile phase ratio (± 0.5%), flow rate (± 0.1 mL/min), and column temperature (± 3°C). Figures for mean recovery (± % confidence interval) as well as relative error were reported.

6.4 *In vitro* and *in vivo* Evaluation

6.4.1 Cell culture and mouse preparation

HT-29 colorectal adenocarcinoma cells were obtained from Boster Biological Technology Co. Ltd (Wuhan, China). Male BALB/c nude mice, aged 5 weeks (18–22 g, SPF grade), were purchased from Dashuo experimental animals Co., Ltd. (Chengdu, China). All animal experiments were conducted under the guidelines approved by the Institutional Animal Care and Use Committee (IACUC) of Chengdu University of Traditional Chinese Medicine.

6.4.2 *In vitro* cytotoxicity on cells

The *in vitro* evaluation was tested on human colorectal adenocarcinoma cell line, HT-29, which was obtained from Boster Biological Technology Co. Ltd (Wuhan, China). Fetal Bovine Serum (FBS, TransSerum® HQ), DMEM/F12 culture medium (HyClone™) and MTT (3-(4,5-dimethylthiazol-2-yl)-2,5-diphenyltetrazolium bromide, Beijing Solarbio Science & Technology Co., Ltd.) were used as received. The cells were cultured in DMEM/F12 medium supplemented with 10% FBS, 100 IU/mL penicillin and then incubated in a humidified incubator containing 5% CO_2 at 37°C.

The cytotoxicity of SICN nanoparticles on HT-29 cells with different environmental pH values were measured by MTT assays. HT-29 cells were firstly seeded in 96-well plate at 8 x 104 cells/100 μL medium and cultured in DMEM/F12 for 24 h. SICN nanoparticle suspension was then added into 96-well plates and incubated with HT-29 cells for 48 h in different pH media (6.5, 7.4 or 7.8). MTT (0.5 mg/ml dissolved in phosphate-buffered saline, 20 μL/well) was added and cells were incubated in the dark at 37 °C for 4 h. Solutions were removed, 150 μL DMSO were added at room temperature to dissolve formazan crystals. Finally, absorbance was measured by a micro-plate reader at 490 nm, and the cells incubated with DMEM/F12 were used as control group. The cell viability in each well was calculated using the equation below:

$$\text{Cell viability (\%)} = (OD_{experimental}) / (OD_{control}) \text{ X } 100\%$$

Where indicates the readout measurement with cells and OD is short for optical density.

6.4.3 *In vitro* uptake efficiency

HT-29 cells were seeded in confocal dishes and cultured in DMEM/F12 for 24 h. SICN nanoparticle suspension (equalling to 50 μM of irinotecan hydrochloride) was

then added into cells and incubated for 1 h in different pH media (6.5, 7.4 or 7.8) before being measured by a Leica TCS SP8 confocal laser scanning microscope (Excitation wavelength, 488 nm). All the parameters kept the same during the whole experiment.

6.4.4 *In vitro* internalisation pathways

HT-29 cells were seeded in confocal dishes and cultured in DMEM/F12 for 24 h. Cells were pre-treated with each inhibitor or at 4°C for 1.5 h and then incubated with SICN nanoparticles (equalling to 50 μM of irinotecan hydrochloride) for 3 h before being analysed by a Leica TCS SP8 confocal laser scanning microscope (Excitation wavelength, 488 nm). All the parameters kept the same during the whole experiment.

6.4.5 *In vivo* therapeutic efficacy and biosafety

HT-29 cell suspension (2×10^6 cells per 200 μL) were subcutaneously injected into the flank of male BALB/c mice. When tumour volume reached around 100 mm^3, the HT-29 tumour bearing nude mice were randomly divided into three groups (four or five mice for each group) and were intravenously injected with PBS, irinotecan hydrochloride (27.5 mg/kg/mouse) or SICN (equivalent irinotecan 27.5 mg/kg/mouse) every other day for consecutive 20 days.

Tumour volume was measured every third day and calculated according to the formula: Tumour volume = length x $width^2/2$. Mice were weighted every three days and the severity of diarrhoea was scored according to the following standards[289]: 0 (normal, normal stool or absent); 1 (slightly wet and soft stool); 2 (moderate, wet and unformed stool with moderate perianal staining of the coat); and 3 (severe, watery stool with severe perianal staining of the coat).

Mice were sacrificed after 5 days of medication discontinuation. Tumours were excised, weighted and photographed. The ex vivo organs (heart, liver, spleen, lung, kidney and brain) and tumours were fixed in 4% paraformaldehyde to prepare paraffin sections. Haematoxylin/eosin (H&E) staining was used for histological analysis.

6.4.6 *Ex vivo* biodistribution

Mice with subcutaneous tumours of around 100 mm^3 in each group were intravenously injected with irinotecan hydrochloride or SICN (equivalent irinotecan 27.5 mg/kg/mouse). Fluorescence based biodistribution images and the average signal of excised tissues were obtained on a FUSION FX7 live animal imaging system.

7. RESULTS AND DISCUSSION

Irinotecan hydrochloride and curcumin were formulated into nanoparticles with a simple precipitation method. The formulation of this nanoparticle system was optimised. An analytical method based on HPLC was developed and validated to characterise the drug content in and the nanoparticle system. The nature of the obtained particles was explored *via* various technologies, which could help to comprehend the self-delivered nano system. Finally, the therapeutic efficacy and bio-safety of this developed nanoparticle system was evaluated on cells and mouse models.

7.1 Nanoparticle Preparation and Characterisation

7.1.1 Nanoparticle preparation and optimisation

The nanoparticles were prepared by using a simple precipitation method. For the construction of the self-delivered nanoparticular systems based on irinotecan hydrochloride and curcumin, several pharmaceutical parameters were explored to optimise the formulation.

Drug ratios

Nanoparticles with different drug ratios were prepared using the same preparation method described before. Their particle sizes, PDI and surface charges of nanoparticles with different drug ratios (molar ratio of irinotecan hydrochloride to curcumin) are shown in the *Table 7.1-1*.

Table 7.1-1 Nanoparticles with different drug ratios

Drug Ratio	Particle sizes (nm) in water	PDI	Surface Charge (mV)
1:3	130.12 ± 1.67	0.125 ± 0.032	-37.42
1:2	120.78 ± 1.46	0.132 ± 0.071	--39.32
1:1	100.78 ± 1.32	0.093 ± 0.032	-42.78
2:1	218.45 ± 4.35	0.425 ± 0.045	-28.23
3:1	315.78 ± 7.32	0.489 ± 0.075	-20.56

As can be seen, when the molar ratio of irinotecan hydrochloride to curcumin is smaller than 1:1, the nanoparticles are uniformly distributed with average dimeters at round 100 nm. These nanoparticles also show negative surface charges with high magnitudes. However, when the molar ratio of irinotecan hydrochloride to curcumin is higher than 1:1, the average sizes of nanoparticles become much larger with multiple peaks and wide distribution (PDI > 0.4). Besides, their surface charges which can

provide the stability of nanoparticles in suspension decrease dramatically. Therefore, the drug ratio of these two molecules is set to 1:1 for further study.

Effects of surfactants

Particles with different content of surfactant (poloxamer 105) were prepared and characterised by DLS. The relevant results are shown in *Table 7.1-2*. As can be seen, with the increase of the content of surfactant poloxamer 105, the hydrodynamic sizes of nanoparticles in water also increase and the size distribution in water becomes wider compared to those without the addition of surfactant. However, the sizes of nanoparticles without surfactant increase by 10 times larger with wide distribution (PDI > 0.5) in PBS while the nanoparticles with 15 weight percent of poloxamer 105 show stabilised particle sizes in both water and PBS. This could be attributed to the steric force provided by the surfactant, which stabilises the particles in suspension with different pH values. Therefore, 15 weight percent of poloxamer 105 is added into the formulation for nanoparticle preparation.

Table 7.1-2 Nanoparticles with different content of surfactant

Poloxamer 105 (W, %)	Particle sizes (nm) in water (pH 7.0)	PDI in water (pH 7.0)	Particle sizes (nm) in PBS (pH 7.4)	PDI in PBS (pH 7.4)
0	100.12 ± 1.67	0.087	1112.78 ± 130.67	0.612
10	112.52 ± 8.37	0.127	228.76 ± 13.64	0.235
15	108.78 ± 2.15	0.102	132.76 ± 1.96	0.112
20	178.52 ± 12.10	0.145	342.23 ± 26.34	0.225
30	224.52 ± 32.72	0.258	782.23 ± 54.34	0.516
50	523.23 ± 56.34	0.425	1042.23 ± 120.46	0.516

7.1.2 Particle sizes and surface charges

The nanoparticles prepared with irinotecan hydrochloride and curcumin with molar ratio 1:1 and 15% of poloxamer 105 under various conditions are characterised by DLS.

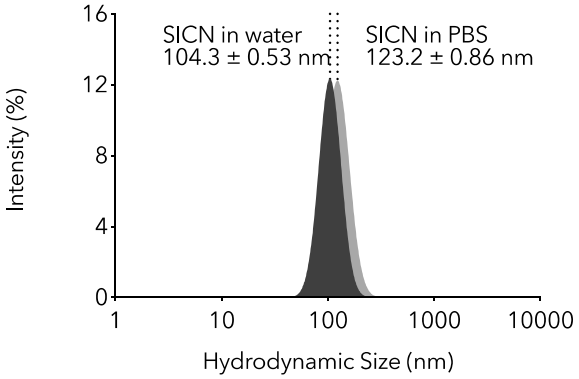

Figure 7.1-1 Size distribution of SICN in water and PBS (pH 7.4).

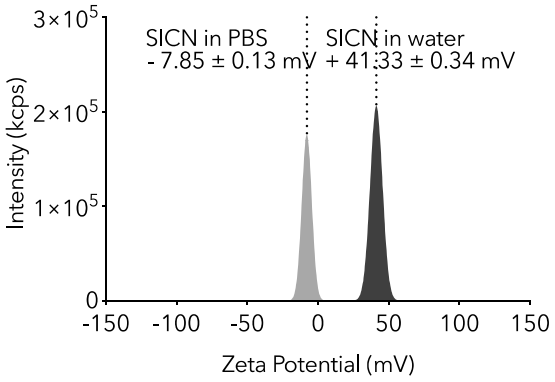

Figure 7.1-2 Surface charges of SICN in water and PBS (pH 7.4).

As can be seen, the average hydrodynamic size of SICN nanoparticles in water is around 100 nm and the surface charge is more than 40 mV. By changing the solvent from water to phosphate buffered saline (PBS, pH = 7.4), the hydrodynamic sizes of SICN nanoparticles increase to around 120 nm (*Figure 7.1-1*) while their surface charges decrease to about -10 mV (*Figure 7.1-2*). The particle sizes change little even though their absolute surface charges decrease by more than 80% in PBS, implying the strong stability of the nanoparticles. This should be attributed to the non-ionic surfactants which provide the nanoparticles additional steric repulsion to prevent them from aggregation[290] and make them become independent of environmental pH values and ionic strength.

Besides, the size distribution (*Figure 7.1-3*) and surface charges (*Figure 7.1-4*) of redispersed SICN nanoparticles in water keep almost the same compared to those before lyophilisation, demonstrating the good stability and redispersibility of the nanoparticles.

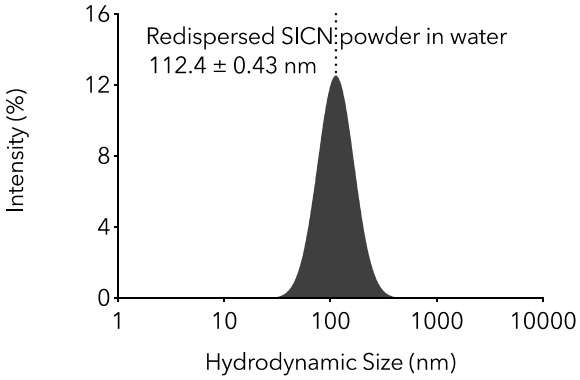

Figure 7.1-3 Size distribution of redispersed SICN powder in water.

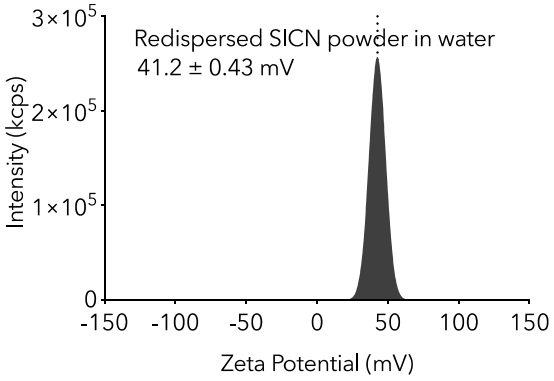

Figure 7.1-4 Surface charges of redispersed SICN powder in water.

The stabilised particle sizes and tuneable surface charges can benefit the drug self-delivery system by ameliorating their biodistribution and enhancing their passively targeted cellular internalisation. Nanoparticles with negative surface charges can be repulsed by the negatively charged cell membrane under normal physiological conditions, resulting in prolonged circulation times[291, 292] and facilitating tumour accumulation via enhanced permeability and retention (EPR) effect[231]. While the positively charged nanoparticles under neutral or acidic environments become efficient at cell penetration, leading to an improved accumulation in acidic tumour tissues[292]. Besides, compared to the commercial irinotecan hydrochloride injections (pH 3.5), the injectable SICN suspension with a pH value close to that of normal blood would reduce the side effects caused to blood vessels during injection and improve the compliance of patients.

7.1.3 Surface morphologies

The morphologies of evaporated SICN nanoparticles and their lyophilised powder with mannitol were observed using a scanning electron microscope (SEM).

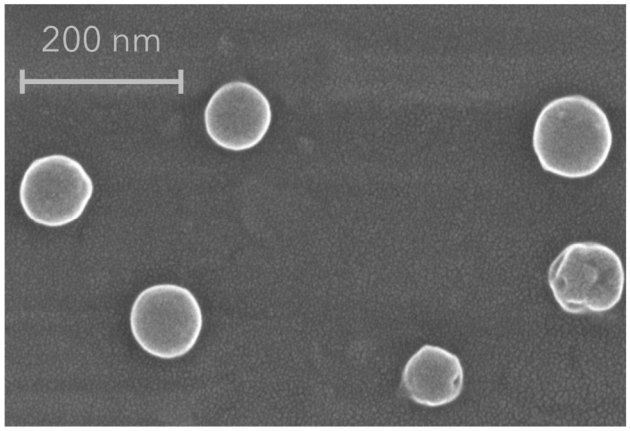

Figure 7.1-5 Surface morphologies of evaporated SICN.

For the evaporated SICN nanoparticles, spherical particles with smooth surfaces (*Figure 7.1-5*) are observed and their sizes are similar to those in suspension (around 100 nm). After lyophilisation with mannitol, we have observed only rod-like crystalline mannitol which has a much larger size than SICN nanoparticles (*Figure 7.1-6*).

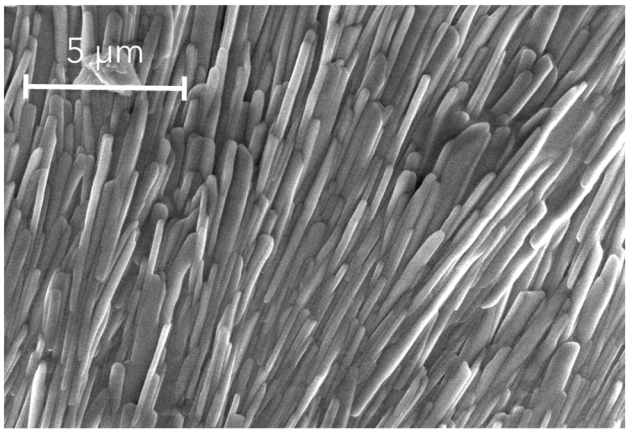

Figure 7.1-6 Surface morphologies of lyophilised SICN with mannitol.

7.1.4 Stability

The stability of SICN nanoparticles under various conditions was characterised by DLS. As shown in *Figure 7.1-7*, the particle sizes, surface charges and size distribution of SICN change little even though the concentration is as low as to about 10 μg/mL in suspension, implying their strong anti-dilution ability which is one of the key

parameters for intravenous injections because the injections would be firstly diluted by large volume of blood after being injected into vessels.

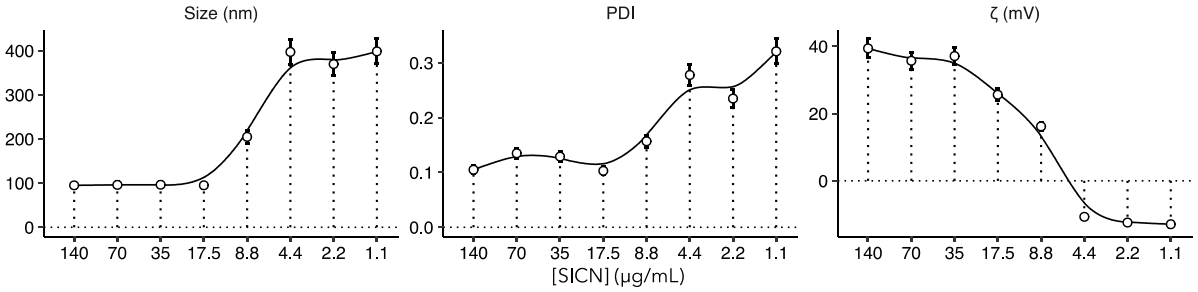

Figure 7.1-7 Anti-dilution ability of SICN nanoparticles.

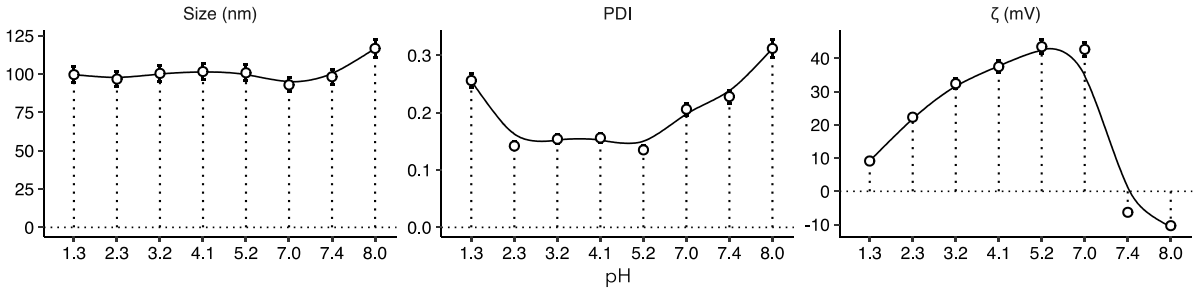

Figure 7.1-8 Physiochemical stability of SICN nanoparticles in water with different pH values.

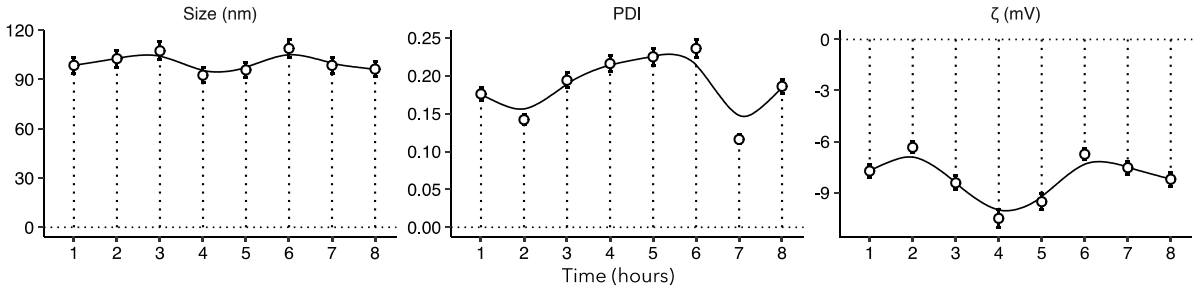

Figure 7.1-9 Storage stability of SICN nanoparticles in PBS (pH 7.4) at 37.5°C.

Besides, although the surface charges of SICN decrease with an increase of acidity in an acidic environment and the addition of alkaline buffer makes the surface charges become negative (*Figure 7.1-8*), the hydrodynamic sizes and size distribution of SICN stay the same with few changes, showing good physiochemical stability. In addition, SICN nanoparticles can keep stable in PBS (pH 7.4) at 37.5°C for up to 8 hours (*Figure 7.1-9*) although their absolute surface charges are less than 10 mV.

All the results evidence the strong stability of SICN nanoparticles under various conditions, which provides the nanoparticles with the probability of being intactly delivered to the targeted organs or tissues without collapse.

7.1.5 PXRD analysis

The PXRD analysis of lyophilised SICN powder and the components are exhibited in *Figure 7.1-10*.

As can be seen, the physical mixture of irinotecan hydrochloride and curcumin with molar ratio 1:1 (*Figure 7.1-10 c*) shows superimposed PXRD patterns of both irinotecan hydrochloride (*Figure 7.1-10 a*) and curcumin (*Figure 7.1-10 b*). Compared to its components (*Figure 7.1-10 a, b, e and f*), the lyophilised SICN powder (*Figure 7.1-10 d*) exhibits new peaks at 11.22°, 23.68°, 25.66°, 28.66° and 29.42°, indicating the formation of a novel crystal. By forming crystalline nanoparticles, not only could the water solubility be improved, but the lactone hydrolysis in irinotecan is also restricted by the strong order effect of crystalline lattices.

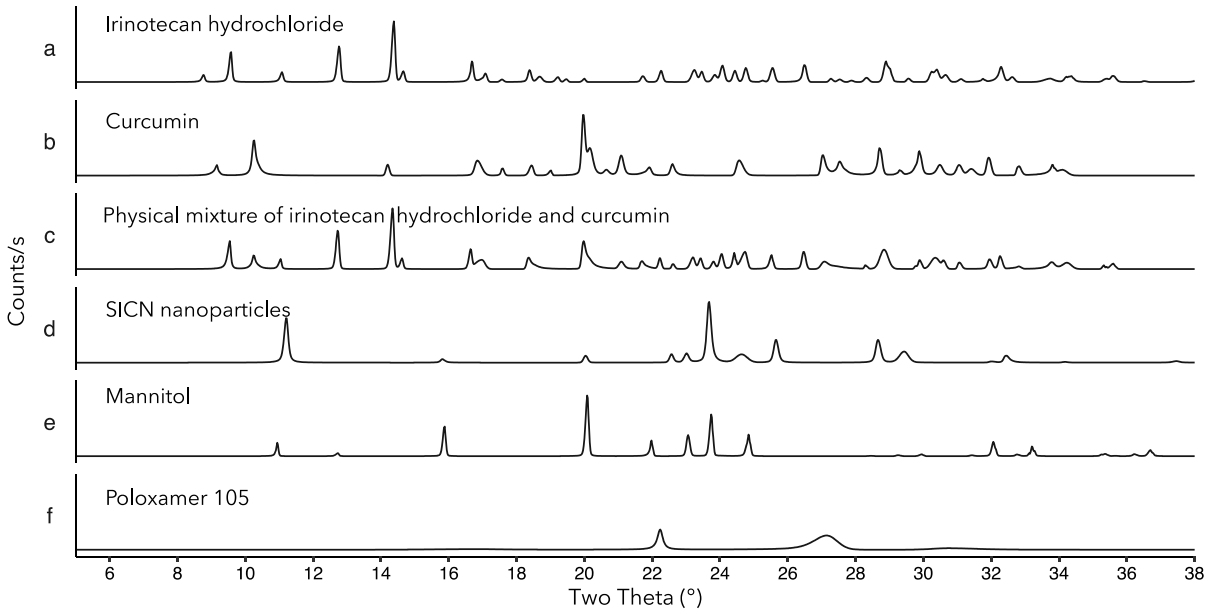

Figure 7.1-10 PXRD analysis of SICN nanoparticles and the components.

7.1.6 Melting behaviour

The melting behaviour of SICN nanoparticles and their components was characterised by DSC.

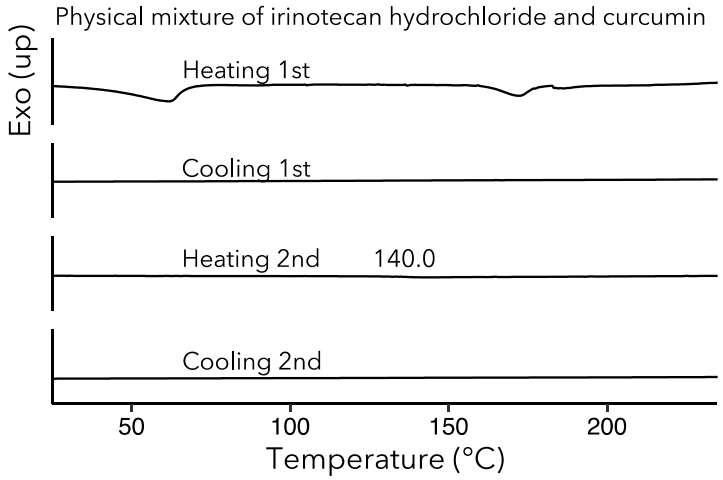

Figure 7.1-11 DSC analysis of irinotecan hydrochloride and curcumin mixture.

In the DSC profile of physical mixture of irinotecan hydrochloride and curcumin (*Figure 7.1-11*), the endothermic peak at about 177 °C in first heating run is attributed to the melting of curcumin crystals[293]. A glass transition state appears at about 140°C in the second heating run, suggesting that the two molecules are in an amorphous form after the first cooling from high temperature to room temperature. The DSC profile of poloxamer 105 in *Figure 7.1-12* reveals its amorphous status. There is a sharp endothermic peak at 166.5°C in the heating runs of lyophilised mannitol powder (*Figure 7.1-13*), which is attributed to the melting process of crystalline mannitol[294].

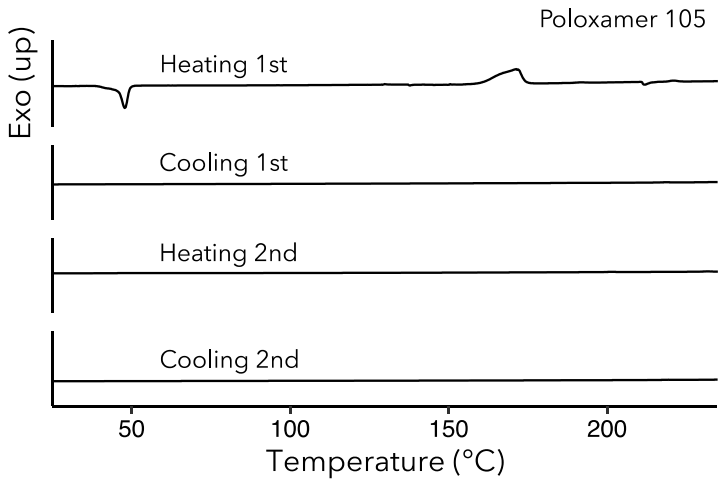

Figure 7.1-12 DSC profile of poloxamer 105.

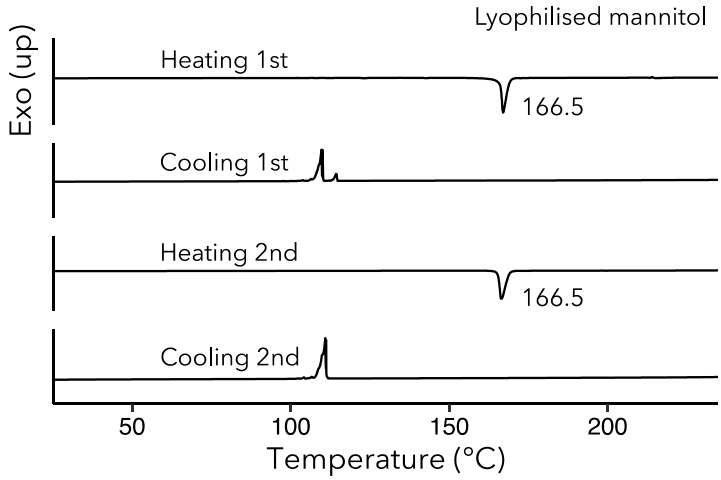

Figure 7.1-13 DSC profile of lyophilised mannitol.

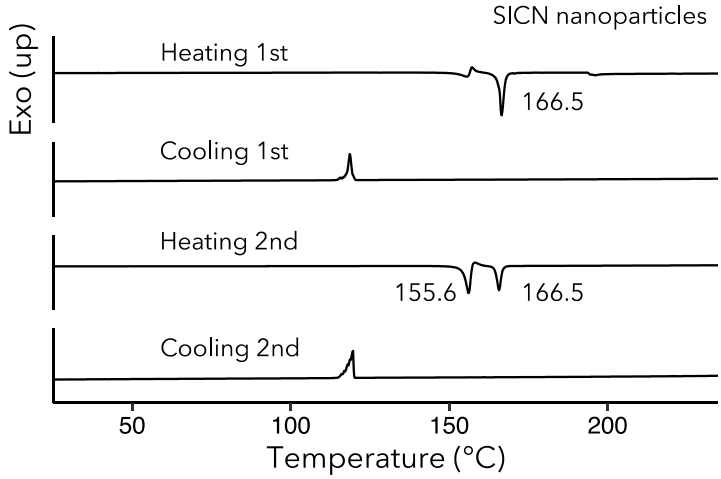

Figure 7.1-14 DSC profile of lyophilised SICN nanoparticles with mannitol.

The DSC profile of lyophilised SICN powder with mannitol in *Figure 7.1-14* displays a unique endothermic peak at 155.6°C except for the peak at 166.5°C, which should be attributable to the melting process of SICN powder. The unique endothermic peak at 155.6°C also implies the crystalline form of SICN nanoparticles.

7.2 Analytical Method based on HPLC

In order to determine the content of irinotecan hydrochloride and curcumin in the self-delivered nano system, a simple and precise analytical method is needed. Here an HPLC analytical method was developed.

7.2.1 Development of HPLC analytical method

Selection of solvents

Curcuminoids eluted with ACN and water containing 4% acetic acid are shown below (*Figure 7.2-1*). The detective wavelength for curcuminoids were set at 420 nm. When the ratio of ACN in the mobile phase decreases from 70% to 50%, three curcuminoids can be well separated and the retention time for bisdemethoxycurcumin, demethoxycurcumin and curcumin were 4.790 min, 5.100 min and 5.560 min, respectively. Besides, the resolutions of two adjacent peaks stand at 2.30 and 2.41, respectively. In addition, the asymmetry factor of 1.00 ± 0.10 demonstrates good symmetry of the chromatographic peaks.

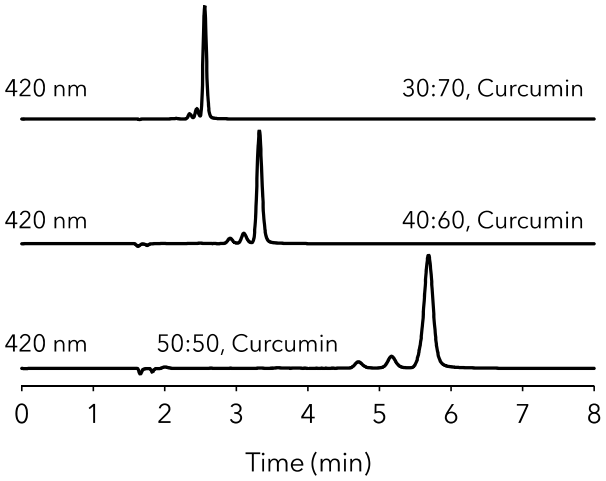

Figure 7.2-1 Curcuminoids eluted with ACN and water containing acetic acid

Irinotecan hydrochloride was also eluted with the same mobile phase and detected at 250 nm. However, as shown in Figure 7.2-2, a tailing peak with an asymmetric factor of 2.01 is observed. Adding DSP (0.002 mol/L) and SDS (0.08 mol/L) into water increases the retention time of irinotecan hydrochloride from 2.187 min. to 3.317 min., and the asymmetric factor decreases to an acceptable value of 1.16 [295]. The addition of DSP and SDS in the mobile phase keeps irinotecan hydrochloride in its neutral form and get rid of the peak tailing. Besides, adding salts does not affect the elution of curcuminoids, hence the mobile phase comprising 50% ACN and 50% water containing DSP (0.002 mol/L), SDS (0.08 mol/L), and acetic acid (4%, v/v) was chosen as the mobile phase for the simultaneous separation and quantification of irinotecan hydrochloride and three curcuminoids.

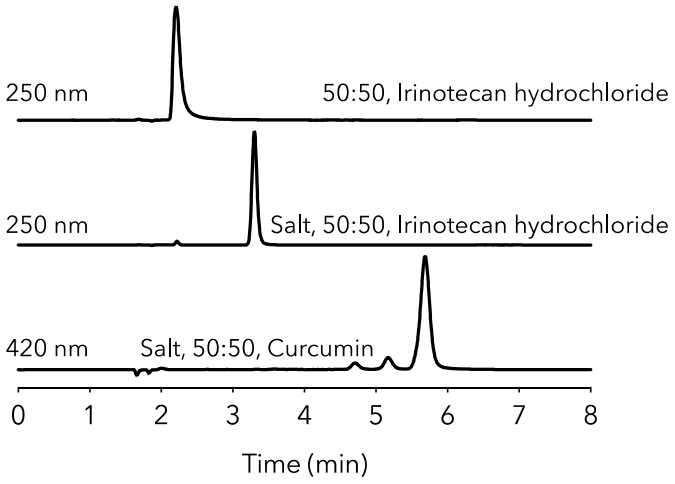

Figure 7.2-2 Chromatograms of irinotecan hydrochloride and curcuminoids

Selection of wavelength

The UV-Vis absorbance profiles of irinotecan hydrochloride and curcuminoids are shown in *Figure 7.2-3*. In order to obtain far more sensitivity and a high degree of precision, the maximum UV-Vis absorption at 256 nm and 424 nm were chosen to detect irinotecan hydrochloride and curcumin, respectively. Since overlap exists in the UV-Vis absorption spectra of irinotecan hydrochloride and curcumin, 379 nm was selected for detecting both irinotecan hydrochloride and curcumin in one chromatogram concurrently.

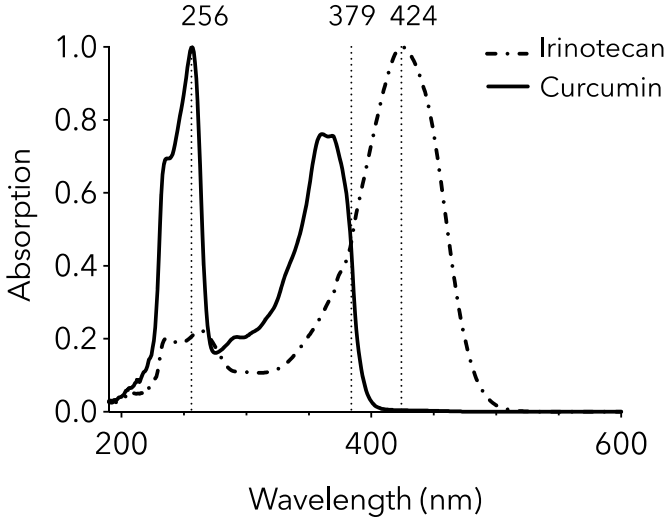

Figure 7.2-3 Selection of wavelengths for the analytical method

7.2.1 Validation of HPLC analytical method

System suitability test

An assay was performed in duplicate 6 times and the detection wavelength was set to 379 nm. The statistical results of the suitability study for the given system is displayed in *Table 7.2-1*.

Table 7.2-1 System suitıability results (379 nm, n = 6)

Parameters	Acceptable Criterion	Irinotecan	Bisdemethoxy-curcumin	Demethoxy-curcumin	Curcumin
Retention Time (min)	N.A.	3.317 ± 0.001	4.795 ± 0.002	5.100 ± 0.001	5.560 ± 0.001
Precision of Retention Time	RSD (%) ≤ 1%	0.03	0.00	0.02	0.02
Precision of Peak Area	RSD (%) ≤ 2%	0.63	0.62	0.96	0.68
Asymmetry factor (European Pharmacopoeia)	0.95 - 1.05	1.02 ± 0.01	1.03 ± 0.01	1.03 ± 0.01	1.01 ± 0.01
Plate number (N)	N ≥ 2000	9785 ± 67	11943 ± 102	11673 ± 83	12197 ± 67
Resolution (European Pharmacopoeia)	≥ 2.0	9.12	2.33	2.35	N.A.

Specificity

The chromatograms of the blank solution, irinotecan hydrochloride, curcumin, and the mixture at 256 nm, 424 nm, and 379 nm are given in *Figure 7.2-4*. Within these, each compound is verified as not interfering with one another.

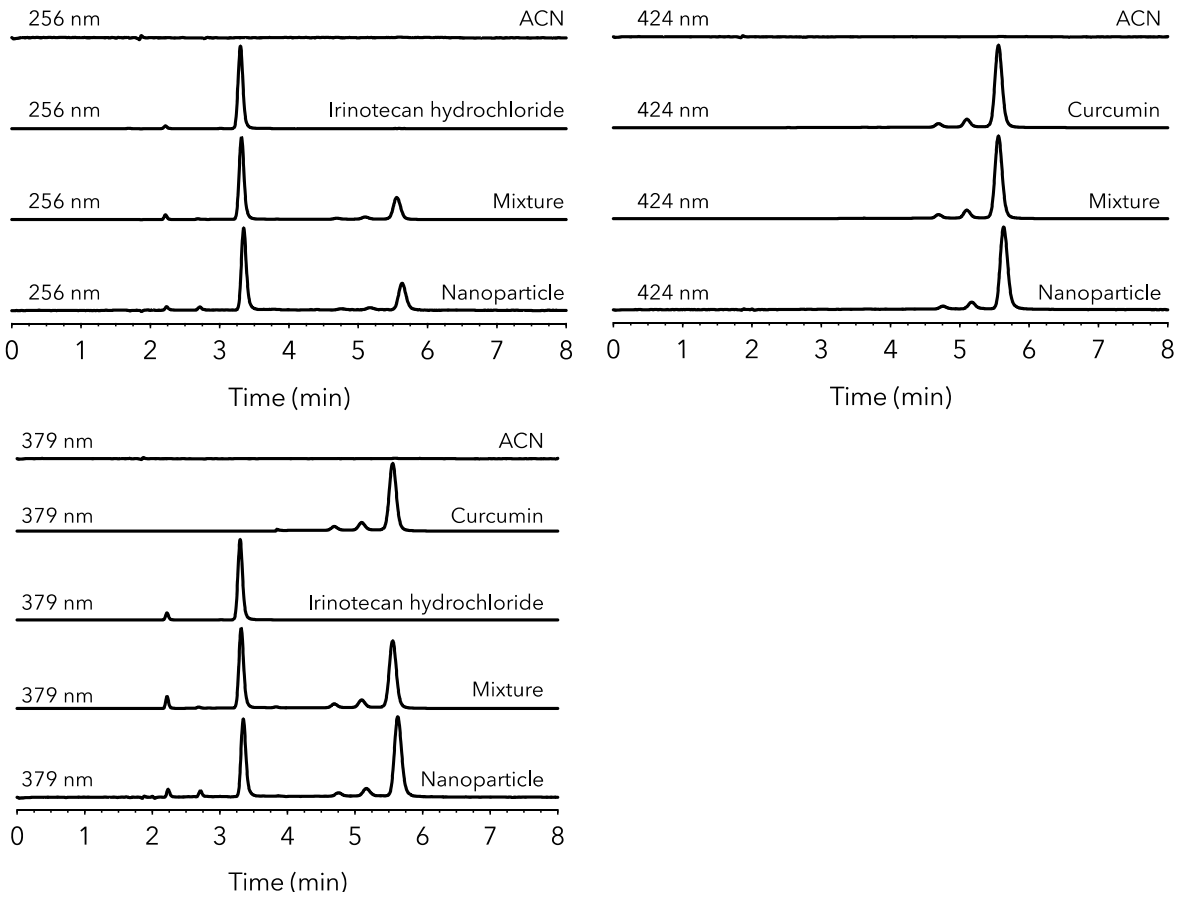

Figure 7.2-4 Specificity of the analytical method

Linearity and range

The assay for each standard was performed in duplicate 3 times and the representative chromatograms of irinotecan hydrochloride and curcuminoids detected at different wavelengths are shown below. The linearity of the detector response for the standards was analysed by least-square regression method and the regression equations for the calibration curves are also displayed in *Figure 7.2-5*. The results showed that the squares of the linear correlation coefficients (R^2) were above 0.999, indicating the good linearity of the calibration curves. ANOVA of regression showed that obtained F values ($F_{obtained}$) are far superior to the critical value ($F_{critical}$) ($F_{critical} << F_{obtained}$), which demonstrates that the linear regression is significant and the method is linear over the whole tested concentration range [296]. The validity of the assay was verified by means of ANOVA, which showed that there is linear regression with no deviation from linearity ($P < 0.001$) and can be used for the quantification of irinotecan hydrochloride and curcumin in the tested range.

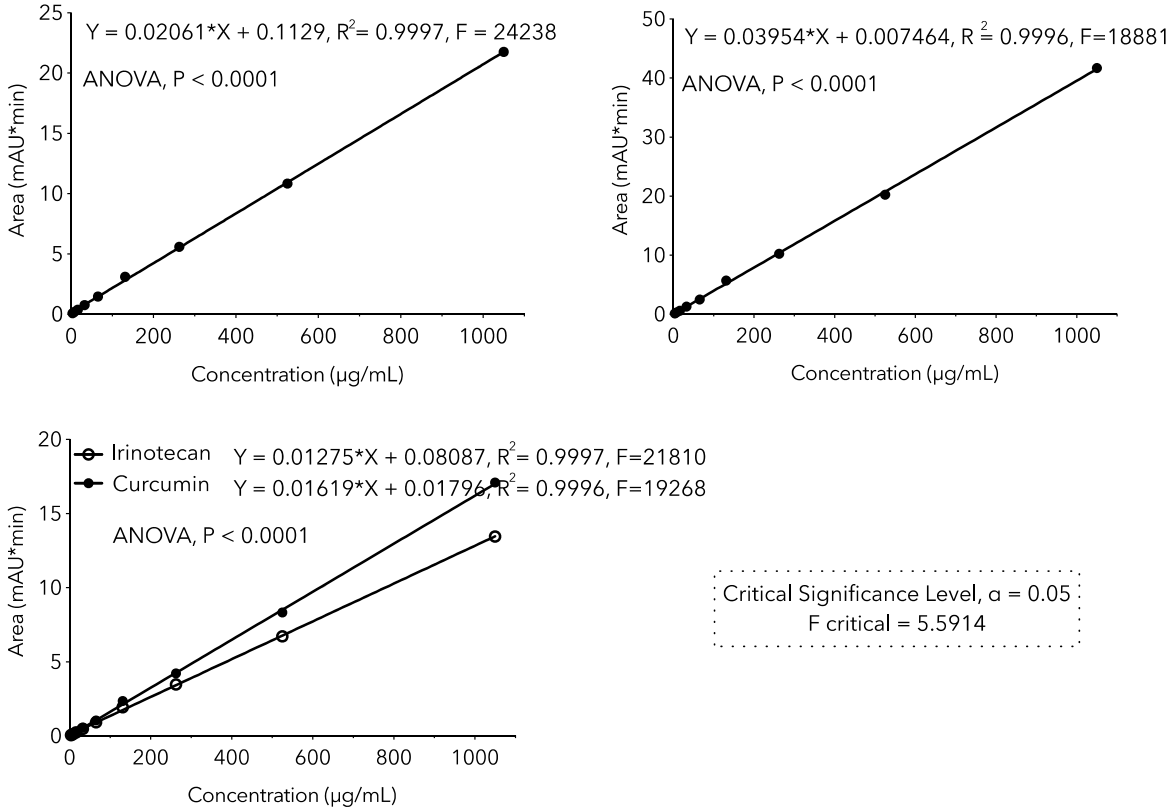

Figure 7.2-5 Linearity of the analytical method

In addition, the regression coefficients of equations at 256 nm and 424 nm, representing the rate of change of one variable (Y) as a function of change in the other (X), are larger than those at 379 nm, demonstrating the greater sensitivity of signal response when altering the concentration of the analytes.

Sensitivity

The calculated method *LODs* for irinotecan hydrochloride at 256 nm and curcumin at 424 nm equal 2.12 ng/mL and 4.94 ng/mL, respectively, hence are lower than those at 379 nm (6.26 ng/mL for irinotecan hydrochloride, 8.71 ng/mL for curcumin), indicating higher sensitivity. The LOQ value was taken as the lowest concentration of calibration curves that could be quantitatively measured, namely 2.05 µg/mL.

Accuracy

Table 7.2-2 details results on the accuracy of the analytical method. The overall recovery (%) determined by multiple analysis is within 101.07 ± 0.54, and the RSD values for the experimental data are less than 1%.

Table 7.2-2 Accuracy of the analytical method

Spike Level (μg/mL)	Measured Concentration (μg/mL) from ***ACN solution***				Measured Concentration (μg/mL) from ***Nanoparticle ACN solution***			
	Irinotecan	Curcumin	Irinotecan	Curcumin	Irinotecan	Curcumin	Irinotecan	Curcumin
30.00	30.18	30.97	30.16	30.22	30.47	30.46	30.25	30.21
	30.11	30.75	30.51	30.71	30.40	30.35	30.27	30.33
	30.19	30.72	30.39	30.44	30.52	30.52	30.64	30.55
RSD (%)	0.14	0.64	0.59	0.81	0.20	0.28	0.72	0.57
Recovery (%)	100.53 ± 0.15	101.82 ± 0.62	101.18 ± 0.59	101.52 ± 0.82	101.54 ± 0.20	101.48 ± 0.29	101.29 ± 0.73	101.21 ± 0.57
200.00	200.35	202.79	203.52	204.19	201.35	202.37	202.54	202.19
	201.53	202.54	203.98	203.53	202.42	200.31	203.9	202.53
	199.86	200.42	201.52	201.23	201.65	201.7	202.51	201.37
RSD (%)	0.43	0.64	0.64	0.77	0.27	0.52	0.39	0.30
Recovery (%)	100.29 ± 0.43	100.96 ± 0.65	101.50 ± 0.65	101.49 ± 0.78	100.90 ± 0.28	100.73 ± 0.53	101.49 ± 0.40	101.02 ± 0.30
500.00	501.52	502.18	503.33	500.14	502.72	501.86	503.76	501.44
	501.76	503.26	505.88	501.37	504.53	503.46	505.46	502.45
	502.49	501.68	500.12	503.34	503.71	502.24	503.98	504.43
RSD (%)	0.10	0.16	0.57	0.32	0.18	0.17	0.18	0.30
Recovery (%)	100.38 ± 0.10	100.47 ± 0.16	100.62 ± 0.58	100.32 ± 0.32	100.73 ± 0.18	100.50 ± 0.17	100.88 ± 0.18	100.55 ± 0.30

Accuracy acceptance criteria, recovery (%), 100 ± 2;

Precision

The precision of this analytical method describes the degree of accord between a series of data from an identical sample [297]. Such precision has been evaluated at three different levels, and the results of inter- and intra-day precision are expressed as RSD (in percent) of a statistically monumental number of experimental samples, as shown in *Table 7.2-3* and *Table 7.2-4*, respectively.

The values of RSD for validation of precision were found to be less than 1.0%, which demonstrates good agreement between the experimental data obtained from multiple analysis of the same sample.

Robustness

Table 7.2-5 details results for robustness under differing chromatographic conditions. The variations in column temperature, flow rate, and mobile phase ratio within given limits that were exhibited engendered mean recoveries (%) ranging between 98.0 and 102.0, while the maximum RSD (%) equalled 1.50, indicating it to be a sufficiently robust method.

Table 7.2-3 Intra-day precision of the analytical method

Spike Level (μg/mL)	Measured Concentration (μg/mL) from ***ACN solution***				Measured Concentration (μg/mL) from ***Nanoparticle ACN solution***			
	Irinotecan (256 nm)	Curcumin (424 nm)	Irinotecan (379 nm)	Curcumin (379 nm)	Irinotecan (256 nm)	Curcumin (424 nm)	Irinotecan (379 nm)	Curcumin (379 nm)
30.00	30.16 ± 0.04	30.81 ± 0.14	30.35 ± 0.18	30.46 ± 0.25	30.59 ± 0.18	30.45 ± 0.29	30.45 ± 0.22	30.36 ± 0.17
RSD (%) [a]	0.14	0.61	0.59	0.81	0.59	0.31	0.65	0.22
Recovery (%)	100.53 ± 0.15	101.82 ± 0.62	101.18 ± 0.59	101.52 ± 0.82	101.97 ± 0.59	101.50 ± 0.95	101.50 ± 0.72	101.20 ± 0.56
200.00	200.58 ± 0.86	201.92 ± 1.30	203.01 ± 1.31	202.98 ± 1.55	203.48 ± 1.15	202.13 ± 1.32	203.01 ± 1.50	202.98 ± 1.55
RSD (%) [a]	0.43	0.64	0.64	0.77	0.57	0.65	0.74	0.76
Recovery (%)	100.29 ± 0.43	100.96 ± 0.65	101.50 ± 0.65	101.49 ± 0.78	101.74 ± 0.57	101.07 ± 0.65	101.51 ± 0.74	101.49 ± 0.76
500.00	501.92 ± 0.51	502.37 ± 0.81	503.11 ± 2.89	501.62 ± 1.61	503.75 ± 1.19	504.97 ± 1.19	502.97 ± 2.19	502.37 ±1.58
RSD (%) [a]	0.10	0.16	0.57	0.32	0.24	0.24	0.44	0.31
Recovery (%)	100.38 ± 0.10	100.47 ± 0.16	100.62 ± 0.58	100.32 ± 0.32	100.75 ± 0.24	100.99 ± 0.24	100.59 ± 0.44	100.47 ± 0.31

[a] Triplicate for each injection; precision acceptance criteria, RSD less than 1% within each level.

Table 7.2-4 Inter-day precision of the analytical method

Spike Level (μg/mL)	Measured Concentration (μg/mL) from ***ACN solution***				Measured Concentration (μg/mL) from ***Nanoparticle ACN solution***			
	Irinotecan (256 nm)	Curcumin (424 nm)	Irinotecan (379 nm)	Curcumin (379 nm)	Irinotecan (256 nm)	Curcumin (424 nm)	Irinotecan (379 nm)	Curcumin (379 nm)
30.00	30.26 ± 0.04	30.21 ± 0.14	30.35 ± 0.18	30.25 ± 0.25	30.19 ± 0.09	30.25 ± 0.09	30.35 ± 0.19	30.26 ± 0.18
RSD (%) [a]	0.15	0.45	0.58	0.62	0.30	0.30	0.63	0.59
Recovery (%)	100.87 ± 0.15	100.70 ± 0.46	101.17 ± 0.57	100.83 ± 0.60	100.63 ± 0.31	100.83 ± 0.30	100.17 ± 0.63	100.87 ± 0.59
P [b] value	0.5471	0.3926	0.2937	0.2578	0.2598	0.3658	0.5478	0.5891
200.00	200.28 ± 0.85	201.72 ± 1.35	202.84 ± 2.42	203.98 ± 1.54	203.45 ± 1.17	201.76 ± 1.19	202.93 ± 1.99	203.47 ± 1.37
RSD (%) [a]	0.42	0.63	1.20	0.79	0.58	0.59	0.98	0.67
Recovery (%)	100.14 ± 0.43	100.86 ± 0.65	101.42 ± 1.23	101.99 ± 0.78	101.73 ± 0.58	100.88 ± 0.59	101.47 ± 0.98	101.74 ± 0.67
P [b] value	0.3651	0.3545	0.5642	0.4201	0.3564	0.6412	0.3574	0.2565
500.00	504.72 ± 0.50	503.57 ± 0.80	505.51 ± 2.90	503.52 ± 1.63	504.35 ± 1.20	501.55 ± 1.70	502.34 ± 2.90	503.46 ± 1.79
RSD (%) [a]	0.12	0.15	0.54	0.36	0.24	0.34	0.58	0.36
Recovery (%)	100.94 ± 0.12	100.71 ± 0.15	101.10 ± 0.58	100.70 ± 0.36	100.87 ± 0.24	100.31 ± 0.34	100.47 ± 0.59	100.69 ± 0.36
P [b] value	0.1471	0.2145	0.2345	0.2634	0.2547	0.1950	0.2314	0.2456

Table 7.2-5 Robustness under differing chromatographic conditions

Parameter	Modification	Mean Recovery (Triplicate for each injection)			
		Irinotecan (256 nm)	Curcumin (424 nm)	Irinotecan (379 nm)	Curcumin (379 nm)
Column temperature	37°C	99.55 ± 1.33	98.54 ± 1.12	99.32 ± 1.45	98.31 ± 1.71
	40°C	99.76 ± 0.73	101.01 ± 0.53	101.54 ± 0.73	100.43 ± 0.63
	43°C	99.26 ± 0.33	99.01 ± 0.53	99.54 ± 0.73	101.20 ± 0.63
	RSD (%)	0.25	1.32	1.22	1.50
Flow Rate	0.9 mL/min	99.47 ± 0.43	99.91 ± 0.67	99.84 ± 0.79	101.20 ± 0.13
	1.0 mL/min	99.76 ± 0.73	101.01 ± 0.53	101.54 ± 0.73	100.43 ± 0.63
	1.1 mL/min	99.86 ± 0.95	99.51 ± 0.43	99.58 ± 0.53	99.20 ± 0.93
	RSD (%)	0.20	0.78	1.06	1.01
Mobile Phase Ratio	50.5:49.5	98.86 ± 0.75	100.51 ± 0.63	101.58 ± 0.93	99.81 ± 0.43
	50:50	99.76 ± 0.73	101.01 ± 0.53	101.54 ± 0.73	100.43 ± 0.63
	49.5:50.5	99.36 ± 0.95	98.51 ± 0.43	99.78 ± 0.83	99.20 ± 0.74
	RSD (%)	0.45	1.32	1.02	0.62

7.3 *In vitro* Evaluation

7.3.1 Cytotoxicity on cells

The *in vitro* cytotoxicity and fluorescence-based cellular uptake efficiency of SICN nanoparticles under various environmental pH values were explored on HT-29 cells.

As shown in *Figure 7.3-1*, the half maximal inhibitory concentration (IC50) of irinotecan hydrochloride on HT-29 cells under normal environment (pH 7.4) is 15.25 μM. The IC50 of SICN nanoparticles on cells with environmental pH of 7.8, 7.4 and 6.5 are 0.278 mg/mL, 0.112 mg/mL and 0.019 mg/mL, equalling to 7.720 μM, 3.112 μM and 0.537 μM of irinotecan hydrochloride, respectively. Significant difference between groups at every dosage level is obtained ($p < 0.001$). Compared to the free irinotecan hydrochloride, the *in vitro* cytotoxicity of SICN is significantly improved by forming nanoparticles. Besides, the acidic environments could result in greater *in vitro* cytotoxicity of SICN on HT-29 cells than the alkaline condition because of the conversional positive surface charges of nanoparticles under tumour environments and the negative surface charges under normal physiological conditions.

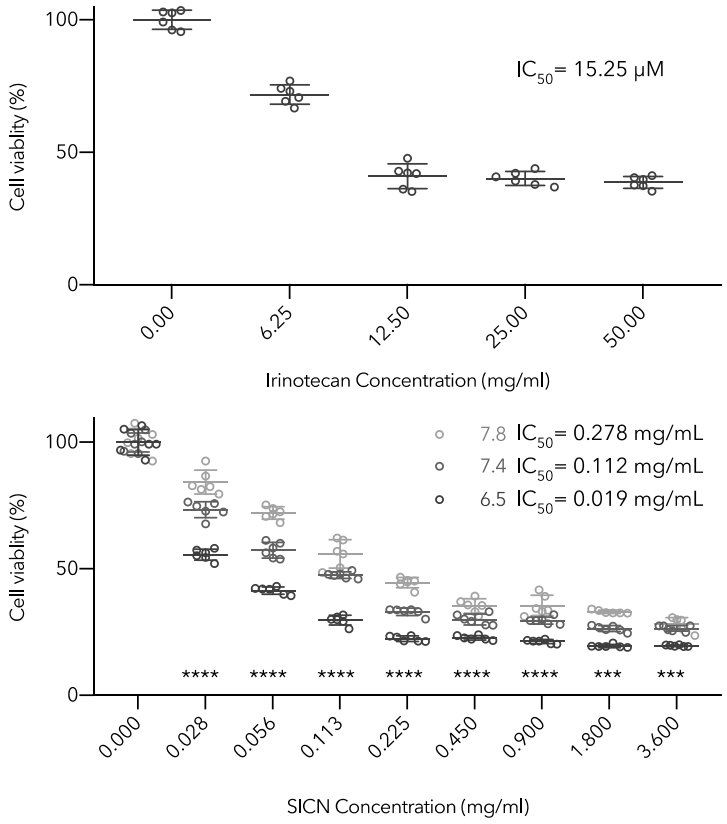

Figure 7.3-1 MTT assay of nanoparticles under different pH values

7.3.2 Fluorescence-based distribution and uptake

The fluorescence-based cellular uptake of SICN nanoparticles under different environmental pH values are shown in *Figure 7.3-2*. The blank group, namely cells under normal conditions without SICN nanoparticles, shows no fluorescence. For SICN groups, cells under acidic environments exhibit significantly stronger fluorescence than those in alkaline conditions ($p < 0.001$), demonstrating the higher uptake efficiency of SICN under tumour environments.

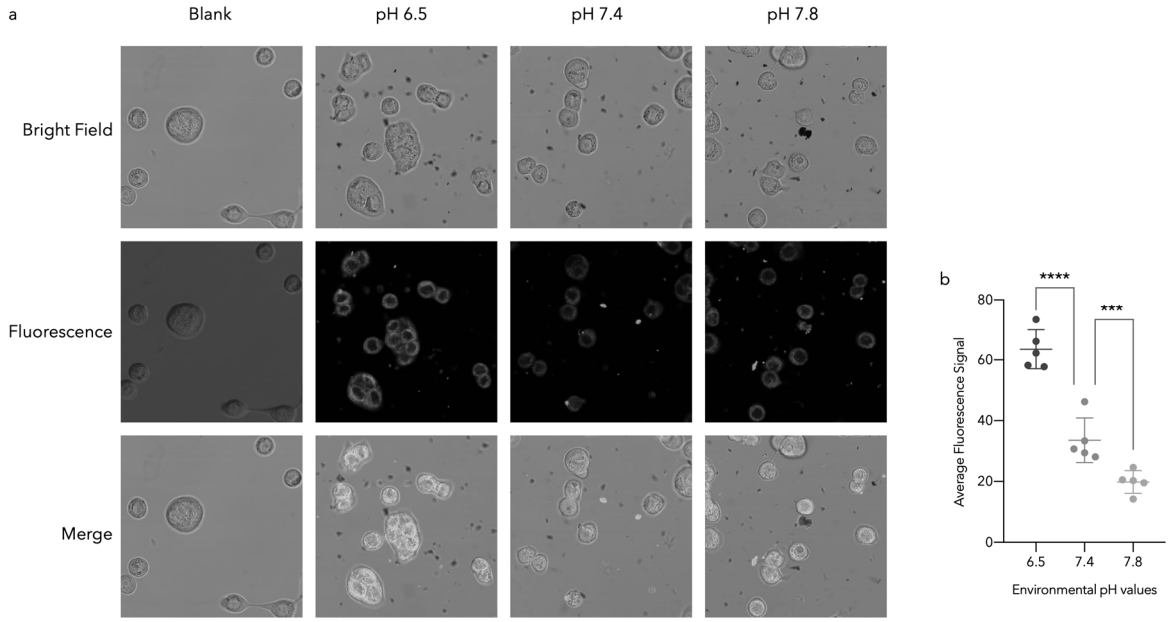

Figure 7.3-2 Fluorescence based uptake and distribution of nanoparticles

7.3.3 Internalisation pathways

The cellular internalization pathways of SICN nanoparticles on HT-29 cells were also tested by confocal laser scanning microscopy (*Figure 7.3-3*). From the statistical results, the cellular uptake of SICN nanoparticles is significantly blocked at 4°C, suggesting an energy-dependent internalization. Moreover, the cellular uptake is not affected by the macropinocytosis inhibitors (cytochalasin D and wortmannin), but significantly inhibited by the clathrin-mediated endocytosis inhibitor (chlorpromazine) and the caveolin inhibitors (genistein and methyl-β-cyclodextrin), indicating the SICN particles are at nano scale during internalization because nano-sized particles (smaller than 500 nm) are mainly endocytosed though clathrin- and caveolin-mediated endocytic pathways while micro-sized particles are internalized *via* macropinocytosis.

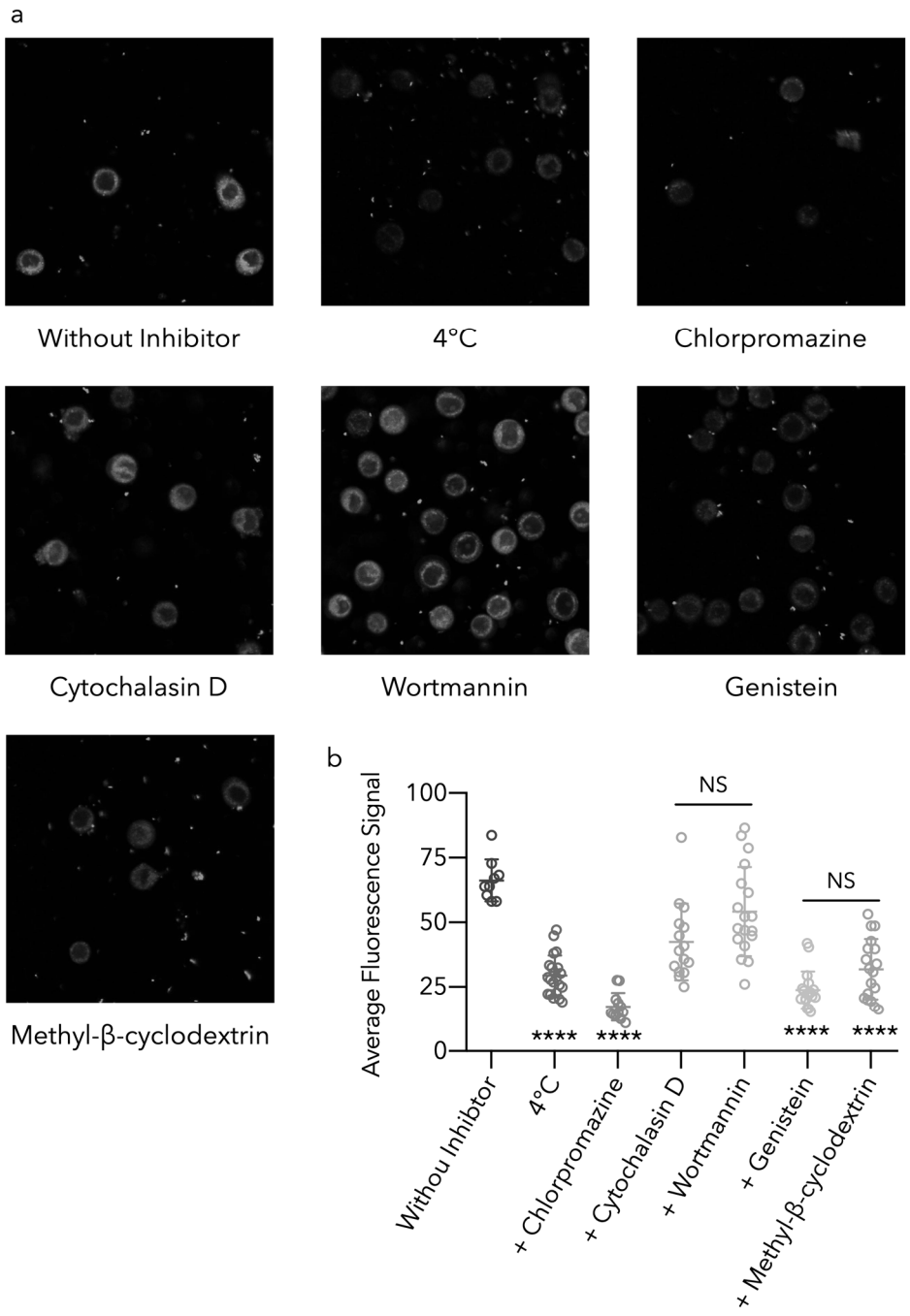

Figure 7.3-3 Cellular internalization pathways of nanoparticles

7.4 *In vivo* Therapeutic Efficacy and Biosafety

The anti-tumour effect of SICN nanoparticles was invested on HT-29 subcutaneous xenograft nude mice. The experimental strategy is illustrated in *Figure 7.4-1*. HT-29 cell suspension were injected into the flank of mice to establish the tumour model. The tumour bearing nude mice were intravenously injected with irinotecan hydrochloride, SICN nanoparticle or PBS every other day for consecutive 20 days and sacrificed after 5 days' discontinuation of medication.

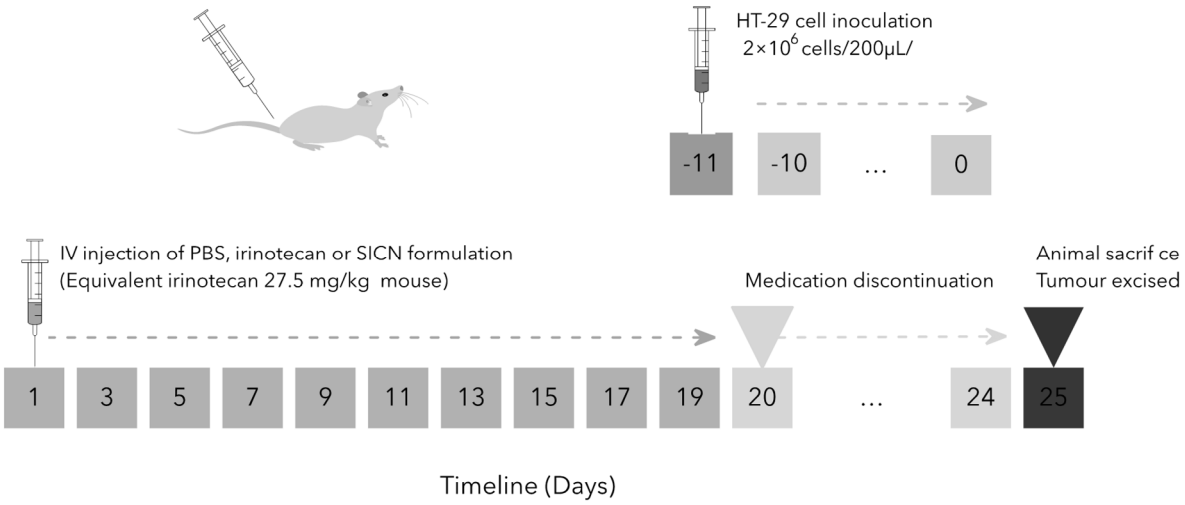

Figure 7.4-1 Experimental design of in vivo anti-tumour efficacy of SICN nanoparticles.

Compared to the PBS group, the average tumour volumes of mice in medication groups are effectively controlled and significant difference occurs on day 9 (around one week post first administration, *Figure 7.4-2*). While the tumour volumes of mice injected with PBS increase by more than 10 days after 20 days post administration.

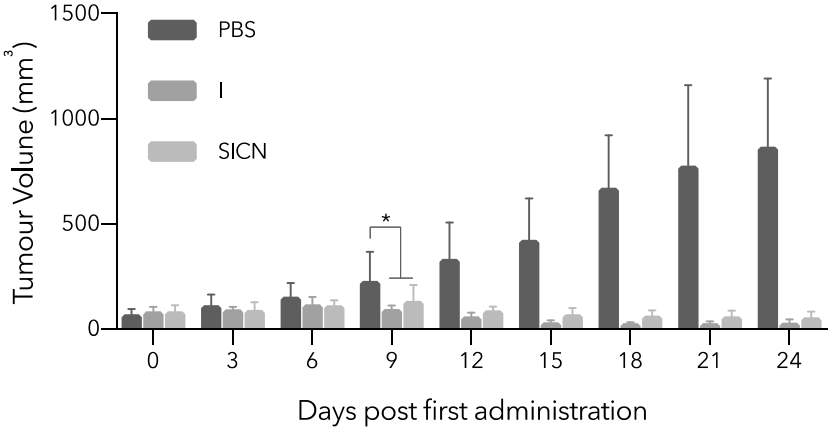

Figure 7.4-2 Tumour volume of mice injected with PBS, irinotecan hydrochloride (I) or SICN.

The regression of tumour volume in the medication groups occurs on day 15 (around two week post first administration, *Figure 7.4-3*), which means the tumour volume from the medication groups are even smaller than their original sizes, demonstrating the good *in vivo* anti-cancer effect of the nanoparticles.

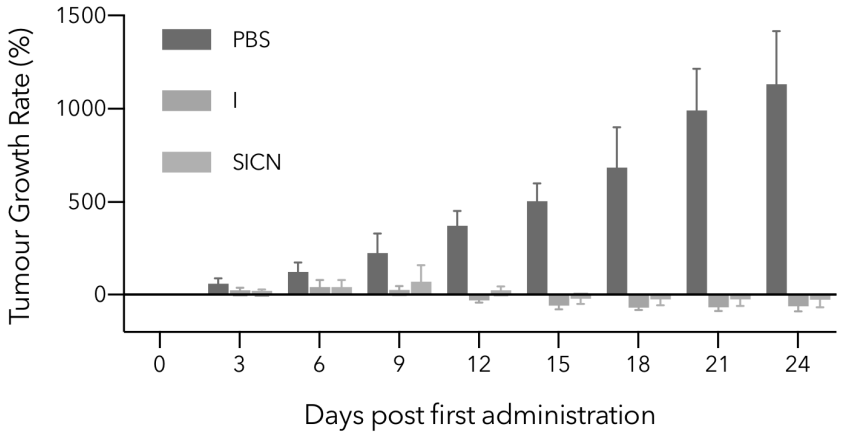

Figure 7.4-3 Tumour growth rate of mice injected with PBS, irinotecan hydrochloride (I) or SICN.

The average weight of tumour from PBS treated group is 0.5 g, as shown in *Figure 7.4-4*. Compared to the PBS treated group, the tumour weight of mice from medication group was significantly repressed ($p < 0.001$) and their average tumour weight is less than 0.1 g. The photography of the excised tumour from different groups is shown in *Figure 7.4-5*. The tumour size of mice from medication group is visually smaller than those from PBS group.

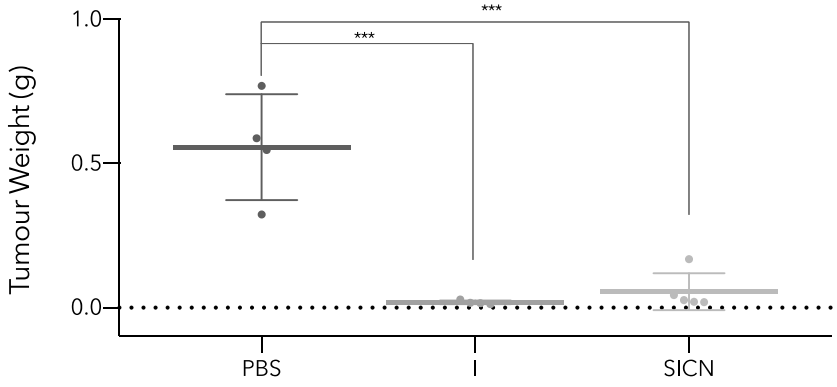

Figure 7.4-4 Tumour growth rate of mice injected with PBS, irinotecan hydrochloride (I) or SICN nanoparticles.

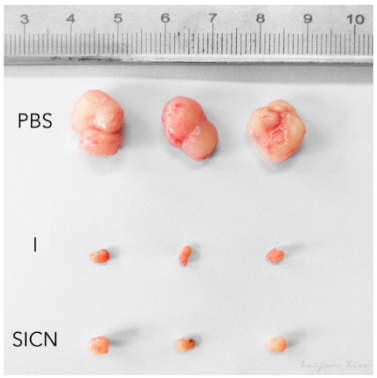

Figure 7.4-5 Tumour appearance from mice injected with PBS, irinotecan hydrochloride or SICN.

No statistical difference between the two medication groups occurs during the whole experiment. These results evidence that SICN is as equally effective in cancer treatment as free irinotecan hydrochloride and the tumour regression effect of SICN is caused by irinotecan instead of curcumin. This should be attributed to the significant difference in half maximal inhibitory concentration of the two molecules. Curcumin can be generally regarded as a biosafe molecule at this dosage level.

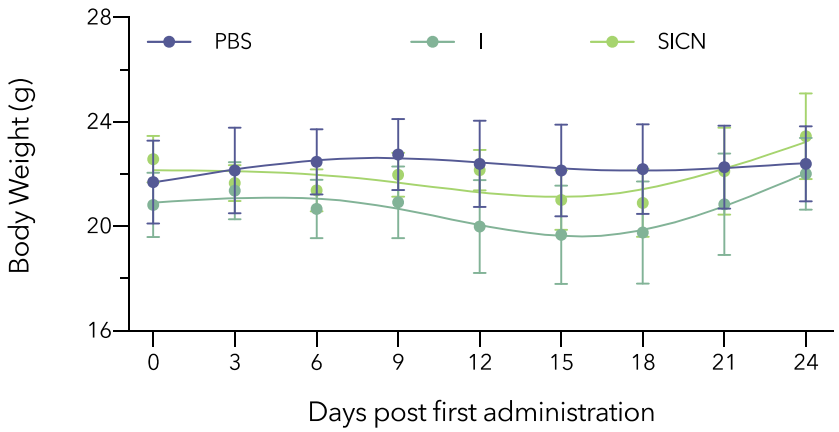

Figure 7.4-6 Body weight of mice injected with PBS, irinotecan hydrochloride or SICN.

During the whole experiment, no significant loss of body weight was observed in all mice, indicating the negligible side effects of SICN nanoparticles for cancer therapy at the employed dose (*Figure 7.4-6*).

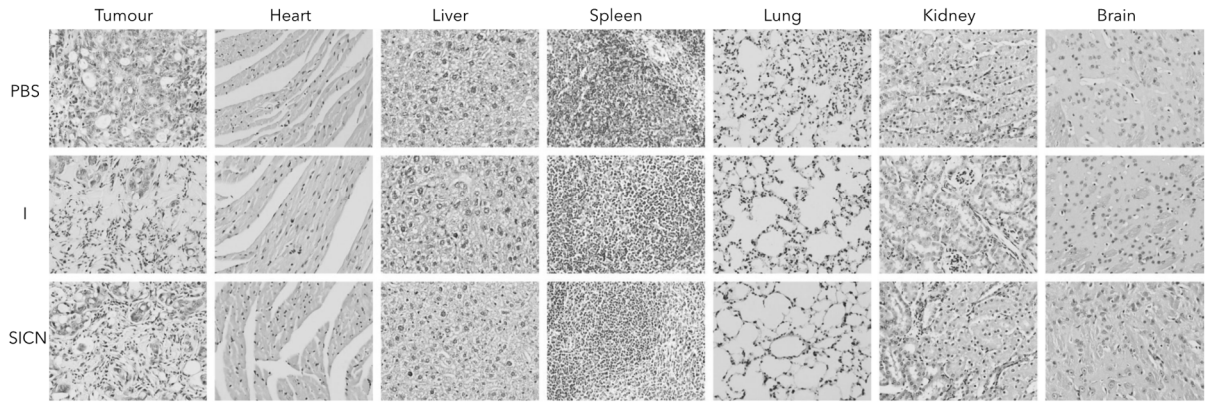

Figure 7.4-7 H&E staining images of tumour tissues from mice treated with PBS, irinotecan hydrochloride or SICN.

The H&E staining images of tumours and major organs from mice treated with PBS, free irinotecan or SICN are shown in *Figure 7.4-7*. Except for the glandular cavities, the H&E staining of colon cancer sections from the PBS group shows intact tumour cell structure. Cells exhibit distinct nuclei with a nearly spherical thin cytoplasmic region. H&E-stained sections of colon cancer from medication groups have distinct damage of tumour cell nuclei and distorted membranes surrounding necrotic tissues. However, compared to the PBS treated group, neither noticeable organ damage nor inflammation lesion can be observed in the medication groups, indicating the negligible organ dysfunction after being treated with SICN nanoparticles or irinotecan. All these results demonstrate that SICN exhibits high biosafety for cancer treatment presenting no significant side effects to the treated mice.

The diarrhoea severity score is shown in *Figure 7.4-8*. As can be seen, severe delayed diarrhoea in the mice treated with free irinotecan occurs on day 10 (10 days post first administration, $p < 0.01$) while no obvious diarrhoea is observed in PBS or SICN treated group during the whole experiment, demonstrating the presence of curcumin in the nano formulation could ameliorate the gut toxicity by alleviating diarrhoea in mice. This can be due to whether the protective effects of curcumin molecule[298] or the formulation changes of irinotecan with the help of curcumin.

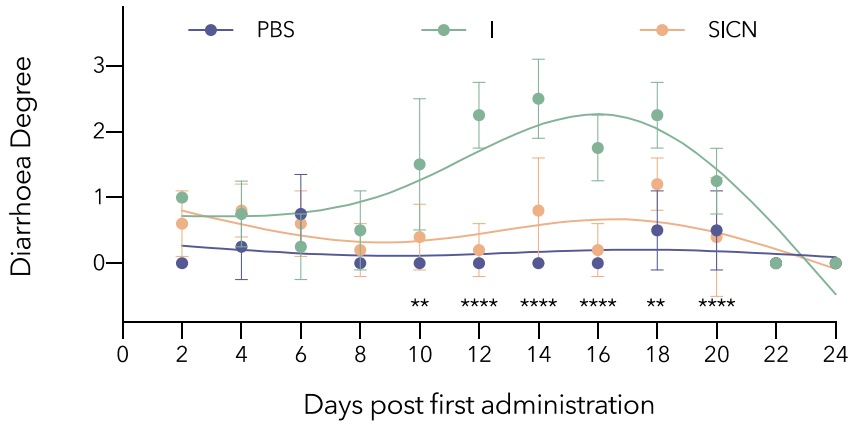

Figure 7.4-8 Diarrhoea degree of mice injected with PBS, irinotecan hydrochloride or SICN.

* significant difference between medication groups (**, $p < 0.01$; ***, $p < 0.001$; ****, $p < 0.0001$)

7.5 *Ex vivo* Biodistribution

The *ex vivo* biodistribution investigation is illustrated in *Figure 7.5-1*. Tumour bearing mice were sacrificed at different time post intravenously injection of irinotecan hydrochloride or SICN nanoparticle suspensions. The excised tissues were imaged immediately.

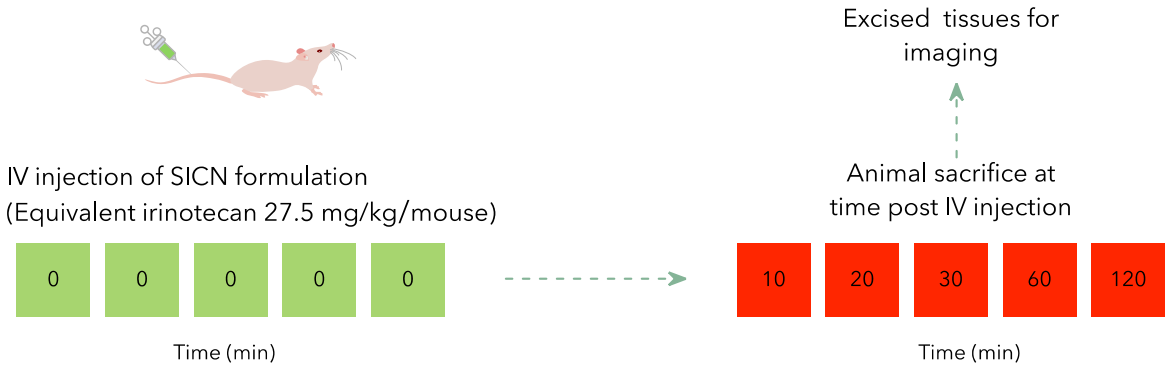

Figure 7.5-1 Experimental design of ex vivo distribution of SICN nanoparticles and irinotecan hydrochloride.

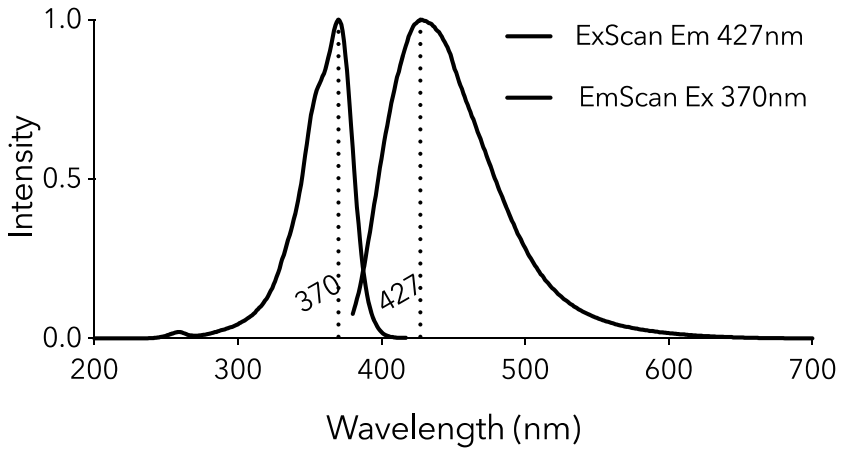

Figure 7.5-2 Normalised fluorescence spectra of irinotecan hydrochloride in DMSO containing 50% of water.

The normalised fluorescence spectra of SICN in PBS (*Figure 7.5-2*) and irinotecan hydrochloride in water containing 50% of DMSO (*Figure 7.5-3*) demonstrate that irinotecan in both forms shows similar fluorescence behaviour with an excitation maximum at around 370 nm and an emission maximum at about 430 nm.

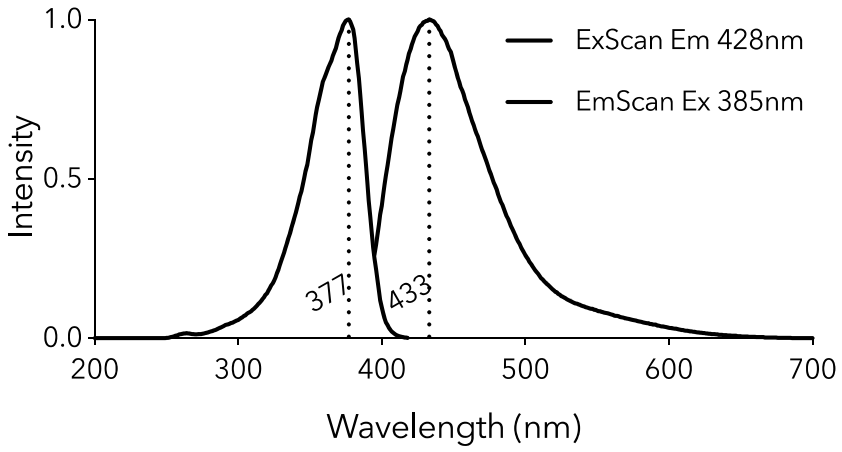

Figure 7.5-3 Normalised fluorescence spectra of SICN nanoparticles in PBS.

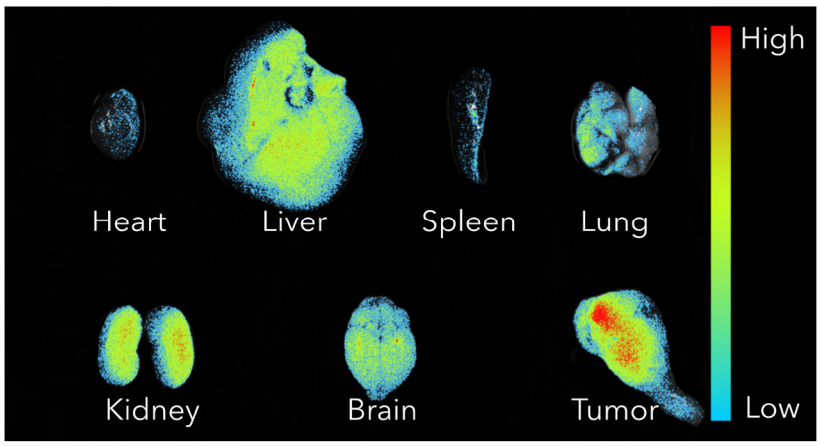

Figure 7.5-4 Fluorescence based biodistribution of irinotecan hydrochloride on ex vivo tissues.

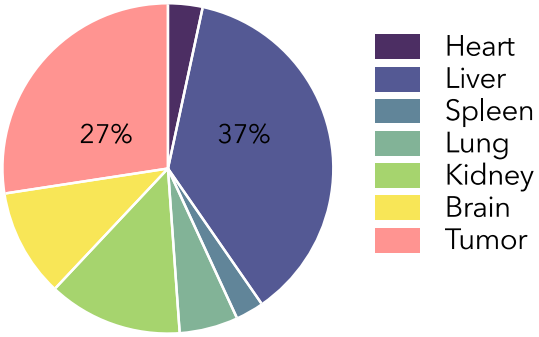

Figure 7.5-5 Relatively average fluorescence of irinotecan hydrochloride from ex vivo tissues.

The fluorescence based biodistribution of irinotecan hydrochloride on excised tissues are shown in *Figure 7.5-4*. Except for the high accumulation of irinotecan hydrochloride in tumour, a relatively higher biodistribution in liver can also be observed. The relatively average fluorescence signal on excised tissues are calculated in *Figure 7.5-5*. The relatively average fluorescence signal from tumour accounts for 27% while the signal from liver is 37%.

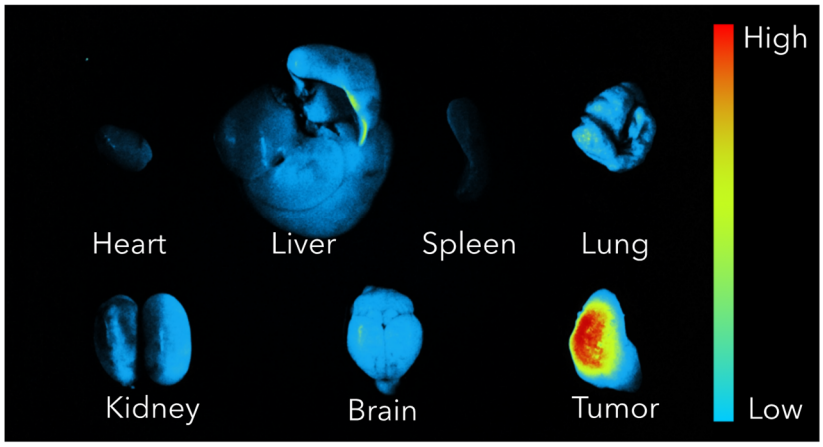

Figure 7.5-6 Fluorescence based biodistribution of SCIN nanoparticles on ex vivo tissues.

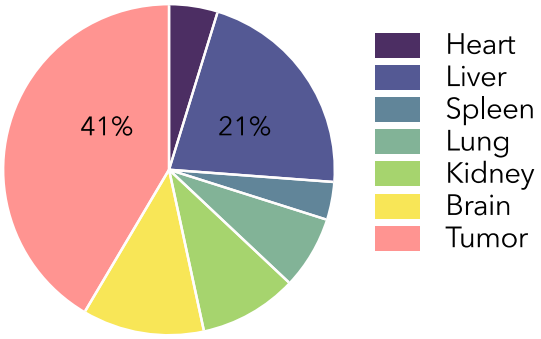

Figure 7.5-7 Relatively average fluorescence signal of SICN nanoparticles from ex vivo tissues.

Compared to irinotecan hydrochloride, a visually higher accumulation of SICN in tumour is observed (*Figure 7.5-6*) and its relatively average signal figures prominently (41% in *Figure 7.5-7*, around 50% larger than that of free irinotecan, 27% in *Figure 7.5-5*), indicating the improved passive tumour targeting of SICN.

Besides, the relative accumulation of SICN in liver is lower (21% in *Figure 7.5-7*) than that of free irinotecan (37% in *Figure 7.5-5*), which might also be one of the reasons that relieve the side effects of SICN nanoparticles.

Clinically, the severe diarrhoea caused by irinotecan is due to the biliary elimination and the subsequent micro-biome reactivation in intestines[299, 300]. Therefore, except for the protective effect of curcumin on intestines[298], the diarrhoea alleviation effect of SICN could also be attributable to the improved passive tumour

targeting, which relatively reduces their quick accumulation in liver and lessens the chances of being rapidly metabolised and excreted into intestines.

To further verify this, the relative accumulation of irinotecan and SICN in tissues including heart, liver, gallbladder, spleen, lung, kidney, brain, tumour and stomach & intestine at different time post intravenous injection were explored in *Figure 7.5-8*.

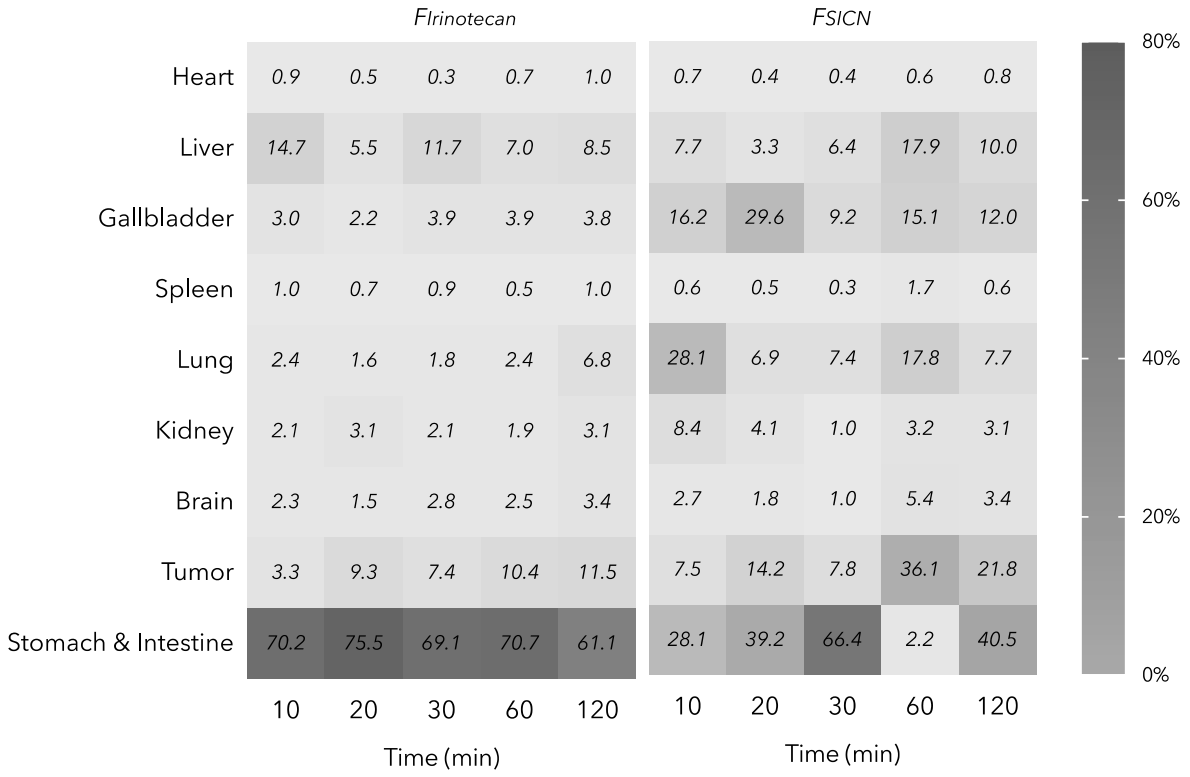

Figure 7.5-8 Heat map of relatively average signal of irinotecan hydrochloride and SICN nanoparticles on tissues within 120 min post intravenous injection.

The relatively average signals of irinotecan hydrochloride are mainly distributed in liver, tumour and stomach & intestine. The relative accumulation in liver decreases from around 15% at 10 minutes to about 8% at 2 hours post injection. The relative biodistribution in tumour increases from around 3% to 12% while the relative accumulation in stomach & intestine keep at about 70%.

However, except for the high accumulation in liver, tumour and stomach & intestine, high distribution of SICN in gallbladder and lung can also be observed. The relatively average signal increase rates of SICN compared to irinotecan hydrochloride within 120 min post intravenous injection are shown in *Figure 7.5-9*.

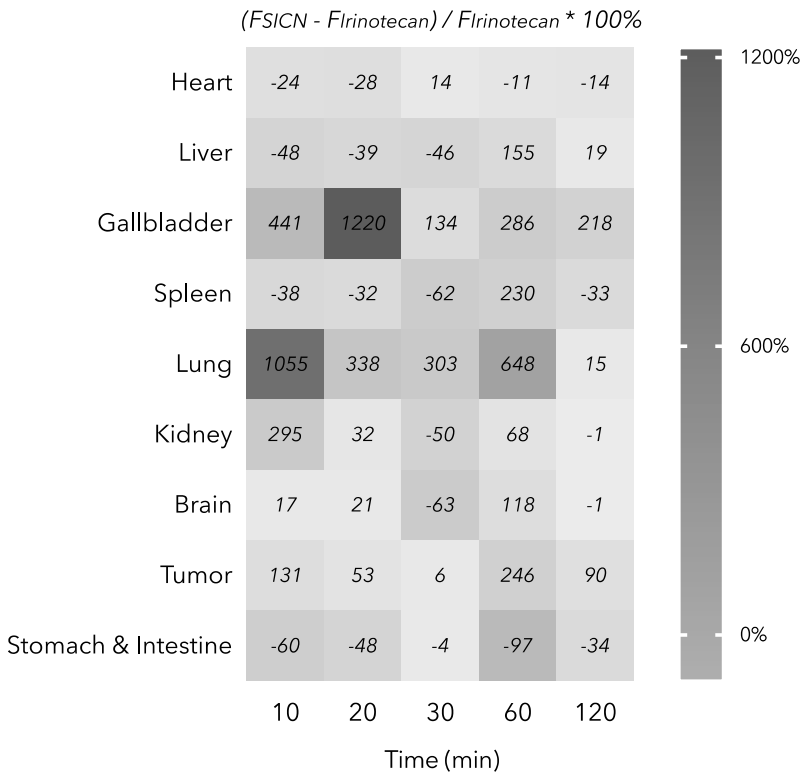

Figure 7.5-9 Heat map of relatively average signal increase rate of SICN compared to irinotecan within 120 min post intravenous injection.

Compared to irinotecan hydrochloride, the relative accumulation of SICN in liver and spleen decrease by around 50% during 30 min post injection, which could benefit the nanoparticles *via* escaping the rapid clearance by mononuclear phagocytic cells and prolonging their residence time in the body. Besides, their relative biodistribution in tumour increase by more than 50%, further evidencing their improved passive targeting due to the uniform nano sizes (EPR effect) and tuneable surface charges. In addition, their relative accumulation in stomach & intestine decrease by about 50%, which directly explains the diarrhoea eradication effect of SICN. More interestingly, the relative accumulation of SICN in gallbladder and lung increase by two or more times. It shows significantly improved accumulation in lung and prolonged residence time in gallbladder, which not only explains the reduced accumulation in stomach & intestine but also brings hope for the treatment of lung and gallbladder cancer and metastatic colorectal cancer.

8. CONCLUSIONS

In the present research project, a novel strategy has been proposed for the construction of drug self-delivery systems for targeted cancer therapy, which can be used for the co-delivery of curcuminoids and irinotecan hydrochloride without using any carriers.

The formulation of the nanoparticles is simply optimised by changing the ratios of the two drug molecules and the nanoparticles are prepared by a simple precipitation method which is suitable for industrial manufactory. These nanoparticles show stabilized particle sizes (100 nm) with mono distribution (PDI $\leqslant$ 0.2) under various conditions and conversional surface charges which increase from around −10 mV in a normal physiological condition (pH 7.4) to +40 mV under acidic tumour environments. The water solubility of curcuminoids is dramatically improved and the lactone hydrolysis of camptothecin derivatives is also restricted to keep their pharmacologically active forms. Besides, the formulation with a pH value close to that of normal blood would reduce the side effects caused to blood vessels and improve the patient compliance compared to commercial injections of camptothecin derivatives (pH 3.5).

A rapid and sensitive HPLC method has been developed and validated for the simultaneous determination of irinotecan hydrochloride and curcuminoids in the co-delivered nanoparticle system. More importantly, *in vivo* mice experiments have demonstrated that, compared to irinotecan itself, the co-delivered irinotecan curcumin nanoparticles exhibited dramatically enhanced lung and gallbladder targeting, improved macrophage-clearance escape and ameliorated colorectal cancer treatment with an eradication of life-threatening diarrhoea, exhibiting great promise for better targeted chemotherapy and clinical translation.

The future work about this research would be focused on the exploration of the inner structures and the forces between molecules in this nanoparticle system, which would be helpful for discovering more similar systems and expanding their potential applications in wider fields.

List of Figures

List of Tables

List of abbreviations

API	Active Pharmaceutical Ingredient
BCS	Biopharmaceutics Classification System
CT	Computed tomography
DDS	Drug Delivery Systems
DLS	Dynamic Light Scattering
DMSO	Dimethyl Sulfoxide
DSDS	Drug Self-Delivery Systems
EPR	Enhanced Permeability and Retention
FDA	The U.S. Food and Drug Administration
MDR	Multiple Drug Resistance
MR	Magnetic Resonance
PBS	Phosphate Buffered Saline
PCL	Polycaprolactone
PEG	Polyethylene Glycol
PET	Positron Emission Tomography
PG	Polyglycerol
PGA	Polyglycolic Acid
PLA	Polylactic Acid
PLGA	Polylactic-coglycolic Acid
PPG	Polypropylene Glycol
QD	Quantum Dots
RBC	Red Blood Cell
RES	Reticulo-Endothelial System
SEM	Scanning Electron Microscope
SICN	Surfactant stabilised irinotecan hydrochloride curcumin nanoparticles

Patents and Publications

Xiao, H., Sedlarik, V. Methods of making nanocrystals with enhanced biological availability and formulation for such nanocrystals preparation for use in anticancer therapy. (2019, WO)

Xiao, H.; Guo, Y.; Liu, H.; Liu, Y.; Wang, Y.; Li, C.; Císař, J.; Škoda, D.; Kuřitka, I.; Guo, L., Structure-based design of charge-conversional drug self-delivery systems for better targeted cancer therapy. Biomaterials 2020, 232, 119701. (IF: 10.317)

Xiao, H.; Sedlařík, V., A Rapid and Sensitive HPLC Method for Simultaneous Determination of Irinotecan Hydrochloride and Curcumin in Co-delivered Polymeric Nanoparticles. Journal of Chromatographic Science 2020. (IF: 1.28)

Xiao, H.; Fei, H, Y.; Li, C.; Sedlarik, V. Self-delivery and self-monitoring of charge-conversional topotecan curcumin nanoparticles for augmented cellular internalisation and enhanced chemotherapy. (To be submitted)

Conferences

Oral presentation on "Drug delivery systems for targeted cancer therapy", Bioengineering seminar series. (California, USA. Apr. 2020)

Oral presentation on "A drug self-delivery system for cancer therapy", 27th Poly-Char World Forum on Advanced Materials. (Naples, Italy. Oct. 2019)

Oral presentation on "Effects of X-shaped reduction-sensitive amphiphilic block copolymer on drug delivery", NewGen Conference - Hydrogel/Bio-mineralised Biomaterial for Bone Tissue Regeneration. (Zlin, Czech Republic, Oct. 2016)

Academic visit

Academic visitor at University of California, Merced, USA. "A drug self-delivery system for cancer treatment based on photodynamic therapy". (Mar. - May. 2020)

Academic visitor at Chengdu University of TCM, China. In vivo therapeutic effects of anti-cancer drugs on nude mice. ("HR Mobility", Mar. - Apr. 2019)

Curriculum Vitae

HAIJUN XIAO XIAO@URZ.ONE

ACADEMIC EDUCATION

2016 – 2020	Tomas Bata University in Zlin Doctoral study in Material Science and Engineering Emphases: Novel DRUG SELF-DELIVERY SYSTEMS
2013 – 2015	University of Macau M.S. in Chinese Medicinal Science
2009 – 2013	China Pharmaceutical University B.S. in Pharmaceutics

Research Interests

- Design and development of nano delivery systems for various applications, including diagnosis and treatment of diseases caused by cancer, viruses and microbial; Nanoparticles for Bio-imaging; Energy transformation for living systems;

RESEARCH EXPERIENCE

09.2016 – 09.2020	Doctoral Researcher at Centre of Polymer Systems (CPS), Tomas Bata University, focuses on novel drug delivery systems for cancer therapy.
03.2020 – 05.2020	Academic visitor to University of California, Merced, USA. A drug self-delivery system for cancer treatment based on photodynamic therapy.
03.2019	"HR Mobility" – Research experience in Chengdu, China. University of TCM. *In vivo* therapeutic effects of anti-cancer drugs on nude mice.
01.2017 – 12.2020	Internal Grant Agency of UTB (IGA/CPS/) Research team member.
2013 – 2015	"Effects of X-shaped reduction-sensitive amphiphilic block copolymer on drug delivery", with emphases on micellar self-assembled behaviour, physical stability, intracellular drug delivery efficiency and anticancer efficacy.

Bibliography

1. Wu, W., et al., *Transformations between co-amorphous and co-crystal systems and their influence on the formation and physical stability of co-amorphous systems.* Molecular Pharmaceutics, 2019. **16**(3): p. 1294-1304.
2. Takagi, T., et al., *A provisional biopharmaceutical classification of the top 200 oral drug products in the United States, Great Britain, Spain, and Japan.* Molecular Pharmaceutics, 2006. **3**(6): p. 631-643.
3. Shim, M.K., et al., *Carrier-free nanoparticles of cathepsin B-cleavable peptide-conjugated doxorubicin prodrug for cancer targeting therapy.* Journal of Controlled Release, 2018. **294**: p. 376-389.
4. Cheetham, A.G., et al., *Self-assembling prodrugs.* Chem. Soc. Rev., 2017. **46**(21): p. 6638-6663.
5. Cabral, H., et al., *Block Copolymer Micelles in Nanomedicine Applications.* Chemical Reviews, 2018. **118**(14): p. 6844-6892.
6. Alasvand, N., et al., *Therapeutic Nanoparticles for Targeted Delivery of Anticancer Drugs.* Multifunctional Systems for Combined Delivery, Biosensing and Diagnostics, 2017: p. 245-259.
7. Organization, W.H., *Latest global cancer data: Cancer burden rises to 18.1 million new cases and 9.6 million cancer deaths in 2018.* International Agency for Research on Cancer. Geneva: World Health Organization, 2018.
8. Torre, L.A., R.L. Siegel, and A. Jemal, *Lung Cancer Statistics.* Adv Exp Med Biol, 2016. **893**: p. 1-19.
9. DeSantis, C.E., et al., *Breast cancer statistics, 2017, racial disparity in mortality by state.* CA Cancer J Clin, 2017. **67**(6): p. 439-448.
10. Siegel, R.L., et al., *Colorectal cancer statistics, 2017.* CA Cancer J Clin, 2017. **67**(3): p. 177-193.
11. Balakrishnan, M., et al., *Changing Trends in Stomach Cancer Throughout the World.* Curr Gastroenterol Rep, 2017. **19**(8): p. 36.
12. Ward, E., et al., *Annual Report to the Nation on the Status of Cancer, 1999-2015, Featuring Cancer in Men and Women ages 20-49.* Journal of the National Cancer Institute, 2019.
13. Ahmad, S., et al. *AGEs, RAGEs and s-RAGE; friend or foe for cancer*. in *Seminars in cancer biology*. 2018. Elsevier.
14. Mattiuzzi, C., F. Sanchis-Gomar, and G. Lippi, *Measuring the potential impact of physical inactivity on worldwide epidemiology of colorectal and breast cancers.* Ann Cancer Epidemiol, 2019.
15. Bonassi, S. and M. Fenech, *Micronuclei and Their Association with Infertility, Pregnancy Complications, Developmental Defects, Anaemias, Inflammation, Diabetes, Chronic Kidney Disease, Obesity, Cardiovascular Disease, Neurodegenerative Diseases and Cancer*, in *The Micronucleus Assay in Toxicology*. 2019. p. 38-78.
16. Petrick, J.L., et al., *Tobacco, alcohol use and risk of hepatocellular carcinoma and intrahepatic cholangiocarcinoma: The Liver Cancer Pooling Project.* British journal of cancer, 2018. **118**(7): p. 1005-1012.
17. Lin, C., S. Franceschi, and G.M. Clifford, *Human papillomavirus types from infection to cancer in the anus, according to sex and HIV status: a systematic review and meta-analysis.* The Lancet Infectious Diseases, 2018. **18**(2): p. 198-206.
18. Collaborators, G.B.D.R.F., *Global, regional, and national comparative risk assessment of 79 behavioural, environmental and occupational, and metabolic risks or clusters of risks, 1990-2015: a systematic analysis for the Global Burden of Disease Study 2015.* Lancet, 2016. **388**(10053): p. 1659-1724.
19. Im, J.H., et al., *Surgery alone versus surgery followed by chemotherapy and radiotherapy in resected extrahepatic bile duct cancer: treatment outcome analysis of 336 patients.* Cancer research and treatment: official journal of Korean Cancer Association, 2016. **48**(2): p. 583.
20. Care, A., *Radiation therapy.* 2019.
21. Wagner, A.D., et al., *Chemotherapy for advanced gastric cancer.* Cochrane database of systematic reviews, 2017(8).

22. Ribas, A. and J.D. Wolchok, *Cancer immunotherapy using checkpoint blockade.* Science, 2018. **359**(6382): p. 1350-1355.
23. Chu, D.-T., et al., *Recent Progress of Stem Cell Therapy in Cancer Treatment: Molecular Mechanisms and Potential Applications.* Cells, 2020. **9**(3): p. 563.
24. Gd, M., et al., *Cancer treatment through hormone therapy and its relationship with Xerostomia and Hyposalivation.* 2020.
25. Lange, M.M., et al., *Urinary dysfunction after rectal cancer treatment is mainly caused by surgery.* British Journal of Surgery, 2008. **95**(8): p. 1020-1028.
26. Sinatra, R.S., J. Torres, and A.M. Bustos, *Pain management after major orthopaedic surgery: current strategies and new concepts.* JAAOS-Journal of the American Academy of Orthopaedic Surgeons, 2002. **10**(2): p. 117-129.
27. Bratzler, D.W., P.M. Houck, and S.I.P.G.W. Workgroup, *Antimicrobial prophylaxis for surgery: an advisory statement from the National Surgical Infection Prevention Project.* The American Journal of Surgery, 2005. **189**(4): p. 395-404.
28. Dayes, I.S., et al., *Long-term results of a randomized trial comparing iridium implant plus external beam radiation therapy with external beam radiation therapy alone in node-negative locally advanced cancer of the prostate.* International Journal of Radiation Oncology* Biology* Physics, 2017. **99**(1): p. 90-93.
29. Barbier, C.E., et al., *Selective internal radiation therapy in patients with progressive neuroendocrine liver metastases.* European journal of nuclear medicine and molecular imaging, 2016. **43**(8): p. 1425-1431.
30. Hodgkinson, G., et al., *Brachytherapy buttress*. 2018, Google Patents.
31. Mandel, S.J. and L. Mandel, *Radioactive iodine and the salivary glands.* Thyroid, 2003. **13**(3): p. 265-271.
32. Asadi, S., et al., *Gold nanoparticle-based brachytherapy enhancement in choroidal melanoma using a full Monte Carlo model of the human eye.* Journal of applied clinical medical physics, 2015. **16**(5): p. 344-357.
33. Mallick, S. and G.K. Rath, *Brachytherapy in Head and Neck Cancers*, in *Practical Radiation Oncology*. 2020, Springer. p. 117-120.
34. Demanes, D.J., *Head and Neck Brachytherapy*, in *Handbook of Image-Guided Brachytherapy*. 2017, Springer. p. 219-272.
35. Huo, J., et al., *Contemporary toxicity profile of breast brachytherapy versus external beam radiation after lumpectomy for breast cancer.* International Journal of Radiation Oncology* Biology* Physics, 2016. **94**(4): p. 709-718.
36. Brenneman, R.J., et al., *Favorable long-term toxicity for salvage low-dose rate prostate brachytherapy for recurrent prostate cancer after external beam radiotherapy from a phase II prospective trial (NRG Oncology/RTOG 0526).* Translational Andrology and Urology, 2019. **8**(Suppl 3): p. S265.
37. Jaber, T., et al., *Targeted therapy in advanced thyroid cancer to resensitize tumors to radioactive iodine.* The Journal of Clinical Endocrinology & Metabolism, 2018. **103**(10): p. 3698-3705.
38. Mai, T.K., et al., *Permanent radioactive I-125 seed implant technique in the treatment of prostate cancer.* 2017.
39. Sourati, A., A. Ameri, and M. Malekzadeh, *Acute side effects of radiation therapy*. 2017: Springer.
40. Jenkins, R.W., D.A. Barbie, and K.T. Flaherty, *Mechanisms of resistance to immune checkpoint inhibitors.* British journal of cancer, 2018. **118**(1): p. 9-16.
41. Tran, E., et al., *T-cell transfer therapy targeting mutant KRAS in cancer.* New England Journal of Medicine, 2016. **375**(23): p. 2255-2262.
42. Lee, J.Y., et al., *Structural basis of checkpoint blockade by monoclonal antibodies in cancer immunotherapy.* Nature communications, 2016. **7**(1): p. 1-10.
43. Sahin, U. and Ö. Türeci, *Personalized vaccines for cancer immunotherapy.* Science, 2018. **359**(6382): p. 1355-1360.

44. Popovic, A., E.M. Jaffee, and N. Zaidi, *Emerging strategies for combination checkpoint modulators in cancer immunotherapy.* The Journal of clinical investigation, 2018. **128**(8): p. 3209-3218.
45. Luen, S.J., et al., *Tumour-infiltrating lymphocytes and the emerging role of immunotherapy in breast cancer.* Pathology, 2017. **49**(2): p. 141-155.
46. June, C.H., et al., *CAR T cell immunotherapy for human cancer.* Science, 2018. **359**(6382): p. 1361-1365.
47. Maude, S.L., et al., *Tisagenlecleucel in children and young adults with B-cell lymphoblastic leukemia.* New England Journal of Medicine, 2018. **378**(5): p. 439-448.
48. Neelapu, S.S., et al., *Axicabtagene ciloleucel CAR T-cell therapy in refractory large B-cell lymphoma.* New England Journal of Medicine, 2017. **377**(26): p. 2531-2544.
49. Kimiz-Gebologlu, I., S. Gulce-Iz, and C. Biray-Avci, *Monoclonal antibodies in cancer immunotherapy.* Molecular biology reports, 2018. **45**(6): p. 2935-2940.
50. Kong, D.-H., et al., *A review of anti-angiogenic targets for monoclonal antibody cancer therapy.* International journal of molecular sciences, 2017. **18**(8): p. 1786.
51. Henriquez, C.M., et al., *Cancer Vaccines*, in *Cancer Immunotherapy and Biological Cancer Treatments*. 2019, IntechOpen.
52. Saxena, M. and N. Bhardwaj, *Re-emergence of dendritic cell vaccines for cancer treatment.* Trends in cancer, 2018. **4**(2): p. 119-137.
53. Carreno, B., et al., *Personalized cancer vaccines and methods therefor*. 2017, Google Patents.
54. Kohlhapp, F.J. and H.L. Kaufman, *Molecular pathways: mechanism of action for talimogene laherparepvec, a new oncolytic virus immunotherapy.* Clinical Cancer Research, 2016. **22**(5): p. 1048-1054.
55. Zahm, C.D., V.T. Colluru, and D.G. McNeel, *DNA vaccines for prostate cancer.* Pharmacology & therapeutics, 2017. **174**: p. 27-42.
56. Ott, P.A., et al., *An immunogenic personal neoantigen vaccine for patients with melanoma.* Nature, 2017. **547**(7662): p. 217-221.
57. Lipford, G.B. and C.M. Zepp, *Immune system modulators*. 2018, Google Patents.
58. Nguyen, R., et al., *The role of interleukin-2, all-trans retinoic acid, and natural killer cells: surveillance mechanisms in anti-GD2 antibody therapy in neuroblastoma.* Cancer Immunology, Immunotherapy, 2018. **67**(4): p. 615-626.
59. Shibuya, S., et al., *Acai Extract Increases the Red Blood Cell Population via Erythropoietin Upregulation in Mice*. 2020.
60. Cox, G.N., *Method to increase the number of circulating platelets by administering PEGylated cysteine variants of IL-11*. 2019, Google Patents.
61. Alsbou, M., et al., *Analysis of Antineoplastics, Immunomodulators, Antibiotics and Analgesics Adverse Drug Reactions Reports Submitted to the Pharmacovigilance Database in Jordan.* Biosciences Biotechnology Research Asia, 2017. **14**(2): p. 541.
62. Whitmore Jr, W.F., *Hormone therapy in prostatic cancer.* The American journal of medicine, 1956. **21**(5): p. 697-713.
63. Mørch, L.S., et al., *Hormone therapy and ovarian cancer.* Jama, 2009. **302**(3): p. 298-305.
64. Maguire, G., *Stem cell therapy without the cells.* Communicative & integrative biology, 2013. **6**(6): p. e26631.
65. Sittinger, M., et al., *Tissue engineering and autologous transplant formation: practical approaches with resorbable biomaterials and new cell culture techniques.* Biomaterials, 1996. **17**(3): p. 237-242.
66. Sirohi, B., et al., *The role of autologous transplantation in patients with multiple myeloma aged 65 years and over.* Bone marrow transplantation, 2000. **25**(5): p. 533-539.
67. Gupta, V., et al., *Comparison of Outcomes of Allogeneic Hematopoietic Cell Transplantation in Patients with Acute Myeloid Leukemia (AML) with Antecedent History of Philadelphia-Negative Myeloproliferative Neoplasm with De Novo AML and with AML Arising from Myelodysplastic*

Syndrome: A Study from the Center for International Blood and Marrow Transplant Research (CIBMTR). Biology of Blood and Marrow Transplantation, 2019. **25**(3): p. S107.
68. Cordonnier, C., et al., *Vaccination of haemopoietic stem cell transplant recipients: guidelines of the 2017 European Conference on Infections in Leukaemia (ECIL 7).* The Lancet Infectious Diseases, 2019.
69. Gibson, C.J., et al., *Clonal hematopoiesis associated with adverse outcomes after autologous stem-cell transplantation for lymphoma.* Journal of clinical oncology, 2017. **35**(14): p. 1598.
70. McCarthy, P.L., et al., *Lenalidomide maintenance after autologous stem-cell transplantation in newly diagnosed multiple myeloma: a meta-analysis.* Journal of Clinical Oncology, 2017. **35**(29): p. 3279.
71. DeVita, V.T. and E. Chu, *A history of cancer chemotherapy.* Cancer research, 2008. **68**(21): p. 8643-8653.
72. Moudi, M., et al., *Vinca alkaloids.* International journal of preventive medicine, 2013. **4**(11): p. 1231.
73. Chatterji, B.P., N.N. Bagban, and R.I. Bhavsar, *Microtubules as Anti-Cancer Drug Targets.* Topics in Anti-Cancer Research, 2017. **6**: p. 31.
74. Huang, C.-Y., et al., *A review on the effects of current chemotherapy drugs and natural agents in treating non–small cell lung cancer.* Biomedicine, 2017. **7**(4).
75. Fu, D., J.A. Calvo, and L.D. Samson, *Balancing repair and tolerance of DNA damage caused by alkylating agents.* Nature Reviews Cancer, 2012. **12**(2): p. 104-120.
76. Reimer, R.R., et al., *Acute leukemia after alkylating-agent therapy of ovarian cancer.* New England Journal of Medicine, 1977. **297**(4): p. 177-181.
77. Lajous, H., et al., *Rethinking alkylating (-like) agents for solid tumor management.* Trends in pharmacological sciences, 2019.
78. Kim, K.-W., et al., *Alkylating Anticancer Drugs*, in *Cancer Drug Discovery*. 2016, Springer. p. 71-94.
79. Berenblum, I., *The modifying influence of dichloro-ethyl sulphide on the induction of tumours in mice by tar.* The Journal of Pathology and Bacteriology, 1929. **32**(3): p. 425-434.
80. Haddow, A. and G. Timmis, *Bifunctional sulphonic acid esters with radiomimetic activity.* Acta-Unio Internationalis Contra Cancrum, 1951. **7**(3): p. 469-471.
81. Agnelli, G., et al., *Early onset life-threatening myelosuppression after low dose of intravesical thiotepa.* Postgraduate medical journal, 1982. **58**(680): p. 380-381.
82. Costa, M., et al., *N-acetylcysteine protects memory decline induced by streptozotocin in mice.* Chemico-biological interactions, 2016. **253**: p. 10-17.
83. Amdam, G., et al., *Proceedings of the National Academy of Science of the United States of America.* Social exploitation of vitellogenin, 2003. **100**: p. 1799-1802.
84. McNaught, A.D. and A. Wilkinson, *Compendium of chemical terminology*. Vol. 1669. 1997: Blackwell Science Oxford.
85. Kimball, D.B. and M.M. Haley, *Triazenes: a versatile tool in organic synthesis.* Angewandte Chemie International Edition, 2002. **41**(18): p. 3338-3351.
86. Blazevic, A., et al. *The effect of temozolomide on pancreatic neuroendocrine tumours and role of MGMT and MMR system in temozolomide resistance*. in *20th European Congress of Endocrinology*. 2018. BioScientifica.
87. Kaitin, K.I., et al., *The new drug approvals of 1990, 1991, and 1992: trends in drug development.* The Journal of Clinical Pharmacology, 1994. **34**(2): p. 120-127.
88. Damia, G. and M. D'lncalci, *Clinical pharmacokinetics of altretamine.* Clinical pharmacokinetics, 1995. **28**(6): p. 439-448.
89. Foye, W.O., *Foye's principles of medicinal chemistry*. 2008: Lippincott Williams & Wilkins.
90. Lee, C.R. and D. Faulds, *Altretamine.* Drugs, 1995. **49**(6): p. 932-953.
91. Tiwari, M., *Antimetabolites: Established cancer therapy.* Journal of Cancer Research & Therapeutics, 2012. **8**(4).
92. Champoux, J.J., *DNA topoisomerases: structure, function, and mechanism.* Annual review of biochemistry, 2001. **70**(1): p. 369-413.

93. Sordet, O., et al., *Apoptosis induced by topoisomerase inhibitors.* Current Medicinal Chemistry-Anti-Cancer Agents, 2003. **3**(4): p. 271-290.
94. Pommier, Y., *DNA topoisomerase I inhibitors: chemistry, biology, and interfacial inhibition.* Chemical reviews, 2009. **109**(7): p. 2894-2902.
95. Chen, J., H. Lin, and M. Hu, *Absorption and metabolism of genistein and its five isoflavone analogs in the human intestinal Caco-2 model.* Cancer chemotherapy and pharmacology, 2005. **55**(2): p. 159-169.
96. Baird, C.L., et al., *The ATPase reaction cycle of yeast DNA topoisomerase II slow rates of ATP Resynthesis and PiRELEASE.* Journal of Biological Chemistry, 2001. **276**(30): p. 27893-27898.
97. Marto, J., et al., *Ethosomes for enhanced skin delivery of griseofulvin.* Colloids and Surfaces B: Biointerfaces, 2016. **146**: p. 616-623.
98. Slobodnick, A., et al., *Update on colchicine, 2017*. Rheumatology, 2018. **57**(suppl_1): p. i4-i11.
99. Martino, E., et al., *Vinca alkaloids and analogues as anti-cancer agents: Looking back, peering ahead.* Bioorganic & medicinal chemistry letters, 2018. **28**(17): p. 2816-2826.
100. Furuse, K., et al., *Phase III study of concurrent versus sequential thoracic radiotherapy in combination with mitomycin, vindesine, and cisplatin in unresectable stage III non–small-cell lung cancer.* Journal of Clinical Oncology, 1999. **17**(9): p. 2692-2692.
101. Smith, I. and T. Powles, *Vindesine in the treatment of breast cancer.* Cancer chemotherapy and pharmacology, 1979. **2**(4): p. 261-262.
102. Retsas, S., K. Newton, and G. Westbury, *Vindesine as a single agent in the treatment of advanced malignant melanoma.* Cancer chemotherapy and pharmacology, 1979. **2**(4): p. 257-260.
103. Pfreundschuh, M., et al., *Lomustine, etoposide, vindesine, and dexamethasone (CEVD) in Hodgkin's lymphoma refractory to cyclophosphamide, vincristine, procarbazine, and prednisone (COPP) and doxorubicin, bleomycin, vinblastine, and dacarbazine (ABVD): a multicenter trial of the German Hodgkin Study Group.* Cancer treatment reports, 1987. **71**(12): p. 1203-1207.
104. Gökbuget, N. and D. Hoelzer, *Vindesine in the treatment of leukaemia.* Leukemia & lymphoma, 1997. **26**(5-6): p. 497-506.
105. Kim, J.O., et al., *Efficacy of Vinorelbine Monotherapy as Third-or Further-Line Therapy in Patients with Advanced Non-Small-Cell Lung Cancer.* Oncology, 2019. **97**(6): p. 356-364.
106. Harbeck, N., et al., *Afatinib plus vinorelbine versus trastuzumab plus vinorelbine in patients with HER2-overexpressing metastatic breast cancer who had progressed on one previous trastuzumab treatment (LUX-Breast 1): an open-label, randomised, phase 3 trial.* The Lancet Oncology, 2016. **17**(3): p. 357-366.
107. Madrid, E., et al., *Taxanes for advanced non-small cell lung cancer.* Cochrane Database of Systematic Reviews, 2018(7).
108. Lim, S.Y. and M.B. Bolster, *Corticosteroids*, in *Neurorheumatology*. 2019, Springer. p. 261-267.
109. Shirley, D.-A. and S. Moonah, *Fulminant amebic colitis after corticosteroid therapy: a systematic review.* PLoS neglected tropical diseases, 2016. **10**(7).
110. Hall, R., *Psychiatric adverse drug reactions: steroid psychosis.* Clin Advances Treatm Psychiatr Disord, 1991. **4**: p. 520-531.
111. Korte, S., *Corticosteroids in relation to fear, anxiety and psychopathology.* Neuroscience & Biobehavioral Reviews, 2001. **25**(2): p. 117-142.
112. Pretorius, E., *Corticosteroids, depression and the role of serotonin.* Reviews in the Neurosciences, 2004. **15**(2): p. 109-116.
113. Jaward, L.R., et al., *Differences in Adverse Effect Profiles of Corticosteroids in Palliative Care Patients.* American Journal of Hospice and Palliative Medicine®, 2019. **36**(2): p. 158-168.
114. Hasselgren, P.-O., et al., *Corticosteroids and muscle wasting role of transcription factors, nuclear cofactors, and hyperacetylation.* Current opinion in clinical nutrition and metabolic care, 2010. **13**(4): p. 423.

115. Simons, M.G., et al., *1185-P: Predictive Model for Hyperglycemic Events after High Dose Corticosteroid Administration*. 2019, Am Diabetes Assoc.
116. Borsi, S.H., et al., *The effects of inhaled corticosteroid on insulin sensitivity in asthmatic patients.* Monaldi Archives for Chest Disease, 2018. **88**(1).
117. Shao, L., et al., *New-Onset Diabetes Mellitus in Patients with Idiopathic Membranous Nephropathy Undergoing Tacrolimus and Low-Dose Corticosteroid Therapy.* Kidney and Blood Pressure Research, 2019. **44**(6): p. 1352-1362.
118. Zhang, L., S.O. Prietsch, and F.M. Ducharme, *Inhaled corticosteroids in children with persistent asthma: effects on growth.* Evidence-Based Child Health: A Cochrane Review Journal, 2014. **9**(4): p. 829-930.
119. Manimaran, V., *A Comparative Study on the Efficacy of inhaler Formulation of Fluticasone Propionate with Budesonide and Beclomethasone Dipropionate in Chronic Obstructive Pulmonary Disease*. 2016, KM College of Pharmacy, Madurai.
120. Chen, H., et al., *Nanonization strategies for poorly water-soluble drugs.* Drug discovery today, 2011. **16**(7-8): p. 354-360.
121. Paolino, D., et al., *Improvement of oral bioavailability of curcumin upon microencapsulation with methacrylic copolymers.* Frontiers in pharmacology, 2016. **7**: p. 485-485.
122. Mourtas, S., et al., *Curcumin-decorated nanoliposomes with very high affinity for amyloid-β1-42 peptide.* Biomaterials, 2011. **32**(6): p. 1635-1645.
123. Kawano, S.-i., et al., *Analysis of keto-enol tautomers of curcumin by liquid chromatography/mass spectrometry.* Chinese Chemical Letters, 2013. **24**(8): p. 685-687.
124. Manolova, Y., et al., *The effect of the water on the curcumin tautomerism: A quantitative approach.* Spectrochimica Acta Part A: Molecular and Biomolecular Spectroscopy, 2014. **132**: p. 815-820.
125. Tønnesen, H.H. and J. Karlsen, *Studies on curcumin and curcuminoids - VI. Kinetics of curcumin degradation in aqueous solution.* Zeitschrift für Lebensmittel-Untersuchung und -Forschung, 1985. **180**(5): p. 402-404.
126. Zebib, B., Z. Mouloungui, and V. Noirot, *Stabilization of curcumin by complexation with divalent cations in glycerol/water system.* Bioinorganic Chemistry and Applications, 2010. **2010**: p. 292760-292760.
127. Priyadarsini, K.I., *The chemistry of curcumin: From extraction to therapeutic agent.* Molecules (Basel, Switzerland), 2014. **19**(12): p. 20091-20112.
128. D'Archivio, A.A. and M.A. Maggi, *Investigation by response surface methodology of the combined effect of pH and composition of water-methanol mixtures on the stability of curcuminoids.* Food chemistry, 2017. **219**: p. 414-418.
129. Lee, W.-H., et al., *Curcumin and its derivatives: their application in neuropharmacology and neuroscience in the 21st century.* Current neuropharmacology, 2013. **11**(4): p. 338-378.
130. Stella, V.J. and K.W. Nti-Addae, *Prodrug strategies to overcome poor water solubility.* Advanced drug delivery reviews, 2007. **59**(7): p. 677-694.
131. Serajuddin, A.T., *Salt formation to improve drug solubility.* Advanced drug delivery reviews, 2007. **59**(7): p. 603-616.
132. Strickley, R.G., *Solubilizing excipients in oral and injectable formulations.* Pharmaceutical research, 2004. **21**(2): p. 201-230.
133. Prasad, D. and H. Chauhan, *Key targeting approaches for pharmaceutical drug delivery.* American Pharmaceutical Review, 2013. **16**(6).
134. Rajani, C., et al., *Cancer-targeted chemotherapy: Emerging role of the folate anchored dendrimer as drug delivery nanocarrier*, in *Pharmaceutical Applications of Dendrimers*. 2020, Elsevier. p. 151-198.
135. Öztürk-Atar, K., H. Eroğlu, and S. Çalış, *Novel advances in targeted drug delivery.* Journal of drug targeting, 2018. **26**(8): p. 633-642.
136. Wakaskar, R.R., *Passive and active targeting in tumor microenvironment.* International journal of drug development and research, 2017. **9**(2): p. 37-41.

137. Patel, J.K. and A.P. Patel, *Passive Targeting of Nanoparticles to Cancer*, in *Surface Modification of Nanoparticles for Targeted Drug Delivery*. 2019, Springer. p. 125-143.
138. Wang, R., et al., *pH-Controlled drug delivery with hybrid aerogel of chitosan, carboxymethyl cellulose and graphene oxide as the carrier.* International journal of biological macromolecules, 2017. **103**: p. 248-253.
139. Yu, F., et al., *Temperature-sensitive copolymer-coated fluorescent mesoporous silica nanoparticles as a reactive oxygen species activated drug delivery system.* International journal of pharmaceutics, 2018. **536**(1): p. 11-20.
140. Chi, Y., et al., *Redox-sensitive and hyaluronic acid functionalized liposomes for cytoplasmic drug delivery to osteosarcoma in animal models.* Journal of Controlled Release, 2017. **261**: p. 113-125.
141. Ojha, T., et al., *Pharmacological and physical vessel modulation strategies to improve EPR-mediated drug targeting to tumors.* Advanced drug delivery reviews, 2017. **119**: p. 44-60.
142. Colombo, M., et al., *Tumour homing and therapeutic effect of colloidal nanoparticles depend on the number of attached antibodies.* Nature communications, 2016. **7**(1): p. 1-14.
143. R Nogueira-Librelotto, D., et al., *Transferrin-conjugated nanocarriers as active-targeted drug delivery platforms for cancer therapy.* Current pharmaceutical design, 2017. **23**(3): p. 454-466.
144. Sun, Y., et al., *Peptide-Based Ligand for Active Delivery of Liposomal Doxorubicin.* Nano Life, 2016. **6**(03n04): p. 1642004.
145. Luo, Z., et al., *Precise glioblastoma targeting by AS1411 aptamer-functionalized poly (l-γ-glutamylglutamine)–paclitaxel nanoconjugates.* Journal of colloid and interface science, 2017. **490**: p. 783-796.
146. Lin, T., et al., *Self-assembled tumor-targeting hyaluronic acid nanoparticles for photothermal ablation in orthotopic bladder cancer.* Acta biomaterialia, 2017. **53**: p. 427-438.
147. Kue, C.S., et al., *Small molecules for active targeting in cancer.* Medicinal research reviews, 2016. **36**(3): p. 494-575.
148. Wang, H., et al., *Tunable fabrication of folic acid-Au@ poly (acrylic acid)/mesoporous calcium phosphate Janus nanoparticles for CT imaging and active-targeted chemotherapy of cancer cells.* Nanoscale, 2017. **9**(38): p. 14322-14326.
149. Wang, X., et al., *Phenylboronic acid-mediated tumor targeting of chitosan nanoparticles.* Theranostics, 2016. **6**(9): p. 1378.
150. Altun, I. and A. Sonkaya, *The Most Common Side Effects Experienced by Patients Were Receiving First Cycle of Chemotherapy.* Iranian journal of public health, 2018. **47**(8): p. 1218-1219.
151. Hu, Z.-Y., Q. Yu, and Y.-S. Zhao, *Dose-dependent association between UGT1A1* 28 polymorphism and irinotecan-induced diarrhoea: A meta-analysis.* European journal of cancer, 2010. **46**(10): p. 1856-1865.
152. Srinivasan, S.S., et al., *Design of a Precision Medication Dispenser: Preventing Overdose by Increasing Accuracy and Precision of Dosage.* IEEE journal of translational engineering in health and medicine, 2018. **6**: p. 1-6.
153. Nikolaou, M., et al., *The challenge of drug resistance in cancer treatment: a current overview.* Clinical & experimental metastasis, 2018. **35**(4): p. 309-318.
154. Konieczkowski, D.J., C.M. Johannessen, and L.A. Garraway, *A convergence-based framework for cancer drug resistance.* Cancer Cell, 2018. **33**(5): p. 801-815.
155. Gottesman, M.M., *Mechanisms of cancer drug resistance.* Annual review of medicine, 2002. **53**(1): p. 615-627.
156. Mansoori, B., et al., *The different mechanisms of cancer drug resistance: a brief review.* Advanced pharmaceutical bulletin, 2017. **7**(3): p. 339.
157. Huang, Y., *Pharmacogenetics/genomics of membrane transporters in cancer chemotherapy.* Cancer and Metastasis Reviews, 2007. **26**(1): p. 183-201.
158. Xiong, J., et al., *Tracing the structural evolution of eukaryotic ATP binding cassette transporter superfamily.* Scientific reports, 2015. **5**: p. 16724.

159. Chaudhary, P.M. and I.B. Roninson, *Expression and activity of P-glycoprotein, a multidrug efflux pump, in human hematopoietic stem cells.* Cell, 1991. **66**(1): p. 85-94.
160. Greaves, M. and C.C. Maley, *Clonal evolution in cancer.* Nature, 2012. **481**(7381): p. 306.
161. Tiwari, G., et al., *Drug delivery systems: An updated review.* International Journal of Pharmaceutical Investigation, 2012. **2**(1): p. 2-11.
162. Zong, A., H. Cao, and F. Wang, *Anticancer polysaccharides from natural resources: A review of recent research.* Carbohydrate polymers, 2012. **90**(4): p. 1395-1410.
163. Yang, J.-D., et al., *Method for producing water-insoluble polysaccharides.* 2005, Google Patents.
164. ASPINALL, G.O., *Classification of polysaccharides*, in *The polysaccharides.* 1983, Elsevier. p. 1-9.
165. Meyers, M.A., et al., *Biological materials: structure and mechanical properties.* Progress in Materials Science, 2008. **53**(1): p. 1-206.
166. Liu, Z., et al., *Polysaccharides-based nanoparticles as drug delivery systems.* Advanced drug delivery reviews, 2008. **60**(15): p. 1650-1662.
167. Chen, K., et al., *Fabrication of Doxorubicin-Loaded Glycyrrhetinic Acid-Biotin-Starch Nanoparticles and Drug Delivery Into HepG2 Cells In Vitro.* Starch-Stärke, 2019. **71**(3-4): p. 1800031.
168. Mohapatra, S., et al., *Doxorubicin loaded carboxymethyl Assam bora rice starch coated superparamagnetic iron oxide nanoparticles as potential antitumor cargo.* Heliyon, 2019. **5**(6): p. e01955.
169. Chen, S., et al., *Nano-micelles based on hydroxyethyl starch-curcumin conjugates for improved stability, antioxidant and anticancer activity of curcumin.* Carbohydrate polymers, 2020. **228**: p. 115398.
170. Hall, M.B., *Determination of starch, including maltooligosaccharides, in animal feeds: Comparison of methods and a method recommended for AOAC collaborative study.* Journal of AOAC International, 2008. **92**(1): p. 42-49.
171. Han, Y., et al., *pH-Sensitive tumor-targeted hyperbranched system based on glycogen nanoparticles for liver cancer therapy.* Applied Materials Today, 2020. **18**: p. 100521.
172. Zhou, J., et al., *Phospholipid-Decorated Glycogen Nanoparticles for Stimuli-Responsive Drug Release and Synergetic Chemophotothermal Therapy of Hepatocellular Carcinoma.* ACS Applied Materials & Interfaces, 2020. **12**(20): p. 23311-23322.
173. Deguchi, S., K. Tsujii, and K. Horikoshi, *Cooking cellulose in hot and compressed water.* Chemical Communications, 2006(31): p. 3293-3295.
174. Omidi, S., M. Pirhayati, and A. Kakanejadifard, *Co-delivery of doxorubicin and curcumin by a pH-sensitive, injectable, and in situ hydrogel composed of chitosan, graphene, and cellulose nanowhisker.* Carbohydrate Polymers, 2020. **231**: p. 115745.
175. El Hadrami, A., et al., *Chitosan in plant protection.* Marine drugs, 2010. **8**(4): p. 968-987.
176. Debode, J., et al., *Chitin mixed in potting soil alters lettuce growth, the survival of zoonotic bacteria on the leaves and associated rhizosphere microbiology.* Frontiers in microbiology, 2016. **7**: p. 565.
177. Tzoumaki, M.V., et al., *Oil-in-water emulsions stabilized by chitin nanocrystal particles.* Food hydrocolloids, 2011. **25**(6): p. 1521-1529.
178. Ding, X., et al., *A pH/ROS-responsive, tumor-targeted drug delivery system based on carboxymethyl chitin gated hollow mesoporous silica nanoparticles for anti-tumor chemotherapy.* Carbohydrate Polymers, 2020: p. 116493.
179. Srivastava, P. and R. Malviya, *Sources of pectin, extraction and its applications in pharmaceutical industry– An overview.* 2011.
180. Kim, W., et al., *Optimization of narirutin extraction during washing step of the pectin production from citrus peels.* Journal of Food Engineering, 2004. **63**(2): p. 191-197.
181. Garna, H., et al., *Effect of extraction conditions on the yield and purity of apple pomace pectin precipitated but not washed by alcohol.* Journal of Food Science, 2007. **72**(1): p. C001-C009.
182. Sundar Raj, A., et al., *A review on pectin: Chemistry due to general properties of pectin and its pharmaceutical uses.* Scientific reports, 2012. **1**: p. 550-1.

183. Cheewatanakornkool, K., et al., *Thiolated pectin–doxorubicin conjugates: Synthesis, characterization and anticancer activity studies.* Carbohydrate polymers, 2017. **174**: p. 493-506.
184. Jayaseelan, C., et al., *Green synthesis of gold nanoparticles using seed aqueous extract of Abelmoschus esculentus and its antifungal activity.* Industrial Crops and Products, 2013. **45**: p. 423-429.
185. Bar, H., et al., *Synthesis of gold nanoparticles of variable morphologies using aqueous leaf extracts of Cocculus hirsutus.* Journal of Experimental Nanoscience, 2012. **7**(1): p. 109-119.
186. Kalaivani, R., et al., *Chitosan mediated gold nanoparticles against pathogenic bacteria, fungal strains and MCF-7 cancer cells.* International Journal of Biological Macromolecules, 2020. **146**: p. 560-568.
187. Salam, F.D., et al., *Anti-bacterial and anti-biofilm efficacies of bioinspired gold nanoparticles.* Materials Letters, 2020. **261**: p. 126998.
188. Yhee, J.Y., J. Im, and R.S. Nho, *Advanced therapeutic strategies for chronic lung disease using nanoparticle-based drug delivery.* Journal of clinical medicine, 2016. **5**(9): p. 82-82.
189. Apaolaza, P., et al., *Hyaluronic acid coating of gold nanoparticles for intraocular drug delivery: Evaluation of the surface properties and effect on their distribution.* Experimental Eye Research, 2020: p. 108151.
190. Ding, Y., et al., *Gold nanoparticles for nucleic acid delivery.* Molecular therapy, 2014. **22**(6): p. 1075-1083.
191. Zhang, X., et al., *Surface functionalization of pegylated gold nanoparticles with antioxidants suppresses nanoparticle-induced oxidative stress and neurotoxicity.* Chemical Research in Toxicology, 2020. **33**(5): p. 1195-1205.
192. Wang, L., et al., *Manipulation of macrophage polarization by peptide-coated gold nanoparticles and its protective effects on acute lung injury.* Journal of nanobiotechnology, 2020. **18**(1): p. 1-16.
193. Keshari, A.K., et al., *Antioxidant and antibacterial activity of silver nanoparticles synthesized by Cestrum nocturnum.* Journal of Ayurveda and integrative medicine, 2020. **11**(1): p. 37-44.
194. Tortella, G., et al., *Silver nanoparticles: Toxicity in model organisms as an overview of its hazard for human health and the environment.* Journal of Hazardous Materials, 2020. **390**: p. 121974.
195. Hemmati, S., et al., *Biosynthesis and chemical characterization of polydopamine-capped silver nanoparticles for the treatment of acute myeloid leukemia in comparison to doxorubicin in a leukemic mouse model.* Applied Organometallic Chemistry, 2020. **34**(2): p. e5277.
196. Mohamed, N., *Synthesis of Hybrid Chitosan Silver Nanoparticles Loaded with Doxorubicin with Promising Anti-cancer Activity.* BioNanoScience, 2020. **10**(3): p. 758-765.
197. Geiser, M., et al., *Cellular uptake and localization of inhaled gold nanoparticles in lungs of mice with chronic obstructive pulmonary disease.* Particle and fibre toxicology, 2013. **10**(1): p. 19-19.
198. Alkilany, A.M. and C.J. Murphy, *Toxicity and cellular uptake of gold nanoparticles: what we have learned so far?* Journal of nanoparticle research, 2010. **12**(7): p. 2313-2333.
199. Shi, H., et al., *Titanium dioxide nanoparticles: a review of current toxicological data.* Particle and fibre toxicology, 2013. **10**(1): p. 15-15.
200. Bailey, F.E., *Alkylene oxides and their polymers*. Vol. 35. 1990: CRC Press.
201. Alconcel, S.N.S., A.S. Baas, and H.D. Maynard, *FDA-approved poly(ethylene glycol)–protein conjugate drugs.* Polym. Chem., 2011. **2**: p. 1442-1448.
202. Klibanov, A.L., et al., *Amphipathic polyethyleneglycols effectively prolong the circulation time of liposomes.* FEBS letters, 1990. **268**(1): p. 235-237.
203. Butcher, N.J., G.M. Mortimer, and R.F. Minchin, *Drug delivery: Unravelling the stealth effect.* Nature nanotechnology, 2016. **11**(4): p. 310-311.
204. Rudmann, D.G., et al., *High Molecular Weight Polyethylene Glycol Cellular Distribution and PEG-associated Cytoplasmic Vacuolation Is Molecular Weight Dependent and Does Not Require Conjugation to Proteins.* Toxicologic Pathology, 2013. **41**(7): p. 970-983.
205. Szebeni, J., *Complement activation-related pseudoallergy: a new class of drug-induced acute immune toxicity.* Toxicology, 2005. **216**(2-3): p. 106-121.

206. Quadir, M.A. and R. Haag, *Biofunctional nanosystems based on dendritic polymers.* Journal of controlled release, 2012. **161**(2): p. 484-495.
207. Ye, H., et al., *Polyester elastomers for soft tissue engineering.* Chem Soc Rev, 2018. **47**(12): p. 4545-4580.
208. McKeen, L., *Renewable resource and biodegradable polymers*. 2012, Elsevier, Amsterdam, The Netherlands. DOI.
209. Englert, C., et al., *Pharmapolymers in the 21st century: Synthetic polymers in drug delivery applications.* Progress in Polymer Science, 2018. **87**: p. 107-164.
210. Drumright, R.E., P.R. Gruber, and D.E. Henton, *Polylactic acid technology.* Advanced materials, 2000. **12**(23): p. 1841-1846.
211. Rasal, R.M., A.V. Janorkar, and D.E. Hirt, *Poly (lactic acid) modifications.* Progress in polymer science, 2010. **35**(3): p. 338-356.
212. Lowe, C.E., *Preparation of high molecular weight polyhydroxyacetic ester*. 1954, Google Patents.
213. Shen, K. and S.L. Yang. *Preparation of high-molecular-weight poly (glycolic acid) by direct melt polycondensation from glycolic acid*. in *Advanced Materials Research*. 2013. Trans Tech Publ.
214. Niu, Z., et al., *PEG-PGA enveloped octaarginine-peptide nanocomplexes: an oral peptide delivery strategy.* Journal of controlled release, 2018. **276**: p. 125-139.
215. Yang, Y.-Y., T.-S. Chung, and N.P. Ng, *Morphology, drug distribution, and in vitro release profiles of biodegradable polymeric microspheres containing protein fabricated by double-emulsion solvent extraction/evaporation method.* Biomaterials, 2001. **22**(3): p. 231-241.
216. Panagi, Z., et al., *Effect of dose on the biodistribution and pharmacokinetics of PLGA and PLGA–mPEG nanoparticles.* International Journal of Pharmaceutics, 2001. **221**(1-2): p. 143-152.
217. Bazile, D., et al., *Body distribution of fully biodegradable [14C]-poly (lactic acid) nanoparticles coated with albumin after parenteral administration to rats.* Biomaterials, 1992. **13**(15): p. 1093-1102.
218. Feng, Q. and R. Tong, *Anticancer nanoparticulate polymer-drug conjugate.* Bioengineering & translational medicine, 2016. **1**(3): p. 277-296.
219. Lee, E.S., K. Na, and Y.H. Bae, *Doxorubicin loaded pH-sensitive polymeric micelles for reversal of resistant MCF-7 tumor.* Journal of Controlled Release, 2005. **103**(2): p. 405-418.
220. Seymour, L.W., et al., *Phase II studies of polymer-doxorubicin (PK1, FCE28068) in the treatment of breast, lung and colorectal cancer.* International journal of oncology, 2009. **34**(6): p. 1629-1636.
221. Paz-Ares, L., et al., *Phase III trial comparing paclitaxel poliglumex vs docetaxel in the second-line treatment of non-small-cell lung cancer.* British Journal of Cancer, 2008. **98**(10): p. 1608-1613.
222. Bobo, D., et al., *Nanoparticle-Based Medicines: A Review of FDA-Approved Materials and Clinical Trials to Date.* Pharmaceutical Research, 2016. **33**(10): p. 1-15.
223. Rideau, E., et al., *Liposomes and polymersomes: a comparative review towards cell mimicking.* Chem. Soc. Rev., 2018. **47**(23): p. 8572-8610.
224. Yadav, D., et al., *Liposomes for Drug Delivery.* Journal of Biotechnology & Biomaterials, 2017. **07**(04).
225. Lyons, D., *Get Vitamins Into Your Body With Liposomes Without Wasting Money*. 2017.
226. Le Meins, J.F., et al., *Hybrid polymer/lipid vesicles: State of the art and future perspectives.* Materials Today, 2013. **16**(10): p. 397-402.
227. Lee, J.S. and J. Feijen, *Polymersomes for drug delivery: design, formation and characterization.* Journal of controlled release, 2012. **161**(2): p. 473-483.
228. Lalatsa, A., et al., *Amphiphilic poly(L-amino acids) - new materials for drug delivery.* Journal of controlled release : official journal of the Controlled Release Society, 2012. **161**(2): p. 523-536.
229. Zhao, L., et al., *A review of polypeptide-based polymersomes.* Biomaterials, 2014. **35**(4): p. 1284-1301.
230. Smart, T., et al., *Block copolymer nanostructures.* Nano Today, 2008. **3**(3-4): p. 38-46.
231. Meng, F., Z. Zhong, and J. Feijen, *Stimuli-responsive polymersomes for programmed drug delivery.* Biomacromolecules, 2009. **10**(2): p. 197-209.

232. Du, Y., et al., *pH-sensitive degradable chimaeric polymersomes for the intracellular release of doxorubicin hydrochloride.* Biomaterials, 2012. **33**(29): p. 7291-7299.
233. Sanson, C., et al., *Temperature responsive poly (trimethylene carbonate)-block-poly (L-glutamic acid) copolymer: polymersomes fusion and fission.* Soft Matter, 2010. **6**(8): p. 1722-1730.
234. Oliveira, H., et al., *Magnetic field triggered drug release from polymersomes for cancer therapeutics.* Journal of Controlled Release, 2013. **169**(3): p. 165-170.
235. Sanson, C., et al., *Doxorubicin loaded magnetic polymersomes: theranostic nanocarriers for MR imaging and magneto-chemotherapy.* ACS nano, 2011. **5**(2): p. 1122-1140.
236. Zhang, J., et al., *pH and reduction dual-bioresponsive polymersomes for efficient intracellular protein delivery.* Langmuir, 2011. **28**(4): p. 2056-2065.
237. GmbH, D.I., *Surfactants & critical micelle concentration (CMC).* 2019.
238. Alexander-Bryant, A.A., W.S.V. Berg-Foels, and X. Wen, *Bioengineering Strategies for Designing Targeted Cancer Therapies.* 2013.
239. Abbasi, E., et al., *Dendrimers: synthesis, applications, and properties.* Nanoscale Research Letters, 2014. **9**(1): p. 247-247.
240. Richards, D.A., A. Maruani, and V. Chudasama, *Antibody fragments as nanoparticle targeting ligands: a step in the right direction.* Chemical science, 2017. **8**(1): p. 63-77.
241. Shukla, R., et al., *HER2 specific tumor targeting with dendrimer conjugated anti-HER2 mAb.* Bioconjugate chemistry, 2006. **17**(5): p. 1109-1115.
242. Kalra, N., et al., *Virosomes: As a Drug Delivery Carrier.* American Journal of Advanced Drug Delivery, 2013. **1**: p. 29-35.
243. Sharma, R. and M. Yasir, *Virosomes: a novel carrier for drug delivery.* Int J Pharm Tech Res, 2010. **2**(4): p. 2327-39.
244. Huang, X., et al., *Cancer cell imaging and photothermal therapy in the near-infrared region by using gold nanorods.* Journal of the American Chemical Society, 2006. **128**(6): p. 2115-2120.
245. Chen, J., et al., *Immuno gold nanocages with tailored optical properties for targeted photothermal destruction of cancer cells.* Nano letters, 2007. **7**(5): p. 1318-1322.
246. Giner-Casares, J.J., et al., *Inorganic nanoparticles for biomedicine: where materials scientists meet medical research.* Materials Today, 2016. **19**(1): p. 19-28.
247. Wang, Y.-X.J., S.M. Hussain, and G.P. Krestin, *Superparamagnetic iron oxide contrast agents: physicochemical characteristics and applications in MR imaging.* European radiology, 2001. **11**(11): p. 2319-2331.
248. Liong, M., et al., *Multifunctional inorganic nanoparticles for imaging, targeting, and drug delivery.* ACS nano, 2008. **2**(5): p. 889-896.
249. Gobin, A.M., et al., *Near-infrared resonant nanoshells for combined optical imaging and photothermal cancer therapy.* Nano letters, 2007. **7**(7): p. 1929-1934.
250. Medarova, Z., et al., *In vivo imaging of siRNA delivery and silencing in tumors.* Nature medicine, 2007. **13**(3): p. 372-372.
251. Sabaeian, M. and A. Khaledi-Nasab, *Size-dependent intersubband optical properties of dome-shaped InAs/GaAs quantum dots with wetting layer.* Applied optics, 2012. **51**(18): p. 4176-4185.
252. Khaledi-Nasab, A., et al., *Kerr nonlinearity due to intersubband transitions in a three-level InAs/GaAs quantum dot: the impact of a wetting layer on dispersion curves.* Journal of Optics, 2014. **16**(5): p. 055004-055004.
253. Olerile, L.D., et al., *Near-infrared mediated quantum dots and paclitaxel co-loaded nanostructured lipid carriers for cancer theragnostic.* Colloids and Surfaces B: Biointerfaces, 2017. **150**: p. 121-130.
254. Chan, W.C.W., et al., *Luminescent quantum dots for multiplexed biological detection and imaging.* Current opinion in biotechnology, 2002. **13**(1): p. 40-46.
255. Soenen, S.J., et al., *Cellular toxicity of inorganic nanoparticles: common aspects and guidelines for improved nanotoxicity evaluation.* Nano today, 2011. **6**(5): p. 446-465.

256. Ihler, G.M., R.H. Glew, and F.W. Schnure, *Enzyme loading of erythrocytes.* Proceedings of the National Academy of Sciences, 1973. **70**(9): p. 2663-2666.
257. Dale, G.L., W. Kuhl, and E. Beutler, *Incorporation of glucocerebrosidase into Gaucher's disease monocytes in vitro.* Proceedings of the National Academy of Sciences, 1979. **76**(1): p. 473-475.
258. Ji, P., S.R. Jayapal, and H.F. Lodish, *Enucleation of cultured mouse fetal erythroblasts requires Rac GTPases and mDia2.* Nature cell biology, 2008. **10**(3): p. 314-314.
259. Muzykantov, V.R., *Drug delivery by red blood cells: vascular carriers designed by mother nature.* Expert opinion on drug delivery, 2010. **7**(4): p. 403-427.
260. Humphreys, J.D. and G. Ihler, *Enhanced stability of erythrocyte-entrapped glucocerebrosidase activity.* The Journal of laboratory and clinical medicine, 1980. **96**(4): p. 682-692.
261. Moran, N.F., et al., *Carrier erythrocyte entrapped thymidine phosphorylase therapy for MNGIE.* Neurology, 2008. **71**(9): p. 686-688.
262. Bridget E, B.A.X., et al., *The entrapment of polyethylene glycol-bound adenosine deaminase (Pegademase) in human carrier erythrocytes*. 1996, Portland Press Limited.
263. Petrikovics, I., et al., *Encapsulation of rhodanese and organic thiosulfonates by mouse erythrocytes.* Toxicological Sciences, 1994. **23**(1): p. 70-75.
264. Pei, L., I. Petrikovics, and J.L. Way, *Antagonism of the lethal effects of paraoxon by carrier erythrocytes containing phosphotriesterase.* Toxicological Sciences, 1995. **28**(2): p. 209-214.
265. Sanz, S., et al., *The influence of enzyme concentration on the encapsulation of glutamate dehydrogenase and alcohol dehydrogenase in red blood cells.* Biotechnology and applied biochemistry, 1995. **22**(2): p. 223-231.
266. Gordon, S. and A. Plüddemann, *Mononuclear Phagocytes*, in *Kelley and Firestein's Textbook of Rheumatology (Tenth Edition)*. 2017, Elsevier. p. 145-168.
267. Xuan, M., et al., *Macrophage cell membrane camouflaged Au nanoshells for in vivo prolonged circulation life and enhanced cancer photothermal therapy.* ACS applied materials & interfaces, 2016. **8**(15): p. 9610-9618.
268. Tao, Y., M. Ning, and H. Dou, *A novel therapeutic system for malignant glioma: nanoformulation, pharmacokinetic, and anticancer properties of cell-nano-drug delivery.* Nanomedicine: Nanotechnology, Biology and Medicine, 2013. **9**(2): p. 222-232.
269. Angsantikul, P., et al., *Cell membrane-coated nanoparticles as an emerging antibacterial vaccine platform.* Vaccines, 2015. **3**(4): p. 814-828.
270. Fang, R.H., et al., *Cancer cell membrane-coated nanoparticles for anticancer vaccination and drug delivery.* Nano letters, 2014. **14**(4): p. 2181-2188.
271. Zhu, J.-Y., et al., *Preferential cancer cell self-recognition and tumor self-targeting by coating nanoparticles with homotypic cancer cell membranes.* Nano letters, 2016. **16**(9): p. 5895-5901.
272. Qin, S.-Y., et al., *Drug self-delivery systems for cancer therapy.* Biomaterials, 2017. **112**: p. 234-247.
273. Ma, W., A.G. Cheetham, and H. Cui, *Building Nanostructures with Drugs.* Nano Today, 2016. **11**(1): p. 13-30.
274. Jia, J., et al., *Mechanisms of drug combinations: Interaction and network perspectives.* Nature Reviews Drug Discovery, 2009. **8**(2): p. 111-128.
275. Administration, U.S.D.o.H.H.S.a.F.D., *Regulatory classification of pharmaceutical co-crystals: Guidance for industry.* Center for Drug Evaluation and Research (CDER), Silver Spring, US, 2018.
276. Cerreia Vioglio, P., M.R. Chierotti, and R. Gobetto, *Pharmaceutical aspects of salt and cocrystal forms of APIs and characterization challenges.* Advanced Drug Delivery Reviews, 2017. **117**: p. 86-110.
277. Duggirala, N.K., et al., *Pharmaceutical cocrystals: along the path to improved medicines.* Chemical communications (Cambridge, England), 2016. **52**(4): p. 640-655.
278. Schultheiss, N. and A. Newman, *Pharmaceutical cocrystals and their physicochemical properties.* Crystal Growth and Design, 2009. **9**(6): p. 2950-2967.

279. Sarmah, K.K., et al., *First-line antituberculosis drug, pyrazinamide, its pharmaceutically relevant cocrystals and a salt.* Acta Crystallographica Section B: Structural Science, Crystal Engineering and Materials, 2017. **73**(Pt 5): p. 1007-1016.
280. Kuminek, G., et al., *How cocrystals of weakly basic drugs and acidic coformers might modulate solubility and stability.* Chemical communications (Cambridge, England), 2016. **52**(34): p. 5832-5835.
281. Elder, D.P., R. Holm, and H.L.d. Diego, *Use of pharmaceutical salts and cocrystals to address the issue of poor solubility.* International Journal of Pharmaceutics, 2013. **453**(1): p. 88-100.
282. Dalpiaz, A., B. Pavan, and V. Ferretti, *Can pharmaceutical co-crystals provide an opportunity to modify the biological properties of drugs?* Drug Discovery Today, 2017. **22**(8): p. 1134-1138.
283. Deng, J.-H., et al., *Dapagliflozin-citric acid cocrystal showing better solid state properties than dapagliflozin.* EUROPEAN JOURNAL OF PHARMACEUTICAL SCIENCES, 2017. **104**: p. 255-261.
284. Zhou, Z., et al., *Resveratrol cocrystals with enhanced solubility and tabletability.* International Journal of Pharmaceutics, 2016. **509**(1-2): p. 391-399.
285. Shevchenko, A., et al., *A new cocrystal and salts of itraconazole: comparison of solid-state properties, stability and dissolution behavior.* International Journal of Pharmaceutics, 2012. **436**(1-2): p. 403-409.
286. Healy, A.M., et al., *Pharmaceutical solvates, hydrates and amorphous forms: A special emphasis on cocrystals.* Advanced Drug Delivery Reviews, 2017. **117**: p. 25-46.
287. Landenberger, K.B., O. Bolton, and A.J. Matzger, *Energetic-Energetic Cocrystals of Diacetone Diperoxide (DADP): Dramatic and Divergent Sensitivity Modifications via Cocrystallization.* Journal of the American Chemical Society, 2015. **137**(15): p. 5074-5079.
288. Borman, P. and D. Elder, *Q2(R1) Validation of Analytical Procedures: An Implementation Guide.* 2017. p. 127-166.
289. Kurita, A., et al., *Modified irinotecan hydrochloride (CPT-11) administration schedule improves induction of delayed-onset diarrhea in rats.* Cancer Chemother Pharmacol, 2000. **46**(3): p. 211-20.
290. Sinha, B., R.H. Müller, and J.P. Möschwitzer, *Bottom-up approaches for preparing drug nanocrystals: Formulations and factors affecting particle size.* International Journal of Pharmaceutics, 2013. **453**(1): p. 126-141.
291. Wang, W.W., et al., *A novel "mosaic-type" nanoparticle for selective drug release targeting hypoxic cancer cells.* Nanoscale, 2019. **11**(5): p. 2211-2222.
292. Zhao, F., et al., *Cellular Uptake, Intracellular Trafficking, and Cytotoxicity of Nanomaterials.* Small, 2011. **7**(10): p. 1322-1337.
293. Hu, K., et al., *Core-shell biopolymer nanoparticle delivery systems: synthesis and characterization of curcumin fortified zein-pectin nanoparticles.* Food chemistry, 2015. **182**: p. 275-281.
294. Koner, J.S., et al., *A Holistic Multi Evidence Approach to Study the Fragmentation Behaviour of Crystalline Mannitol.* Scientific Reports, 2015. **5**(1): p. 16352-16352.
295. Raju, T.V., et al., *Development and Validation of a Precise, Single HPLC Method for the Determination of Tolperisone Impurities in API and Pharmaceutical Dosage Forms.* Sci Pharm, 2013. **81**(1): p. 123-38.
296. Mishra, A., et al., *A simple reversed phase high-performance liquid chromatography (RP-HPLC) method for determination of curcumin in aqueous humor of rabbit.* J Adv Pharm Technol Res, 2014. **5**(3): p. 147-9.
297. Sousa, F., V.M.F. Goncalves, and B. Sarmento, *Development and validation of a rapid reversed-phase HPLC method for the quantification of monoclonal antibody bevacizumab from polyester-based nanoparticles.* Journal of Pharmaceutical and Biomedical Analysis, 2017. **142**: p. 171-177.
298. Johnson, J.J. and H. Mukhtar, *Curcumin for chemoprevention of colon cancer.* Cancer Letters, 2007. **255**(2): p. 170-181.
299. Pommier, Y., M. Cushman, and J.H. Doroshow, *Novel clinical indenoisoquinoline topoisomerase I inhibitors: a twist around the camptothecins.* Oncotarget, 2018. **9**(99): p. 37286-37288.

300. Guthrie, L., et al., *Human microbiome signatures of differential colorectal cancer drug metabolism.* Npj Biofilms and Microbiomes, 2017. **3**.

Appendixes

1. Xiao, H., Sedlarik, V. Methods of making nanocrystals with enhanced biological availability and formulation for such nanocrystals preparation for use in anticancer therapy. (2019, WO)

2. Xiao, H.; Guo, Y.; Liu, H.; Liu, Y.; Wang, Y.; Li, C.; Císař, J.; Škoda, D.; Kuřitka, I.; Guo, L., Structure-based design of charge-conversional drug self-delivery systems for better targeted cancer therapy. Biomaterials 2020, 232, 119701. (IF: 10.317)

3. Xiao, H.; Sedlařík, V., A Rapid and Sensitive HPLC Method for Simultaneous Determination of Irinotecan Hydrochloride and Curcumin in Co-delivered Polymeric Nanoparticles. Journal of Chromatographic Science 2020. (IF: 1.28)

(12) INTERNATIONAL APPLICATION PUBLISHED UNDER THE PATENT COOPERATION TREATY (PCT)

(19) World Intellectual Property Organization
International Bureau

(43) International Publication Date
07 May 2020 (07.05.2020)

WIPO | PCT

(10) International Publication Number
WO 2020/088702 A1

(51) International Patent Classification:
A61K9/14 (2006.01) *A61K 31/4745* (2006.01)
A61K9/19 (2006.01)

(21) International Application Number:
PCT/CZ2019/050048

(22) International Filing Date:
16 October 2019 (16.10.2019)

(25) Filing Language: Czech

(26) Publication Language: English

(30) Priority Data:
PV 2018-591 30 October 2018 (30.10.2018) CZ
PV 2019-630 09 October 2019 (09.10.2019) CZ

(71) Applicant: **TOMAS BATA UNIVERSITY IN ZLIN** [CZ/CZ]; Nam. T.G. Masaryka 5555, 76001 Zlin (CZ).

(72) Inventors: **XIAO, Haijun;** Tonghui South Road, 256, Dongli Guanghua Xinglin Community, Qingyang District, Chengdu, Sichuan (CN). **SEDLARIK, Vladimir;** Jar. Stasi 1148, 76302 Zlin, Malenovice (CZ).

(74) Agent: **GÖRIG, Jan;** Korabova 98, 763 16 Frystak (CZ).

(81) Designated States *(unless otherwise indicated, for every kind of national protection available)*: AE, AG, AL, AM, AO, AT, AU, AZ, BA, BB, BG, BH, BN, BR, BW, BY, BZ, CA, CH, CL, CN, CO, CR, CU, CZ, DE, DJ, DK, DM, DO, DZ, EC, EE, EG, ES, FI, GB, GD, GE, GH, GM, GT, HN, HR, HU, ID, IL, IN, IR, IS, JO, JP, KE, KG, KH, KN, KP, KR, KW, KZ, LA, LC, LK, LR, LS, LU, LY, MA, MD, ME, MG, MK, MN, MW, MX, MY, MZ, NA, NG, NI, NO, NZ, OM, PA, PE, PG, PH, PL, PT, QA, RO, RS, RU, RW, SA, SC, SD, SE, SG, SK, SL, SM, ST, SV, SY, TH, TJ, TM, TN, TR, TT, TZ, UA, UG, US, UZ, VC, VN, ZA, ZM, ZW.

(84) Designated States *(unless otherwise indicated, for every kind of regional protection available)*: ARIPO (BW, GH, GM, KE, LR, LS, MW, MZ, NA, RW, SD, SL, ST, SZ, TZ, UG, ZM, ZW), Eurasian (AM, AZ, BY, KG, KZ, RU, TJ, TM), European (AL, AT, BE, BG, CH, CY, CZ, DE, DK, EE, ES, FI, FR, GB, GR, HR, HU, IE, IS, IT, LT, LU, LV, MC, MK, MT, NL, NO, PL, PT, RO, RS, SE, SI, SK, SM, TR), OAPI (BF, BJ, CF, CG, Cl, CM, GA, GN, GQ, GW, KM, ML, MR, NE, SN, TD, TG).

Published:
— *with international search report (Art. 21(3))*
— *in black and white; the international application as filed contained color or greyscale and is available for download from PATENTSCOPE*

(54) **Title:** METHODS OF MAKING NANOCRYSTALS WITH ENHANCED BIOLOGICAL AVAILABILITY AND FORMULATION FOR SUCH NANOCRYSTALS PREPARATION FOR USE IN ANTICANCER THERAPY

C

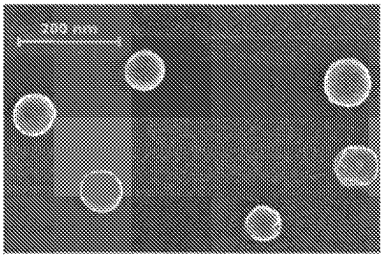

Fig. 4

(57) Abstract: The method of nanocrystal preparation is based on the procedure of the crystalline nanoparticles preparation in powder form that comprises a) dissolving the protonated nitrogen containing derivatives of camptothecin and curcuminoids in an organic solvent leading to formation of self-assembled ionic complex followed by subsequent addition of nonionogenic injectable surfactant, b) transferring the obtained mixture into aqueous medium under continuous homogenization including mixing, shaking and/or using ultrasound, c) removing the solvent in order to obtain powder form, d) lyophilisation of the product with the previously added cryoprotectant. Composition for nanocrystal preparation through the method according to the invention consists of injectable nonionic surfactant and self-assembled ionic complex that contains curcuminoids and protonated nitrogen containing derivatives of camptothecin and its analogues in the molar ratios in the range between 10: 1 and 1:10. Analogues of camptothecin include preferably camptothecin and homocamptothecin. Protonated nitrogen containing camptothecin derivatives preferably have the protonated nitrogen included in their chemical structure through at least one functional group including primary amine, secondary amine, tertiary amine, cyclic amine and/or their combinations. Utilization of nanocrystals prepared for the anticancer injectable drug application consists in the dissolution of 3 wt. % nanocrystals in powder form in the liquid medium based on distilled water with 5 wt. % of glucose.

WO 2020/088702 A1

METHODS OF MAKING NANOCRYSTALS WITH ENHANCED BIOLOGICAL AVAILABILITY AND FORMULATION FOR SUCH NANOCRYSTALS PREPARATION FOR USE IN ANTICANCER THERAPY

Field of Invention

The invention describes method of preparation of nanocrystals based on ionic complexes forming self-assembled nanostructures and compositions prepared by this method. The composition and the obtained nanocrystals can be used for preparation of agents with enhanced biological availability that can be utilized especially in the field of preparation and application of cytostatics with reduced side effects.

State of the Art

The analogues of camptothecin and their derivatives are potent therapeutic agents for chemical treatment of various oncological diseases. These molecules and their active metabolites can specifically bind to topoisomerase I-DNA complex, thereby preventing reconnection of the single-stranded fracture and stopping DNA replication. Curcuminoids (curcumin (CAS 458-37-7), desmethoxycurcumin (CAS 22608-11-3) and bis-demethoxycurcumin (CAS 24939-16-0)) are natural polyphenols found in the extract of *Curcuma longa,* one of the widely used medicinal plants particularly in Asian countries. Curcuminoids show pharmacological effects, such as anti-inflammatory, antioxidant and antimicrobial properties. Furthermore, they are described through an anti-cancer effect, too.

However, the usage of camptothecin and its derivatives for chemotherapeutic treatment of cancer can cause side effects to oncological patients in form of stomach problems, nausea, diarrhoea. Another undesirable phenomenon reducing the effect of treatment is the gradual development of tumour cell tolerance to the drug.

Additionally, the hydrophobicity (very low water solubility), which can be also found in combination with other substances, significantly reduces the possibilities of biological effects of curcuminoids in the body. Another limitation of the wider biological utilization of curcuminoid therapeutic potential is their rapid metabolization causing a low rate of plasma protein binding described in WO 2010013224 (EP 2349237).

Patent CN102885800B (issued August 6, 2014) reveals that by combining irinotecan (a camptothecin derivative) with curcuminoids some of the above-mentioned side effects can be suppressed. The combination of camptothecin and curcuminoid in the form of nanocrystals is

also discussed in patent application CN104546728, which describes the stabilization of nanocrystals by an amphoteric molecule, for example a poloxamer, and the possibility of its subsequent use in the preparation of injectable solutions. This takes into account the tendency of curcuminoids to metabolize rapidly. Nevertheless, a specific implementation of a combination suitable for injection is not described herein.

The aim of the invention is therefore to provide an easy-to-manufacture and stable composition intended for immediate use in injection applications which is based on curcuminoids and camptothecin derivatives, is suitable for use as an anticancer agent and gentle to the patient's gastrointestinal tract, i.e. does not show the above-mentioned side effects.

Ground of Invention

The aforesaid disadvantages and drawbacks of the above-mentioned biologically active substances used up to now for the treatment of oncological diseases are largely eliminated by the composition for the preparation of nanocrystals for the substances with enhanced biological availability according to the invention and the method of its preparation.

The ground of the method of preparation of nanocrystals according to the invention consists in that the preparation of nanocrystalline particles in powder form contains the following steps:

a) dissolving the protonated nitrogen containing derivatives of camptothecin and curcuminoids in an organic solvent leading to formation of a self-assembled ionic complex followed by subsequent addition of nonionogenic injectable surfactant;

b) transferring the obtained mixture into an aqueous medium under continuous homogenization, including mixing, shaking and / or using ultrasound;

c) removing the solvent to obtain a powder form;

d) lyophilisation of the product with the previously added cryoprotectant.

The organic solvent used in step a) is preferably dimethylsulfoxide (CAS 67-68-5), propylene carbonate (CAS 108-32-7), acetonitrile (CAS 75-05-8), acetone (CAS 67-64-1) , dimethylformamide (CAS 68-12-2), tetrahydrofuran (CAS 109-99-9), methylpyrrolidone (CAS 872-50-4), hexamethylphosphoramide (CAS 680-31-9), methanol (CAS 67-56-1), ethanol (CAS 64-17-5), acetic acid (CAS 64-19-7) or combinations thereof.

The cryoprotectant used in step d) is preferably lactose (CAS 63-42-3), mannitol (CAS 69-65-8), sucrose (CAS 57-50-1), trehalose (CAS 99-20-7), fructose (CAS 57-48-7), glucose (CAS 50-99-7), sodium alginate (CAS 9005-38-3), gelatin (CAS 9000-70-8) or combinations thereof.

The ground of the composition prepared by the method according to the invention consists in that the composition consists of an injectable nonionic surfactant and a self-assembled ionic complex containing curcuminoids and protonated nitrogen comprising camptothecin derivatives and analogues thereof in a molar ratio of components ranging from 10: 1 to 1:10.

Camptothecin analogues preferably include camptothecin (CAS 7689-03-4) and homocamptothecin (CAS 186669-19-2). The protonated nitrogen is contained in camptothecin derivatives preferably in the form of at least one functional group including a primary amine, a secondary amine, a tertiary amine, a cyclic amine and / or a combination thereof. The primary amine-containing camptothecin derivative may be one or more substances from the following groups: 9-aminocamptothecin (CAS 91421-43-1), exatecan (CAS 171335-80-1), delimotecan (CAS 187852-63-7), namitecan (CAS 372105-27-6). Preferably, the secondary amine-containing camptothecin derivative is belotecan (CAS 256411-32-2). The tertiary amine-containing camptothecin derivative may be topotecan (CAS 123948-87-8) and / or lipotecan (CAS 1432176-87-8). Camptothecin derivatives containing a cyclic amine in their structure are represented by one or more substances from the group of: irinotecan (CAS 100286-90-6), lurtotecan (CAS 149882-10-0), afeletecan (CAS 215604-75-4), simmitecan (CAS 1247847-78-4), elomotecan (CAS 220998-10-7).

The nitrogen-containing camptothecin analogue derivatives are preferably present in the composition in the form of salts with organic or inorganic acids selected from the group comprising hydrochloric acid (CAS 7647-01-0), sulfuric acid (CAS 7664-93-9), phosphoric acid (CAS 7664 -38-2), hydrobromic acid (CAS 10035-10-6), perchloric acid (CAS 7601-90-3), methanesulfonic acid (CAS 75-75-2p, acetic acid (CAS 64-19-7), maleic acid (CAS 110-16-7), tartaric acid (CAS 526-83-0), citric acid (CAS 77-92-9) or combinations thereof.

The ground of the use of the nanocrystals according to the invention for the preparation of an anticancer agent for injection applications consists in that the nanocrystals in the form of a powder are dissolved in a liquid medium which is distilled water containing 5% wt. glucose, wherein the weight ratio of nanocrystals to liquid medium is in the range of 0.01: 99.99 to 3:97.

Based on the ionic complexes according to the the present invention, injectable nanocrystalline self-assembled systems with therapeutic and anti-inflammatory effects and better tolerability in

the body are produced. Combining them with the nonionic components according to the invention provides compositions for immediate or sequential use in injection applications, based on nanocrystals with cytostatic properties and exhibiting increased stability over a wide pH range.

The advantage of the composition according to the invention is the narrow particle size distribution and their stability, but also the increased water solubility of the hydrophobic curcuminoid molecules, which significantly enhances their use in injectable applications and the so-called biological availability - the possible actions inside the body. Thus, their therapeutic effect in the treatment of cancer is enhanced.

The nanocrystals based on the composition according to the invention can be prepared either in powder form without specific requirements for temperature, pressure or stabilizing additives, which is favorable from the viewpoint of commercial production of chemotherapeutic agents, or directly as a liquid substance for injectable applications.

Overview of Images in Drawings

The attached drawings show the chemical structures for the composition according to the invention and the obtained properties of the nanocrystals:

Fig. 1 - Chemical structures of amphiphilic camptothecin analogues and hydrophobic curcuminoids;

Fig. 2 - Fluorescence characteristics of self-assembled ionic complexes based on irinotecan hydrochloride and curcumin (Excitation (A), emission (B) and synchronous (C) fluorescence spectra of irinotecan with different curcumin concentrations in dimethylformamide at 25°C; (D) Stem-Volmer plot showing fluorescence quenching of irinotecan at 25 ° C; (E) Plot of (Io/ I-1) versus logarithm of curcuminoid concentration (mol / L);

Note: Io and I represent the fluorescence intensity of irinotecan in the absence (I_0) and in the presence of (I) curcuminoids. ($\tau o_)$ and (x) are the fluorescence lifetimes of irinotecan in the absence and in the presence of curcumin, respectively; Ci is the concentration of irinotecan; Cc is the concentration of curcuminoids;

Fig. 3 - Chemical structures of protonated nitrogen containing camptothecin analogue derivatives;

Fig. 4 - Representation of a typical hydrodynamic diameter (A) and zeta potential (B) of nanocrystals dispersed in distilled water and their scanning electron microscope images (C) with measuring scale showing the length of 200 nm; the yield of relevant camptothecin analogue derivatives from nanocrystals based on topotecan (TCN) / curcumin, belotecan (BCN) / curcumin and exatecan / curcumin (ECN);

Fig. 5 - Changes in nanocrystalline properties in suspension in water (A) at different pH values (after 8 hours at 37.5 ° C) and in phosphate buffer (B) at different times (pH = 7.4 , 37. 5 ° C);

Fig. 6 - XRD spectra on powder samples: A - irinotecan hydrochloride, B - curcumin, C - mixture of pure components of irinotecan hydrochloride and curcumin, D - nanocrystals based on self-assembled ionic complexes - final product, E - pure cryoprotectant mannitol after dissolution in water and subsequent evaporation, F - pure constituents of irinotecan hydrochloride and curcumin after dissolution in methanol and subsequent evaporation;

Figures 7 to 13 - procedure for verifying the anti-cancer effect of injectable irinotecan-curcumin hydrochloride (ICN) according to the invention in nano-form of HT-29 on a tumour produced by a subcutaneous graft applied in mouse (nude mouse) *in vivo* :

Fig. 7 is a schematic diagram of an experiment for testing anti-tumour efficacy using colorectal tumour graft applied in nude mice;

Fig. 8 - tumour volume applied in mice injected with PBS, I or ICN (PBS = Phosphate-buffered saline, Ph 7.4; I = irinotecan hydrochloride alone; ICN = combination I with curcumin according to the invention);

Figure 9 - Tumour volume change after injection of PBS, I or ICN;

Figure 10 - Tumour mass change after injection of PBS, I or ICN;

Fig. 11 - images of extracted tumours;

Fig. 12 - weight of tested animals after injection of PBS, I or ICN;

Fig. 13 - intensity of side effect in experimental animals (in the form of diarrhea); considerable difference between the ICN and I group, no difference between ICN and PBS group. The significance of the differences observed between the groups was analyzed using a two-way ANOVA analysis (parameters * $p < 0.05$, ** $P < 0.01$, *** $P < 0.001$, **** $P < 0.0001$).

Detailed description of the detected dependences:

Camptothecin analogue derivatives have fluorescent properties. It can be seen from Figures 2A, 2B and 2C that irinotecan (a nitrogen containing camptothecin derivative) exhibits an excitation peak at a wavelength of 385 nm and an emission peak at 428 nm. The addition of curcuminoid causes the quenching (decreasing intensity) of the excitatory, emission and synchronous spectra of irinotecan. The data obtained from the measured values within the quenching process analysed using the Stem-Volmer model (Fig. 2D) show changes in fluorescence intensities, but without changing its lifetime, indicating the formation of a complex with curcuminoid (static quenching) at a 1: 1 molar ratio (Fig. 2E). The above mentioned properties can also be observed for other protonated nitrogen-containing derivatives of camptothecin and its analogues, the structures of which are shown in Fig. 3. The above stated shows that curcuminoids and protonated nitrogen-containing derivatives of camptothecin and its analogues form at specific organic solvent environments ionic surfactants that are self-organized through intermolecular interactions (e.g. hydrophobic and electrostatic interactions).

The nanoparticles based on curcuminoid (7.4 mg) and another protonated nitrogen containing camptothecin derivative or salt thereof, e.g. topotecan hydrochloride (4.6 mg), belotecan (4.3 mg) or exatecan (5.3 mg), were - based on this finding - also prepared by the method according to the invention with similar results.

It has been found out that the parameters of nanocrystals prepared from the above mentioned ionic complexes are best controlled in the range of hydrodynamic diameter of 50-1000 nm with a polydispersity less than or equal to 0.2 in suspension. The zeta potential of nanocrystals ranges from -10 mV to +60 mV depending on the pH and ionic strength of the environment. The molar ratio of curcuminoid and protonated nitrogen-containing camptothecin derivatives and analogues thereof is in the range of 10: 1 to 1:10.

However, the sizes of nanocrystals based solely on ionic complexes are strongly dependent on the pH and ionic strength of the surrounding environment, which may lead to their uncontrolled changes. Therefore, the addition of nonionic surfactants to the above mentioned compositions was further tested. The addition of non-ionic surfactants (e.g., cholesterol, poloxamer, polyoxylic castor oil and polysorbates) results in reaching the stability of nanocrystals over a wide pH range due to the impact of steric interparticle forces. Despite the fact that the surface tension of the particles decreases to almost zero value, there are shown only slight changes in their size. Nanocrystals based on a mixture of the above mentioned ionic and nonionic complexes exhibit an increase in solubilization resistance of at least 40% compared to nanocrystals based on only ionic complexes.

The XRD spectra on powder samples (Fig. 6) show the creation of new crystalline structures formed during the preparation of the composition according to the invention.

The nanosuspension can be prepared by mixing nanocrystals in an injectable liquid containing, for example, 5 wt. % glucose and 0.96 % wt. sodium chloride.

The values and dependences shown in Figures 7 to 13 will be described and analysed directly in Example 11.

Examples

Example 1

Preparation of nanocrystals based on irinotecan and curcumin - structure see Fig. 1 and 3

Irinotecan hydrochloride (6.2 mg) and curcumin (7.4 mg) in a molar ratio of 1: 2 were dissolved in 0.5 mL of dimethylsulfoxide at room temperature. Subsequently, 15 wt. % of poloxamer 105 as a nonionic surfactant was added. The resulting mixture was transferred to an aqueous medium - added to 30 mL of distilled water and stirred at 500 rpm for 5 min at room temperature. (In addition to water, an aqueous medium with a pH of max. 9 may be used for transfer to an aqueous medium.)

The obtained suspension was subjected to dialysis in order to remove the organic solvent; a membrane with a MWCO (molecular weight cutoff) of 500 D was used.

Dialysis was performed against distilled water for 3 hours. Before lyophilization, 20 % wt. mannitol was added, which served as a cryoprotectant.

The size of the resulting nanocrystals was around 100 nm (see Fig. 4A and 4B). The nanocrystals had a positive surface charge of +43 mV and showed a narrow size distribution represented by a polydispersity index of 0.107. According to the scanning electron microscope (SEM) analysis, the above mentioned nanocrystalline particles had an almost globular shape close to spheres and a smooth surface (Fig. 4C). Changes in the selected characteristics of nanoparticles (hydrodynamic diameter, polydispersity index and zeta potential) when exposed to different pH or ionic strength are shown in Fig. 5. The surface tension of nanoparticles decreased with the increasing acidity of the environment (pH less than 7). Negative zeta potential values of nanocrystals were monitored in an alkaline environment (pH greater than 7). On the other hand, there were slight changes in the size of nanocrystals and the breadth of their polydispersity as a result of further impact of repulsive steric forces. In addition, nanoparticles

are stable even after 8 hours in phosphate buffer (pH 7.4) at 37.5 ° C, with a slight increase in particle diameter and their polydispersity. Their surface tension was below +10 mV.

The concentration of both bioactive substances was verified by high performance liquid chromatography. The detected proportion of bioactive substances in the particles was 70% by weight. The ratios between camptothecin derivatives and curcuminoids in nanoparticles were almost the same as the concentration ratio at the beginning of the reaction.

The combination of the ionic complex and the non-ionic surfactant resulted in nanocrystals having cytostatic properties that showed increased stability over a wide pH range.

Example 2

Preparation of nanocrystals of irinotecan and curcumin (ICN) - structure see Fig. 1 and 3

Irinotecan hydrochloride (6.2 mg) and curcumin (7.4 mg) at a molar ratio of 1: 2 were dissolved in 0.4 mL of dimethylsulfoxide (DMSO) at room temperature to form a self-assembled ionic complex, to which 3 mg of cholesterol was subsequently added as nonionic surfactant. The organic solution thus obtained was then added to 30 mL of distilled water and stirred under the same conditions as in Example 1. The obtained suspension was dialyzed to remove the organic solvent; a MWCO 300 D membrane was used. Dialysis was performed against distilled water for 2 hours. Before lyophilization, 1% wt. mannitol serving as a cryoprotectant was added to the compound. In this way, nanocrystals were obtained in the form of a powder, from which a nanosuspension was prepared by dissolving in distilled water containing 5% wt. glucose.

The combination of the ionic complex and the non-ionic surfactant resulted in nanocrystals having cytostatic properties that showed increased stability over a wide pH range.

Example 3

Preparation of nanocrystals based on topotecan and curcumin (TCN) - structure see Fig. 3

Topotecan hydrochloride (4.6 mg) and curcumin (4.0 mg) in a 1: 1 molar ratio were dissolved in 0.3 mL of dimethylformamide (DMF) at room temperature to form a self-assembled ionic complex, to which 1.3 mg of polysorbate 80 was subsequently added - serving as a nonionic surfactant. The organic solution thus obtained was then added to 15 mL of distilled water and stirred as in Example 1, after which the suspension obtained was subjected to dialysis to remove the organic solvent - MWCO 500 D membrane. Dialysis was performed against distilled water for 2 hours. Before lyophilization, 1% wt. mannitol serving as a cryoprotectant was added to

the compound. A nanocrystalline powder was obtained from which the nanosuspension for application was prepared by dissolving in distilled water containing 5 % wt. glucose.

The parameters of the product obtained, as well as the products of Examples 4 to 10 below, will be listed and summarized in the final section of this chapter.

Example 4

Preparation of nanocrystals based on belotecan and curcumin (BCN) - structure see Fig. 3.

Belotecan hydrochloride (4.3 mg) and curcumin (3.5 mg) in a 1: 1 molar ratio were dissolved in 0.3 mL dimethylsulfoxide (DMSO) at room temperature to form a self-assembled ionic complex, to which 3.4 mg of nonionic surfactant- polyoxylated castor oil - was subsequently added. The organic solution thus obtained was then added to 15 mL of distilled water and stirred as in Example 1, and the suspension obtained was again dialyzed with a MWCO 500 D membrane. Dialysis was performed against distilled water for 1 hour. Before lyophilization, 1% wt. mannitol serving as a cryoprotectant was added to the compound. A powder was obtained from which the nanosuspension was subsequently prepared by dissolving in distilled water containing *5%* wt. glucose.

Example 5

Preparation of nanocrystals based on exatecan and curcumin (ECN) - structure see Fig. 3

Exatecan mesylate (5.3 mg) and curcumin (7.0 mg) at a molar ratio of 1:2 were dissolved in 0.4 mL DMF at room temperature to form a self-assembled ionic complex, to which 1.8 mg of a nonionic poloxamer 105 surfactant was subsequently added The organic solution thus obtained was then added to 20 mL of distilled water and stirred as in Example 1, the suspension obtained was dialyzed using a MWCO 300 D membrane. Dialysis was performed against distilled water for 3 hours. Before lyophilization, 1% wt. mannitol serving as a cryoprotectant was added to the compound. In this way, a nanocrystalline powder was obtained from which the nanosuspension for use was prepared by dissolving the powder in distilled water containing 5% wt. glucose.

Example 6

Preparation of nanocrystals based on lipotecan and curcumin (LiCN) - structure see Fig. 3

Lipotecan hydrochloride (8.8 mg) and curcumin (3.5 mg) in a 1:1 molar ratio were dissolved in 0.3 mL of DMF at room temperature to form a self-assembled ionic complex, to which 1.8 mg

of nonionic surfactant poloxamer 105 was subsequently added. The organic solution thus obtained was then added to 30 mL of distilled water and stirred as in Example 1, the suspension obtained was dialyzed with a membrane of MWCO 500 D. Dialysis was performed against distilled water for 2 hours. Before lyophilization, 1% wt. mannitol serving as a cryoprotectant was added to the compound. In this way, a powder was obtained from which the nanosuspension was prepared before use by dissolving the powder in distilled water containing 5 wt. % glucose and 0.96 wt. % sodium chloride.

Example 7

Preparation of nanocrystals based on afeletecan and curcumin (ACN) - structure see Fig. 3

Afeletecan hydrochloride (9.0 mg) and curcumin (7.5 mg) at a molar ratio of 1:2 were dissolved in 0.5 mL DMSO at room temperature to form a self-assembled ionic complex, to which 2.5 mg of a nonionic surfactant poloxamer 105 was subsequently added. The organic solution thus obtained was then added to 40 mL of distilled water and stirred as in Example 1, and the suspension obtained was dialyzed with a MWCO 1000 D membrane to remove the organic solvent. Dialysis was performed against distilled water for 2 hours. Before lyophilization, 1% wt. mannitol serving as a cryoprotectant was added to the compound. Thus a powder was obtained from which a nanosuspension was subsequently prepared by dissolving in distilled water containing 5% wt. glucose in a weight ratio of 0.01:99.99 (lyophilisate: medium).

Example 8

Preparation of nanocrystals based on lurtotecan and curcumin (LuCN) - structure see Fig. 3

Lurtotecan dihydrochloride (6.0 mg) and curcumin (3.5 mg) in a 1:1 molar ratio were dissolved in 0.3 mL DMSO at room temperature to form a self-assembled ionic complex, to which 1.4 mg of a nonionic surfactant poloxamer 105 was subsequently added The organic solution thus obtained was then added to 15 mL of distilled water and stirred as in the previous examples, the obtained suspension was dialyzed using a MWCO 300 D membrane, the process was performed against distilled water for 2 hours. Before lyophilization, 1% wt. mannitol serving as a cryoprotectant was added to the compound. Within this procedure a powder was obtained from which the nanosuspension was prepared for purposes of application by dissolving in distilled water containing 5% wt. glucose in a weight ratio of 2:98 (lyophilisate: medium).

Example 9

Preparation of nanocrystals based on simmitecan and curcumin (SCN) - structure see Fig. 3

Simmitecan hydrochloride (6.2 mg) and curcumin (7.4 mg) at a molar ratio of 1:2 were dissolved in 0.4 mL of DMF at room temperature to form a self-assembled ionic complex, to which 2 mg of poloxamer 105 was subsequently added as a nonionic surfactant. The organic solution thus obtained was then added to 30 mL of distilled water and stirred as in the previous examples, and the suspension obtained was dialyzed using a MWCO 300 D membrane. Dialysis was performed against distilled water for 3 hours. Before lyophilization, 1% wt. mannitol serving as a cryoprotectant was added to the compound. In this way a powder was obtained from which the nanosuspension was prepared for application by dissolving in distilled water containing 5% wt. glucose in a weight ratio of 3:97 (lyophilisate: medium).

Example 10

Preparation of nanocrystals based on elomotecan and curcumin (EmCN) - structure see Fig. 3

Elomotecan hydrochloride (5.5 mg) and curcumin (7.4 mg) in a molar ratio of 1:2 were dissolved in 0.4 mL DMSO at room temperature to form a self-assembled complex, to which 2 mg of poloxamer 105 were subsequently added. The organic solution thus obtained was then added to 30 mL of distilled water and stirred as in the previous examples, the obtained suspension was dialyzed using a MWCO 300 D membrane. Dialysis was performed against distilled water for 3 hours. Before lyophilization, 1% wt. mannitol serving as a cryoprotectant was added to the compound. In this way a powder was obtained from which the application nanosuspension was prepared by dissolving in distilled water containing 5% wt. glucose in a weight ratio of 2:98 (lyophilisate: medium).

The compositions described in Examples 3 to 10 exhibited the following properties:

In the case of nanoparticles based on curcumininoid and other protonated nitrogen-containing derivatives of camptothecin and its analogues as shown in Examples 3 to 10, e.g. topotecan hydrochloride (TCN), belotecan hydrochloride (BCN), exatecan mesylate (ECN), lipotecan hydrochloride (LiCN)), afeletecan hydrochloride (ACN), lurtotecan dihydrochloride (LuCN), simmitecan hydrochloride (SCN) or elomotecan hydrochloride (EmCN), they were discovered to have similar properties to irinotecan based particles in terms of size, size distribution, surface charge and morphology.

The concentration of bioactive components (ICN, TCN, BCN and ECN) - see Examples 1 to 5 in the prepared nanoparticles was verified by high performance liquid chromatography (HPLC). As can be seen from Fig. 4D, the detected proportion of bioactive substances in the particles

was 70% wt. In the case of camptothecin and curcuminoid derivatives, their proportional presence in nanoparticles was almost identical with the initial ratio before the start of the reaction.

Changes in the selected characteristics of irinotecan-based nanoparticles were also observed under various environmental conditions. Fig. 5 shows the behaviour of nanoparticles at different pH or ionic strength. The surface tension of nanoparticles decreased with the increasing acidity of the environment (pH less than 7). Negative zeta potential values of nanoparticles were recorded in an alkaline environment (pH greater than 7). On the contrary, only minor changes occurred in the size of nanoparticles and the width of their polydispersity as a consequence of further impact of repulsive steric forces induced by the presence of nonionic complexes. In addition, nanoparticles are stable even after 8 hours in phosphate buffer (pH 7.4) at 37.5 ° C, with a slight increase in particle diameter and polydispersity.

Example 11

Preparation of the composition and experimental verification of the therapeutic effect - see Fig. 7 - 13.

Irinotecan hydrochloride 6.2 mg and curcumin 3.7 mg were dissolved in 0.4 mL dimethylsulfoxide (DMSO) at room temperature and 15% wt. d. poloxamer 105 was added. The obtained organic solution was added to 20 mL of distilled water with stirring (500 rpm) for 4 min at room temperature. The obtained suspension was transferred to a dialysis tube where MWCO (molecular-weight-cut-off) = 300 D, and dialyzed against distilled water to remove the organic solvent. Mannitol was added as a cryoprotectant. Irinotecan-curcumin powder was obtained by lyophilisation. By dissolving it in distilled water containing 5% wt. glucose, an anticancer emulsion for injection applications was obtained.

The anti-cancer effects of this injectable formulation were investigated *in vivo* using intestinal cells of the HT-29 line on a tumour created by subcutaneous graft of these cells applied in mouse (nude mouse). The experiment strategy is shown in Fig. 7.

Progress and monitoring:

Once the average tumour volume reached about 100 mm^3, mice were randomly separated into three groups of 4-5 in each group and injected intravenously with 1) PBS, 2) I, 3) ICN (equivalent to the amount of irinotecan alone - 27.5 mg / kg) every other day for a total of 19 days.

Course of treatment: Body weight and tumour volume were measured every 3 days. Tumour volume was calculated according to the formula Tv = length x width^2/2. 5 days after interruption of medication, mice were sacrificed, by tumours were subsequently (day 25 from the start of the experiment) removed, weighed and photographed.

Monitoring of undesirable side effects: Diarrhea was reported according to the following scale: stool 0 - normal or none, 1 - slightly wet and soft, 2 - moderately soft and unshaped with moderate peri-anal contamination, 3 - intense, watery with critical contamination in the peri-anal area.

Evaluation of therapeutic effects:

Compared to the PBS group in mice in both treatment groups, the average tumour volumes were effectively regulated and there were significant differences from the untreated group at day 9 (about 1 week after the first administration - Fig. 8). Tumour volume decline occurred in the treatment groups on day 15 (about 2 weeks after the first administration, Fig. 9). The treatment groups also show significant differences in tumour weight compared to PBS (blind) - Fig. 10. Photodocumentation of the removed tumours is shown in Fig. 11.

There was no statistical difference between the two treatment groups throughout the experiment. The results confirm that the efficacy of the combined nanoformulation of the ICN according to the invention is the same as the anti-cancer effect of irinotecan hydrochloride itself, and that the tumour regression effect is induced by irinotecan instead of curcumin in the ICN according to the invention. This can be attributed to a significant difference in half maximal inhibitory concentration of the both substances. Curcumin can generally be considered as biologically safe at the therapeutic level / concentration of irinotecan used.

In addition, no significant weight loss was observed in any of the mice throughout the whole experiment, which would indicate even minor side effects of the ICN nano-formulation according to the invention at the dosage used in the treatment of the tumour - Fig. 12.

Evaluation of undesirable side effects:

As can be seen from Fig. 13, diarrhea was significantly delayed in mice treated with irinotecan alone on day 10 after the first administration ($p < 0.01$), with no distinct diarrhea in the PBS group (blind - no treatment) throughout the whole experiment, but also not in the ICN group (mice treated with the composition according to the invention). Reduction of diarrhea in mice in this group shows that the presence of curcumin together with irinotecan in the

nanofonnulation according to the invention can reduce intestinal load and thus protect the intestines, thus increasing the patients' comfort. This can be attributed either to the therapeutic effects of the curcumin molecule or to a change in the drug formulation from irinotecan alone to its combination with curcumin according to the invention.

Industrial applicability

The composition for the preparation of nanocrystals for medicaments with the enhanced biological availability, the method of the preparation of nanocrystals and the use of nanocrystals in injectable applications according to the invention will find use preferably in the field of production of medicaments with the increased requirement for biological availability and tolerability. It will be used especially in the field of preparation of cytostatics - anticancer agents.

CLAIMS

1. A method of preparation of nanocrystals with enhanced biological availability, characterized by that the procedure of preparation in the powder form contains the following steps:

a) dissolving the protonated nitrogen containing derivatives 15of camptothecin and curcuminoids in an organic solvent leading to formation of self-assembled ionic complex followed by subsequent addition of nonionogenic injectable surfactant;

b) transferring the obtained mixture into aqueous medium under continuous homogenization including mixing, shaking and/or using ultra-sound;

c) removing the solvent in order to obtain powder form;

d) lyophilisation of the product with the previously added cryoprotectant.

2. The method of preparation of nanocrystals according to claim 1, characterized by that the organic solvent used in the step a) is dimethylsulphoxide, propylen carbonate, acetonitrile, acetone, dimethylformamide, tetrahydrofurane, methylpyrrolidone, hexamethylphosphoramide, methanol, ethanol, acetic acid or their combination.

3. The method of preparation of nanocrystals according to claim 1, characterized by that the cryoprotectant used in step d) is lactose, mannitol, sucrose, trehalose, fructose, glucose, sodium alginate, gelatine or their combination.

4. A composition for preparation of nanocrystals with enhanced biological availability and nanocrystals prepared from this composition by the method according to claim 1, characterized by that the composition comprises of injectable nonionic surfactant and self-assembled ionic complex based on curcuminoids and protonated nitrogen containing camptothecin derivatives and its analogues in the molar ratio between 10:1 and 1:10.

5. A composition for preparation of nanocrystals according to claim 4, characterized by that the camptothecin analogues contain protonated nitrogen and include camptothecin and homocamptothecin.

6. A composition for preparation of nanocrystals according to claim 4 and 5, characterized by that the protonated nitrogen containing derivatives of camptothecin contain in their chemical structure at least one of functional groups including primary amine, secondary amine, tertiary amine, cyclic amine and/or their combinations.

7. A composition for preparation of nanocrystals according to claim 4 and 6, characterized by that the derivatives of camptothecin, which contain primary amine included in their chemical structure, include one or more substances from the group of 9-aminokamptothecin, exatecan, delimotecan, namitecan.

8. A composition for preparation of nanocrystals according to claim 4 and 6, characterized by that the derivatives of camptothecin, containing secondary amine in their chemical structure, include belotecan.

9. A composition for preparation of nanocrystals according to claim 4 and 6, characterized by that the derivatives of camptothecin, containing tertiary amine in their chemical structure, include topotecan and/or lipotecan.

10. A composition for preparation of nanocrystals according to claim 4 and 6, characterized by that the derivatives of camptothecin containing cyclic amine in their chemical structure, include one or more compounds from the group of irinotekan, lurtotecan, afeletecan, simmitecan, elomotecan.

11. A composition for preparation of nanocrystals according to claim 4, characterized by that the derivatives of nitrogen containing camptothecin analogues are present in form of salts of organic or inorganic acids selected from the group including hydrochloric acid, sulphuric acid, phosphoric acid, hydrobromic acid, perchloric acid, methanesulfonic acid, acetic acid, maleic acid, tartaric acid, citric acid or their combinations.

12. A composition for preparation of nanocrystals according to claim 4, characterized by in that the injectable nonionogenic surfactant is based on cholesterol, poloxamers, polyoxyl castor oil, polysorbates or their combinations.

13. Utilization of nanocrystals prepared according to the claim 1 for the anticancer injectable drug application, characterized by that the nanocrystals in the powder form are dissolved in the liquid medium comprised of distilled water with 5 wt. % of

glucose where the weight ratio of nanocrystals and liquid medium is in the range between 0.01:99.99 and 3:97.

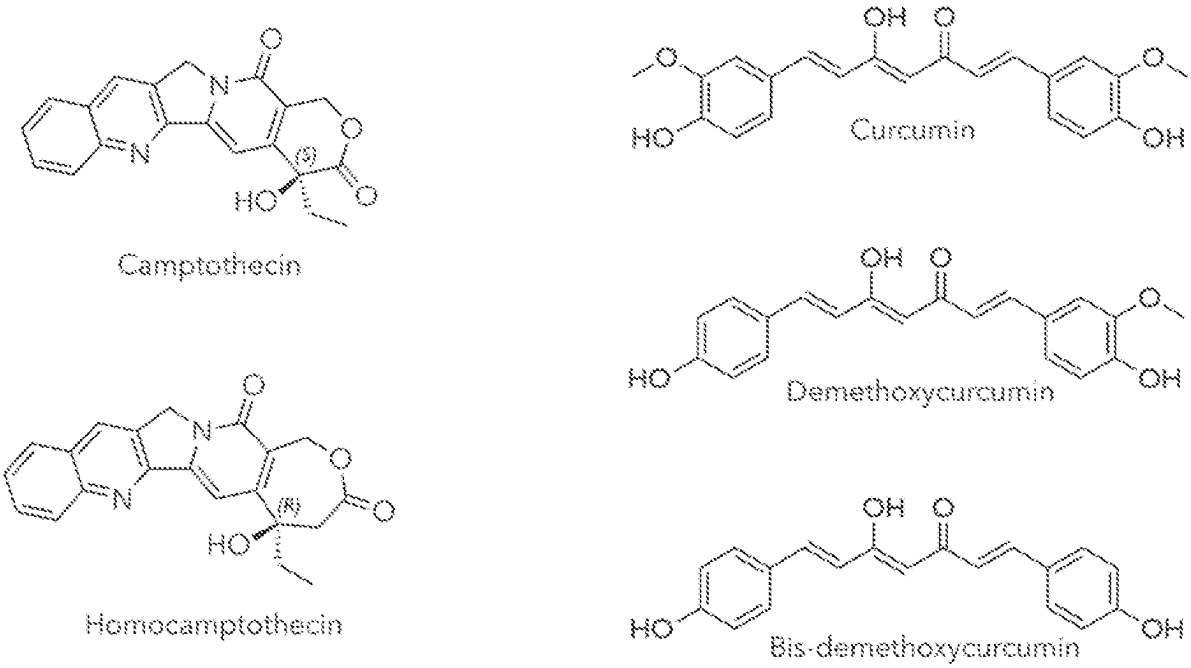
Camptothecin
Curcumin
Demethoxycurcumin
Homocamptothecin
Bis-demethoxycurcumin

Fig. 1

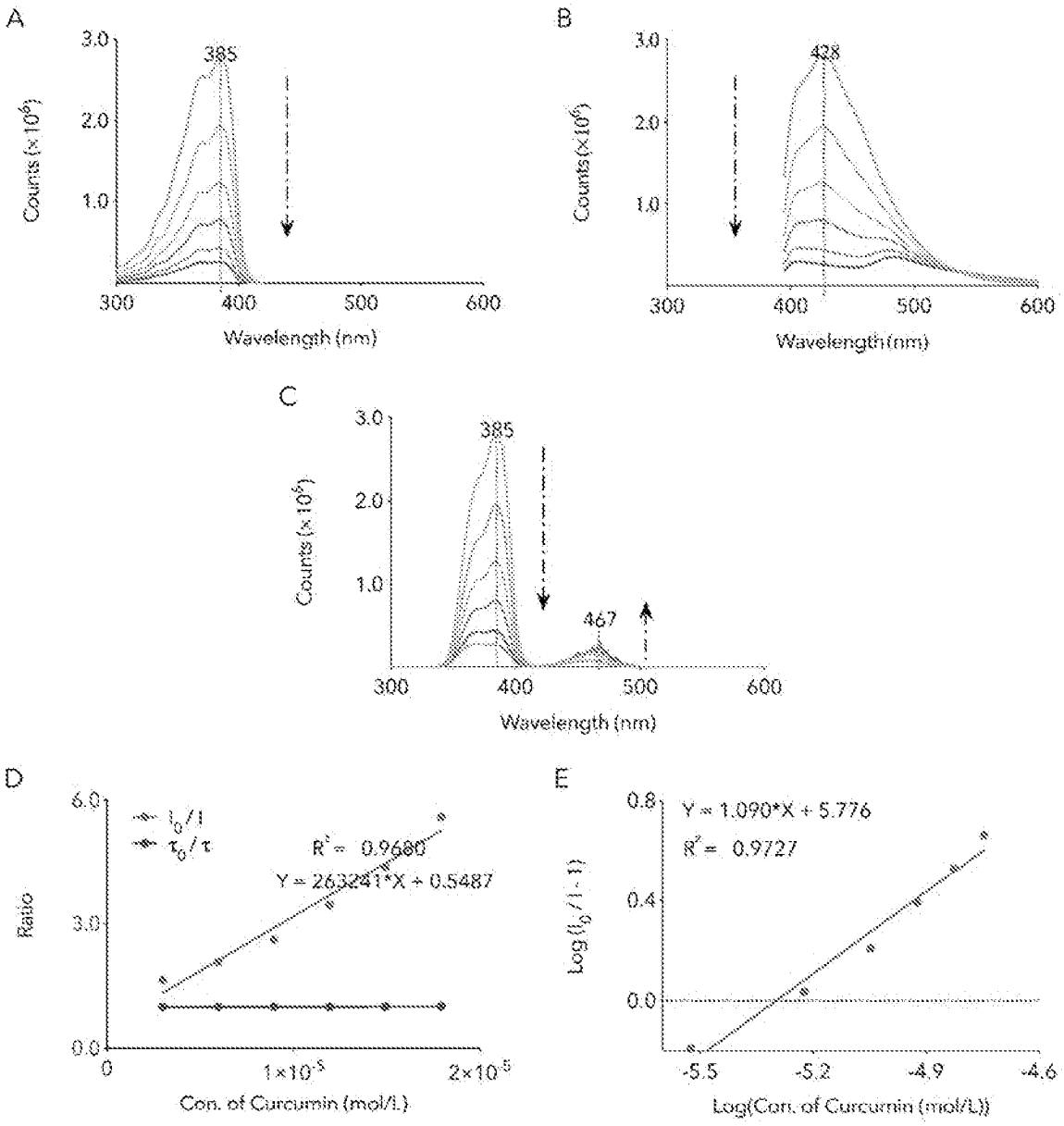
A
385
Counts (×10⁶)
Wavelength (nm)
B
428
Counts (×10⁶)
Wavelength (nm)
C
385
467
Counts (×10⁶)
Wavelength (nm)
D
I₀/I
τ₀/τ
R² = 0.9680
Y = 263241*X + 0.5487
Ratio
Con. of Curcumin (mol/L)
E
Y = 1.090*X + 5.776
R² = 0.9727
Log (I₀/I - 1)
Log(Con. of Curcumin (mol/L))

Fig. 2 A-E

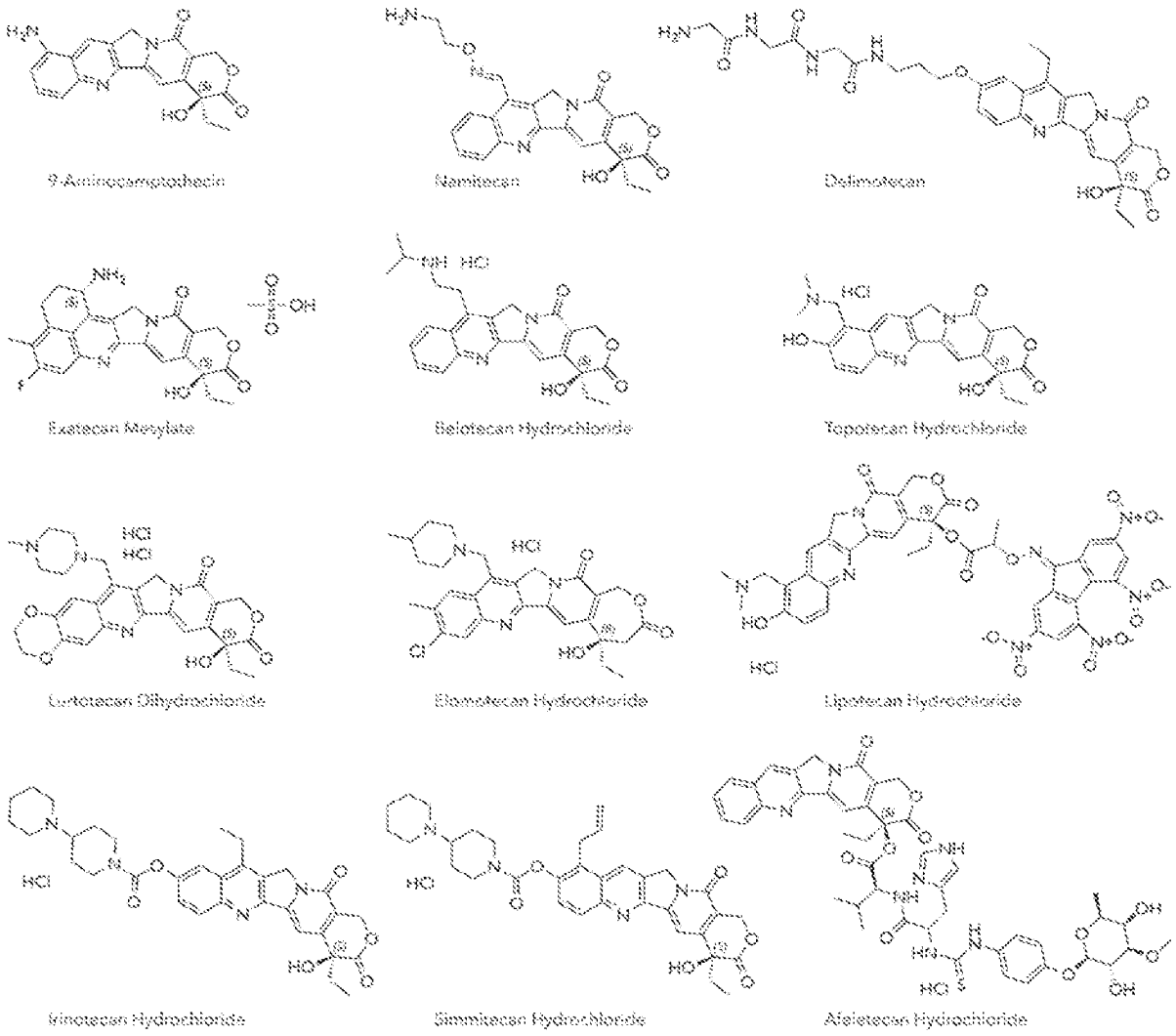
9-Aminocamptothecin
Namitecan
Delimotecan
Exatecan Mesylate
Belotecan Hydrochloride
Topotecan Hydrochloride
Lurtotecan Dihydrochloride
Elomotecan Hydrochloride
Lipotecan Hydrochloride
Irinotecan Hydrochloride
Simmitecan Hydrochloride
Afelotecan Hydrochloride

Fig. 3

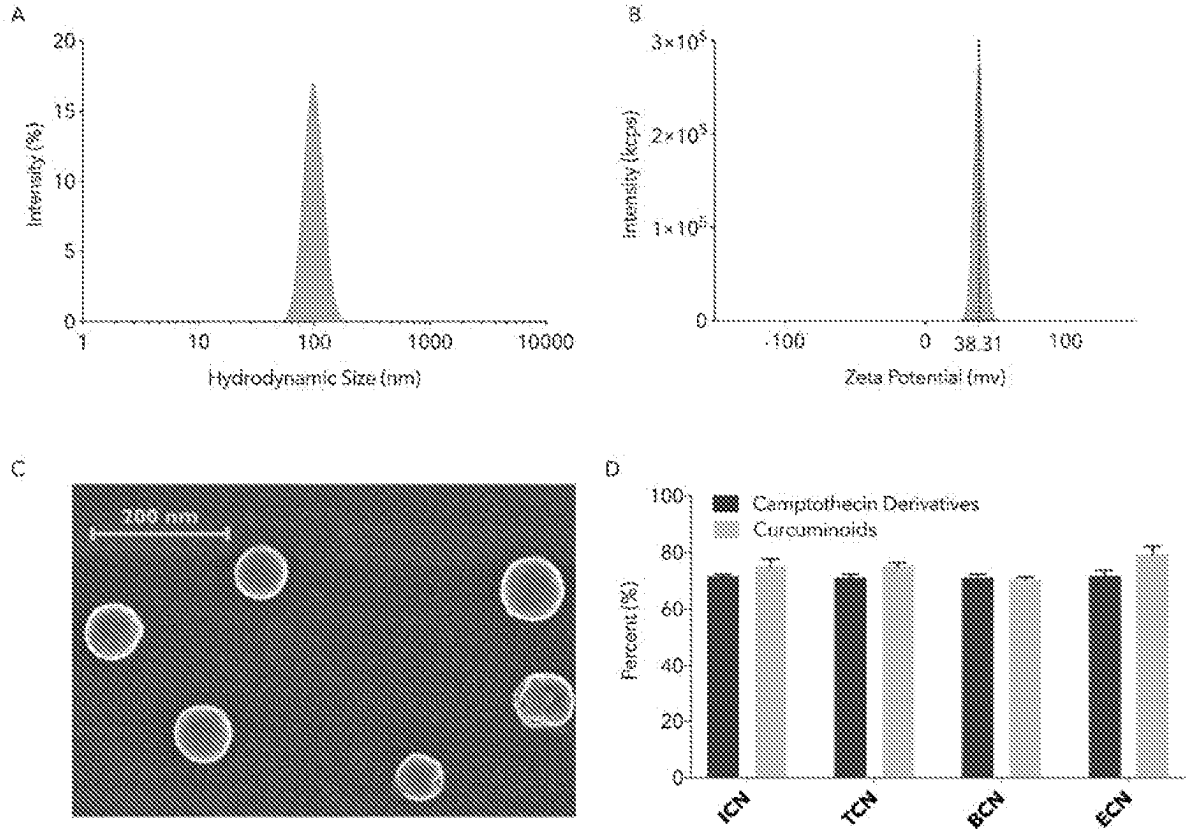
A
Intensity (%)
Hydrodynamic Size (nm)
B
Intensity (kcps)
Zeta Potential (mv)
38.31
C
D
Camptothecin Derivatives
Curcuminoids
Percent (%)
ICN
TCN
BCN
ECN

Fig. 4 A-D

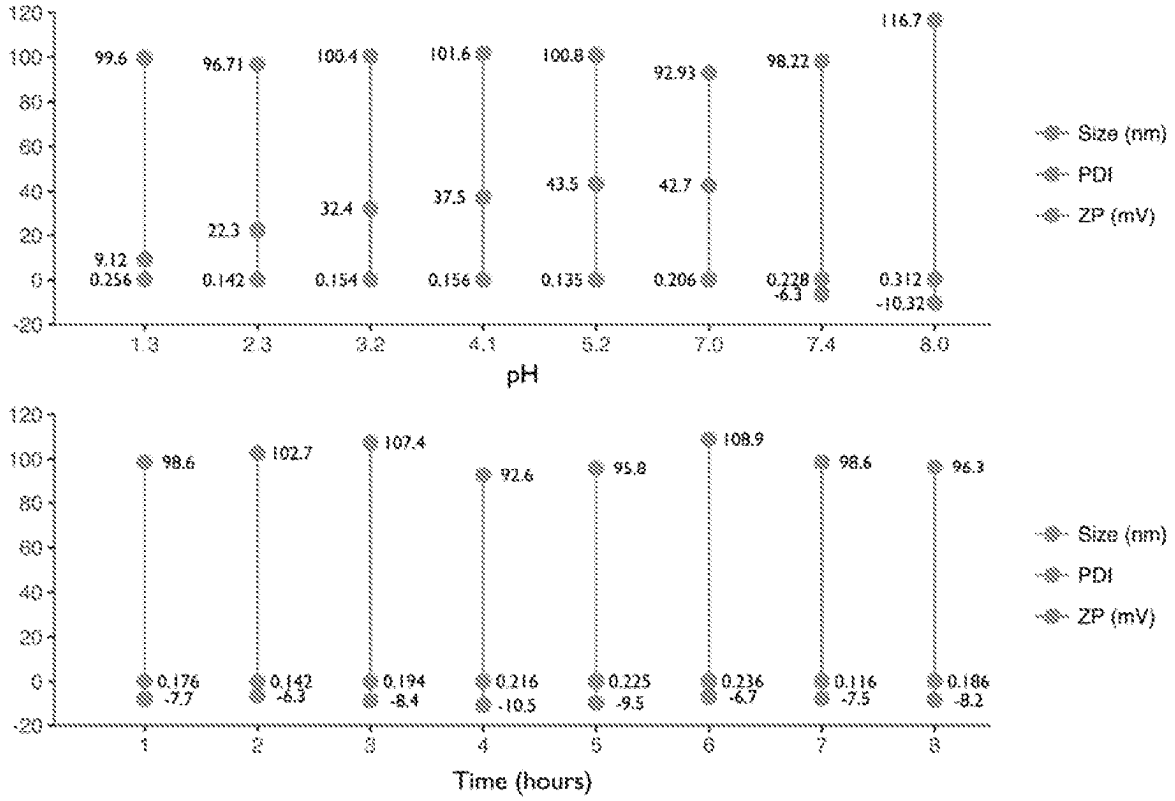
120
100
80
60
40
20
0
-20
99.6
96.71
100.4
101.6
100.8
92.93
98.22
116.7
9.12
0.256
22.3
0.142
32.4
0.154
37.5
0.156
43.5
0.135
42.7
0.206
0.228
-6.3
0.312
-10.32
1.3
2.3
3.2
4.1
5.2
7.0
7.4
8.0
pH
Size (nm)
PDI
ZP (mV)
98.6
102.7
107.4
92.6
95.8
108.9
98.6
96.3
0.176
-7.7
0.142
-6.3
0.194
-8.4
0.216
-10.5
0.225
-9.5
0.236
-6.7
0.116
-7.5
0.186
-8.2
1
2
3
4
5
6
7
8
Time (hours)
Size (nm)
PDI
ZP (mV)

Fig. 5

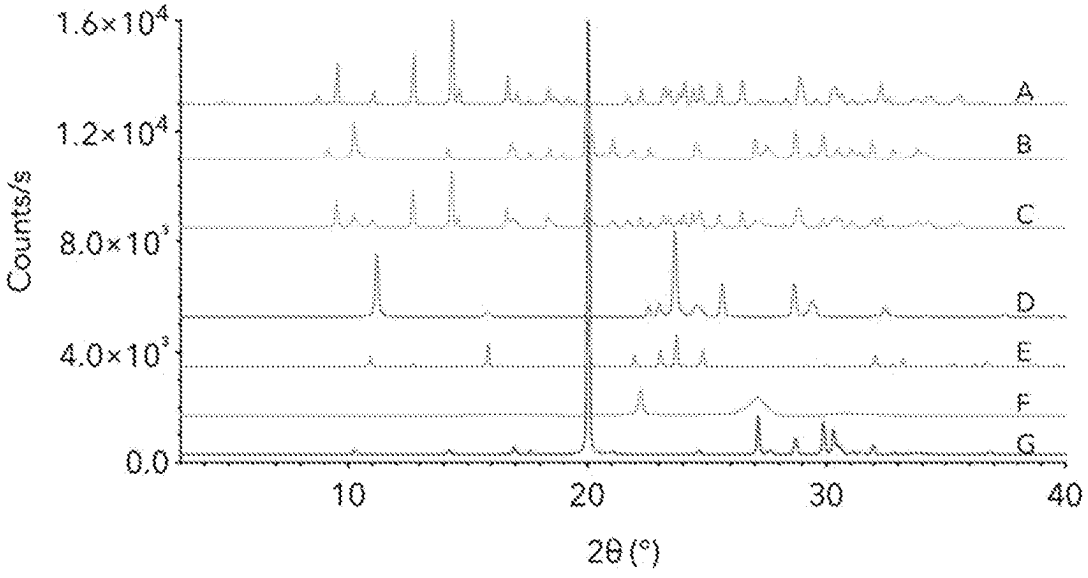
1.6×10⁴
1.2×10⁴
8.0×10³
4.0×10³
0.0
Counts/s
A
B
C
D
E
F
G
10
20
30
40
2θ (°)

Fig. 6

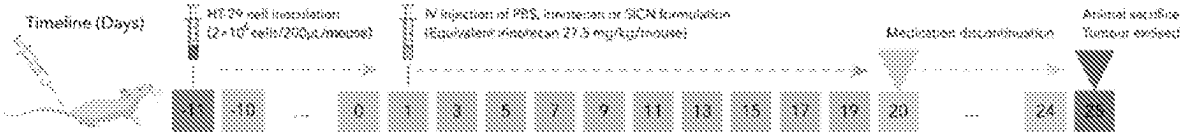

Fig. 7

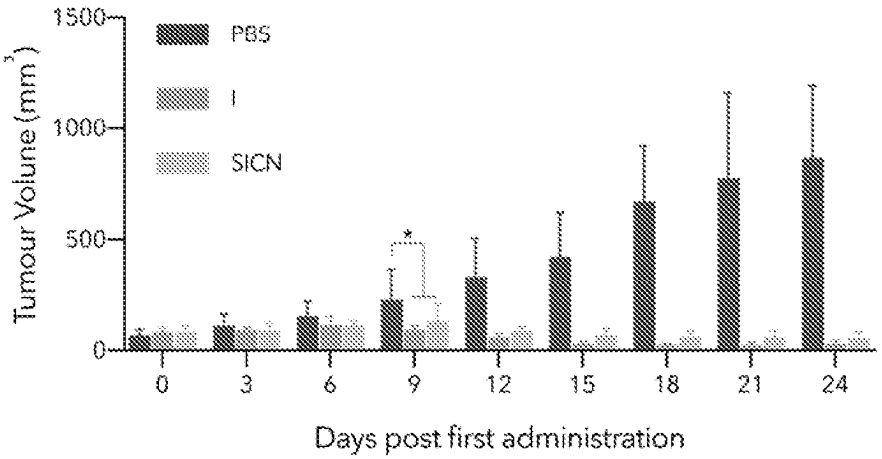

Fig. 8

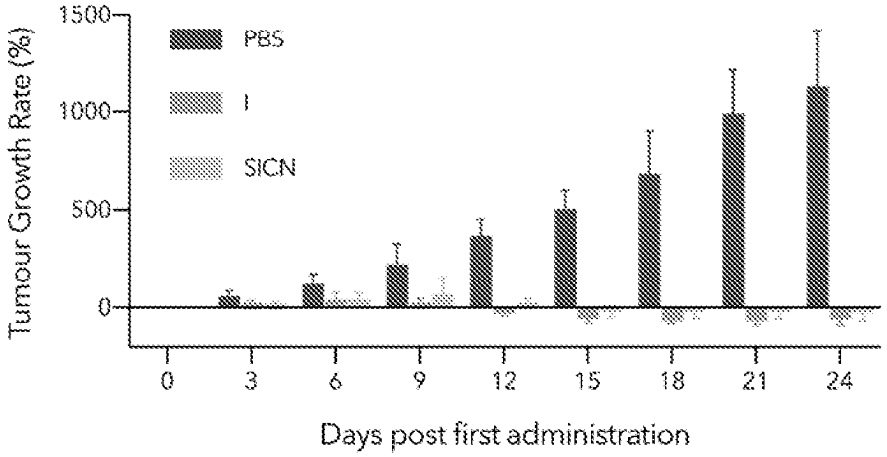

Fig. 9

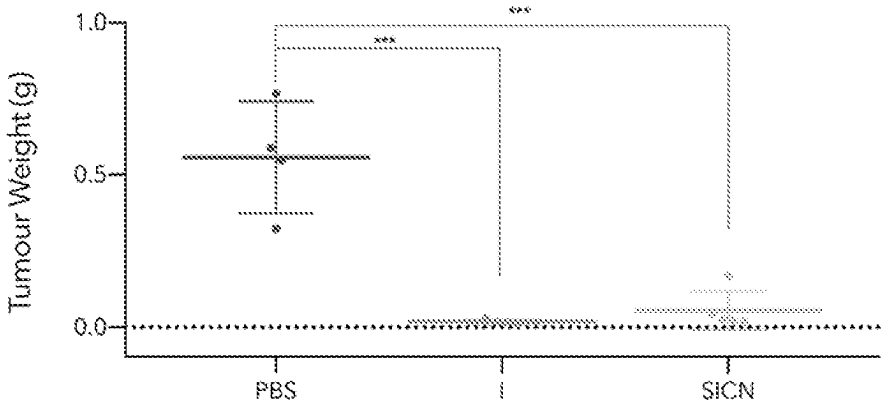

Fig. 10

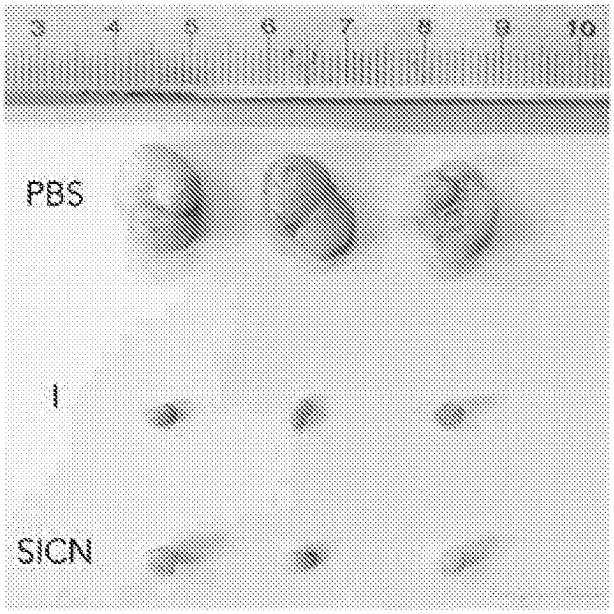

Fig. 11

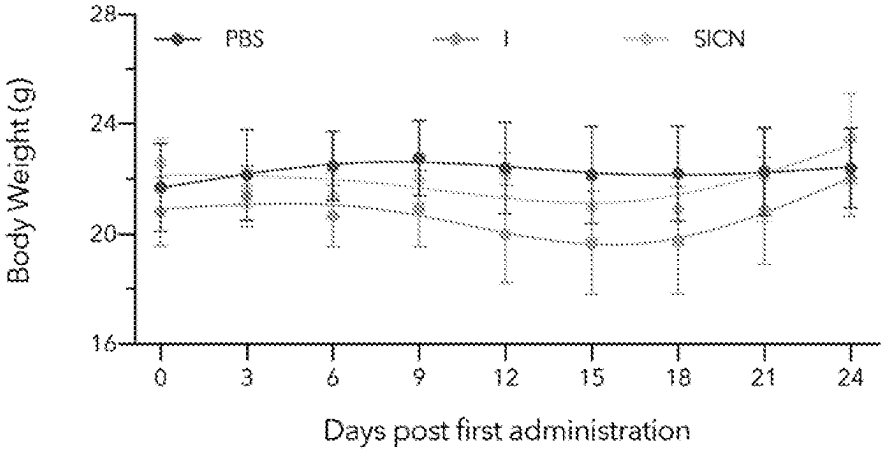
PBS
I
SICN
Body Weight (g)
28
24
20
16
0
3
6
9
12
15
18
21
24
Days post first administration

Fig. 12

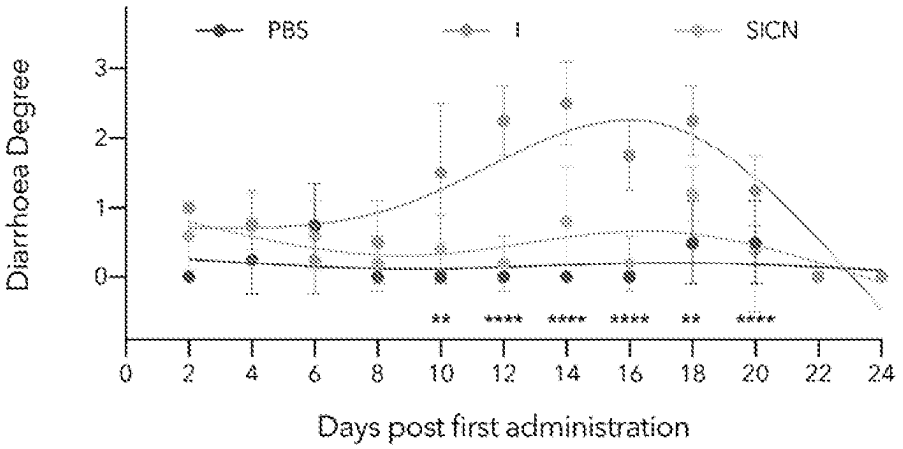
PBS
I
SICN
Diarrhoea Degree
3
2
1
0
**
****
****
****
**
****
0
2
4
6
8
10
12
14
16
18
20
22
24
Days post first administration

Fig. 13

INTERNATIONAL SEARCH REPORT

International application No
PCT/CZ2019/050048

A. CLASSIFICATION OF SUBJECT MATTER
INV. A61K9/14 A61K9/19 A61K31/4745
ADD.

According to International Patent Classification (IPC) or to both national classification and IPC

B. FIELDS SEARCHED

Minimum documentation searched (classification system followed by classification symbols)
A61K

Documentation searched other than minimum documentation to the extent that such documents are included in the fields searched

Electronic data base consulted during the international search (name of data base and, where practicable, search terms used)
EPO-Internal , WPI Data

C. DOCUMENTS CONSIDERED TO BE RELEVANT

Category*	Citation of document, with indication, where appropriate, of the relevant passages	Relevant to claim No.
X Y	WO 02/064064 A1 (SUPERGEN INC [US]; RTP PHARMA INC [CA] ET AL.) 22 August 2002 (2002-08-22) the whole document claims 1-131 -----	4-13 1-13
Y	WO 2005/002546 A1 (SMITHKLINE BEECHAM CORP [US]; OH CHOON K [US]; IGNATIOUS FRANCIS [US]) 13 January 2005 (2005-01-13) the whole document claims 1-8; examples 1-6 -----	1-13

☐ Further documents are listed in the continuation of Box C.

☒ See patent family annex.

* Special categories of cited documents :

"A" document defining the general state of the art which is not considered to be of particular relevance

"E" earlier application or patent but published on or after the international filing date

"L" document which may throw doubts on priority claim(s) orwhich is cited to establish the publication date of another citation or other special reason (as specified)

"O" document referring to an oral disclosure, use, exhibition or other means

"P" document published prior to the international filing date but later than the priority date claimed

"T" later document published after the international filing date or priority date and not in conflict with the application but cited to understand the principle or theory underlying the invention

"X" document of particular relevance; the claimed invention cannot be considered novel or cannot be considered to involve an inventive step when the document is taken alone

"Y" document of particular relevance; the claimed invention cannot be considered to involve an inventive step when the document is combined with one or more other such documents, such combination being obvious to a person skilled in the art

"&" document member of the same patent family

Date of the actual completion of the international search	Date of mailing of the international search report
21 January 2020	28/01/2020

Name and mailing address of the ISA/	Authorized officer
European Patent Office, P.B. 5818 Patentlaan 2 NL - 2280 HV Rijswijk Tel. (+31-70) 340-2040, Fax: (+31-70) 340-3016	Felder, Christian

1

INTERNATIONAL SEARCH REPORT

Information on patent family members

International application No
PCT/CZ2019/050048

Patent document cited in search report	Publication date	Patent family member(s)	Publication date
WO 02064064 A1	22-08-2002	EP 1365705 A1	03-12-2003
		WO 02064064 A1	22-08-2002
WO 2005002546 A1	13-01-2005	EP 1643972 A1	12-04-2006
		JP 2007522085 A	09-08-2007
		US 2006222694 A1	05-10-2006
		WO 2005002546 A1	13-01-2005

Biomaterials 232 (2020) 119701

Contents lists available at ScienceDirect

Biomaterials

journal homepage: www.elsevier.com/locate/biomaterials

Structure-based design of charge-conversional drug self-delivery systems for better targeted cancer therapy

Haijun Xiao[a,1], Yiping Guo[b,1], Hongmei Liu[c], Yushi Liu[c], Yumin Wang[a], Changqing Li[b,d], Jaroslav Císař[a], David Škoda[a], Ivo Kuřitka[a], Li Guo[c,e,*], Vladimír Sedlařík[a,**]

[a] Centre of Polymer Systems, Tomas Bata University in Zlin, Zlin, 76001, Czech Republic
[b] Quantitative and Systems Biology Program, University of California, Merced, CA, 95343, USA
[c] School of Pharmacy, Chengdu University of Traditional Chinese Medicine, Chengdu, 611137, China
[d] Department of Bioengineering, University of California, Merced, CA, 95343, USA
[e] State Key Laboratory of Characteristic Chinese Medicine Resources in Southwest China, Chengdu University of Traditional Chinese Medicine, Chengdu, 611137, China

ARTICLE INFO

Keywords:
Irinotecan
Curcumin
Charge conversion
Self-delivery
Targeting therapy
Diarrhea

ABSTRACT

Various design and fabrication strategies of carrier-based drug delivery systems have been quickly established and applied for cancer therapy in recent years. These systems contribute greatly to current cancer treatments but further development needs to be made to eliminate obstacles such as low drug loading capacity and severe side effects. To achieve better drug delivery, we propose an innovative strategy for the construction of easy manufactured drug self-delivery systems based on molecular structures, which can be used for the co-delivery of curcuminoids and all the nitrogen-containing derivatives of camptothecin for better targeted cancer therapy with minimized side effects. The formation mechanism investigation demonstrates that the rigid planar structures of camptothecin derivatives and curcuminoids with relevant leaving hydrogens make it possible for them to be assembled into nanoparticles under suitable conditions. These nanoparticles show stabilized particle sizes (100 nm) under various conditions and tunable surface charges which increase from around −10 mV in a normal physiological condition (pH 7.4) to +40 mV under acidic tumor environments. In addition, *in vivo* mice experiments have demonstrated that, compared to irinotecan (a derivative of camptothecin) itself, the co-delivered irinotecan curcumin nanoparticles exhibited significantly enhanced lung and gallbladder targeting, improved macrophage-clearance escape and ameliorated colorectal cancer treatment with an eradication of life-threatening diarrhea, bringing hope for better targeted chemotherapy and clinical translation. Lastly, the strategy of structure based design of drug self-delivery systems may inspire more research and discoveries of similar self-delivered nano systems for wider pharmaceutical applications.

1. Introduction

Cancer is the second largest cause of death globally. Chemotherapy based on small molecules remains one of the most effective ways to fight against various cancers. For example, topotecan (Fig. 1a), a derivative of camptothecin, has been used for the treatment of ovarian cancer, cervical cancer and lung cancer, among which lung cancer causes the largest cancer-related death in 2018 (1.8 million deaths) and still remains the leading diagnosed malignancy in 2018 (2.1 million new cases). Irinotecan (Fig. 1a), another camptothecin derivative, has been used as the first-line treatment for colorectal cancer [1], the third most commonly diagnosed malignancy (1.8 million new cases in 2018) causing the second largest number of cancer-related deaths (0.86 million deaths in 2018). These small molecular chemotherapeutic agents are usually intravenously injected into the body yielding systemic effects. This approach is especially advantageous when dealing with metastatic cancer but the concomitant challenge involves balancing the therapeutic effects of the drug with their undesirable side effects [2].

Many approaches have been explored to minimize the adverse effects of drugs as well as to solve other problems, such as the poor water solubility of more than 80% of drug candidates [3,4], including altering their chemical structures by covalently conjugating with hydrophilic moieties [5,6] and making advantages of various carriers [7]. Nevertheless, these newly introduced moieties or carriers themselves need

* Corresponding author. School of Pharmacy, Chengdu University of Traditional Chinese Medicine, Chengdu, 611137, China.
** Corresponding author. Centre of Polymer Systems, Tomas Bata University in Zlin, Zlin, 76001, Czech Republic.
E-mail addresses: guoli@cdutcm.edu.cn (L. Guo), sedlarik@utb.cz (V. Sedlařík).
[1] Both authors contributed equally to this project.

https://doi.org/10.1016/j.biomaterials.2019.119701
Received 29 August 2019; Received in revised form 21 November 2019; Accepted 18 December 2019
Available online 19 December 2019
0142-9612/

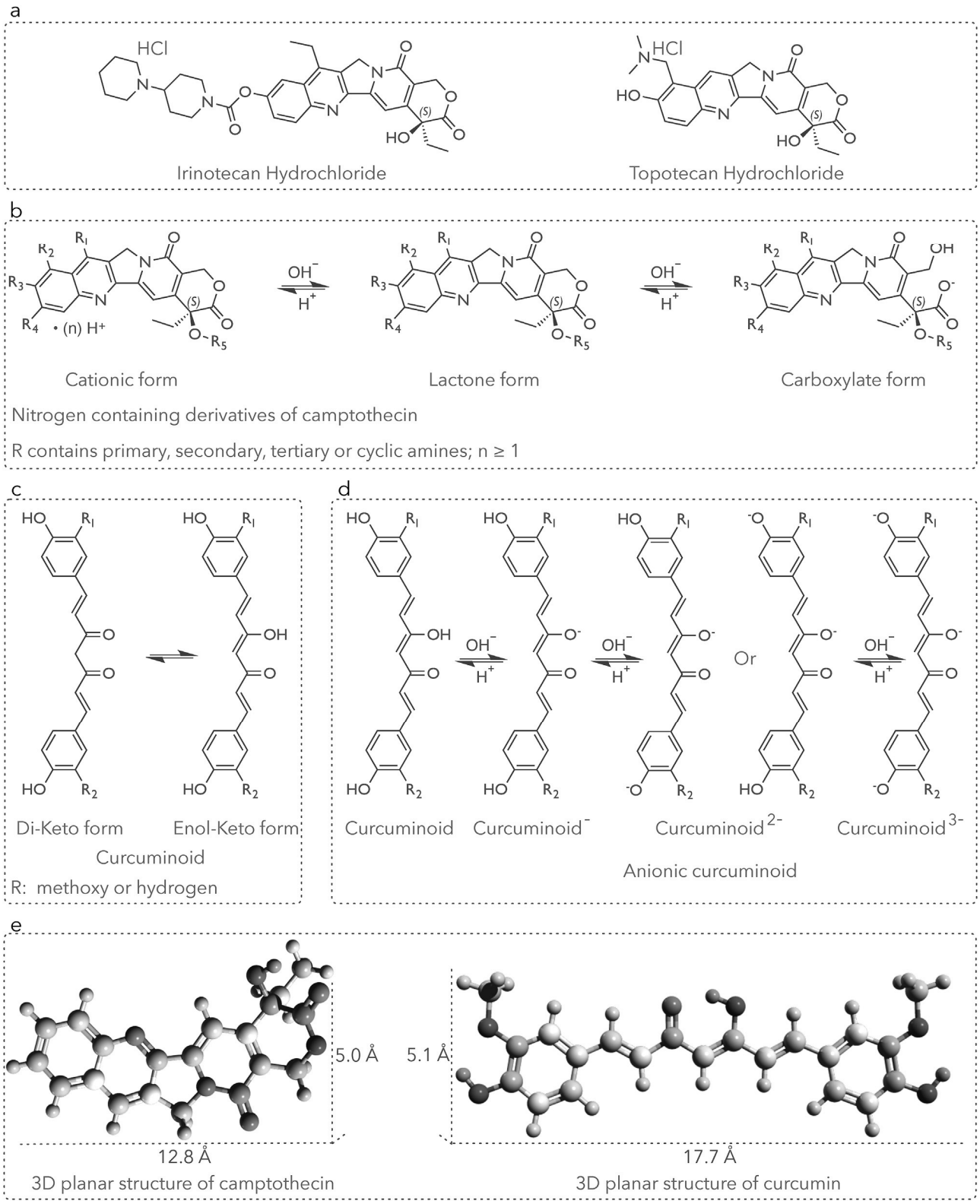

Fig. 1. Structures and properties of camptothecin derivatives and curcuminoids. (a) Chemical structures of irinotecan hydrochloride and topotecan hydrochloride. (b) Protonated nitrogen-containing derivatives of camptothecin by forming salts with medicinal acids (left); the pH-dependent lactone hydrolysis equilibria of camptothecin derivatives (right). (c) Chemical structures of curcuminoids in enol-keto tautomeric equilibria. (d) Dissociation equilibria between curcuminoids and their anions. (e) Three-dimensional grid planar structures and sizes of camptothecin and curcumin (color by partial charge; red, negative; blue, positive; Å, angstrom).

vigorous trials before clinical use [8] and they usually display a more complicated path through the clinic [9]. Furthermore, the involute design and fabrication procedures of many nanomedicines become real obstacles in the practical industrial manufacture [10–12].

Camptothecin is a natural hydrophobic alkaloid with multiple conjugated aromatic rings and rigid planar structure [13,14] (Fig. 1e), allowing it to sustain the DNA/topoisomerase complex and subsequently result in cell death [15]. Due to the lone pairs, the nitrogen-containing camptothecin derivatives are industrially protonated by forming salts with relevant medicinal acids to further improve their water solubility and minimize the toxicity (Fig. 1b). However, one common problem for all the derivatives of camptothecin is that they undergo pH-dependent lactone hydrolysis to get pharmacologically inactive carboxylate forms which show little topoisomerase inhibitory activity [16,17]. Besides, these camptothecin derivatives also cause many side effects, such as the vascular discomfort due to the low pH value (pH 3.5) of their commercial injections and the severely life-threatening diarrhea [18].

Curcuminoids (Fig. 1c) are linear diarylheptanoids extracted from *Curcuma longa*. They exhibit many pharmacological effects and have been reported to attenuate cell resistance [19,20], ameliorate gastrointestinal toxicity [21], protect heart tissue [22] and also possess antitumor activities [23,24]. However, the applications of curcuminoids are heavily limited due to their extremely poor water solubility.

So far, no nano formulations based on these two molecular species have been reported. For the first time, we propose a strategy for the construction of easy manufactured drug self-delivery systems based on molecular structures, which can be used for the co-delivery of curcuminoids and all the nitrogen-containing derivatives of camptothecin for better targeted cancer therapy *via* charge conversion. The formation mechanism investigation demonstrates that the two molecular species can self-assemble into complex of ion pairs in polar organic solvents through intermolecular non-covalent interactions, resulting in a uniform distribution with certain molar ratios before being penetrated into anti-solvents to form nanoparticles. As shown in Scheme 1, these nanoparticles show stabilized particle sizes (100 nm) under various conditions and tunable surface charges which increase from around −10 mV in a normal physiological condition (pH 7.4) to +40 mV under acidic tumor environments. The water solubility of curcuminoids is dramatically improved and the lactone hydrolysis of camptothecin derivatives is also restricted to keep their pharmacologically active forms. Besides, the formulation with a pH value close to that of normal blood would reduce the side effects caused to blood vessels and improve the patient compliance compared to commercial injections of camptothecin derivatives (pH 3.5). More importantly, *in vivo* mice experiments have confirmed that, compared to irinotecan itself, the co-delivered irinotecan curcumin nanoparticles exhibited dramatically enhanced lung and gallbladder targeting, improved macrophage-clearance escape and better colorectal cancer treatment with an eradication of life-threatening diarrhea, which brings great hope for better targeted chemotherapy and clinical translation. The strategy of construction of drug self-delivery systems based on molecular structures may inspire more discoveries of similar formulations for wider pharmaceutical applications.

2. Materials and methods

2.1. Materials

Irinotecan hydrochloride, topotecan hydrochloride, curcumin, poloxamer 105, mannitol, glucose, paraformaldehyde and dimethyl sulfoxide (DMSO) were purchased from Sigma-Aldrich and used as received. Wortmannin, cytochalasin D, genistein and methyl-β-cyclodextrin were purchased from Meilun Biotechnology Co. Ltd (Dalian, China). Chlorpromazine was obtained from Selleck Chemicals (China). Phosphate buffered saline (PBS, pH = 7.4) was prepared in laboratory and ultrapure water was produced using a Milli-Q integral water purification system.

2.2. Nanoparticle preparation

Surfactant stabilized irinotecan hydrochloride curcumin nanoparticles (SICN) were prepared based on a simple precipitation method. Briefly, irinotecan hydrochloride (6.2 mg) and curcumin (3.7 mg)

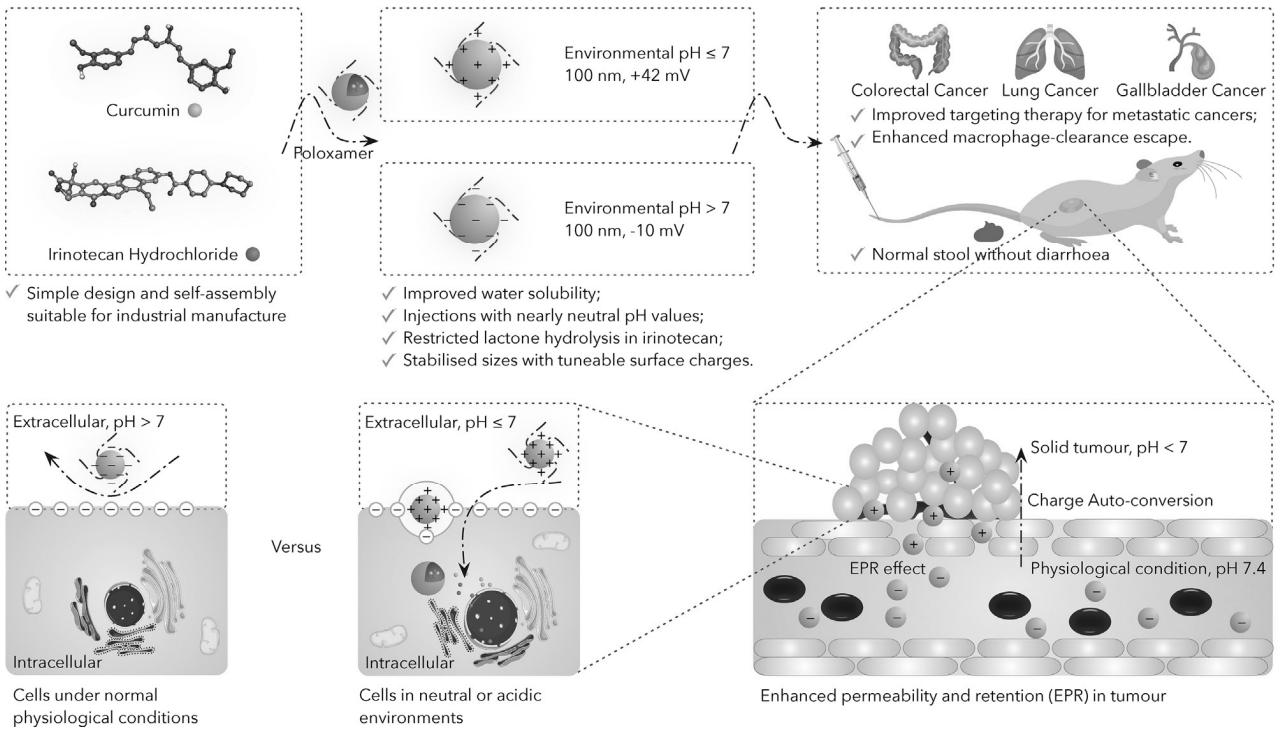

Scheme 1. Construction of charge-conversional drug self-delivery systems for better targeted cancer therapy.

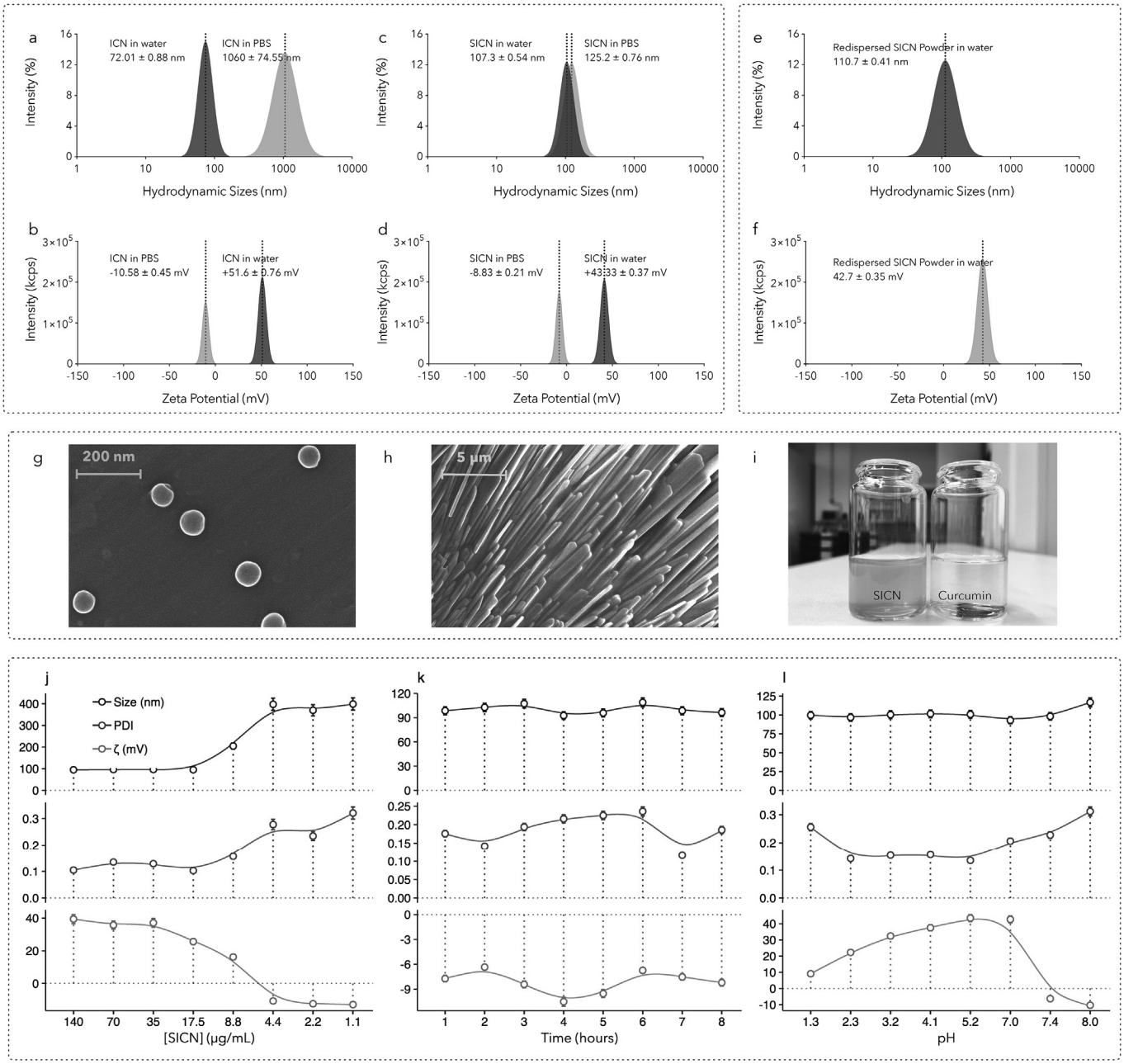

Fig. 2. Sizes, surface charges, redispersity, morphologies, appearance and stability of nanoparticles. (a) Particle sizes of ICN increase from about 70 nm in water to 1000 nm in PBS while (b) its surface charges decrease from 50 mV to -10 mV; (c) Stabilized particle sizes of SICN under various conditions; (d) Tunable surface charges of SICN increase from -7 mV in PBS (pH 7.4) to + 41 mV in water; SICN powder shows easy redispersity with narrow size distribution (e) and strong surface charges (f); (g) Spherical SICN with smooth surfaces; (h) Morphology of lyophilized SICN with mannitol; (i) Apparent appearance of SICN and curcumin in water exhibits the dramatically improved water solubility of curcumin by forming nanoparticles with irinotecan hydrochloride. (j) Anti-dilution ability of SICN in water after serial dilution; (k) Storage stability of SICN in PBS at 37.5°C; (l) SICN shows stabilized sizes and distribution although its surface charges decrease with an increase of acidity in an acidic environment and the addition of alkaline buffer makes the surface charges become negative. < br > Tag as simple para: < br > Abbreviation: ICN: Irinotecan hydrochloride Curcumin Nanoparticles; SICN: Surfactant stabilized Irinotecan hydrochloride Curcumin Nanoparticles; PBS: Phosphate Buffer Saline, pH = 7.4.

(Molar ratio 1:1) were dissolved in dimethyl sulfoxide (DMSO, 300 μL), inside which 0.5 mg of injectable non-ionic surfactant poloxamer 105 was added. The obtained organic solution was added into ultrapure water (30 mL) with magnetic stirring to get a suspension which was then dialyzed to remove the organic solvent. Nanoparticle powder was obtained after lyophilization with mannitol, which was then dispersed into ultrapure water containing glucose to get an injectable nanoparticle suspension.

Irinotecan hydrochloride curcumin nanoparticles without surfactants (ICN) and topotecan hydrochloride curcumin nanoparticles without surfactant (TCN) were also prepared using the same procedures.

2.3. Nanoparticle characterization

The hydrodynamic sizes and surface charges of nanoparticles in different conditions were characterized by dynamic light scattering (DLS). To investigate the morphologies of nanoparticles, a drop of

nanoparticle water suspension was evaporated on an aluminum foil. All nanoparticles were coated with a thin layer of gold (conductive coating) before investigation under a scanning electron microscope (SEM). The diffraction and thermal behavior of nanoparticles were characterized by powder x-ray diffraction (PXRD) and differential scanning calorimetry (DSC), respectively.

2.4. Fluorescence quenching

The stock solution was prepared by dissolving 10 mg of irinotecan hydrochloride or curcumin into 10 mL of DMSO. The working solution was obtained by mixing 10 μL of irinotecan hydrochloride stock solution with different volumes (from 1 μL to 10 μL) of curcumin stock solution and the final volume was adjusted to 1 mL with DMSO. The fluorescence spectra and lifetime were recorded on a spectrophotometer (FL980, Edinburgh, England). The excitation and emission wavelengths were set at 385 nm and 428 nm, respectively. For fluorescence synchronous spectra, the emission off wavelength was 43 nm.

The working solution containing topotecan was prepared using the same method. The excitation and emission wavelengths were set at 395 nm and 433 nm, respectively. For fluorescence synchronous spectra, the emission off wavelength was 38 nm.

2.5. Cells and mice

HT-29 colorectal adenocarcinoma cells were obtained from Boster Biological Technology Co. Ltd (Wuhan, China). Male BALB/c nude mice, aged 5 weeks (18–22 g, SPF grade), were purchased from Dashuo experimental animals Co., Ltd. (Chengdu, China). All animal experiments were conducted under the guidelines approved by the Institutional Animal Care and Use Committee (IACUC) of Chengdu University of Traditional Chinese Medicine.

2.6. In vivo therapeutic efficacy and biosafety

HT-29 cell suspension (2×10^6 cells per 200 μL) were subcutaneously injected into the flank of male BALB/c mice. When tumor volume reached around 100 mm^3, the HT-29 tumor bearing nude mice were randomly divided into three groups (four or five mice for each group) and were intravenously injected with PBS, irinotecan hydrochloride (27.5 mg/kg/mouse) or SICN (equivalent irinotecan 27.5 mg/kg/mouse) every other day for consecutive 20 days. Tumor volume was measured every third day and calculated according to the formula: Tumor volume = length x $width^2/2$. Mice were weighted every three days and the severity of diarrhea was scored according to the following standards [25]: 0 (normal, normal stool or absent); 1 (slightly wet and soft stool); 2 (moderate, wet and unformed stool with moderate perianal staining of the coat); and 3 (severe, watery stool with severe perianal staining of the coat). Mice were sacrificed after 5 days of medication discontinuation. Tumors were excised, weighted and photographed. The excised tissues (heart, liver, spleen, lung, kidney, brain and tumor) were fixed in 4% paraformaldehyde to prepare paraffin sections. Hematoxylin/eosin (H&E) staining was used for histological analysis.

2.7. Ex vivo biodistribution

Mice with subcutaneous tumors of around 100 mm^3 were intravenously injected with irinotecan hydrochloride or SICN (equivalent irinotecan 27.5 mg/kg/mouse). Fluorescence based visual distribution of drugs and their average signal on excised tissues were obtained on a FUSION FX7 live animal imaging system.

3. Results and discussion

3.1. Stabilized particle sizes and tunable surface charges

The hydrodynamic sizes and surface charges of ICN nanoparticles under various conditions are displayed in Fig. 2. As can be seen, by changing the solvent from water to PBS (pH 7.4), the particle sizes of ICN increase from about 70 nm to more than 1000 nm (Fig. 2a) while their surface charges decrease from around 50 mV to about −10 mV (Fig. 2b). Compared to ICN in water, the addition of injectable non-ionic surfactant poloxamer 105 slightly increases the hydrodynamic sizes of SICN nanoparticles to around 100 nm (Fig. 2c) while slightly decreases their surface charges to about 40 mV in water (Fig. 2d). In addition, altering the solvent to PBS further decreases the surface charges of SICN to around −10 mV, while their hydrodynamic sizes keep almost the same due to the additional steric repulsion provided by the non-ionic surfactants [26], making SICN become independent of environmental pH values and ionic strength.

The stabilized particle sizes and tunable surface charges can benefit the drug self-delivery system by ameliorating their biodistribution and enhancing their passively targeted cellular internalization. Nanoparticles with negative surface charges can be repulsed by the negatively charged cell membrane under normal physiological conditions, resulting in prolonged circulation times [27,28] and facilitating tumor accumulation *via* enhanced permeability and retention (EPR) effect [29]. While the positively charged nanoparticles under neutral or acidic environments become efficient at cell penetration, leading to an improved accumulation in acidic tumor tissues [28]. Besides, compared to the commercial irinotecan hydrochloride injection (pH 3.5), the injectable SICN suspension with a pH value close to that of normal blood would reduce the side effects caused to blood vessels during injection and improve the compliance of patients.

3.2. Morphology and appearance

The morphologies of evaporated SICN nanoparticles and their lyophilized powder with mannitol were characterized by SEM. For the evaporated SICN, spherical particles with smooth surfaces are displayed in Fig. 2g and their sizes are similar to those in suspension (around 100 nm). The morphologies and sizes of evaporated SICN nanoparticles under environments with different pH values keep almost the same (Figs. S1 and S2), demonstrating the good stability of nanoparticle. After lyophilization with mannitol, from Fig. 2h, we have observed only rod-like crystalline mannitol. The apparent appearance of SICN and curcumin in water is shown in Fig. 2i. Compared to pure curcumin in water, the water solubility of curcumin is markedly improved by forming nanoparticles with irinotecan hydrochloride.

3.3. Stability

The stability of SICN nanoparticles under various conditions was characterized by DLS. As shown in Fig. 2j, the particle sizes, surface charges and size distribution of SICN change little even though the concentration is low to about 10 μg/mL in suspension, implying their strong anti-dilution ability. Besides, SICN can keep stable in PBS (pH 7.4) at 37.5 °C for 8 h (Fig. 2k) though their absolute surface charges are less than 10 mV. Besides, although the surface charges of SICN decrease with an increase of acidity in an acidic environment and the addition of alkaline buffer makes the surface charges become negative (Fig. 2l), the hydrodynamic sizes and size distribution of SICN stay the same with few changes. In addition, the size and surface charges of redispersed SICN powder in water (Fig. 2e and f) keep almost the same compared to those before lyophilization. All these results demonstrate the good stability and easy redispersity of SICN nanoparticles.

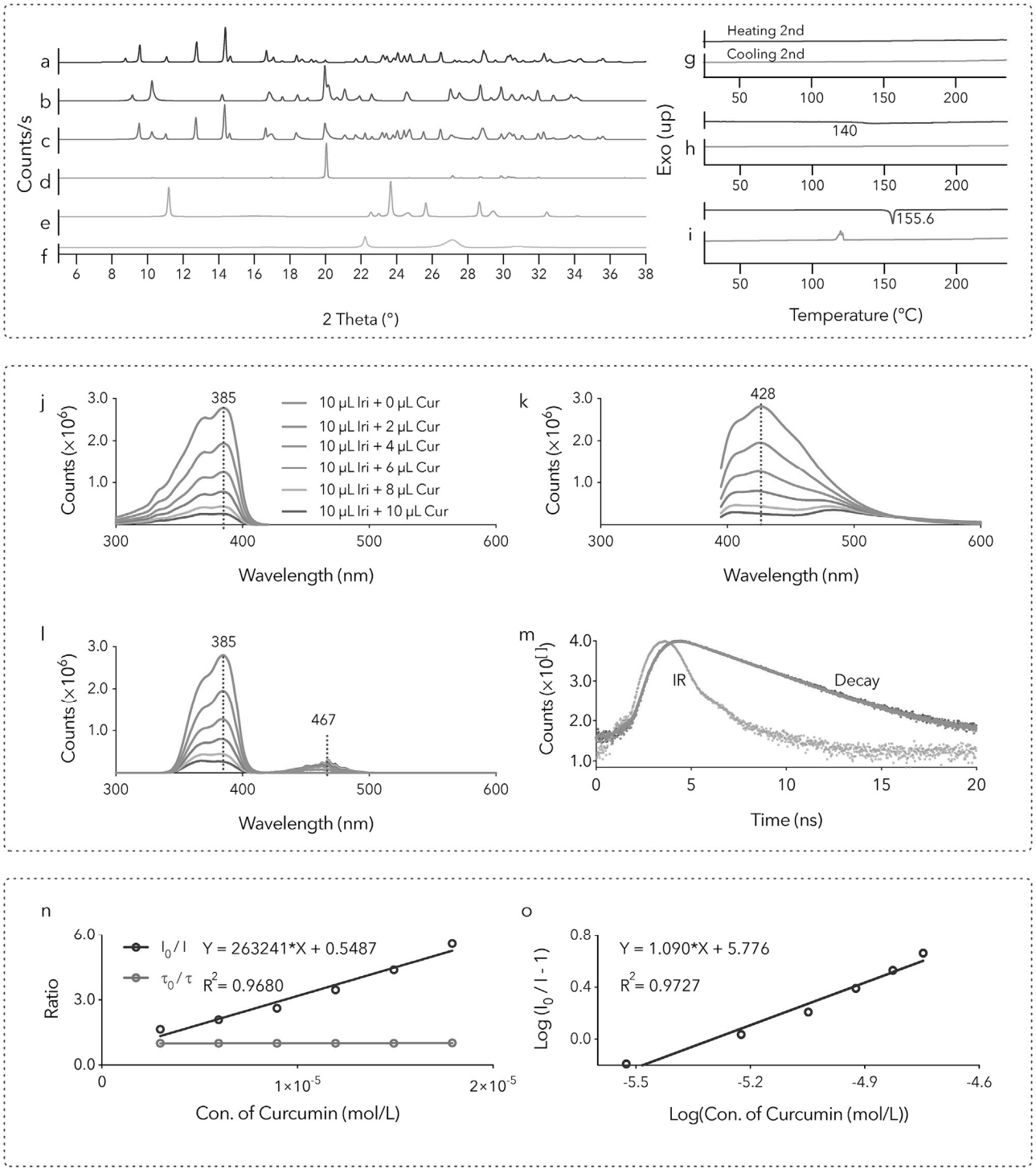

Fig. 3. Crystalline profiles of SICN nanoparticles and fluorescence quenching of irinotecan chloride in DMSO caused by curcumin. Physical mixture of irinotecan hydrochloride and curcumin (c, molar ratio 1:1) shows superimposed PXRD patterns of both irinotecan hydrochloride (a) and curcumin (b); vacuum dried powder of methanol solution containing irinotecan hydrochloride and curcumin (d, molar ratio 1:1) shows evident novel diffraction peaks; SICN (e) shows new peaks at 11.22°, 23.68°, 25.66°, 28.66° and 29.42° compared to its components including irinotecan hydrochloride (a), curcumin (b) and P105 (f). DSC profile of P105 (g) implies its amorphous state; DSC profile of irinotecan hydrochloride and curcumin mixture (h, ratio 1:1) indicates their amorphous state after cooling from high temperature; Melting point of SICN at 155.6°C (i). The fluorescence excitation (j, emission at 428 nm), emission (k, excitation at 385 nm), synchronous (l, emission off 43 nm) spectra and fluorescent lifetime (m, excitation at 385 nm, emission at 428 nm) of irinotecan hydrochloride (Iri) in presence of various amounts of curcumin (Cur) in DMSO at room temperature; (n) The Stern-Volmer plots for the fluorescence quenching of irinotecan hydrochloride at room temperature; (o) The plots of log (I < span data-format = "subscript" > 0 < /span > /I - 1) versus log(concentration of quencher (mol/L)). < br > Tag simple para as: < br > Abbreviation: PXRD, powder x-ray diffraction; DSC, differential scanning calorimetry; SICN, Surfactant stabilized Irinotecan hydrochloride Curcumin Nanoparticles; IR, instrumental response; DMSO, dimethyl sulfoxide; < br > Notes: I < span data-format = "subscript" > 0 < /span > and I represent the fluorescent intensity of irinotecan hydrochloride in the absence and presence of curcumin, respectively. τ < span data-format = "subscript" > 0 < /span > and τ represent the fluorescent lifetime of irinotecan hydrochloride in the absence and presence of curcumin, respectively.

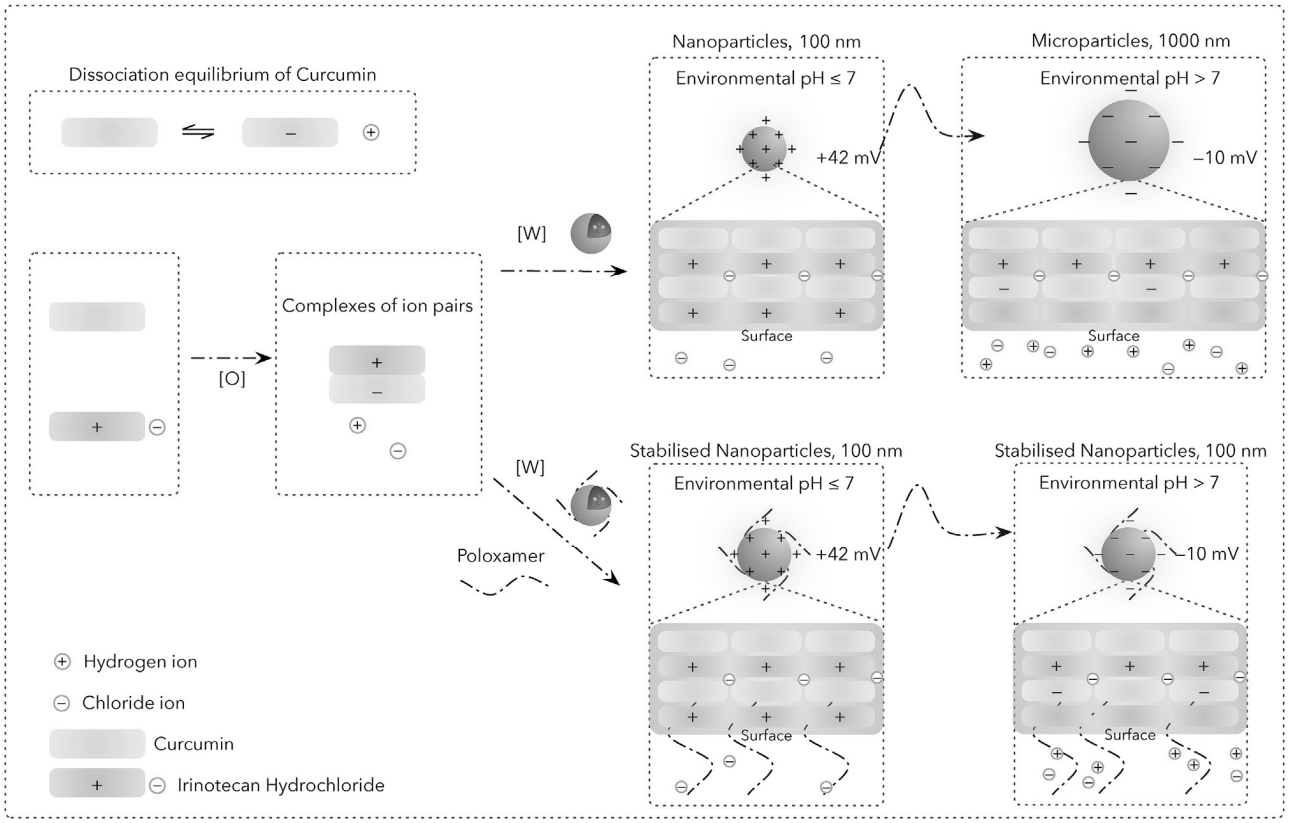

Fig. 4. Iillustration of the formation of surfactant stabilized irinotecan hydrochloride and curcumin nanoparticles. Irinotecan hydrochloride and curcumin initially self-assemble into homogeneous complexes of ion pairs in polar organic solvents. Nanoparticles are obtained by precipitation in presence of large volume of their unfavorable solvents regarding to the solubility. Surfactant stabilized nanoparticles become independent of environmental pH values and ionic strength because of the additional steric force provided by surfactants. < br > Tag as simple para: Abbreviation: [O], oil phase; [W], aqueous phase.

3.4. PXRD analysis

The PXRD analysis of SICN and its components is displayed in Fig. 3. As can be seen, the physical mixture of irinotecan hydrochloride and curcumin with molar ratio 1:1 (Fig. 3c) shows superimposed diffraction patterns of both irinotecan hydrochloride (Fig. 3a) and curcumin (Fig. 3b). While the vacuum dried powder of methanol solution containing both irinotecan and curcumin (Fig. 3d) shows several evident novel diffraction peaks, indicating these two molecules are ordered in a new crystalline state with the help of methanol. SICN powder (Fig. 3e) shows new diffraction peaks at 11.22°, 23.68°, 25.66°, 28.66° and 29.42° compared to its components (Fig. 3a, b, and 3f), implying the formation of a novel crystal. By forming cocrystals, not only could the water solubility be improved (Fig. 2i), but the lactone hydrolysis in irinotecan is also restricted by the strong order effect of crystalline lattices.

3.5. Melting behavior

The melting and crystallization behavior of SICN and its components were analyzed by DSC. In the DSC curves of surfactant poloxamer 105 (Fig. 3g), no evident endothermic or exothermic peaks appears in both the heating and cooling runs, indicating its amorphous state. In the second heating run of physical mixture of curcumin and irinotecan hydrochloride (molar ratio 1:1, Fig. 3h), a glass transition occurs at about 140 °C, which implies that the mixture stays in an amorphous state after the first cooling from high temperature. However, there is a sharp endothermic peak at 155.6 °C in the heating run and an exothermic peak at 119 °C in the cooling run of SICN (Fig. 3i), which should be attributable to the melting and crystallization processes, respectively. The unique melting point of SICN at 155.6 °C also demonstrates they are in a crystalline form because an amorphous solid does not have a definite melting point.

3.6. Static quenching

The fluorescence excitation (Fig. 3j), emission (Fig. 3k), synchronous (Fig. 3l) spectra and fluorescent lifetime (Fig. 3m) of irinotecan hydrochloride in DMSO in the presence of various amounts of curcumin were measured by a fluorospectrometer at room temperature. Irinotecan hydrochloride shows an excitation maximum at 385 nm and an emission maximum at 428 nm. The addition of curcumin causes the fluorescence quenching in excitation, emission and synchronous spectra. However, the fluorescence lifetime of irinotecan hydrochloride keeps the same.

The fluorescence quenching data are analyzed by the Stern-Volmer equation [30]:

$$I_0/I = 1 + K_{sv} * [Q] = 1 + k_q * \tau_0 * [Q]$$

The binding number is calculated according to the following equation [30]:

$$\mathrm{Log}\,(I_0/I - 1) = \mathrm{Log}\,K_a + n * \log[Q]$$

where I_0 and I represent the fluorescent intensity of irinotecan hydrochloride in the absence and presence of curcumin, respectively. K_{sv} is the Stern–Volmer quenching constant and K_q is the bimolecular quenching constant; τ_0 is the fluorescence lifetime of fluorophore in the absence of quencher. K_a is the association constant, n is the binding number and [Q] represents the concentration of quencher.

As shown in Fig. 3n, a linear Stern-Volmer plot and the unchanged fluorescence lifetime in the absence and presence of curcumin (Fig. 3m) reveals that the quenching of irinotecan hydrochloride in DMSO is

caused by assembling into ground state complexes with curcumin (static quenching) [30] with a molar ratio of 1:1 (Fig. 3o) through intermolecular interactions, such as hydrophobic interactions, hydrogen bonding, π-π stacking [31] and electrostatic adsorption [32].

3.7. Formation mechanism

Based on all the evidence obtained, a possible formation process of the SICN nanoparticles is illustrated in Fig. 4. Curcumin and irinotecan hydrochloride self-assemble into complexes of ion pairs in polar organic solvents through intermolecular interactions. The extremely poor water-solubility of curcumin and camptothecin (the parent compound of irinotecan), the relatively exposed hydrogen atoms and the rigid planar structures (Fig. 1e) of both molecules with multiple conjugated aromatic rings [33–35] provide the possibility of hydrophobic interactions, hydrogen bonding and π-π stacking between these two molecules [36], respectively. In addition, due to the active methylene hydrogen of β-diketones and two other phenolic hydrogen in curcumin, there are three pKa values for the dissociation of acidic protons in curcumin, namely 7.8, 8.5 and 9.0 (Fig. 1d) [36–38]. The partial ionization of weak acids in polar organic solvents [39] grants curcumin the opportunity to interact with cationic irinotecan which is protonated by forming salts with hydrochloride. In return, the electrostatic adsorption between cationic irinotecan and anionic curcumin promotes the dissociation of curcumin in polar organic solvents.

The organic solution of ionic complexes is then drop-wisely added into large volume of their unfavorable solvents regarding to the solubility to form nanoparticles by precipitation [40], during which the presence of water with pH values lower than the pKa of curcumin results in the shifts of curcumin dissociation equilibria towards the molecular form [38] and therefore leads to the positively charged surface of SICN nanoparticles. The high magnitudes of surface charges play a pivotal role during the formation of nanoparticles, which allows them to be repulsed from each other electrostatically and prevented from aggregation in suspension.

However, the positive surface charges attributed from the protonated irinotecan also result in the environmental pH sensitivity of the ICN nanoparticles (Fig. 2a). The relatively alkaline nano-environment deprotonates not only cationic irinotecan but also the weakly acidic curcumin molecules, therefore leading to the neutral irinotecan molecules and partially negatively charged curcumin (depending on the specific pH values of the environment) on the surface of nanoparticles (Fig. 2b). In addition, the high ionic strength in suspension compresses the electric double layer of the nanoparticles [41], further leading to the decrease of their surface charges. The relatively lower magnitudes of the surface charges decrease the electrostatic repulsion between nanoparticles, resulting in the failure in preventing their aggregation and subsequently obtaining microscale particles.

The introduction of non-ionic surfactant, which is partially hybridized inside SICN nanoparticles through hydrophobic interactions, not only will not interrupt the electrostatic interactions between irinotecan hydrochloride and curcumin during the formation of nanoparticles, but also provides an additional repulsive steric force to prevent their aggregation [41], making the particle size and distribution of SICN nanoparticles become independent of environmental pH values and ionic strength (Fig. 2c).

3.8. Mechanism verification

The strategy for design of drug self-delivery systems based on the molecular structures of curcuminoids and camptothecin derivatives was verified by preparing topotecan hydrochloride curcumin nanoparticles (TCN) using the same method. As can be seen in Fig. 5a, TCN shows a hydrodynamic size of around 126 nm with a narrow size distribution (PDI 0.18) in water and they also have positive surface charges with large magnitudes (Fig. 5b). TCN also shows smoothly spherical structure (Fig. 5d). In addition, similar fluorescence quenching behavior (Fig. 5j, k and 5l) and lifetime decay (Fig. 5m) between topotecan hydrochloride and curcumin in DMSO were observed, revealing the static quenching between the two molecules.

The physical mixture of topotecan hydrochloride and curcumin (molar ratio 1:1, Fig. 5g) shows superimposed diffraction patterns of both topotecan hydrochloride (Fig. 5e) and curcumin (Fig. 5f). However, TCN shows novel diffraction peaks at 11.20°, 23.67°, 24.57, 25.66°, 28.66° and 29.44° (Fig. 5h), demonstrating the different crystal state of TCN. More interestingly, these patterns have the same diffraction angles with those of ICN nanoparticles (Fig. 5i), further verifying that molecules with the same chemical skeletons of camptothecin and curcumin can form nanoparticles *via* the similar formation mechanism by utilizing this strategy. However, their dissimilar relative diffraction intensity (e.g., 24.57° and 29.44°) and different melting points (Fig. 5c) evince the divergent subtle structures in both nanoparticles and also indicate their different molecular composition and arrangements.

3.9. In vitro cytotoxicity, uptake efficiency and internalization pathways

The *in vitro* cytotoxicity and fluorescence-based cellular uptake efficiency of SICN nanoparticles under various environmental pH values were explored on HT-29 cells.

As shown in Fig. S3, the half maximal inhibitory concentration (IC_{50}) of irinotecan hydrochloride on cells under normal environment (pH 7.4) is 15.25 μM. The IC_{50} of SICN nanoparticles on cells with environmental pH of 7.8, 7.4 and 6.5 are 0.278 mg/mL, 0.112 mg/mL and 0.019 mg/Ml, equaling to 7.720 μM, 3.112 μM and 0.537 μM of irinotecan hydrochloride, respectively. Significant difference between groups at every dosage level is obtained ($p < 0.001$). Compared to the free irinotecan hydrochloride, the *in vitro* cytotoxicity of SICN is significantly improved by forming nanoparticles. Besides, the acidic environments could result in greater *in vitro* cytotoxicity of SICN on HT-29 cells than the alkaline condition because of the conversional positive surface charges of nanoparticles under tumor environments and the negative surface charges under normal physiological conditions.

The fluorescence-based cellular uptake of SICN nanoparticles under different environmental pH values are shown in Fig. S4. The blank group, namely cells under normal conditions without SICN nanoparticles, shows no fluorescence. For SICN groups, cells under acidic environments exhibit significantly stronger fluorescence than those in alkaline conditions ($p < 0.001$), demonstrating the higher uptake efficiency of SICN under tumor environments.

The cellular internalization pathways of SICN nanoparticles on HT-29 cells were also tested by confocal laser scanning microscopy (Fig. S5). From the statistical results, the cellular uptake of SICN nanoparticles is significantly blocked at 4 °C, suggesting an energy-dependent internalization. Moreover, the cellular uptake is not affected by the macropinocytosis inhibitors (cytochalasin D and wortmannin), but significantly inhibited by the clathrin-mediated endocytosis inhibitor (chlorpromazine) and the caveolin inhibitors (genistein and methyl-β-cyclodextrin), indicating the SICN particles are at nano scale during internalization because nano-sized particles (smaller than 500 nm) are mainly endocytosed though clathrin- and caveolin-mediated endocytic pathways while micro-sized particles are internalized *via* macropinocytosis [42,43]. Besides, as shown in Figs. S4 and S5, SICN nanoparticles are evenly distributed in the cytosol around the nucleus due to the caveolin-mediated endocytosis which can bypass lysosomes [43].

3.10. Nanoparticle disposition

The plasma concentration-time profiles of free irinotecan hydrochloride and SICN nanoparticles are shown in Fig. S6. The plasma concentration for irinotecan hydrochloride group decreases by around 80% after 2 h while the concentration for SICN group still keeps at about 50% in plasma. Mice receiving a single injection of SICN

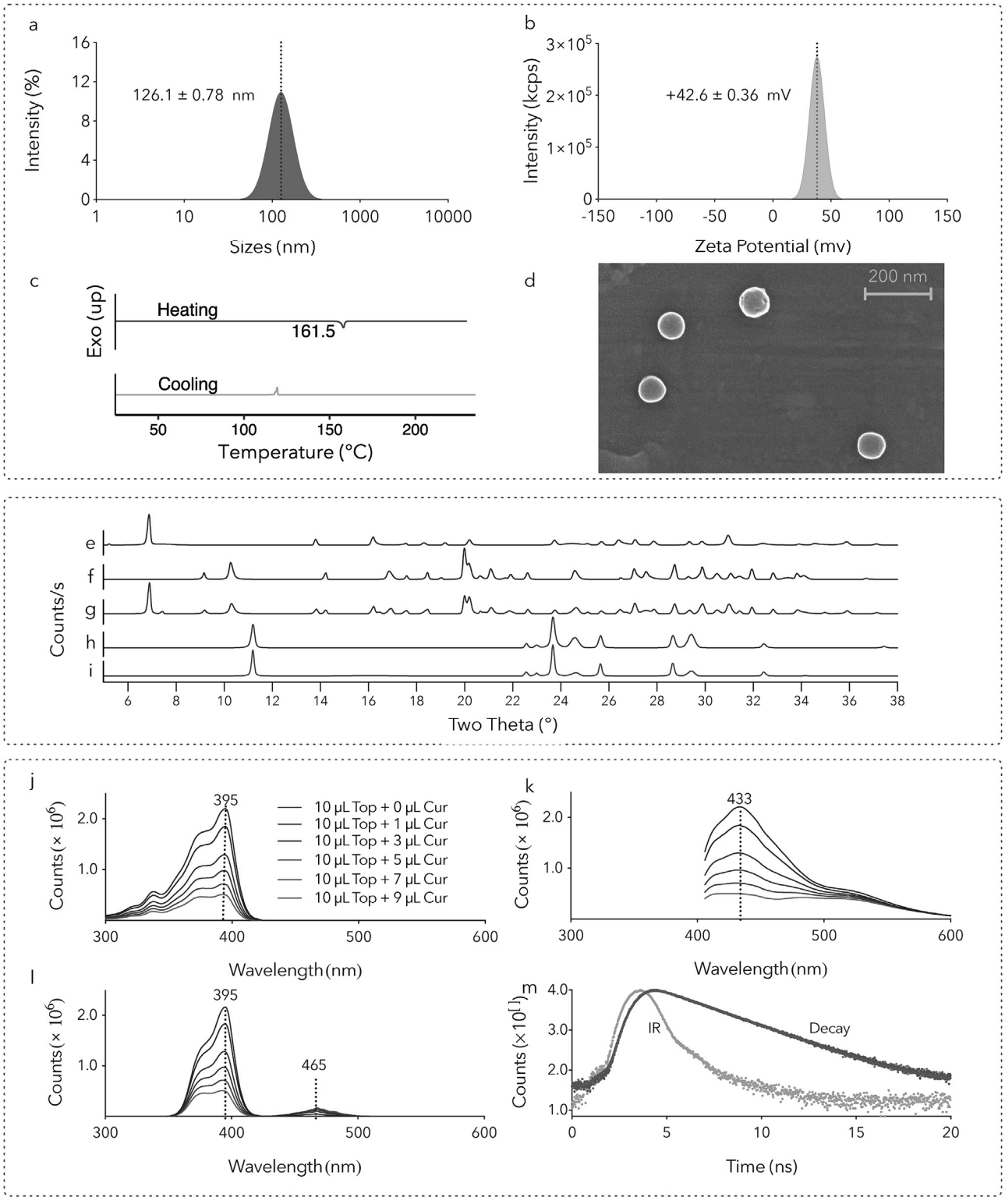

Fig. 5. Sizes, surface charges, morphologies and crystalline profiles of TCN nanoparticles and fluorescence quenching of topotecan hydrochloride in the presence of curcumin in DMSO. Typical hydrodynamic distribution (a) and surface charges (b) of TCN in water; (c) DSC profile of TCN shows its melting point at 161.5°C; (d) Smoothly spherical structure of evaporated TCN. Physical mixture of topotecan hydrochloride and curcumin (g, molar ratio 1:1) shows superimposed PXRD patterns of both topotecan hydrochloride (e) and curcumin (f); TCN (h, molar ratio 1:1) shows new peaks at 11.22°, 23.68°, 25.66°, 28.66° and 29.42° compared to its components including topotecan hydrochloride (e) and curcumin (f); TCN (h) and ICN (i) show similar diffraction patterns. The fluorescence excitation (j, emission at 433 nm), emission (k, excitation at 395 nm), synchronous (l, emission off 38 nm) spectra and fluorescent lifetime (m, excitation at 395 nm, emission at 433 nm) of topotecan hydrochloride (Top) in presence of various amounts of curcumin (Cur) in DMSO at room temperature. < br > Tag as simple para: < br > Abbreviation: PXRD, powder x-ray diffraction; DSC, differential scanning calorimetry; TCN, Topotecan hydrochloride Curcumin Nanoparticles; SICN: Surfactant stabilized Irinotecan hydrochloride Curcumin Nanoparticles. DMSO, dimethyl sulfoxide.

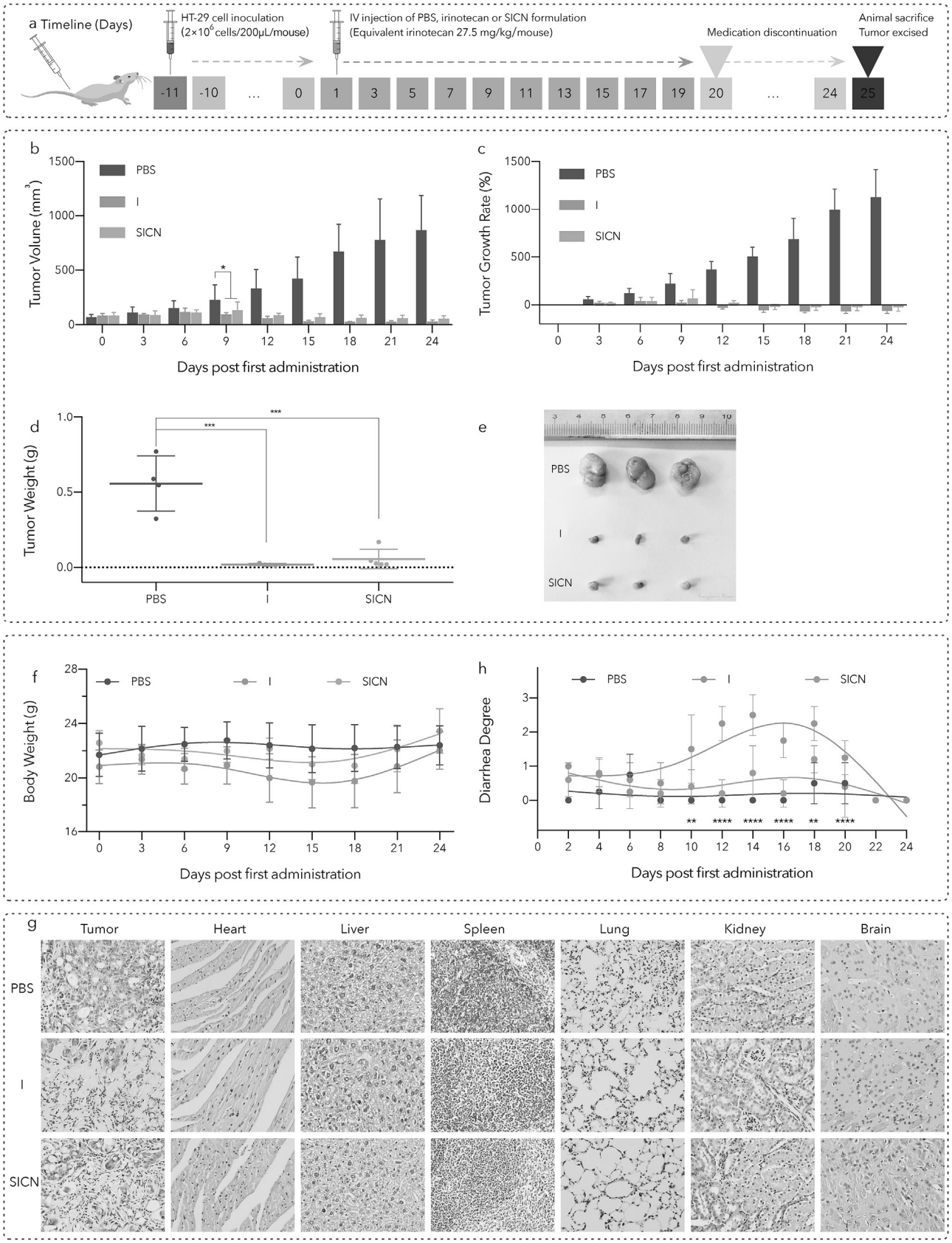

(caption on next page)

Fig. 6. < span data-format = "italic" > In vivo < /span > anticancer efficacy of SICN on HT-29 subcutaneous xenograft nude mice. (a) A schematic diagram of the experimental design of anticancer efficacy; (b) Tumor volume (b), tumor growth rate (c), tumor weight (d) and tumor images (e) from mice treated with PBS, I or SICN; (f) Negligible changes of Body weight; (g) H&E staining images of excised tumors and major organs (magnification of 400x). (h) Delayed diarrhea degree of mice (significant difference between SICN and I treated groups, no statistical difference between SICN and PBS treated groups). < br > Tag as simple para: < br > Abbreviation: IV, intravenous therapy; PBS, Phosphate buffered saline, pH 7.4; I, Irinotecan hydrochloride; SICN, Surfactant stabilized Irinotecan hydrochloride and Curcumin Nanoparticles. Significance of differences between groups are analyzed using 2way ANOVA. * p < 0.05, ** P < 0.01, *** P < 0.001, **** P < 0.0001.

nanoparticles achieve an obvious improvement in plasma concentration and exposure compared to free irinotecan, which is consistent with the previous report in literature [44].

3.11. In vivo therapeutic efficacy and biosafety

The anti-tumor effect of SICN nanoparticles was invested on HT-29 subcutaneous xenograft nude mice. The experimental strategy is illustrated in Fig. 6a. Compared to the PBS group, the average tumor volumes of mice in medication groups are effectively controlled and significant difference occurs on day 9 (around one week post first administration, Fig. 6b). The regression of tumor volume in the medication groups occurs on day 15 (around two week post first administration, Fig. 6c). The medication groups also show significant differences in tumor weight (Fig. 6d) and the photography of excised tumor is shown in Fig. 6e. No statistical difference between the two medication groups occurs during the whole experiment. These results confirm that the SICN nanoparticles is as equally effective in colorectal cancer treatment as free irinotecan hydrochloride and the tumor regression effect of SICN is caused by irinotecan instead of curcumin. This should be attributed to the significant difference in half maximal inhibitory concentration of the two molecules. Curcumin can be generally regarded as a biosafe molecule at the dose level.

No significant loss of body weight was observed in all the mice during the whole experiment, indicating the negligible side effects of the SICN nanoparticles for tumor therapy at the employed dose (Fig. 6f). Besides, the H&E staining images of tumors and major organs (heart, liver, spleen, lung, kidney and brain) from HT-29 tumor-bearing mice treated with PBS, free irinotecan or SICN are shown in Fig. 6g. Except for the glandular cavities, the H&E staining of colon cancer sections from the PBS group shows intact tumor cell structure. Cells exhibit distinct nuclei with a nearly spherical thin cytoplasmic region. H&E-stained sections of colon cancer from medication groups have distinct damage of tumor cell nuclei and distorted membranes surrounding necrotic tissues. However, compared to the PBS treated group, neither noticeable organ damage nor inflammation lesion can be observed in the medication groups, indicating the negligible organ dysfunction after being treated with SICN nanoparticles or irinotecan. All these results demonstrate that the SICN nanoparticles exhibit high biosafety for cancer treatment presenting no significant side effects to the treated mice.

As shown in Fig. 6h, significant delayed diarrhea in the mice treated with free irinotecan occurs on day 10 (10 days post first administration, $p < 0.01$) while no obvious diarrhea is observed in PBS or SICN treated group during the whole experiment, demonstrating the presence of curcumin in the nano formulation could protect the intestine and ameliorate the gut toxicity by alleviating diarrhea in mice. This can be due to whether the protective effects of curcumin molecule [21] or the formulation changes of irinotecan with the help of curcumin.

3.12. Ex vivo biodistribution

The *ex vivo* biodistribution investigation was carried out according to Fig. 7a. The normalized fluorescence spectra of irinotecan hydrochloride in water containing 50% of DMSO (Fig. 7b) and SICN in PBS (Fig. 7c) show that irinotecan in both forms display similar fluorescence behavior with an excitation maximum at around 370 nm and an emission maximum at about 430 nm.

The fluorescence based biodistribution of irinotecan hydrochloride and SICN on excised tissues are shown in Fig. 7d and e, respectively. Except for the high accumulation of irinotecan hydrochloride in tumor (Fig. 7d), a relatively higher biodistribution in liver can also be observed. Their relatively average signals are 27% and 37%, respectively (Fig. 7f). Compared to irinotecan hydrochloride, a visually higher accumulation of SICN in tumor is observed (Fig. 7e) and its relatively average signal figures prominently (36% in Fig. 7g, around 33% larger than that of free irinotecan, 27% in Fig. 7f), showing an improved tumor targeting of SICN. Besides, the relative accumulation of SICN in liver is lower (18% in Fig. 7g) than that of free irinotecan (37% in Fig. 7f), which might also be one of the reasons that relieve the side effects. Clinically, the severe diarrhea caused by irinotecan hydrochloride is due to the biliary elimination and the subsequent microbiome reactivation in intestines [45,46]. Therefore, except for the protective effect of curcumin on intestines [21], the diarrhea alleviation effect of SICN could also be attributable to the improved tumor targeting, which relatively reduces their quick accumulation in liver and lessens the chances of being rapidly metabolized and excreted into intestines.

To further verify this, the relative accumulation of irinotecan and SICN in tissues including heart, liver, gallbladder, spleen, lung, kidney, brain, tumor and stomach & intestine at different time post intravenous injection were explored in Fig. 7h. The relatively average signals of irinotecan are mainly distributed in liver, tumor and stomach & intestine. The relative accumulation in liver decreases from around 15% at 10 min to about 8% at 2 h post injection. The relative biodistribution in tumor increases from around 3%–12% while the relative accumulation in stomach & intestine keep at about 70%. However, except for the high accumulation in liver, tumor and stomach & intestine, high distribution of SICN in gallbladder and lung can also be observed. Compared to free irinotecan, the relative accumulation of SICN in liver and spleen decrease by around 50% during 30 min post injection (Fig. 7i), which could benefit the nanoparticles *via* escaping the rapid clearance by mononuclear phagocytic cells and prolonging their residence time in the body. Besides, their relative biodistribution in tumor increase by more than 50%, further evidencing their improved tumor targeting due to the uniform nano sizes (EPR effect) and convertible surface charges. In addition, their relative accumulation in stomach & intestine decrease by about 50%, which directly explains the diarrhea eradication effect of SICN. More interestingly, the relative accumulation of SICN in gallbladder and lung increase by two or more times. It shows significantly improved accumulation in lung and prolonged residence time in gallbladder, which not only explains the reduced accumulation in stomach & intestine but also brings hope for the treatment of lung and gallbladder cancer.

4. Conclusions

For the first time, we propose a strategy for the construction of drug self-delivery systems based on molecular structures, which can be used for the co-delivery of curcuminoids and all the nitrogen-containing derivatives of camptothecin for better targeted cancer therapy. The formation mechanism investigation demonstrates that these two molecular species can self-assemble into complex of ion pairs in polar organic solvents through intermolecular non-covalent interactions,

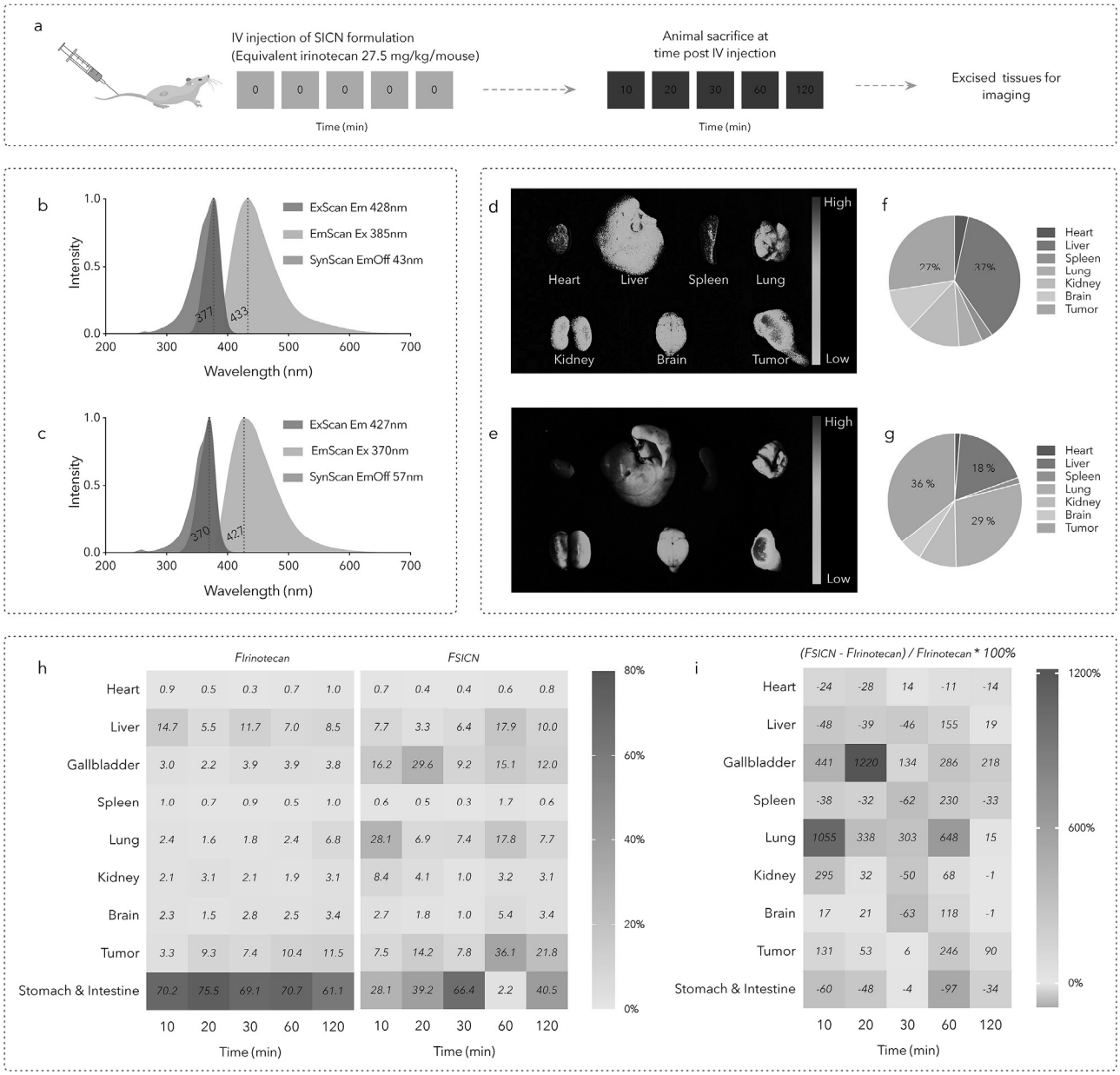

Fig. 7. < span data-format = "italic" > Ex < /span > < span data-format = "italic" > vivo < /span > distribution of SICN nanoparticles on HT-29 subcutaneous xenograft nude mice. (a) A schematic diagram of the experimental design of ex vivo biodistribution by using HT-29 tumor-bearing nude mice; Irinotecan hydrochloride in water containing 50% of DMSO (b) and SICN in PBS (c) exhibit similar behavior in their normalized fluorescence spectra; Fluorescence based relative biodistribution of irinotecan hydrochloride (d) and SICN nanoparticles (e) on tissues from mice sacrificed at 10 min post intravenous injection; The relatively average signal of irinotecan hydrochloride (f) and SICN nanoparticles (g) on excised tissues; (h) Heat map of relatively average signal of irinotecan and SCIN on tissues within 120 min post intravenous injection; (i) Heat map of relatively average signal increase rate of SICN compared to irinotecan within 120 min post intravenous injection. < br > Tag as simple para: < br > Abbreviation: PBS, Phosphate buffered saline, pH 7.4; SICN, Surfactant stabilised Irinotecan hydrochloride Curcumin Nanoparticles.

resulting in a uniform distribution of them before being penetrated into anti-solvents to form nanoparticles. These nanoparticles show stabilized particle sizes (100 nm) with mono distribution (PDI $\leq$ 0.2) under various conditions and conversional surface charges which increase from around -10 mV in a normal physiological condition (pH 7.4) to $+40$ mV under acidic tumor environments. The water solubility of curcuminoids is dramatically improved and the lactone hydrolysis of camptothecin derivatives is also restricted to keep their pharmacologically active forms. Besides, the formulation with a pH value close to that of normal blood would reduce the side effects caused to blood vessels and improve the patient compliance compared to commercial injections of camptothecin derivatives (pH 3.5). More importantly, *in vivo* mice experiments have demonstrated that, compared to irinotecan itself, the co-delivered irinotecan curcumin nanoparticles exhibited dramatically enhanced lung and gallbladder targeting, improved macrophage-clearance escape and ameliorated colorectal cancer treatment with an eradication of life-threatening diarrhea, exhibiting great promise for better targeted chemotherapy and clinical translation. Lastly, the strategy of structure based design of drug self-delivery systems may inspire more research and discoveries of similar self-delivered nano systems for wider pharmaceutical applications.

Declaration

The authors state no conflict of interest.

Author contributions

Conceptualization, H.X.; Methodology & Investigation, H.X., Y.G., H.L., Y.L., Y.W., J.C. and D.S.; Formal Analysis, H.X.; Resources, I.K., L.G. and V.S.; Writing - Original Draft, H.X.; Writing – Review & editing, C.L., H.X., Y.G. and V.S.; Visualization, H.X.; Supervision, V.S. and L.G., Funding Acquisition, V.S., L.G. and C.L.

Acknowledgments

We express our great appreciation to Jiayi Sun at Innovative Institute of Chinese Medicine and Pharmacy, Chengdu University of Traditional Chinese Medicine, for the assistance with confocal laser scanning microscopy, Haojie Fei at Centre of Polymer Systems, Tomas Bata University in Zlin, for the help with scanning electron microscopy, Juanru Liu at School of Pharmacy, Chengdu University of Traditional Chinese Medicine, for the assistance during *in vitro* evaluation and all the technicians who helped us during this research. This work was co-funded by the Ministry of Education, Youth and Sports of the Czech Republic [Grant No. LO 1504]; Internal Grant Agency of the Tomas Bata University in Zlin [Grant No. IGA/CPS/2017/005, Grant No. IGA/CPS/2018/003, Grant No. IGA/CPS/2019/006]; Fund for Fostering Talents in Basic Science of the National Natural Science Foundation of China [J1310034-18] and graduate student summer fellowship of Quantitative and Systems Biology program, University of California, Merced, United States.

Appendix A. Supplementary data

Supplementary data to this article can be found online at https://doi.org/10.1016/j.biomaterials.2019.119701.

References

[1] W. Wulaningsih, A. Wardhana, J. Watkins, N. Yoshuantari, D. Repana, M. Van Hemelrijck, Irinotecan chemotherapy combined with fluoropyrimidines versus irinotecan alone for overall survival and progression-free survival in patients with advanced and/or metastatic colorectal cancer, Cochrane Database System. Rev. 2016 (2) (2016) CD008593-CD008593.

[2] V. Schirrmacher, From chemotherapy to biological therapy: a review of novel concepts to reduce the side effects of systemic cancer treatment (Review), Int. J. Oncol. 54 (2) (2019) 407–419.

[3] W. Wu, Y. Wang, K. Loebmann, H. Grohganz, T. Rades, Transformations between co-amorphous and co-crystal systems and their influence on the formation and physical stability of co-amorphous systems, Mol. Pharm. 16 (3) (2019) 1294–1304.

[4] T. Takagi, C. Ramachandran, M. Bermejo, S. Yamashita, L.X. Yu, G.L. Amidon, A provisional biopharmaceutical classification of the top 200 oral drug products in the United States, Great Britain, Spain, and Japan, Mol. Pharm. 3 (6) (2006) 631–643.

[5] M.K. Shim, J. Park, H.Y. Yoon, S. Lee, W. Um, J.-H. Kim, S.-W. Kang, J.-W. Seo, S.-W. Hyun, J.H. Park, Y. Byun, I.C. Kwon, K. Kim, Carrier-free nanoparticles of cathepsin B-cleavable peptide-conjugated doxorubicin prodrug for cancer targeting therapy, J. Control. Release 294 (2018) 376–389.

[6] A.G. Cheetham, R.W. Chakroun, W. Ma, H. Cui, Self-assembling prodrugs, Chem. Soc. Rev. 46 (21) (2017) 6638–6663.

[7] H. Cabral, K. Miyata, K. Osada, K. Kataoka, Block copolymer micelles in nanomedicine applications, Chem. Rev. 118 (14) (2018) 6844–6892.

[8] Y. Zhao, F. Fay, S. Hak, J.M. Perez-Aguilar, B.L. Sanchez-Gaytan, B. Goode, R. Duivenvoorden, C.d.L. Davies, A. Bjorkoy, H. Weinstein, Z.A. Fayad, C. Perez-Medina, W.J.M. Mulder, Augmenting drug-carrier compatibility improves tumour nanotherapy efficacy, Nat. Commun. 7 (1) (2016) 11221.

[9] V.J. Venditto, F.C. Szoka, Cancer nanomedicines: so many papers and so few drugs!, Adv. Drug Deliv. Rev. 65 (1) (2013) 80–88.

[10] R. Ghadi, N. Dand, BCS class IV drugs: highly notorious candidates for formulation development, J. Control. Release 248 (2017) 71–95.

[11] S.W. Morton, K.P. Herlihy, K.E. Shopsowitz, Z.J. Deng, K.S. Chu, C.J. Bowerman, J.M. DeSimone, P.T. Hammond, Scalable manufacture of built-to-order nanomedicine: spray-assisted layer-by-layer functionalization of PRINT nanoparticles, Advanced materials (Deerfield Beach, Fla, 25 (34) (2013) 4707–4713.

[12] K. Liu, Z. Zhu, X. Wang, D. Gonçalves, B. Zhang, A. Hierlemann, P. Hunziker, Microfluidics-based single-step preparation of injection-ready polymeric nanosystems for medical imaging and drug delivery, Nanoscale 7 (40) (2015) 16983–16993.

[13] J. Lopes-de-Araujo, S. Reis, C. Nunes, Topotecan effect on the structure of normal and cancer plasma membrane lipid models: a multi-model approach, Eur. J. Pharm. Sci. 123 (2018) 515–523.

[14] B.L. Staker, M.D. Feese, M. Cushman, Y. Pommier, D. Zembower, L. Stewart, A.B. Burgin, Structures of three classes of anticancer agents bound to the human topoisomerase I-DNA covalent complex, J. Med. Chem. 48 (7) (2005) 2336–2345.

[15] S.K. Das, I. Rehman, A. Ghosh, S. Sengupta, P. Majumdar, B. Jana, B.B. Das, Poly (ADP-ribose) polymers regulate DNA topoisomerase i (Top1) nuclear dynamics and camptothecin sensitivity in living cells, Nucleic Acids Res. 44 (17) (2016) 8363–8375.

[16] S. Palakurthi, Challenges in SN38 drug delivery: current success and future directions, Expert Opin. Drug Deliv. 12 (12) (2015) 1911–1921.

[17] T.Y. Ci, T. Li, G.T. Chang, L. Yu, J.D. Ding, Simply mixing with poly(ethylene glycol) enhances the fraction of the active chemical form of antitumor drugs of camptothecin family, J. Control. Release 169 (3) (2013) 329–335.

[18] F.N.U.A.U. Rahman, S. Ali, M.W. Saif, Update on the role of nanoliposomal irinotecan in the treatment of metastatic pancreatic cancer, Therap. Adv. Gastroenterol. 10 (7) (2017) 563–572.

[19] P. Su, Y. Yang, G. Wang, X. Chen, Y. Ju, Curcumin attenuates resistance to irinotecan via induction of apoptosis of cancer stem cells in chemoresistant colon cancer cells, Int. J. Oncol. 53 (3) (2018) 1343–1353.

[20] M. Murakami, S. Ohnuma, M. Fukuda, E.E. Chufan, K. Kudoh, K. Kanehara, N. Sugisawa, M. Ishida, T. Naitoh, H. Shibata, Y. Iwabuchi, S.V. Ambudkar, M. Unno, Synthetic analogs of curcumin modulate the function of multidrug resistance–linked ATP-binding cassette transporter ABCG2, Drug Metab. Dispos. 45 (11) (2017) 1166–1177.

[21] J.J. Johnson, H. Mukhtar, Curcumin for chemoprevention of colon cancer, Cancer Lett. 255 (2) (2007) 170–181.

[22] O. Ciftci, N.B. Turkmen, A. Taslıdere, Curcumin protects heart tissue against irinotecan-induced damage in terms of cytokine level alterations, oxidative stress, and histological damage in rats, Naunyn Schmiedeberg's Arch. Pharmacol. 391 (8) (2018) 783–791.

[23] M.C. Bonferoni, S. Rossi, G. Sandri, F. Ferrari, Nanoparticle formulations to enhance tumor targeting of poorly soluble polyphenols with potential anticancer properties, Semin. Cancer Biol. 46 (2017) 205–214.

[24] J. Adiwidjaja, A.J. McLachlan, A.V. Boddy, Curcumin as a clinically-promising anticancer agent: pharmacokinetics and drug interactions, Expert Opin. Drug Metabol. Toxicol. 13 (9) (2017) 953–972.

[25] A. Kurita, S. Kado, N. Kaneda, M. Onoue, S. Hashimoto, T. Yokokura, Modified irinotecan hydrochloride (CPT-11) administration schedule improves induction of delayed-onset diarrhea in rats, Cancer Chemother. Pharmacol. 46 (3) (2000) 211–220.

[26] B. Sinha, R.H. Müller, J.P. Möschwitzer, Bottom-up approaches for preparing drug nanocrystals: formulations and factors affecting particle size, Int. J. Pharm. 453 (1) (2013) 126–141.

[27] W.W. Wang, X.Y. Li, Z.H. Wang, J.F. Zhang, X. Dong, Y.Z. Wu, C. Fang, A.W. Zhou, Y.L. Wu, A novel "mosaic-type" nanoparticle for selective drug release targeting hypoxic cancer cells, Nanoscale 11 (5) (2019) 2211–2222.

[28] F. Zhao, Y. Zhao, Y. Liu, X.L. Chang, C.Y. Chen, Y.L. Zhao, Cellular uptake, intracellular trafficking, and cytotoxicity of nanomaterials, Small 7 (10) (2011) 1322–1337.

[29] F. Meng, Z. Zhong, J. Feijen, Stimuli-responsive polymersomes for programmed drug delivery, Biomacromolecules 10 (2) (2009) 197–209.

[30] J.R. Lakowicz, Principles of Fluorescence Spectroscopy, Springer Science & Business Media, 2013.

[31] H.M. Su, H.M. He, Y.Y. Tian, N. Zhao, F.X. Sun, X.M. Zhang, Q. Jiang, G.S. Zhu, Syntheses and characterizations of two curcumin-based cocrystals, Inorg. Chem. Commun. 55 (2015) 92–95.

[32] D. Ke, Q.Q. Yang, M.L. Yang, Y. Wu, J.B. Li, H.B. Zhou, X.Y. Wang, Effect of the spacer length on the electrostatic interactions of cationic gemini surfactant micelles with trianionic curcumin, Colloids Surf., A 436 (2013) 80–86.

[33] P.P.N. Rao, T. Mohamed, K. Teckwani, G. Tin, Curcumin binding to beta amyloid: a computational study, Chem. Biol. Drug Des. 86 (4) (2015) 813–820.

[34] Y.C. Pommier, A foot in the door. Targeting the genome beyond Topoisomerase I with Camptothecins and novel anticancer drugs: importance of DNA replication, repair and cell cycle checkpoints, Curr. Med. Chem. Anti Cancer Agents 4 (2004) 429–434.

[35] S. Mourtas, M. Canovi, C. Zona, D. Aurilia, A. Niarakis, B. La Ferla, M. Salmona, F. Nicotra, M. Gobbi, S.G. Antimisiaris, Curcumin-decorated nanoliposomes with very high affinity for amyloid-β1-42 peptide, Biomaterials 32 (6) (2011) 1635–1645.

[36] E. Gazit, A possible role for pi-stacking in the self-assembly of amyloid fibrils, FASEB J. 16 (1) (2002) 77–83.

[37] H.H. Tønnesen, J. Karlsen, Studies on curcumin and curcuminoids - VI. Kinetics of curcumin degradation in aqueous solution, Z. Lebensm. Unters. Forsch. 180 (5) (1985) 402–404.

[38] W.-H. Lee, C.-Y. Loo, M. Bebawy, F. Luk, R.S. Mason, R. Rohanizadeh, Curcumin and its derivatives: their application in neuropharmacology and neuroscience in the 21st century, Curr. Neuropharmacol. 11 (4) (2013) 338–378.

[39] K. Sarmini, E. Kenndler, Ionization constants of weak acids and bases in organic solvents, J. Biochem. Biophys. Methods 38 (2) (1999) 123–137.

[40] S. Khan, M. de Matas, J.W. Zhang, J. Anwar, Nanocrystal preparation: low-energy precipitation method revisited, Cryst. Growth Des. 13 (7) (2013) 2766–2777.

[41] B.J. Palla, D.O. Shah, Stabilization of high ionic strength slurries using the

synergistic effects of a mixed surfactant system, J. Colloid Interface Sci. 223 (1) (2000) 102–111.
[42] J. Rejman, V. Oberle, I.S. Zuhorn, D. Hoekstra, Size-dependent internalization of particles via the pathways of clathrin- and caveolae-mediated endocytosis, Biochem. J. 377 (Pt 1) (2004) 159–169.
[43] X.Y. Sun, Q.Z. Gan, J.M. Ouyang, Size-dependent cellular uptake mechanism and cytotoxicity toward calcium oxalate on Vero cells, Sci. Rep. 7 (2017) 41949.
[44] A. Carie, J. Rios-Doria, T. Costich, B. Burke, R. Slama, H. Skaff, K. Sill, IT-141, a polymer micelle encapsulating SN-38, induces tumor regression in multiple colorectal cancer models, J. Drug. Deliv. 2011 (2011) 869027.
[45] Y. Pommier, M. Cushman, J.H. Doroshow, Novel clinical indenoisoquinoline topoisomerase I inhibitors: a twist around the camptothecins, Oncotarget 9 (99) (2018) 37286–37288.
[46] L. Guthrie, S. Gupta, J. Daily, L. Kelly, Human microbiome signatures of differential colorectal cancer drug metabolism, Npj Biofilm. Microbiol. 3 (2017).

Journal of Chromatographic Science, 2020, Vol. 00, No. 00, 1–10
doi: 10.1093/chromsci/bmaa033
Article

Article

A Rapid and Sensitive HPLC Method for Simultaneous Determination of Irinotecan Hydrochloride and Curcumin in Co-delivered Polymeric Nanoparticles

Haijun Xiao and Vladimír Sedlařík*

Center of Polymer Systems, Tomas Bata University in Zlin, Tr. T. Bati 5678, 760 01 Zlin, Czech Republic

*Author to whom correspondence should be addressed. E-mail: sedlarik@utb.cz

Received 6 September 2019; Revised 27 April 2020; Accepted 5 June 2020

Abstract

In recent years, a great deal of attention has been paid to the combined use of multiple antitumor drugs for better cancer treatment. The aims of the study are to construct a nanoparticle drug delivery system for the co-delivery of irinotecan hydrochloride and curcumin and to develop an analytical method for simultaneously quantifying these molecules, which is essential for further studies of the co-delivered nano system. The irinotecan hydrochloride and curcumin co-delivered nanoparticle (ICN) were prepared by combinatorially entrapping them into polyethylene glycol–poly lactic acid-co-glycolic acid (PEG–PLGA) polymeric nanoparticles. A simple, sensitive and rapid high-performance liquid chromatography method was developed and validated to simultaneously quantify the compounds in the co-delivered nanoparticle system. Acetonitrile and ultrapure water containing sodium dodecyl sulfate (0.08 mol/L), disodium phosphate (Na_2HPO_4, 0.002 mol/L) and acetic acid (4%, v/v) were used as the mobile phase and their ratio was set at 50:50. The flow rate was set to 1.0 mL/min, and the temperature in the column oven was maintained at 40°C. The analysis was carried out at 256 and 424 nm to assess irinotecan hydrochloride and curcumin, respectively. Detectors with only one channel can also visualize both analytes in one chromatogram at 379 nm and still demonstrate acceptable sensitivity. The retention times for irinotecan hydrochloride and curium were 3.317 and 5.560 min, respectively. The method developed was confirmed to be sensitive, accurate (recovery, 100 ± 2%), precise (relative standard deviation, RSD ≤ 1%), robust and linear ($R^2 \geq 0.9996$) in the range from 2.05 to 1050 μg/mL. The presented method has been used to quantify irinotecan hydrochloride and curcumin in the co-delivered ICN nano system to assess the drug delivery quality of the nanoparticles and can also be used for routine analysis because of its simplicity and accuracy.

Introduction

Combining multiple antitumor drugs in the treatment of cancer has been demonstrated as one of the most effective ways to reduce the side effects of drugs, overcome multiple drug resistance (MDR) and improve the therapeutic efficacy of the same (1, 2). Many novel pharmaceutical systems have been designed to simultaneously deliver a number of active ingredients to achieve synergistic effects in cancer therapy (3–5).

Irinotecan hydrochloride is a potent inhibitor of topoisomerase I, which has been utilized to treat various cancers, especially colorectal and lung conditions (6). Irinotecan is prone to interconversion

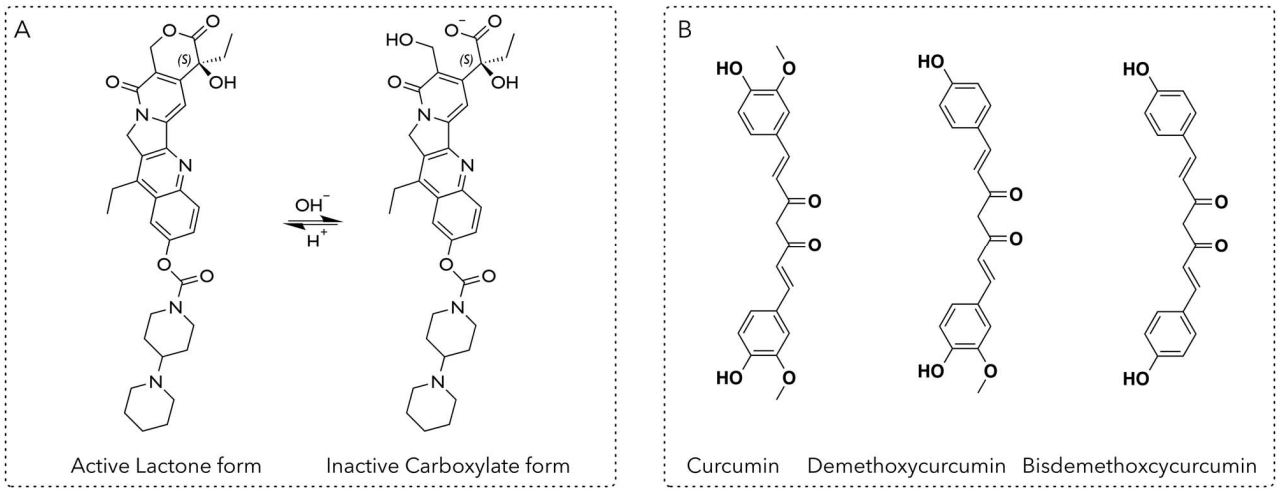

Figure 1. Chemical structures of irinotecan and curcuminoids. (A) Irinotecan undergoes pH-dependent hydrolysis to form the pharmacologically inactive carboxylate form; (B) Three representative components of curcuminoids.

between its carboxylate and lactone forms (Figure 1A), exhibited through changes in the pH of the molecular environment; notably, only the closed lactone form is pharmacologically active (7).

Curcuminoids are naturally hydrophobic polyphenols found in the extract of *Curcuma longa*, a medicinal plant widely used in Asian countries (8). As shown in Figure 1B, they contain three main components, namely curcumin, demethoxycurcumin and bisdemethoxycurcumin. These molecules evince an intrinsic anticancer effect and other pharmacological properties, such as anti-inflammatory, antioxidant and antimicrobial qualities (9). But their clinical use has been very limited due to the extremely low water solubility (10).

When combined with curcuminoids, the anticancer effect of irinotecan hydrochloride can be heightened by regulating relevant pathways inside cancer cells (11, 12), or by furthering the apoptosis of cancer cells (13). Co-delivering irinotecan hydrochloride and curcuminoids via nanotechnologies could represent a good strategy to overcome the drawbacks of the two molecular species as well as to achieve an enhanced cancer treatment. The authors, however, are unaware of any studies in the literature on the co-delivery and simultaneous determination of these compounds despite that many separate nano systems (14, 15) and analytical methods for both molecular species (16–18) have been reported.

The present study prepares a nanoparticle drug delivery system for the co-delivery of irinotecan hydrochloride and curcuminoids and provides a high-performance liquid chromatography (HPLC) method for simultaneously separating and analyzing these molecules. Chromatographic conditions are optimized to separate and quantify the compounds by adjusting the composition of the mobile phase and selecting UV-Vis wavelengths suitable for detection. The analysis was carried out at 256 and 424 nm to assess irinotecan hydrochloride and curcumin, respectively. Detectors with only one channel can also visualize both analytes in one chromatogram at 379 nm and still demonstrate acceptable sensitivity. The method has proven to be sensitive, accurate (recovery, 100 ± 2%), precise (relative standard deviation, RSD ≤ 1%), robust and linear ($R^2 \geq 0.9996$) in the range from 2.0 to 1050 μg/mL. The presented method has been used to quantify irinotecan hydrochloride and curcumin in the co-delivered irinotecan hydrochloride and curcumin co-delivered nanoparticle (ICN) nano system to assess the drug delivery quality of the nanoparticles and can also be used for routine analysis with related analytes.

Materials and Methods

Materials and instrumentation

Curcumin (curcuminoid content ≥94%, curcumin ≥80%), irinotecan hydrochloride (≥ 98% HPLC, powder), acetonitrile (ACN, HPLC grade), methanol (MeOH, HPLC grade), dimethyl sulfoxide (DMSO, HPLC grade), acetic acid (HPLC grade), hydrochloride, sodium dodecyl sulfate (SDS, ≥ 98% GC, powder) and polyethylene glycol–poly lactic acid-co-glycolic acid ($PEG_{Mn\ 2000}$–$PLGA_{Mn\ 4500}$,) were purchased from Sigma-Aldrich (Czech Republic) and utilized as received. Disodium phosphate (DSP, Na_2HPO_4) was provided by PENTA s.r.o. (Czech Republic). Ultrapure water was prepared in laboratory using a Milli-Q integral water purification system. Spectroscopic analyses were performed on a DIONEX UltiMate 3000 HPLC system, equipped with an LPG-3400SD Standard Quaternary Pump and a DAD-3000 Diode Array Detector (DAD).

Nanoparticle preparation

The ICN were prepared via an antisolvent method using PEG–PLGA as drug carriers. Briefly, curcumin (1.0 mg), irinotecan hydrochloride (1.0 mg) and PLGA-PEG (10 mg) were dissolved in DMSO (1.0 mL), which was then added dropwise into ultrapure water (10 mL) under stirring (400 RPM, 10 min). Nanoparticle water suspension was obtained after removing organic solvent by dialysis against ultrapure water (Molecular Weight Cut-Off of dialysis membrane, 3000). The hydrodynamic sizes and surface charges of nanoparticles were recorded by dynamic light scattering (DLS).

Assessment of drug delivery quality

To assess the drug delivery quality of this nanoparticle co-delivery system, ICN nanoparticle suspensions with or without centrifugation (10,000 RPM, 10 min) were diluted with ACN before being injected into HPLC to determine any difference in drug content prior to and following centrifugation. The drug-loading capacity (DL %), drug entrapment efficiency (EE %) and drug molar ratio (DR) were calculated according to the following equations:

$$\text{DL (\%, irinotecan hydrochloride)} = (I_{1\ \text{or}\ 2})/(I_0 + P_0) \times 100\% \quad (1).$$

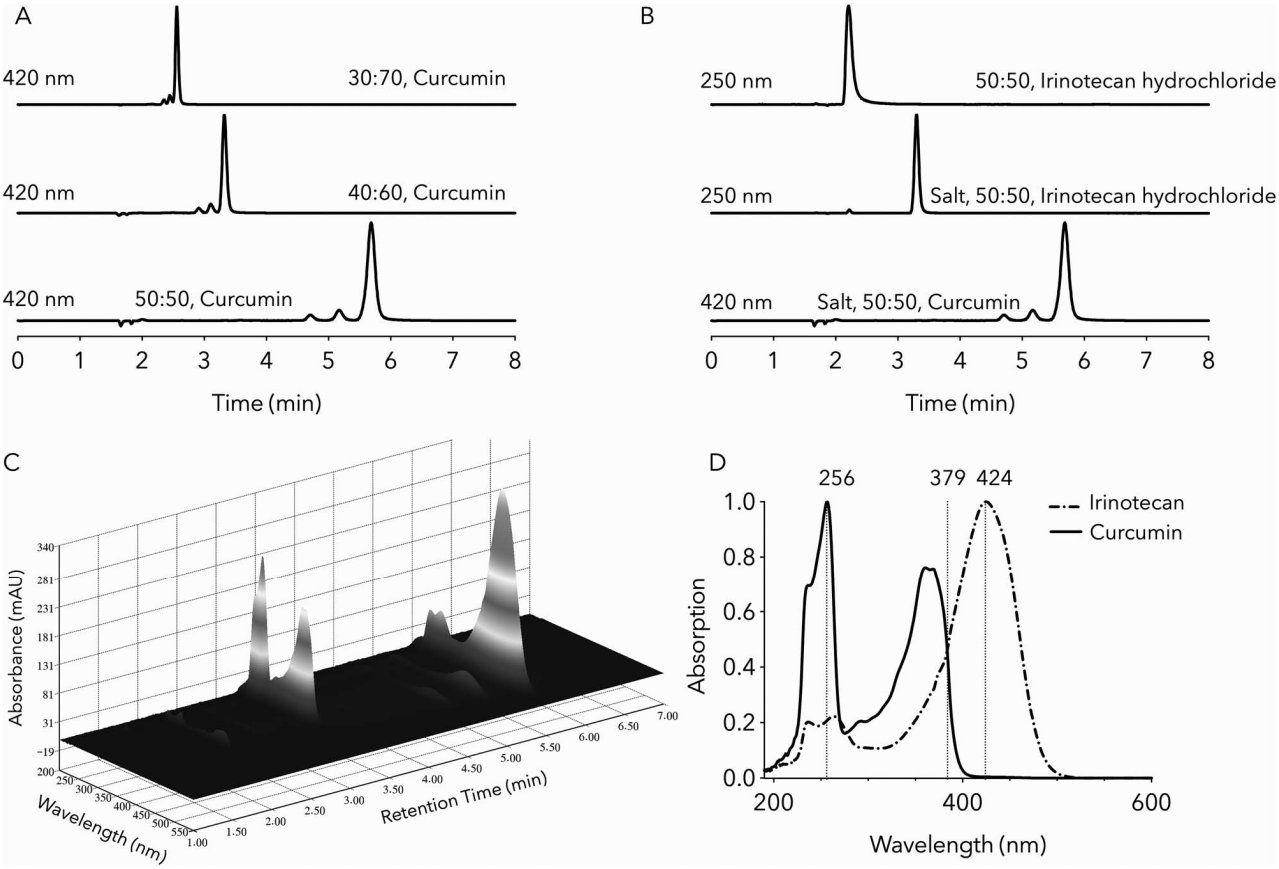

Figure 2. The optimization of chromatographic conditions. (A) Curcuminoids were eluted with acetonitrile and water (containing 4% acetic acid). Three curcuminoids can be well separated by decreasing the amount of acetonitrile from 70 to 50%; (B) Adding salts (sodium phosphate and sodium dodecyl sulfate) overcomes the peak tailing of irinotecan and does not affect the elution of curcuminoids; (C) 3D UV-Vis absorption of irinotecan and curcuminoids; (D) Overlap of UV-Vis absorption of irinotecan and curcumin.

DL (%, curcumin) = $(C_{1\text{ or }2})/(C_0 + P_0) \times 100\%$ (2).

EE (%, irinotecan hydrochloride) = $I_{1\text{ or }2}/I_0 \times 100\%$ (3).

EE (%, curcumin) = $C_{1\text{ or }2}/C_0 \times 100\%$ (4).

DR = molar amount of C_2/molar amount of I_2 (5).

Above, DL represents the drug-loading capacity, EE represents the drug entrapment efficiency and DR means drug molar ratio. *C* stands for the weight of curcumin, *I* represents the weight of irinotecan hydrochloride and *P* represents the weight of polymer PEG–PLGA. The right subscript 0 represents the amount of relevant drug molecule initially added; the right subscripts 1 and 2 represent the amount of relevant drug molecule before and after centrifugation, respectively.

Preparation of stock solution

Curcumin stock solution (1.05 mg/mL) was prepared by accurately weighing 10.5 mg of curcumin and dissolving it into 10 mL of ACN. Irinotecan hydrochloride stock solution (1.05 mg/mL) was prepared by weighing 10.5 mg of irinotecan hydrochloride and dissolving it into 10 mL of ACN. Additionally, to prepare a combined stock solution containing both curcumin and irinotecan hydrochloride, 10.5 mg of curcumin and 10.5 mg of irinotecan hydrochloride were accurately weighed and dissolved into 10 mL of ACN. All the prepared stock solutions were stored at 4°C in darkness for further use.

Development of analytical method

Chromatographic separation was carried out on a C_{18} column (Kinetex 2.6 μ C_{18} 100A, 150 mm × 4.6 mm) fitted with a pre-column (WATREX 50 mm × 4 mm, ReproSil 100 C_{18}, 5 μm). ACN and ultrapure water containing DSP (0.002 mol/L), SDS (0.08 mol/L) or acetic acid (4%, v/v) were used as the mobile phase. The flow rate was set to 1.0 mL/min, and the temperature in the column oven was maintained at 40°C. The volume injected for all injections equaled 0.5 μL. The UV-Vis absorption of curcumin or irinotecan hydrochloride was determined by HPLC, on the aforementioned system equipped with a DAD detector.

Validation of analytical method

Validation of the method was carried out according to current guidelines issued by the International Conference on Harmonization (ICH), ref. Q2 (R1) (ICH, 2017) (19).

Specificity. Blank ACN, standard curcumin solution, standard irinotecan hydrochloride solution, mixed irinotecan hydrochloride curcumin solution and ICN nanoparticles diluted with ACN were injected into HPLC so as to determine the specificity of the analytical method.

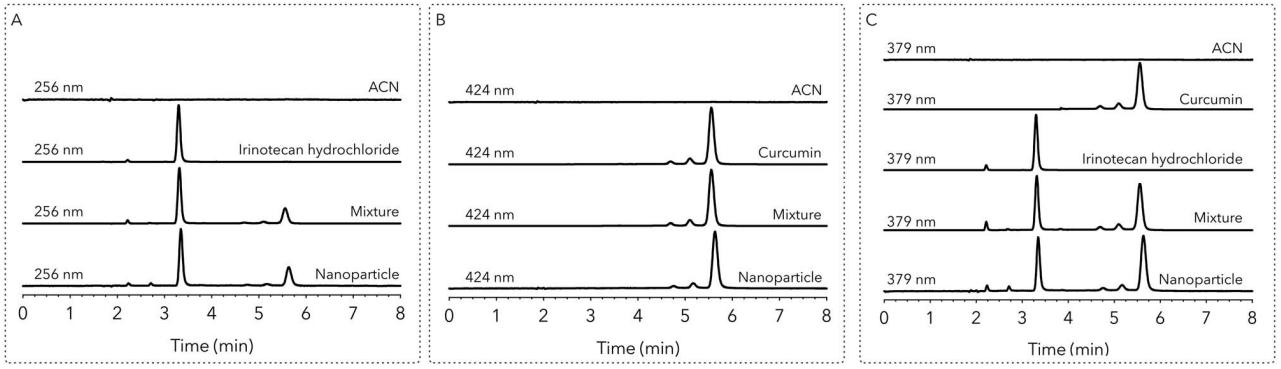

Figure 3. Specificity for detecting irinotecan and/or curcuminoids in different forms under various wavelengths. (A) Specificity for detecting irinotecan at 256 nm; (B) Specificity for detecting curcuminoids at 424 nm; (C) Specificity for detecting both irinotecan and curcuminoids at 379 nm.

Linearity and range. Serial dilutions were prepared of a mixture of curcumin and irinotecan hydrochloride in ACN at concentrations ranging from 2.05 μg/mL to 1.05 mg/mL. The calibration curve was plotted in triplicate, displaying peak area versus concentration. Analysis of least square regression was conducted on the data obtained and analysis of variance (ANOVA) test ($\alpha = 0.05$) was used to assess the regression significance.

Sensitivity. The sensitivity of the analysis method was observed with respect to the limit of detection (LOD) and limit of quantitation (LOQ). The LOQ was determined as the first concentration of calibration curves. The LOD was estimated based on the standard deviation (σ) of y-intercepts and the slopes (s) of the regression lines. The equations are represented below:

$$\text{LOD} = 3.3\,\sigma/\text{s} \quad (6).$$

Accuracy. To evaluate the accuracy of the method, a recovery experiment was performed. Three different levels (30, 200 and 500 μg/mL) of curcumin and irinotecan hydrochloride were added to the matrix samples: ACN and nanoparticle ACN solution. Their responses were estimated from the relevant calibration curve. Accuracy was determined by recovery with a relative error based upon actual and estimated concentrations.

Precision. Repeatability was analyzed by injecting three different levels (30, 200 and 500 μg/mL) of curcumin and irinotecan hydrochloride solution into the HPLC system in three replicates within a single day. Intermediate precision was also determined by analyzing the same three concentrations of curcumin and irinotecan hydrochloride solutions on 2 days in five replicates. RSD (%) with a confidence interval pertaining to the estimated concentrations was calculated for each set of data according to the calibration curve.

Robustness. The robustness of the proposed method was determined by changing a chromatographic condition, such as the mobile phase ratio (±0.5%), flow rate (±0.1 mL/min) and column temperature (±3°C). Figures for mean recovery (± % confidence interval) as well as relative error were reported.

Results

Development of analytical method

Selection of solvents

Curcuminoids eluted with ACN and water containing 4% acetic acid are shown in Figure 2A. The detective wavelength of curcuminoids used during solvent selection was set at 420 nm according to the literature report (20). When the ratio of ACN in the mobile phase decreases from 70 to 50%, three curcuminoids can be well separated and the retention time for bisdemethoxycurcumin, demethoxycurcumin and curcumin were 4.790, 5.100 and 5.560 min, respectively. Besides, the resolutions of two adjacent peaks stand at 2.30 and 2.41, respectively. In addition, the asymmetry factor of 1.00 ± 0.10 demonstrates good symmetry of the chromatographic peaks.

Irinotecan hydrochloride was also eluted with the same mobile phase and detected at 250 nm (21). However, as shown in Figure 2B, a tailing peak with an asymmetric factor of 2.01 is observed. Adding DSP (0.002 mol/L) and SDS (0.08 mol/L) into water increases the retention time of irinotecan hydrochloride from 2.187 to 3.317 min, and the asymmetric factor decreases to an acceptable value of 1.16 (22). The addition of DSP and SDS in the mobile phase keeps irinotecan hydrochloride in its neutral form and gets rid of the peak tailing. Besides, adding salts does not affect the elution of curcuminoids, hence the mobile phase comprising 50% ACN and 50% water containing DSP (0.002 mol/L), SDS (0.08 mol/L) and acetic acid (4%, v/v) was chosen as the mobile phase for the simultaneous separation and quantification of irinotecan hydrochloride and three curcuminoids.

Selection of wavelength. Figure 2C shows 3D UV-Vis absorbance profile of irinotecan hydrochloride and curcuminoids, within which the representative chromatographic peaks are well separated from each other. In order to obtain far more sensitivity and a high degree of precision, the maximum UV-Vis absorption at 256 and 424 nm (Figure 2D) were chosen to detect irinotecan hydrochloride and curcumin, respectively. Since overlap exists in the UV-Vis absorption spectra of irinotecan hydrochloride and curcumin, 379 nm was selected for detecting both irinotecan hydrochloride and curcumin in one chromatogram concurrently.

Validation of analytical method

System suitability test. An assay was performed in duplicate six times, the detection wavelength having been set to 379 nm. The statistical results of the suitability study for the given system are displayed in Table I.

Specificity. The chromatograms of the blank solution, irinotecan hydrochloride, curcumin and the mixture at 256, 424 and 379 nm are given in Figures 3A, B and C, respectively. Within these, each compound is verified as not interfering with one another.

Table I. System Suitability Results (379 nm, $n = 6$)

Parameters	Acceptable criterion	Irinotecan	Bisdemethoxycucumin	Demethoxycucumin	Curcumin
Retention time (min)	N.A.	3.317 ± 0.001	4.795 ± 0.002	5.100 ± 0.001	5.560 ± 0.001
Precision of retention time	RSD (%) ≤ 1%	0.03	0.00	0.02	0.02
Precision of peak area	RSD (%) ≤ 2%	0.63	0.62	0.96	0.68
Asymmetry factor (European pharmacopoeia)	0.95–1.05	1.02 ± 0.01	1.03 ± 0.01	1.03 ± 0.01	1.01 ± 0.01
Plate number (N)	N ≥ 2000	9785 ± 67	11943 ± 102	11673 ± 83	12197 ± 67
Resolution (European pharmacopoeia)	≥ 2.0	9.12	2.33	2.35	N.A.

Linearity and range. The assay for each standard was performed in duplicate three times and the representative chromatograms of irinotecan hydrochloride and curcuminoids detected at different wavelengths are shown in Figure 4. The linearity of the detector response for the standards was analyzed by least-square regression method and the regression equations for the calibration curves are displayed below:

For irinotecan hydrochloride detected at 256 nm:

$Y = 0.02061 * X + 0.1129$, $R^2 = 0.9997$ and $F = 24238$.

For curcumin detected at 424 nm:

$Y = 0.03954 * X + 0.007464$, $R^2 = 0.9996$ and $F = 18881$

For irinotecan detected at 379 nm:

$Y = 0.01275 * X + 0.08087$, $R^2 = 0.9997$ and $F = 21810$

For curcumin detected at 379 nm:

$Y = 0.01619 * X + 0.01796$, $R^2 = 0.9996$ and $F = 19268$

The results showed that the squares of the linear correlation coefficients (R^2) were above 0.999, indicating the good linearity of the calibration curves. ANOVA of regression showed that obtained F values ($F_{obtained}$) are far superior to the critical value ($F_{critical} = 5.5914$) ($F_{critical} < < F_{obtained}$), which demonstrates that the linear regression is significant and the method is linear over the whole tested concentration range (23). The validity of the assay was verified by means of ANOVA, which showed that there is linear regression with no deviation from linearity ($P < 0.001$) and can be used for the quantification of irinotecan hydrochloride and curcumin in the tested range.

In addition, the regression coefficients of equations at 256 and 424 nm, representing the rate of change of one variable (Y) as a function of change in the other (X), are larger than those at 379 nm, demonstrating the greater sensitivity of signal response when altering the concentration of the analytes.

Sensitivity. The calculated method LODs for irinotecan hydrochloride at 256 nm and curcumin at 424 nm equal 2.12 and 4.94 ng/mL, respectively, hence are lower than those at 379 nm (6.26 ng/mL for irinotecan hydrochloride and 8.71 ng/mL for curcumin), indicating higher sensitivity. The LOQ value was taken as the lowest concentration of calibration curves that could be quantitatively measured, namely 2.05 μg/mL.

Accuracy. Table II details results on the accuracy of the analytical method. The overall recovery (%) determined by multiple analysis is within 101.07 ± 0.54, and the RSD values for the experimental data are less than 1%.

Precision. The precision of this analytical method describes the degree of accord between a series of data from an identical sample (24). Such precision has been evaluated at three different levels, and the results of inter- and intra-day precision are expressed as RSD (in percent) of a statistically monumental number of experimental samples, as shown in Tables III and IV, respectively.

The values of RSD for validation of precision were found to be less than 1%, which demonstrates good agreement between the experimental data obtained from multiple analysis of the same sample.

Robustness. Table V details results for robustness under differing chromatographic conditions. The variations in column temperature, flow rate and mobile phase ratio within given limits that were exhibited engendered mean recoveries (%) ranging between 98.0 and 102.0, while the maximum RSD (%) equaled 1.50, indicating it to be a sufficiently robust method.

Application of analytical method

As shown in Figure 5, the average hydrodynamic size of ICN nanoparticles in water is 210.7 ± 0.9074 nm, with a polydispersity index (PDI) of 0.206 ± 0.013; hence sufficient to instigate enhanced permeability and retention (EPR) for the treatment of solid cancers. The surface Zeta Potential of ICN nanoparticles in water suspension stood at −24.19 ± 0.954 mV, indicating good stability under normal conditions.

Regarding HPLC analysis, as shown in Figure 3, no unexpected peaks or variations in the chromatograms were found, this being an analytical method considered specific to and practicable for simultaneously quantifying both curcumin and irinotecan hydrochloride in the given ICN nanoparticle water suspensions. Variations in drug content in the nanoparticles preceding and subsequent to centrifugation are presented as DL (%) and EE (%), as displayed in Figure 5. DL reflects the amount of drug delivered per amount encapsulated and EE is the percentage of drug that is successfully entrapped into the nanoparticles. No significant differences were discerned between either group, indicating that the prepared ICN nanoparticles were uniformly distributed and suspended in water and that the irinotecan hydrochloride and curcumin molecules are not adsorbed on the nanoparticle surface. The loss of drugs should be because of the operation during preparation and harvest.

Discussion

In the present study, a drug co-delivery polymeric nanoparticle system based on irinotecan hydrochloride and curcumin was constructed. Their drug loading and entrapment quality was assessed based on the established HPLC method. Optimization of HPLC conditions was performed by adjusting the mobile phase and selecting

Table II. Accuracy of the Analytical Method

Spike level (μg/mL)	Measured concentration (μg/mL) from ACN solution				Measured concentration (μg/mL) from Nanoparticle ACN solution			
	Irinotecan (256 nm)	Curcumin (424 nm)	Irinotecan (379 nm)	Curcumin (379 nm)	Irinotecan (256 nm)	Curcumin (424 nm)	Irinotecan (379 nm)	Curcumin (379 nm)
30.00	30.18	30.97	30.16	30.22	30.48	30.47	30.26	30.22
	30.11	30.75	30.51	30.71	30.41	30.35	30.41	30.31
	30.19	30.72	30.39	30.44	30.59	30.52	30.69	30.54
RSD (%)	0.14	0.64	0.59	0.81	0.30	0.29	0.72	0.54
Recovery (%)	100.53 ± 0.15	101.82 ± 0.62	101.18 ± 0.59	101.52 ± 0.82	101.64 ± 0.30	101.49 ± 0.29	101.51 ± 0.73	101.19 ± 0.55
200.00	200.35	202.79	203.52	204.19	201.37	203.31	205.52	204.19
	201.53	202.54	203.98	203.53	202.4	204.35	203.98	203.53
	199.86	200.42	201.52	201.23	203.66	201.72	202.52	201.23
RSD (%)	0.43	0.64	0.64	0.77	0.57	0.65	0.74	0.77
Recovery (%)	100.29 ± 0.43	100.96 ± 0.65	101.50 ± 0.65	101.49 ± 0.78	101.24 ± 0.57	101.56 ± 0.66	102.00 ± 0.75	101.49 ± 0.78
500.00	501.52	502.18	503.33	500.14	502.42	501.34	503.26	501.74
	501.76	503.26	505.88	501.37	504.13	503.42	505.71	502.94
	502.49	501.68	500.12	503.34	504.71	501.59	499.95	505.43
RSD (%)	0.10	0.16	0.57	0.32	0.24	0.23	0.57	0.37
Recovery (%)	100.38 ± 0.10	100.47 ± 0.16	100.62 ± 0.58	100.32 ± 0.32	100.75 ± 0.24	100.42 ± 0.23	100.59 ± 0.58	100.67 ± 0.38

Accuracy acceptance criteria, recovery (%), 100 ± 2

Table III. Intra-day Precision of the Analytical Method in Matrices (ACN solution and Nanoparticle solution)

Spike level (μg/mL)	Measured concentration (μg/mL) from ACN solution				Measured concentration (μg/mL) from Nanoparticle ACN solution			
	Irinotecan (256 nm)	Curcumin (424 nm)	Irinotecan (379 nm)	Curcumin (379 nm)	Irinotecan (256 nm)	Curcumin (424 nm)	Irinotecan (379 nm)	Curcumin (379 nm)
30.00	30.16 ± 0.04	30.81 ± 0.14	30.35 ± 0.18	30.46 ± 0.25	30.49 ± 0.09	30.45 ± 0.09	30.45 ± 0.22	30.36 ± 0.17
RSD (%) [a]	0.14	0.61	0.59	0.81	0.30	0.29	0.72	0.54
Recovery (%)	100.53 ± 0.15	101.82 ± 0.62	101.18 ± 0.59	101.52 ± 0.82	101.64 ± 0.30	101.49 ± 0.29	101.51 ± 0.73	101.19 ± 0.55
200.00	200.58 ± 0.86	201.92 ± 1.30	203.01 ± 1.31	202.98 ± 1.55	202.48 ± 1.15	203.13 ± 1.32	204.01 ± 1.50	202.98 ± 1.55
RSD (%) [a]	0.43	0.64	0.64	0.77	0.57	0.65	0.74	0.77
Recovery (%)	100.29 ± 0.43	100.96 ± 0.65	101.50 ± 0.65	101.49 ± 0.78	101.24 ± 0.57	101.56 ± 0.66	102.00 ± 0.75	101.49 ± 0.78
500.00	501.92 ± 0.51	502.37 ± 0.81	503.11 ± 2.89	501.62 ± 1.61	503.75 ± 1.19	502.12 ± 1.14	502.97 ± 2.89	503.37 ± 1.88
RSD (%) [a]	0.10	0.16	0.57	0.32	0.24	0.23	0.57	0.37
Recovery (%)	100.38 ± 0.10	100.47 ± 0.16	100.62 ± 0.58	100.32 ± 0.32	100.75 ± 0.24	100.42 ± 0.23	100.59 ± 0.58	100.67 ± 0.38

[a]Triplicate for each injection; precision acceptance criteria, RSD less than 1% within each level.

Table IV. Inter-day Precision of the Analytical Method in Matrices (ACN solution and Nanoparticle solution)

Spike level (µg/mL)	Measured concentration (µg/mL) from *ACN solution*				Measured concentration (µg/mL) from Nanoparticle ACN solution			
	Irinotecan (256 nm)	Curcumin (424 nm)	Irinotecan (379 nm)	Curcumin (379 nm)	Irinotecan (256 nm)	Curcumin (424 nm)	Irinotecan (379 nm)	Curcumin (379 nm)
30.00	30.26 ± 0.04	30.21 ± 0.14	30.35 ± 0.18	30.25 ± 0.25	30.19 ± 0.09	30.25 ± 0.09	30.05 ± 0.22	30.26 ± 0.17
RSD (%) [a]	0.15	0.45	0.58	0.62	0.30	0.29	0.72	0.54
Recovery (%)	100.87 ± 0.15	100.70 ± 0.46	101.17 ± 0.57	100.83 ± 0.60	100.63 ± 0.31	100.83 ± 0.30	100.17 ± 0.72	100.87 ± 0.55
P [b] value	0.5471	0.3926	0.2937	0.2578	0.2598	0.3658	0.5478	0.5891
200.00	200.28 ± 0.85	201.72 ± 1.35	202.84 ± 2.42	203.98 ± 1.54	203.45 ± 1.15	202.76 ± 1.19	202.34 ± 2.45	203.47 ± 3.27
RSD (%) [a]	0.42	0.63	1.20	0.79	0.57	0.58	0.72	0.58
Recovery (%)	100.14 ± 0.43	100.86 ± 0.65	101.42 ± 1.23	101.99 ± 0.78	101.73 ± 0.57	101.38 ± 0.61	101.17 ± 1.24	101.74 ± 1.62
P [b] value	0.3651	0.3545	0.5642	0.4201	0.3564	0.6412	0.3574	0.2565
500.00	504.72 ± 0.50	503.57 ± 0.80	505.51 ± 2.90	503.52 ± 1.63	504.35 ± 1.19	504.27 ± 1.19	501.57 ± 2.80	505.57 ± 1.89
RSD (%) [a]	0.12	0.15	0.54	0.36	0.24	0.23	0.57	0.38
Recovery (%)	100.94 ± 0.12	100.71 ± 0.15	101.10 ± 0.58	100.70 ± 0.36	100.87 ± 0.25	100.85 ± 0.24	100.31 ± 0.59	101.11 ± 0.38
P [b] value	0.1471	0.2145	0.2345	0.2634	0.2547	0.1950	0.2314	0.2456

Precision acceptance criteria, RSD less than 1% within each level. [a]Triplicate in two different days. [b]Student's t-test with significance level of 95% for 2 days.

Table V. Robustness Results under Different Chromatographic Conditions

Parameter	Modification	Mean recovery (Triplicate for each injection)			
		Irinotecan (256 nm)	Curcumin (424 nm)	Irinotecan (379 nm)	Curcumin (379 nm)
Column temperature	37°C	99.55 ± 1.33	98.54 ± 1.12	99.32 ± 1.45	98.31 ± 1.71
	40°C	99.76 ± 0.73	101.01 ± 0.53	101.54 ± 0.73	100.43 ± 0.63
	43°C	99.26 ± 0.33	99.01 ± 0.53	99.54 ± 0.73	101.20 ± 0.63
	RSD (%)	0.25	1.32	1.22	1.50
Flow rate	0.9 mL/min	99.47 ± 0.43	99.91 ± 0.67	99.84 ± 0.79	101.20 ± 0.13
	1.0 mL/min	99.76 ± 0.73	101.01 ± 0.53	101.54 ± 0.73	100.43 ± 0.63
	1.1 mL/min	99.86 ± 0.95	99.51 ± 0.43	99.58 ± 0.53	99.20 ± 0.93
	RSD (%)	0.20	0.78	1.06	1.01
Mobile phase ratio	50.5:49.5	98.86 ± 0.75	100.51 ± 0.63	101.58 ± 0.93	99.81 ± 0.43
	50:50	99.76 ± 0.73	101.01 ± 0.53	101.54 ± 0.73	100.43 ± 0.63
	49.5:50.5	99.36 ± 0.95	98.51 ± 0.43	99.78 ± 0.83	99.20 ± 0.74
	RSD (%)	0.45	1.32	1.02	0.62

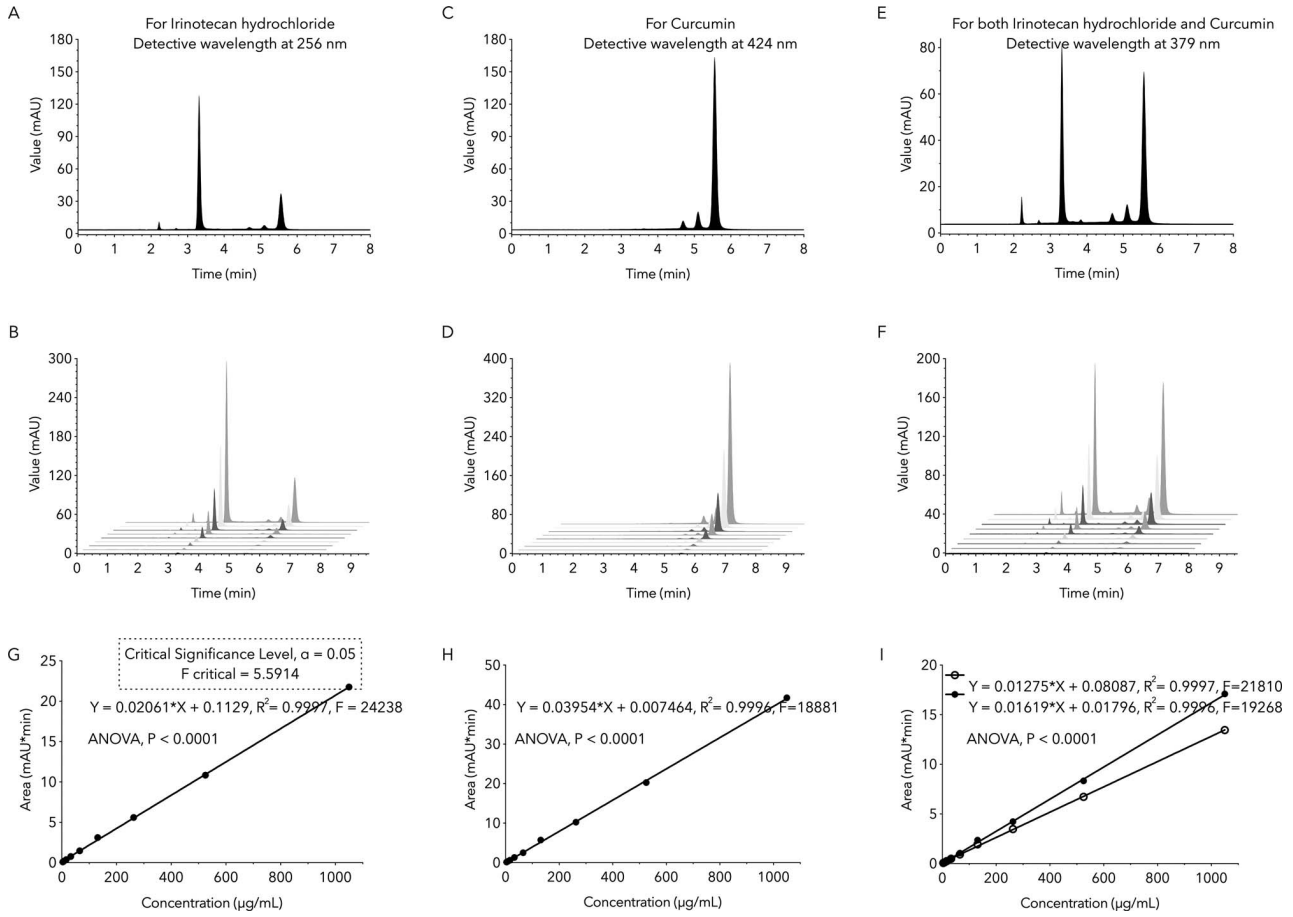

Figure 4. Chromatogram at 256 nm for detection of irinotecan (A) with different concentrations (B); Chromatogram at 424 nm for detection of curcuminoids (C) with different concentrations (D); Chromatogram at 379 nm for detection of both irinotecan and curcuminoids (E) with different concentrations (F); Regressed calibration curve at 256 nm (G), 424 nm (H) and 379 nm (I).

the detective wavelengths. Acetonitrile and ultrapure water containing sodium dodecyl sulfate (0.08 mol/L), disodium phosphate (Na_2HPO_4, 0.002 mol/L) and acetic acid (4%, v/v) were used as the mobile phase and their ratio was set at 50:50. DSP and SDS were used in the mobile phase to keep irinotecan hydrochloride in its neutral form and get rid of the peak tailing. The analysis can be carried out to simultaneously quantify irinotecan hydrochloride and curcumin at two different detective wavelengths, namely 256 and 424 nm. Detectors with only one channel can also visualize both analytes in one chromatogram at 379 nm and still demonstrate acceptable sensitivity. The method developed was validated to be sensitive, accurate (recovery, $100 \pm 2\%$), precise (RSD $\leq 1\%$), robust and linear ($R^2 \geq 0.9996$) in the tested range.

The molar ratio of curcumin to irinotecan hydrochloride in the co-delivered nanoparticles was approximately 2:1, indicating more hydrophobic curcumin molecules entrapped inside the nanoparticles than amphiphilic irinotecan hydrochloride. The authors surmise that during formation of the nanoparticles the extremely hydrophobic curcumin molecules aggregate together with the hydrophobic part of PLGA–PEG polymer, forming hard inner cores, and the hydrophobic portion of the irinotecan molecules are embedded inside the inner cores; this is due to hydrophobic interactions between the molecules themselves. The water-soluble part of PLGA–PEG and hydrophilic piperidine rings of irinotecan (25) stretch out and decrease the contact area between the nanoparticles, thereby boosting the stability of the nanoparticles owing to steric repulsion. During the formation of nanoparticles, the functions of curcumin and irinotecan hydrochloride differ. The hydrophobic curcumin molecules form an inner core with the hydrophobic part of PLGA–PEG. Meanwhile, the entire amphiphilic irinotecan hydrochloride molecule serves as a surfactant and heightens particle stability (26, 27).

Based on the current assessment of the drug loading and entrapment quality of this co-delivered nanoparticle system, further work such as the *in vitro* and *in vivo* therapeutic efficacy of both molecules will be carried out on relevant cancer models.

Conclusions

In this research, development has focused on innovative pharmaceutical systems for co-delivering irinotecan hydrochloride and curcumin, giving rise to the simple, sensitive and rapid analytical method described herein with its basis on HPLC. The analytical method developed was confirmed to be sensitive, accurate (recovery, $100 \pm 2\%$), precise (RSD $\leq 1\%$), robust and linear ($R^2 \geq 0.9996$) in the range from 2.0 to 1050 μg/mL, which has been used for the simultaneous quantification of irinotecan hydrochloride and curcumin in the co-delivered pharmaceutical systems to assess their drug delivery quality

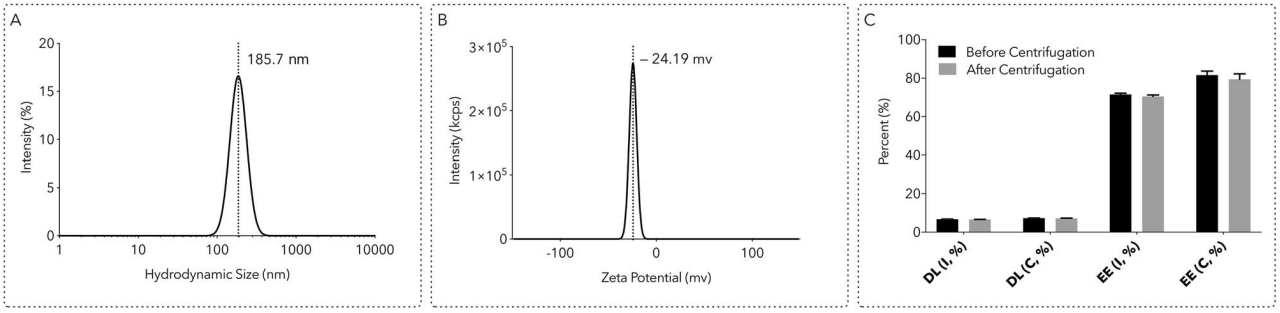

Figure 5. Typical hydrodynamic size (A) and zeta potential (B) of irinotecan and curcuminoids co-delivered nanoparticles. The drug-loading capacity and drug entrapment efficiency prior to and following centrifugation process (C).
Abbreviation: DL (I, %), drug-loading capacity of irinotecan; DL (C, %), drug- loading capacity of curcumin; EE (I, %), drug Entrapment Efficiency of irinotecan; EE (C, %), drug Entrapment Efficiency of curcumin.

and can also be used for routine analysis with related analytes because of its simplicity and accuracy.

Declaration

The authors state no conflicts of interest exist to their knowledge.

Acknowledgments

This work was co-funded by the Ministry of Education, Youth and Sports of the Czech Republic (project no. LO1504) and by the Internal Grant Agency of Tomas Bata University in Zlin (project no. IGA/CPS/2020/002).

References

1. Shim, G., Kim, M.G., Kim, D., Park, J.Y., Oh, Y.K.; Nanoformulation-based sequential combination cancer therapy; *Adv Drug Deliv Rev*, (2017); 115: 57–81.
2. Hu, Q., Sun, W., Wang, C., Gu, Z.; Recent advances of cocktail chemotherapy by combination drug delivery systems; *Adv Drug Deliv Rev*, (2016); 98: 19–34.
3. Li, Y., Thambi, T., Lee, D.S.; Co-delivery of drugs and genes using polymeric nanoparticles for synergistic cancer therapeutic effects; *Advanced Healthcare Materials*, (2018); 7.
4. Arranz-Romera, A., Esteban-Perez, S., Garcia-Herranz, D., Aragon-Navas, A., Bravo-Osuna, I., Herrero-Vanrell, R.; Combination therapy and co-delivery strategies to optimize treatment of posterior segment neurodegenerative diseases; *Drug Discov Today*, (2019); 24: 1644–1653.
5. Pan, J.Y., Rostamizadeh, K., Filipczak, N., Torchilin, V.P.; Polymeric co-delivery systems in cancer treatment: An overview on component drugs' dosage ratio effect; *Molecules*, (2019); 24: 1035.
6. Bailly, C.; Irinotecan: 25 years of cancer treatment; *Pharmacol Res*, (2019); 148: 104398.
7. Palakurthi, S.; Challenges in SN38 drug delivery: Current success and future directions; *Expert Opin Drug Del*, (2015); 12: 1911–1921.
8. Amanolahi, F., Mohammadi, A., Oskuee, R.K., Nassirli, H., Malaekeh-Nikouei, B.; A simple, sensitive and rapid isocratic reversed-phase high-performance liquid chromatography method for determination and stability study of curcumin in pharmaceutical samples; *Avicenna J Phytomedi*, (2017); 7: 444–453.
9. Kotha, R.R., Luthria, D.L.; Curcumin: biological, pharmaceutical, nutraceutical, and analytical aspects; *Molecules*, (2019); 24: 2930.
10. Ching, Y.C., Gunathilake, T.M.S., Chuah, C.H., Ching, K.Y., Singh, R., Liou, N.-S.; Curcumin/tween 20-incorporated cellulose nanoparticles with enhanced curcumin solubility for nano-drug delivery: Characterization and in vitro evaluation; *Cellulose*, (2019); 26: 5467–5481.
11. Huang, Y.F., Zhu, D.J., Chen, X.W., Chen, Q.K., Luo, Z.T., Liu, C.C. *et al.*; Curcumin enhances the effects of irinotecan on colorectal cancer cells through the generation of reactive oxygen species and activation of the endoplasmic reticulum stress pathway; *Oncotarget*, (2017); 8: 40264–40275.
12. Neerati, P., Sudhakar, Y.A., Kanwar, J.R.; Curcumin regulates colon cancer by inhibiting P-glycoprotein in in-situ cancerous colon perfusion rat model; *J Cancer Sci Ther*, (2013); 5: 313–319.
13. Zhu, D.J., Chen, X.W., Wang, J.Z., Ju, Y.L., Yang, M.Z.O., Zhang, W.J.; Proteomic analysis identifies proteins associated with curcumin-enhancing efficacy of irinotecan-induced apoptosis of colorectal cancer LOVO cell; *Int J Clin Exp Patho*, (2014); 7: 1–15.
14. Si, J., Zhao, X., Gao, S., Huang, D., Sui, M.; Advances in delivery of irinotecan (CPT-11) active metabolite 7-ethyl-10-hydroxycamptothecin; *Int J Pharm*, (2019); 568: 118499.
15. Yavarpour-Bali, H., Ghasemi-Kasman, M., Pirzadeh, M.; Curcumin-loaded nanoparticles: A novel therapeutic strategy in treatment of central nervous system disorders; *Int J Nanomedicine*, (2019); 14: 4449–4460.
16. Korany, M.A., Haggag, R.S., Ragab, M.A.A., Elmallah, O.A.; A validated stability-indicating HPLC method for simultaneous determination of silymarin and curcumin in various dosage forms; *Arab J Chem*, (2017); 10: S1711–S1725.
17. Zhuang, Q., Liu, X., Sun, Z., Wang, H., Jiang, J.; A validated UPLC-MS/MS method to determine free and total irinotecan and its two metabolites in human plasma after intravenous administration of irinotecan hydrochloride liposome injection; *J Pharmaceut Biomed*, (2019); 170: 112–123.
18. Tommasini, M., *et al.*; Monitoring of Irinotecan in Human Plasma: Sensitive Fluorescent Nanogels by Molecular Imprinting. *ChemRxiv*. (2019).
19. Borman, P., Elder, D.; Q2(R1) validation of analytical procedures: An implementation guide. 2017, p. 127–166.
20. Carolina Alves, R., Perosa Fernandes, R., Fonseca-Santos, B., Damiani Victorelli, F., Chorilli, M.; A critical review of the properties and analytical methods for the determination of curcumin in biological and pharmaceutical matrices; *Crit Rev Anal Chem*, (2019); 49: 138–149.
21. Kumar, V.K., Raju, N.A., Rani, N., Rao, J., Satyanarayana, T.; The estimation of irinotecan HCl in parenterals by RP-HPLC; *Asian J Res Chem*, (2009); 2: 54–56.
22. Raju, T.V., Seshadri, R.K., Arutla, S., Mohan, T.S., Rao, I.M., Nittala, S.R.; Development and validation of a precise, single HPLC method for the determination of Tolperisone impurities in API and pharmaceutical dosage forms; *Sci Pharm*, (2013); 81: 123–138.
23. Mishra, A., Dewangan, G., Singh, W.R., Hazra, S., Mandal, T.K.; A simple reversed phase high-performance liquid chromatography (RP-HPLC) method for determination of curcumin in aqueous humor of rabbit; *J Adv Pharm Technol Res*, (2014); 5: 147–149.

24. Sousa, F., Goncalves, V.M.F., Sarmento, B.; Development and validation of a rapid reversed-phase HPLC method for the quantification of monoclonal antibody bevacizumab from polyester-based nanoparticles; *J Pharmaceut Biomed*, (2017); 142: 171–177.
25. Li, J., Li, B., Sun, L., Duan, B., Huang, S., Yuan, Y. *et al.*; Self-delivery nanoparticles of an amphiphilic irinotecan–enediyne conjugate for cancer combination chemotherapy; *J Mater Chem B*, (2019); 7: 103–111.
26. Huang, P., Hu, M.X., Zhou, L.Z., Wang, Y., Pang, Y., Tong, G.S. *et al.*; Self-delivery nanoparticles from an amphiphilic covalent drug couple of irinotecan and bendamustine for cancer combination chemotherapy; *Rsc Adv*, (2015); 5: 86254–86264.
27. Hu, S.Q., Lee, E., Wang, C., Wang, J.Q., Zhou, Z.X., Li, Y.X. *et al.*; Amphiphilic drugs as surfactants to fabricate excipient-free stable nanodispersions of hydrophobic drugs for cancer chemotherapy; *J Control Release*, (2015); 220: 175–179.